The Astrophysical Journal, 893:77 (90pp), 2020 April 10 https://doi.org/10.3847/1538-4357/ab0a86

A Comprehensive Statistical Study of Gamma-Ray Bursts

Feifei Wang[1,2], Yuan-Chuan Zou[1], Fuxiang Liu[3], Bin Liao[1], Yu Liu[1], Yating Chai[1], and Lei Xia[1]
[1] School of Physics, Huazhong University of Science and Technology, Wuhan 430074, People's Republic of China; zouyc@hust.edu.cn
[2] School of Mathematics and Physics, Qingdao University of Science and Technology, Qingdao 266061, People's Republic of China; wangfeifei@qust.edu.cn
[3] College of Science and TGMRC, China Three Gorges University, Yichang 443002, People's Republic of China; lfxshufe@gmail.com
Received 2018 March 2; revised 2019 February 8; accepted 2019 February 13; published 2020 April 16

Abstract

In order to obtain an overview of gamma-ray bursts (GRBs), we need a full sample. In this paper, we collected 6289 GRBs (from GRB 910421 to GRB 160509A) from the literature, including their prompt emission, afterglow, and host galaxy properties. We hope to use this large sample to reveal the intrinsic properties of GRBs. We have listed all of the data in machine-readable tables, including the properties of the GRBs, correlation coefficients and linear regression results of two arbitrary parameters, and linear regression results of any three parameters. These machine-readable tables could be used as a data reservoir for further studies on the classifications or correlations. One may find some intrinsic properties from these statistical results. With these comprehensive tables, it is possible to find relations between different parameters and to classify the GRBs into different subgroups. Upon completion, they may reveal the nature of GRBs and may be used as tools like pseudo-redshift indicators, standard candles, etc. All of the machine-readable data and statistical results are available.

Key words: astronomical databases: miscellaneous – gamma-ray burst: general – methods: statistical – stars: statistics

Supporting material: figure sets, machine-readable tables

1. Introduction

Gamma-ray bursts (GRBs) were first detected in 1967 (Klebesadel et al. 1973) by the Vela Satellite Network. They have been intensively studied since the 1990s, especially after the Burst and Transient Source Experiment (BATSE) on board the *Compton Gamma Ray Observatory* (Meegan et al. 1992) began operations. For a single event, the fluence is between 10^{-7} and 10^{-5} erg cm^{-2}, and the isotropic energy is from about 10^{48} to 10^{55} erg (Nakar 2007; Zhang et al. 2011; Gehrels & Razzaque 2013; Berger 2014; Kumar & Zhang 2015). Thus, GRBs are the most violent and energetic stellar explosions in distant galaxies known to humankind (Kumar & Zhang 2015). The nature of GRBs is still undiscovered, even though there are many research works that have been going on for many years. The fireball model is one historical model that explains the mechanism of GRBs (Rees & Meszaros 1992; Piran et al. 1993; Wijers et al. 1997; Mészáros 1998, 2006). It implies that GRBs are produced by highly relativistic and collimated jets. The interaction of blobs in the jet is believed to produce the prompt emission, and the interaction of the jet with the ambient material produces the multiwavelength afterglow (X-ray, optical, and sometimes also radio). For a clear view of the current understanding of GRBs, some recent books and reviews could be read, such as the books by Kouveliotou et al. (2012) and Zhang (2018); Piran (1999, 2004), Zhang & Mészáros (2004), Mészáros (2006), Zhang (2007), and Kumar & Zhang (2015) for the general physics; Nakar (2007) and Berger (2014) for short GRBs (SGRBs); Gehrels et al. (2009), who concentrated on the observations; Woosley & Bloom (2006) and Maeder & Meynet (2012) on the progenitors; Wang et al. (2015) and Dainotti & Del Vecchio (2017) on the empirical correlations; and Lee et al. (2000) on the central engines.

In order to explain the physics of GRBs, many attempts have been made to describe the spectra in different physical frameworks, and significant progress has been achieved. There are two main frameworks. One is internal or external shocks, the emissions of which are assumed to be nonthermal intrinsically (Katz 1994; Rees & Meszaros 1994; Tavani 1996; Sari et al. 1998; Gao et al. 2015b). Another is photospheric emission, which is predicted to occur in the "fireball" model (Mészáros & Rees 2000; Rees & Mészáros 2005; Pe'er et al. 2007; Thompson et al. 2007). Racz et al. (2017) found that synchrotron radiation is significant in *Fermi*/Gamma-ray Burst Monitor (GBM) spectra. Subphotospheric dissipation (Rees & Mészáros 2005; Giannios 2006; Pe'er et al. 2006a; Chhotray & Lazzati 2015), which can broaden the spectrum, has been suggested as the emission mechanism in some bursts. Ahlgren et al. (2015) was first to provide a full physical model, Dissipation with Radiative Emission as A table Model, which is based on subphotospheric dissipation, and gave acceptable fits to GRB 090618 and GRB 100724B for more details. If we take subphotospheric dissipation and/or high-latitude effects (Lundman et al. 2013), the photospheric model can account for a large diversity of spectra. Recent observations of GRB spectra have shown a mixture of thermal and nonthermal spectra (Ryde 2005; Ryde & Pe'er 2009; Guiriec et al. 2010; Nappo et al. 2017), which implies that there is an interplay between different emission mechanisms. The existence of GRB subgroups might be the consequence of different emission mechanisms (Bégué & Burgess 2016). Acuner & Ryde (2018) searched the full *Fermi*/GBM catalog using Gaussian Mixture Models to cluster bursts according to the low-energy photon index of the Band model (Band et al. 1993; $\alpha_{\rm Band}$), the high-energy photon index of the Band model ($\beta_{\rm Band}$), the spectral peak energy of the Band model ($E_{\rm p,Band}$), the fluence ($F_{\rm g}$), and the duration of 5%–95% γ-ray fluence (T_{90}) in order to divide bursts into those with a photospheric origin and those with a synchrotron origin. They thought both emission from the photosphere and optically thin synchrotron radiation are

operating, but different emissions dominate differently for individual GRBs. They found that one-third of the bursts are consistent with synchrotron radiation and that two-thirds of all bursts are consistent with photospheric emission. Besides the two main groups, they also found subgroups. This maybe due to the dissipation pattern in the jet; alternatively, it maybe due to whether the jet is dominated by thermal or magnetic energy, or due to the viewing angle (Acuner & Ryde 2018). For the afterglows of GRBs, we can also find thermal and nonthermal components. To date, there have been a total of 16 GRBs reported to have thermal components in the X-ray light curves (LCs; Campana et al. 2006; Page et al. 2011; Starling et al. 2011; Thöne et al. 2011; Sparre & Starling 2012; Starling et al. 2012; Friis & Watson 2013; Nappo et al. 2017). Valan et al. (2018) reported six detections of additional thermal components in the GRBs' early X-ray afterglows. A cocoon breaking out from a thick wind or late prompt emission may be the explanation for the additional thermal components, which might be hidden by bright afterglows in the majority of GRBs. This is why a small fraction of afterglows are detected with additional thermal components (Valan et al. 2018). Some other possible explanations include shock breakout appearing for GRBs with associated supernova (Campana et al. 2006), or the cocoon that surrounds the jet (Mészáros & Rees 2001; Pe'er et al. 2006b; Ghisellini et al. 2007; Starling et al. 2012), or the jet itself (Friis & Watson 2013; Irwin & Chevalier 2016; Nappo et al. 2017).

Statistical study of accumulated data might be able to reveal the underlying physics. This can be roughly split into classification and correlation-seeking. Nowadays, the classification of GRBs is still uncertain. Traditionally, they are grouped into SGRBs and long GRBs (LGRBs), depending on whether T_{90} is smaller or greater than 2 s, where T_{90} is the time difference between the 95th and 5th percentile of the total counts, which is often taken as the typical duration of a GRB. Kouveliotou et al. (1993) analyzed the $\log T_{90}$ distribution of 222 BATSE GRBs. They found that the distribution is bimodal, and the dividing line is about 2 s. However, T_{90} is a function of the energy band. Consequently, this value is detector-dependent (Bromberg et al. 2013; Resmi 2017). Bromberg et al. (2013) calculated a useful threshold duration that separates collapsars (long) from noncollapsars (short), $T_{90} = 3.1 \pm 0.5$ s in BATSE, $T_{90} = 1.7^{+0.4}_{-0.6}$ s in *Fermi* GBM, and $T_{90} = 0.8 \pm 0.3$ s in *Swift*. LGRBs are rich in low-energy photons. They are thought to have originated from the gravitational collapse of massive stars, owing to observational evidence of some LGRBs associated with Type Ic supernovae (SNe; Galama et al. 1998; Hjorth et al. 2003; Stanek et al. 2003; Woosley & Bloom 2006; Hjorth & Bloom 2012; Xu et al. 2013). The host galaxies of LGRBs have low metallicity, sometimes interacting with other galaxies (Sahu et al. 1997; Bloom et al. 1998, 2002; Chary et al. 2002; Christensen et al. 2004; Savaglio et al. 2009; Krühler et al. 2015), high star-forming rate, and small host galaxy offset (Bloom et al. 2002; Fruchter et al. 2006; Blanchard et al. 2016). Compared to LGRBs, the SGRBs are rich in higher energy photons. They are thought to be the product of compact binary mergers with at least one neutron star, such as a black hole and a neutron star (BH–NS), or two neutron stars (NS–NS; Eichler et al. 1989; Paczynski 1991; Narayan et al. 1992; Nakar 2007; Zhang et al. 2009). Some studies prefer other compact merger models, like an ONeMg with a CO white dwarf (WD) merger model (Lyutikov & Toonen 2017), however. The presence of kilonova emission (Berger et al. 2013; Tanvir et al. 2013) and the locations of SGRBs (Berger et al. 2013) provide evidence for the compact merger model. Therefore, SGRBs might be candidate sources of gravitational waves (GWs; e.g., Eichler et al. 1989; Nakar 2007; Piro & Thrane 2012; Berger 2014). To date, the advanced Laser Interferometer Gravitational Wave Observatory (LIGO) has detected some GWs, such as GW150914 (Abbott et al. 2016a), GW151226 (Abbott et al. 2016b), GW170104 (Abbott et al. 2017a), and GW170817 (Abbott et al. 2017b). The observation of the association of GW170817 and GRB 170817A confirms the NS–NS merger as a progenitor of SGRBs (Abbott et al. 2017b, 2017c; Goldstein et al. 2017; Granot et al. 2017; Pozanenko et al. 2017; Xiao et al. 2017; Zou et al. 2018). The host galaxies of SGRBs include late-type and early-type galaxies, and have a large offset, which is about five times larger than LGRBs (Fong et al. 2010a). Some SGRBs have been putatively associated with r-process-powered "kilonovae/macronovae," like GRB 130603B, GRB 060614, and probably GRB 080503 and GRB 050709 as well (Li & Paczyński 1998; Metzger et al. 2010; Berger et al. 2013; Tanvir et al. 2013; Gao et al. 2015a; Yang et al. 2015; Jin et al. 2016).

With the increasing number of instruments used for detecting GRBs, such as *BeppoSAX*/GRBM (40–700 keV; Boella et al. 1997), Konus-*Wind* (10 keV–10 MeV; Aptekar et al. 1995), *HETE*-2 (6–400 keV; Ricker et al. 2003), *INTEGRAL* (15–200 keV; Mereghetti et al. 2003), *Swift*/XRT (0.2–10 keV; Gehrels et al. 2004; Burrows et al. 2005), *Swift*/BAT (15–150 keV; Gehrels et al. 2004; Barthelmy et al. 2005), *Polar* (10–500 keV; Produit et al. 2018), *HXMT* (10–500 keV; Zhang et al. 2014b), *Fermi*/LAT (20 MeV–300 GeV; GLAST Facility Science Team 1999; Ackermann et al. 2012), *Fermi*/GBM (8 keV–40 MeV; GLAST Facility Science Team 1999; Meegan et al. 2009), the Alpha Magnetic Spectrometer (AMS-02, 0.5 GeV–2 TeV; Kounine 2012), the DArk Matter Particle Explorer (DAMPE, called Wukong, 5 GeV–10 TeV; Chang et al. 2017), we can have much better quality data to analyze. Some researchers have argued that a third class of GRBs might exist (e.g., de Ugarte Postigo et al. 2011). Tsutsui et al. (2013a) identified subclasses of LGRBs using cumulative LCs of the prompt emission. Different subclasses have different fundamental planes, which is a correlation among $L_{\rm pk}$, $E_{\rm pk}$, and $T_{\rm L}$ ($T_{\rm L} = E_{\rm iso}/L_{\rm pk}$; Tsutsui et al. 2011). Furthermore, Tsutsui & Shigeyama (2014) confirmed that a third class of GRBs does exist in addition to SGRBs and LGRBs. The classification method is based on two properties, both quantified with the LC shapes of the prompt emission: the absolute deviation of their cumulative LCs from constant luminosity and the ratio of the mean counts to the maximum counts (Tsutsui et al. 2013a; Tsutsui & Shigeyama 2014). A new class of GRBs with thousands of seconds of duration, known as ultra-long bursts, has been discovered (Stratta et al. 2013; Levan et al. 2014; Cucchiara et al. 2015; Horesh et al. 2015; Gompertz & Fruchter 2017). Possible candidates for the origin of ultra-long bursts are blue supergiant collapsars, magnetars, and WD tidal disruption events caused by massive black holes (Stratta et al. 2013; Greiner et al. 2015; Ioka et al. 2016; Perets et al. 2016; Gompertz & Fruchter 2017). However, Evans et al. (2014) considered and rejected the possibility that the ultra-LGRB 130925A was a form of tidal disruption event, and instead showed that if the circumburst density around the ultra-LGRB 130925A is low, the long duration of the burst and faint external

shock emission are naturally explained. On the contrary, Gompertz & Fruchter (2017) suggested a high-density circumburst environment for the ultra-LGRB 111209A, which was powered by the spindown of a highly magnetized millisecond pulsar. Norris & Bonnell (2006) found the existence of an intermediate class (IC), or SGRBs with Extended Emission (SGRBsEE), which show properties mixed between SGRBs and LGRBs. Some models have been proposed to explain SGRBsEE, like fallback accretion onto a newborn magnetar (Rowlinson & O'Brien 2012; Rowlinson et al. 2014; Rea et al. 2015; Gibson et al. 2017; Stratta et al. 2018). Horváth (1998, 2002) investigated 797 and 1929 BASTE GRBs, respectively, and found that a three-Gaussian (3-G) distribution is better than a two-Gaussian (2-G) one statistically. Similar results can be found in the analysis of *BeppoSAX* (Horváth 2009), *Swift* /BAT (Horváth et al. 2008; Horváth & Tóth 2016), *Fermi*/GBM (Tarnopolski 2015), etc. The analysis method is χ^2 fitting (Horváth 1998; Tarnopolski 2015) or the Maximum Likelihood method (Horváth 2002, 2009; Horváth et al. 2008), and the rejection probability is less than 0.5%. Zitouni et al. (2015) investigated 248 *Swift*/BAT GRBs and also prefer the 3-G distribution, but they prefer the 2-G distribution for BATSE bursts. It was suggested by Zitouni et al. (2015) that, because the distribution of the envelope masses of the progenitors is nonsymmetric, the duration distribution corresponding to the collapsar scenario might not be symmetric. Chattopadhyay & Maitra (2017) even found five kinds of GRBs in the BATSE catalog using the Gaussian Mixture model. However, some recent works still insisted on only two components (Tarnopolski 2015, 2016; Yang et al. 2016b; Zhang et al. 2016a; Bhave et al. 2017; Kulkarni & Desai 2017) and showed that the intermediate GRB class is unlikely. A plausible explanation for the bimodal distribution of the duration is that the two-class GRB duration distributions are intrinsically nonsymmetric (Tarnopolski 2016). This indicates that we need more GRB parameters to evaluate the optimum number of components, and T_{90} should not be the unique criterion. Because we have found that some SGRBs have properties of LGRBs, and LGRBs have properties of SGRBs, the duration criterion is not enough to reveal the physical origin of GRBs. For example, GRB 060505, GRB 060614, and GRB 111005A have T_{90} greater than 2 s, but we have no detection of a supernova associated with these three GRBs (Dong et al. 2018). They are also called long-SGRBs or SN-less LGRBs (Wang et al. 2017). GRB 060614 is also more like an SGRB based on its temporal lag and peak luminosity (Gehrels et al. 2006). Several models have been proposed to explain GRB 060614, including the merger of an NS and a massive WD (King et al. 2007), the tidal disruption of a star by an intermediate-mass black hole (Lu et al. 2008), and the merger of a stellar-mass BH and a WD (Dong et al. 2018). A near-infrared bump was discovered in the afterglow, which probably arose from a Li–Paczyński macronova (Li & Paczyński 1998; Dong et al. 2018), supporting the compact binary merger model for GRB 060614 (Yang et al. 2015). On the contrary, the T_{90} of GRB 090426 is 1.24 s, but it lies in a blue, star-forming, and interacting host galaxy. The afterglow is located at a small offset from the center of its host galaxy, and it is in the LGRB region of the $E_{\rm p,rest}$–$E_{\rm iso}$ plot (Antonelli et al. 2009; Levesque et al. 2010b), where $E_{\rm p,rest}$ is the spectral peak energy in the rest frame and $E_{\rm iso}$ is the isotropic γ-ray energy. All of these properties indicate that its origin might be the collapse of a massive star. Zhang et al. (2009) suggested that we need multiwavelength criteria to determine the physical origin of individual GRBs. Li et al. (2016) gave a comparative overlapping study of the properties of SGRBs and LGRBs, and found that the three best parameters for classification purposes are T_{90}, $f_{\rm eff}$, and $F_{\rm light}$, where $f_{\rm eff}$ is the effective amplitude parameter (Lü et al. 2014) and $F_{\rm light}$ is the surface brightness fraction. Ruffini et al. (2016) divided LGRBs and SGRBs further into two subclasses, depending on whether a BH is formed in the merger or in the hypercritical accretion process exceeding the NS critical mass, and they indicated two additional progenitor systems: WD–NS and BH–NS. Therefore, given the complexity of GRBs, multi-dimensional analyses based on more complete data are likely to reveal the true classification, which needs a comprehensive data collection.

The other method is to seek the underlying correlation between different properties. The most quoted relations are the Amati relation (Amati et al. 2002, 2009; Lamb et al. 2004; Sakamoto et al. 2004; Amati 2006; Virgili et al. 2012; Demianski et al. 2017) and the Ghirlanda relation (Ghirlanda et al. 2004b). Amati et al. (2002) found a correlation between $E_{\rm iso}$ in the rest-frame $1–10^4$ keV energy band and the spectral peak energy ($E_{\rm pk}$) in 12 *BeppoSAX* GRBs. It might be due to the fact that GRBs with a larger initial Lorentz factor Γ_0 also have a larger peak energy (Ghirlanda et al. 2012), or an optically thin synchrotron shock model (Lloyd et al. 2000b). Amati et al. (2008) updated the samples. They used 70 LGRBs and XRFs (X-ray flashes), and analyzed the correlation between the rest-frame peak energy ($E_{\rm pk,i}$) and $E_{\rm iso}$. They also pointed out that the $E_{\rm pk,i}$–$E_{\rm iso}$ correlation is not affected by significant selection effects. However, this relation has been challenged by other works (Band & Preece 2005; Nakar & Piran 2005). Ghirlanda et al. (2004b) used 40 GRBs to derive a correlation between collimation-corrected energy and $E_{\rm pk}$. They gave a further test for this correlation later (Ghirlanda et al. 2007). Yonetoku et al. (2004) also gave a reliable correlation between $E_{\rm pk}$ and peak luminosity $L_{\rm pk}$ (Yonetoku correlation) using the data of *BeppoSAX* and BATSE. Then they estimated the redshifts and GRB formation rate for some GRBs without known distances. Afterwards, a growing number of samples was used to investigate the Yonetoku correlation (Ghirlanda et al. 2004a, 2005; Lu et al. 2010; Yonetoku et al. 2010; Tsutsui et al. 2013b). Yonetoku et al. (2010) reanalyzed the Amati and Yonetoku relation with 101 GRBs, examined how the truncation of the detector sensitivity affects the correlations, and concluded that they are surely intrinsic properties of GRBs. Firmani et al. (2006) reported that adding $T_{\rm R45}$ (Reichart et al. 2001) can reduce the dispersion of the Yonetoku correlation. As such, they discovered a correlation among $L_{\rm pk}$, $E_{\rm pk}$, and $T_{\rm R45}$. However, the studies of Rossi et al. (2008) and Collazzi & Schaefer (2008) did not confirm this relation. Tsutsui et al. (2009) investigated the correlation between the residuals of $L_{\rm pk}$ and $E_{\rm iso}$ from the best-fit function, and found that the luminosity time ($T_{\rm L} = E_{\rm iso}/L_{\rm pk}$) can improve the Amati and Yonetoku relations. Later, Tsutsui et al. (2011) discovered a new relation among $T_{\rm L}$, $L_{\rm pk}$, and $E_{\rm pk}$ when considering systematic errors. Tsutsui et al. (2010) pointed out that the intrinsic dispersion of the correlations among $E_{\rm pk}$, $L_{\rm pk}$, and $E_{\rm iso}$ depends on the quality of the data set. Tsutsui et al. (2013b) analyzed the Amati and Yonetoku relations for 13 SGRBs, and the correlations are dimmer than those for LGRBs for the same $E_{\rm pk}$. Zhang & Wang (2018) used the $E_{\rm pk}$ and $L_{\rm pk}$ correlation with 16 SGRBs to study the luminosity function and formation rate of SGRBs. Tu & Wang (2018) studied the correlation between isotropic energy and

duration of GRBs and found $T_{90} \propto E_{\rm iso}^{1/3}$, which can be explained by magnetic reconnection. Isotropic luminosity ($L_{\rm iso}$) and $E_{\rm pk}$ are also found to have a good correlation (Schaefer 2003a; Frontera et al. 2012; Nava et al. 2012). Schaefer et al. (2001) and Schaefer (2003a) noted that the $E_{\rm pk}$ and $L_{\rm iso}$ correlation is due to their dependence on Γ_0. With this correlation, we can further study the structure of ultrarelativistic outflow, shock acceleration, and magnetic field generation (Lloyd-Ronning & Petrosian 2002). Dichiara et al. (2016) found a highly significant anticorrelation in 123 LGRBs between $E_{\rm pk,i}$ and the power density spectra (PDS) slope α. They put forward a model based on magnetic reconnection for this phenomenon. $E_{\rm pk,i}$ and α are linked to the ejecta magnetization at the dissipation site, so that more magnetized outflows would produce more variable GRB LCs at short timescales, shallower PDS, and higher values of $E_{\rm pk,i}$. Addition to the relations extracted from the spectra, some relations are obtained from the GRB LCs. Norris et al. (2000) found an anticorrelation between $L_{\rm pk}$ and spectral lag in 174 BATSE GRBs. Tsutsui et al. (2008) obtained a new spectral lag–$L_{\rm pk}$ relation using 565 BATSE GRBs, which is different from the result of Norris et al. (2000). This anticorrelation might contain indirect connections to Γ_0, and it has been confirmed by several studies (Salmonson 2000; Schaefer et al. 2001; Daigne & Mochkovitch 2003; Zhang et al. 2006b). The interpretation of this relation might be kinematic effect (Salmonson 2000) or energy formation affecting the development of the pulse much more than dissipation (Norris et al. 2000). The correlation between variability and $L_{\rm pk}$ can be used to estimate the GRB redshift and luminosities (Fenimore & Ramirez-Ruiz 2000; Reichart et al. 2001). The origin of this correlation may be relativistically shocked jets (Schaefer 2007). Mallozzi et al. (1995) found a correlation between $E_{\rm pk}$ and the peak photon flux ($P_{\rm pk}$) in the 256 ms time bin of 50–300 keV. Lloyd et al. (2000a) simulated 1000 GRBs in the 50–300 keV energy band and found a similar strong correlation between $E_{\rm pk}$ and $F_{\rm g}$. Goldstein et al. (2010) used this correlation to classify LGRBs and SGRBs, and confirmed the presence of two GRB classes. There have been many similar works to confirm this correlation (Borgonovo & Ryde 2001; Ghirlanda et al. 2010, 2011; Guiriec et al. 2010; Lu et al. 2012a). With the estimated Γ_0, some related correlations were also found, such as Γ_0–$E_{\rm iso}$ (Liang et al. 2010), Γ_0–$L_{\rm iso}$ (Lü et al. 2012), and $L_{\rm iso}$–$E_{\rm pk,i}$–Γ_0 (Liang et al. 2015). Willingale et al. (2007a) showed that a source-frame characteristic photon energy to peak luminosity ratio, K_z, can be constructed, and it is constant within a factor of 2 for all bursts. The existence of K_z indicates that the mechanism responsible for the prompt emission from all GRBs is probably predominantly thermal (Willingale et al. 2007a). Willingale et al. (2010) analyzed the individual prompt pulses of a GRB. They showed that the luminosity of the pulses is correlated with the peak energy of the pulse spectrum and anticorrelated with the time since ejection of the pulse.

Aside from the study of individual GRB prompt emission, the statistics of afterglows are also helpful in understanding their nature. A correlation was found between the early optical/UV luminosity (measured at rest-frame 200 s) and average decay rate (measured from 200 s; Oates et al. 2009, 2012). The luminosity–decay correlation also exists in the X-ray band, and is consistent with the optical/UV (Oates et al. 2015, 2016; Racusin et al. 2016). At the same time, the early optical/UV luminosity (measured at rest-frame 200 s) is correlated with the isotropic energy $E_{\rm iso}$ and rest-frame peak spectral energy $E_{\rm pk}$ (D'Avanzo et al. 2012; Margutti et al. 2013; Oates et al. 2015). Evans et al. (2007, 2009) provided the methods and results of an automatic analysis of a complete sample of *Swift*–XRT observations of GRBs. Liang et al. (2008a, 2008b) performed a more detailed analysis of the jet breaks (Liang et al. 2008a) and the early shallow decay to late jet-like decay phases (Liang et al. 2008b). Yi et al. (2016) gave a comprehensive study of the X-ray flares from GRBs observed by *Swift*. They analyzed the 10 year X-ray flare data of *Swift*/XRT until the end of 2015 March and studied the distributions of energy, duration, waiting time, rise time, decay time, peak time, and peak flux. After that, Yi et al. (2017) statistically studied GRB optical flares from the *Swift*/UVOT catalog. They found that optical flares and X-ray flares may share a similar physical origin, and both of them are possibly related to central engine activities. Jia et al. (2016) statistically studied GRB X-ray flares to prove the ubiquitous bulk acceleration in the emission region. With the recent development of networks of robotic telescopes, we are able to follow up the early optical emission of GRBs and to find a peak in the optical afterglow LCs ($t_{\rm pkOpt}$) of some GRBs. This is due to the dynamics of the fireball deceleration. So, $t_{\rm pkOpt}$ can provide the Γ_0 of the fireball before deceleration, and Γ_0 represents the maximum value attained by the outflow during this dynamical evolution. The bulk Lorentz factor Γ_0 of GRBs is very important. We can use it to compute the GRBs' comoving frame properties, shedding light on their physics (Ghirlanda et al. 2018). We can use $t_{\rm pkOpt}$ to derive the distribution of Γ_0 (Rykoff et al. 2009; Ghirlanda et al. 2012, 2018), and also use other methods to estimate Γ_0 (Sari & Piran 1999; Molinari et al. 2007; Ghisellini et al. 2010; Zou & Piran 2010; Zhang 2011; Lü et al. 2012; Nava et al. 2013; Nappo et al. 2014; Zou et al. 2015). Geng & Huang (2016) developed a numerical method to calculate the dynamics of a system consisting of a forward shock and a reverse shock. They found that the steep optical rebrightenings would be caused by the fallback accretion of black holes, while the shallow optical rebrightenings are the consequence of the injection of the electron–positron-pair wind from the central magnetar. Dainotti et al. (2008) examined the available X-ray decay curves of all GRBs measured by *Swift*. They found a correlation between $\log[T_{\rm a}/(1+z)]$ (time at the end of the X-ray plateau in the rest frame) and $\log[L_{\rm X}(T_{\rm a})]$ (X-ray luminosity at time $T_{\rm a}$), hereafter also referred to as LT. The slope is $-0.74^{+0.2}_{-0.19}$. This LT anticorrelation shows that the shorter the plateau duration, the more luminous the plateau. Dainotti et al. (2008) believed that this LT anticorrelation is a further tool for the standardization of GRBs as a distance indicator. This result is confirmed by Ghisellini et al. (2009) and Yamazaki (2009). A physical subsample of LGRBs with a significant LT anticorrelation in the GRB rest frame has been discovered (Dainotti et al. 2010). Dainotti et al. (2016) revealed that the subsample of LGRBs associated with SNe presents a very high LT anticorrelation. This analysis may open new perspectives in future theoretical investigations of GRBs with a plateau emission and associated with SNe (Dainotti & Del Vecchio 2017). Many researches have been carried out on the LT relation, such as expanding the sample (Dainotti et al. 2011a, 2015b; Mangano et al. 2012), or investigating the influence of the selection biases on the slope of the relation (Dainotti et al. 2013a, 2018; Dainotti & Amati 2018). There are also many correlations between the prompt and the afterglow. For the LT relation, Xu & Huang (2012) added $E_{\rm iso}$ as a third parameter to get a tighter three-parameter correlation. When adding the peak luminosity to the

prompt emission $L_{\rm pk}$, Dainotti et al. (2016) also found a good correlation. Similarly, Si et al. (2018) analyzed the optical LCs of 50 GRBs. They calculated the break time of optical plateaus and the break luminosity. When they added $E_{\rm iso}$, a significantly tighter correlation was found. Dainotti et al. (2015a) demonstrated that $L_{\rm pk}$ (the peak luminosity in the prompt emission) and $L_{\rm prompt}$ (the average prompt luminosity) have intrinsic correlations with $L_{\rm X}(T_{\rm a})$. Liang & Zhang (2005) derived a three-parameter correlation, which is among $E_{\gamma,\rm iso}$, the spectral peak energy in the rest frame, and the rest-frame break time of the optical afterglow LCs. Zaninoni et al. (2016) gave a comprehensive statistical analysis of *Swift* X-ray LCs of GRBs collected from 2004 December to 2014 June, and found a three-parameter correlation between $E_{\rm iso}$ in the rest-frame $1–10^4$ keV energy band, $E_{\rm pk,i}$, and $E_{\rm X,iso}$ (X-ray energy emitted in the rest frame 0.3–30 keV; Margutti et al. 2013).

There have also been some researches on GRB host galaxies. The LGRB host galaxy offsets (the distance from the site of the GRBs to the center of its host galaxies) are consistent with the expected distribution of massive stars (Bloom et al. 2002), and SGRB host galaxy offsets are in good agreement with NS binary mergers (Fong et al. 2010a; Church et al. 2011). SGRBsEE seem to be a subgroup of SGRBs, because SGRBsEE mostly have smaller projected physical offsets (Troja et al. 2008) and occur closer to their host galaxies in denser interstellar environments (Malesani et al. 2007). SGRBs without extended emission are the opposite. It also implies that SGRBs possibly have two distinct populations. SGRBsEE are due to NS–BH mergers, and SGRBs without extended emission are due to NS–NS mergers (Troja et al. 2008). Furthermore, the correlation between X-ray absorption column densities and SGRB host galaxy offsets gives another evidence that SGRBs possibly have two distinct populations (Kopač et al. 2012). Japelj et al. (2016) studied the host galaxies of a complete sample of bright LGRBs to investigate the impact of the environment on GRB formation. Arabsalmani et al. (2018) studied the mass–metallicity (MZ) relation of 33 GRB hosts spanning a redshift range between ∼0.3 and ∼3.4 and a mass range from $10^{8.2}\,M_{\odot}$ to $10^{11.1}\,M_{\odot}$. They found that GRB hosts track the MZ relation of the general star-forming galaxy population with an average offset of 0.15 ± 0.15 dex below the MZ relation of the general population, and metallicity measurements can influence the relation result (Arabsalmani et al. 2018). The offset may be the result of the different methods used to select their respective galaxy populations (Kocevski & West 2011). There are also some relations between the host galaxy and afterglow emission (or prompt emission; Wang et al. 2018). Zhang et al. (2017) carried out some statistical analysis and found possible correlations between SGRB afterglow luminosities and their host galaxy offset. This may be due to the number density of circumburst medium decreasing with the distance to the host galaxy center. However, there are some other uncertainties related to this correlation, including the angle between the line of sight, the host galaxy disk, and SGRBs occurring in a globular cluster (Zhang et al. 2017). Selection effects usually occur when the sample observed is not representative of the true population itself (Dainotti & Del Vecchio 2017).

All previous statistical studies were based on original data or data from catalogs. For each individual study, one needs to collect the data from the beginning. Here we are trying to collect all of the data and keep them in a reservoir for future studies. The data were all manually collected from the literature, including almost all of the properties belonging to GRBs, i.e., prompt emission, afterglows, and host galaxies. Compared with the automatic gathering of data by machine, the manual collection is slow. However, it is hard for the machine to recognize the variety of symbols, and many of the data are expressed in different ways, which makes the task even harder. Before advances in machine algorithm, for precision in data gathering, we can only manually collect them in the present stage. This paper is organized as follows. In Section 2, we introduce the data preparation, including the data gathering from published papers. The table is in machine-readable format, while a sample of the table is shown in Table 1. Error imputation for the data with central values but without error bars is introduced in Section 3. In Section 4, we introduce our statistical methods. We give the distributions for each parameter in the observer frame and those for some parameters in the rest frame. All histograms are shown in Figure Set 1. We show two histograms in Figure 1. We give scatter plots between two parameters with at least five samples. All plots are shown in Figure Set 2, and two scatter plots are given in Figure 2. We analyzed the linear coefficient and nonlinear correlation ratio between two parameters that are available for at least five GRBs. We excluded trivial results, like the T_{90} and $T_{90,\rm i}$ correlation, which is obvious but does not give extra information. A small portion of all the results are shown in Table 3, and the comprehensive results are shown in a machine-readable table. We give all linear regression results between two and three parameters that are available for at least five GRBs. A small portion of all the results are shown in Tables 4 and 5, and all the results are given in two machine-readable tables. Results are given in Sections 5 and 6; we give a more detailed analysis for some good results and give some reasonable explanation for these good results. A discussion is given in Section 7, and we conclude in Section 8. A concordance cosmology with parameters $H_0 = 67.8 \pm 0.9\ {\rm km\ s^{-1}\ Mpc^{-1}}$ and $\Omega_{\rm M} = 0.308 \pm 0.012$ (Planck Collaboration et al. 2016) is adopted in this work.

2. Samples

We collected all of the possible data for 6289 GRBs, from GRB 910421 (1991 April 21) to GRB 160509A (2016 May 9). There are 46 parameters in this catalog, including the basic information, the prompt emission, the afterglow, and the host galaxy.

For the basic information on each GRB, we recorded the trigger time, instrument, trigger number, coordinate, and position error. Most of the basic information are from the Gamma-ray Coordinates Network (GCN) and published papers, while most of the information on the BATSE GRBs are from BATSE website.[4] The basic information is quite important. It can help us make sure whether or not some GRBs with the same names are different GRBs. Because some GRBs detected by different instruments have the same GRB name, we changed the names for a small number of GRBs. For example, there is a Fermi GRB 100911, while there is also a MAXI GRB 100911. They have the same name in different papers; however, the trigger time is different. Therefore, they must be different GRBs. We call the Fermi GRB as GRB 100911A and the MAXI GRB as GRB 100911B, following their trigger times. Further, some GRBs have different names in different papers. For all GRBs that have different names or whose names were changed by us, we use the flag "A" to note this. Not all of

[4] https://gammaray.msfc.nasa.gov/batse/grb/catalog/current/

Table 1
Big Table Samples

Label	Units	Description
GRB	⋯	GRB identifier
f_GRB	⋯	Flag on GRB[a]
T.h	hr	Trigger time in UTC (hour)
T.m	minute	Trigger time in UTC (minutes)
T.s	s	Trigger time in UTC (s)
Det	⋯	Detector used to obtain the data
TrigNo	⋯	Trigger number
RAh	hr	Hour of R.A. (J2000)
RAm	minutes	Minute of R.A. (J2000)
RAs	s	Second of R.A. (J2000)
DE-	⋯	Decl. sign (J2000)
DEd	deg	Degree of decl. (J2000)
DEm	arcmin	Arcminute of decl. (J2000)
DEs	arcsec	Arcsecond of decl. (J2000)
ePos	arcsec	Position uncertainty
z	⋯	Redshift
E_z	⋯	Positive error on z in the 1σ error bar
e_z	⋯	Negative error on z in the 1σ error bar
r_z	⋯	Reference for redshift
DL	10 + 28 cm	Luminosity distance
E_DL	10 + 28 cm	Positive error on DL
e_DL	10 + 28 cm	Negative error on DL
r_DL	⋯	Reference for luminosity distance
f_DL	⋯	Flag on luminosity distance[a]
T90	s	Burst duration with 5%–95% of fluence
E_T90	s	Positive error on T90 in the 1σ error bar
e_T90	s	Negative error on T90 in the 1σ error bar
r_T90	⋯	Reference for T90
f_T90	⋯	Flag on T90[a]
T50	s	Burst duration with 25%–75% of fluence
E_T50	s	Positive error on T50 in the 1σ error bar
e_T50	s	Negative error on T50 in the 1σ error bar
r_T50	⋯	Reference for T50
f_T50	⋯	Flag on T50[a]
TR45	s	Burst duration with 45% of brightest fluence according to the definition of Reichart et al. (2001).
E_TR45	s	Positive error on TR45 in the 1σ error bar
e_TR45	s	Negative error on TR45 in the 1σ error bar
r_TR45	⋯	Reference for TR45
f_TR45	⋯	Flag on TR45[a]
variability1	⋯	Variability, based on the Fenimore & Ramirez-Ruiz (2000) definition
E_variability1	⋯	Positive error on variability1 in the 1σ error bar
e_variability1	⋯	Negative error on variability1 in the 1σ error bar
r_variability1	⋯	Reference for variability1
f_variability1	⋯	Flag on variability1[a]
variability2	⋯	Variability, based on the Reichart et al. (2001) definition
E_variability2	⋯	Positive error on variability2 in the 1σ error bar
e_variability2	⋯	Negative error on variability2 in the 1σ error bar
r_variability2	⋯	Reference for variability2
variability3	⋯	Variability, based on the Schaefer (2007) definition
E_variability3	⋯	Positive error on variability3 in the 1σ error bar
e_variability3	⋯	Negative error on variability3 in the 1σ error bar

Table 1
(Continued)

Label	Units	Description
r_variability3	⋯	Reference for variability3
Fg	10–9 J m^{-2}	Fluence in the 20–2000 keV energy band
E_Fg	10–9 J m^{-2}	Positive error on fluence in the 1σ error bar
e_Fg	10–9 J m^{-2}	Negative error on fluence in the 1σ error bar
r_Fg	⋯	Reference for fluence
f_Fg	⋯	Flag on fluence[a]
HR	⋯	Hardness ratio between 100–2000/20–100 keV
E_HR	⋯	Positive error on HR in the 1σ error bar
e_HR	⋯	Negative error on HR in the 1σ error bar
r_HR	⋯	Reference for HR
f_HR	⋯	Flag on HR[a]
Eiso	10 + 52 erg	Isotropic energy in the rest-frame 1–10 + 4 keV energy band
E_Eiso	10 + 52 erg	Positive error on Eiso in the 1σ error bar
e_Eiso	10 + 52 erg	Negative error on Eiso in the 1σ error bar
r_Eiso	⋯	Reference for Eiso
f_Eiso	⋯	Flag on Eiso[a]
Lpk	10 + 52 erg s^{-1}	Isotropic peak luminosity in the 1 s time bin in the rest-frame 1–10 + 4 keV energy band
E_Lpk	10 + 52 erg s^{-1}	Positive error on Lpk in the 1σ error bar
e_Lpk	10 + 52 erg s^{-1}	Negative error on Lpk in the 1σ error bar
r_Lpk	⋯	Reference for Lpk
f_Lpk	⋯	Flag on Lpk[a]
Fpk1	10–9 J m^{-2} s^{-1}	Peak flux in the 1 s time bin in the rest-frame 1–10 + 4 keV energy band
E_Fpk1	10–9 J m^{-2} s^{-1}	Positive error on Fpk1 in the 1σ error bar
e_Fpk1	10–9 J m^{-2} s^{-1}	Negative error on Fpk1 in the 1σ error bar
r_Fpk1	⋯	Reference for Fpk1
f_Fpk1	⋯	Flag on Fpk1[a]
Fpk2	10–9 J m^{-2} s^{-1}	Peak flux in the 64 ms time bin in the rest-frame 1–10 + 4 keV energy band
E_Fpk2	10–9 J m^{-2} s^{-1}	Positive error on Fpk2 in the 1σ error bar
e_Fpk2	10–9 J m^{-2} s^{-1}	Negative error on Fpk2 in the 1σ error bar
f_Fpk2	⋯	Flag on Fpk2[a]
Fpk3	10–9 J m^{-2} s^{-1}	Peak flux in the 256 ms time bin in the rest-frame 1–10 + 4 keV energy band
E_Fpk3	10–9 J m^{-2} s^{-1}	Positive error on Fpk3 in the 1σ error bar
e_Fpk3	10–9 J m^{-2} s^{-1}	Negative error on Fpk3 in the 1σ error bar
f_Fpk3	⋯	Flag for Fpk3[a]
Fpk4	10–9 J m^{-2} s^{-1}	Peak flux in the 1024 ms time bin in the rest-frame 1–10 + 4 keV energy band
E_Fpk4	10–9 J m^{-2} s^{-1}	Positive error on Fpk4 in the 1σ error bar
e_Fpk4	10–9 J m^{-2} s^{-1}	Negative error on Fpk4 in the 1σ error bar
f_Fpk4	⋯	Flag for Fpk4[a]
Ppk1	ph cm^{-2} s^{-1}	Peak photon flux in the 64 ms time bin of 10–1000 keV
E_Ppk1	ph cm^{-2} s^{-1}	Positive error on Ppk1 in the 1σ error bar
e_Ppk1	ph cm^{-2} s^{-1}	Negative error on Ppk1 in the 1σ error bar
r_Ppk1	⋯	Reference for Ppk1
f_Ppk1	⋯	Flag on Ppk1[a]
Ppk2	ph cm^{-2} s^{-1}	Peak photon flux in the 256 ms time bin of 10–1000 keV
E_Ppk2	ph cm^{-2} s^{-1}	Positive error on Ppk2 in the 1σ error bar
e_Ppk2	ph cm^{-2} s^{-1}	

Table 1
(Continued)

Label	Units	Description
		Negative error on Ppk2 in the 1σ error bar
r_Ppk2	⋯	Reference for Ppk2
f_Ppk2	⋯	Flag on Ppk2[a]
Ppk3	ph cm^{-2} s^{-1}	Peak photon flux in the 1024 ms time bin of 10–1000 keV
E_Ppk3	ph cm^{-2} s^{-1}	Positive error on Ppk3 in the 1σ error bar
e_Ppk3	ph cm^{-2} s^{-1}	Negative error on Ppk3 in the 1σ error bar
r_Ppk3	⋯	Reference for Ppk3
f_Ppk3	⋯	Flag on Ppk3[a]
Ppk4	ph cm^{-2} s^{-1}	Peak photon flux in the 1 s time bin of 10–1000 keV
E_Ppk4	ph cm^{-2} s^{-1}	Positive error on Ppk4 in the 1σ error bar
e_Ppk4	ph cm^{-2} s^{-1}	Negative error on Ppk4 in the 1σ error bar
r_Ppk4	⋯	Reference for Ppk4
f_Ppk4	⋯	Flag on Ppk4[a]
alphaband	⋯	Opposite value of the low-energy spectrum index of the Band model
E_alphaband	⋯	Positive error on alpha.band in the 1σ error bar
e_alphaband	⋯	Negative error on alpha.band in the 1σ error bar
r_alphaband	⋯	Reference for alpha.band
f_alphaband	⋯	Flag on alpha.band[a]
betaband	⋯	Opposite value of the high-energy spectrum index of the Band model
E_betaband	⋯	Positive error on beta.band in the 1σ error bar
e_betaband	⋯	Negative error on beta.band in the 1σ error bar
r__betaband	⋯	Reference for beta.band
f__betaband	⋯	Flag on beta.band[a]
Epband	keV	Spectral peak energy of the Band model
E_Epband	keV	Positive error on Ep.band in the 1σ error bar
e_Epband	keV	Negative error on Ep.band in the 1σ error bar
r_Epband	⋯	Reference for Ep.band
f_Epband	⋯	Flag on Ep.band[a]
alphacpl	⋯	Opposite value of the spectrum index of the cutoff power-law (CPL) model
E_alphacpl	⋯	Positive error on alpha.cpl in the 1σ error bar
e_alphacpl	⋯	Negative error on alpha.cpl in the 1σ error bar
r_alphacpl	⋯	Reference for alpha.cpl
f_alphacpl	⋯	Flag on alpha.cpl[a]
Epcpl	keV	Spectral peak energy of the cutoff power-law (CPL) model
E_Epcpl	keV	Positive error on Ep.cpl in the 1σ error bar
e_Epcpl	keV	Negative error on Ep.cpl in the 1σ error bar
r_Epcpl	⋯	Reference for Ep.cpl
f_Epcpl	⋯	Flag on Ep.cpl[a]
alphaspl	⋯	Opposite value of the spectrum index of the simple power-law (SPL) model
E_alphaspl	⋯	Positive error on alpha.spl in the 1σ error bar
e_alphaspl	⋯	Negative error on alpha.spl in the 1σ error bar
r_alphaspl	⋯	Reference for alpha.spl

Table 1
(Continued)

Label	Units	Description
f_alphaspl	⋯	Flag on alpha.spl[a]
thetaj	rad	Jet-opening angle
E_thetaj	rad	Positive error on theta.j in the 1σ error bar
e_thetaj	rad	Negative error on theta.j in the 1σ error bar
r_thetaj	⋯	Reference for theta.j
f_thetaj	⋯	Flag on theta.j[a]
spectrallag	ms MeV^{-1}	Spectral time lag, for every GRB, we can get the time lag, t, between the low-energy band E1–E2 and the high-energy band E3–E4, then we use the value of $t/[(E4–E3)/2–(E2–E1)/2]$, in order to avoid the influence of the different E1, E2, and E3, E4; thus, it is in units of ms MeV^{-1}.
E_spectrallag	ms MeV^{-1}	Positive error on spectral.lag in the 1σ error bar
e_spectrallag	ms MeV^{-1}	Negative error on spectral.lag in the 1σ error bar
r_spectrallag	⋯	Reference for spectral.lag
f_spectrallag	⋯	Flag on spectral.lag[a]
Gamma0	⋯	Initial Lorentz factor
E_Gamma0	⋯	Positive error on Gamma0 in the 1σ error bar
e_Gamma0	⋯	Negative error on Gamma0 in the 1σ error bar
r_Gamma0	⋯	Reference for Gamma0
f_Gamma0	⋯	Flag on Gamma0[a]
[tburst]	s	Duration of the GRB central engine defined by both gamma-ray and X-ray light curves in logarithm; the definition is from Zhang et al. (2014a)
E_[tburst]	s	Positive error on t_burst in the 1σ error bar
e_[tburst]	s	Negative error on t_burst in the 1σ error bar
r_[tburst]	⋯	Reference for t_burst
tpkX	s	Peak flux time in the X-ray band
E_tpkX	s	Positive error on t.pkX in the 1σ error bar
e_tpkX	s	Negative error on t.pkX in the 1σ error bar
r_tpkX	⋯	Reference for t.pkX
f_tpkX	⋯	Flag on t.pkX[a]
tpkOpt	s	Peak flux time in the optical band
E_tpkOpt	s	Positive error on t.pkOpt in the 1σ error bar
e_tpkOpt	s	Negative error on t.pkOpt in the 1σ error bar
r_tpkOpt	⋯	Reference for t.pkOpt
f_tpkOpt	⋯	Flag on t.pkOpt[a]
FX11hr	Jy	Flux density in the X-ray band 11 hr after the trigger time of the burst
E_FX11hr	Jy	Positive error on F.X11hr in the 1σ error bar
e_FX11hr	Jy	Negative error on F.X11hr in the 1σ error bar
r_FX11hr	⋯	Reference for F.X11hr
f_FX11hr	⋯	Flag on F.X11hr[a]
betaX11hr	⋯	Index in the X-ray band 11 hr after the trigger time of the burst
E_betaX11hr	⋯	

Table 1
(Continued)

Label	Units	Description
		Positive error on beta.X11hr in the 1σ error bar
e_betaX11hr	⋯	Negative error on beta.X11hr in the 1σ error bar
r_betaX11hr	⋯	Reference for beta.X11hr
FOpt11hr	Jy	Flux density in the optical band 11 hr after the trigger time of the burst
E_FOpt11hr	Jy	Positive error on F.Opt11hr in the 1σ error bar
e_FOpt11hr	Jy	Negative error on F.Opt11hr in the 1σ error bar
r_FOpt11hr	⋯	Reference for F.Opt11hr
f_FOpt11hr	⋯	Flag on F.Opt11hr[a]
tradiopk	s	Peak radio time in the afterglow
E_tradiopk	s	Positive error on t.radiopk in the 1σ error bar
e_tradiopk	s	Negative error on t.radiopk in the 1σ error bar
r_tradiopk	⋯	Reference for t.radiopk
f_tradiopk	⋯	Flag on t.radiopk[a]
Fradiopk	Jy	Peak flux density in the radio band at 8.46 GHz
E_Fradiopk	Jy	Positive error on F.radiopk in the 1σ error bar
e_Fradiopk	Jy	Negative error on F.radiopk in the 1σ error bar
r_Fradiopk	⋯	Reference for F.radiopk
f_Fradiopk	⋯	Flag on F.radiopk[a]
offset	kpc	Distance from the burst location to the center of the host galaxy
E_offset	kpc	Positive error on the offset in the 1σ error bar
e_offset	kpc	Negative error on the offset in the 1σ error bar
r_offset	⋯	Reference for the offset
f_offset	⋯	Flag on the offset[a]
metallicity	⋯	Metallicity of the host; the value is $12 + \log[O/H]$
E_metallicity	⋯	Positive error on the metallicity in the 1σ error bar
e_metallicity	⋯	Negative error on the metallicity in the 1σ error bar
r_metallicity	⋯	Reference for the metallicity
f_metallicity	⋯	Flag on the metallicity[a]
Mag	mag	Absolute magnitude in the 3.5 um rest wavelength
E_Mag	mag	Positive error on Mag in the 1σ error bar
e_Mag	mag	Negative error on Mag in the 1σ error bar
r_Mag	⋯	Reference for Mag
f_Mag	⋯	Flag on Mag[a]
NH	$10 + 21$ cm^{-2}	Column density of hydrogen
E_NH	$10 + 21$ cm^{-2}	Positive error on N_H in the 1σ error bar
e_NH	$10 + 21$ cm^{-2}	Negative error on N_H in the 1σ error bar
r_NH	⋯	Reference for N_H
f_NH	⋯	Flag on N_H[a]
AV	⋯	Dust extinction
E_AV	⋯	Positive error on A_V in the 1σ error bar
e_AV	⋯	Negative error on A_V in the 1σ error bar
r_AV	⋯	Reference for A_V
f_AV	⋯	Flag on A_V[a]
SFR	solMass yr^{-1}	Star formation rate

Table 1
(Continued)

Label	Units	Description
E_SFR	solMass yr^{-1}	Positive error on SFR in the 1σ error bar
e_SFR	solMass yr^{-1}	Negative error on SFR in the 1σ error bar
r_SFR	⋯	Reference for SFR
f_SFR	⋯	Flag on SFR[a]
[SSFR]	[Gyr^{-1}]	Specific star formation rate in logarithm
E_[SSFR]	[Gyr^{-1}]	Positive error on [SSFR] in the 1σ error bar
e_[SSFR]	[Gyr^{-1}]	Negative error on [SSFR] in the 1σ error bar
r_[SSFR]	⋯	Reference for [SSFR]
f_[SSFR]	⋯	Flag on [SSFR][a]
Age	Myr	The age of the GRB host galaxy
E_Age	Myr	Positive error on Age in the 1σ error bar
e_Age	Myr	Negative error on Age in the 1σ error bar
r_Age	⋯	Reference for Age
f_Age	⋯	Flag on Age[a]
[Mass]	[solMass]	Stellar mass in logarithm
E_[Mass]	[solMass]	Positive error on [Mass] in the 1σ error bar
e_[Mass]	[solMass]	Negative error on [Mass] in the 1σ error bar
r_[Mass]	⋯	Reference for [Mass]
f_[Mass]	⋯	Flag on [Mass][a]

Note.
[a] Flags include A: we changed the GRB name, or the name is a little different in different papers and GCN, because some different GRBs have the same name in different instruments. For example, Fermi GRB 110916 and MAXI GRB 110916 are two different GRBs with different trigger times, but they have the same GRB name, so we changed Fermi GRB 110916 to GRB 110916A, and MAXI GRB 110916 to GRB 110916B. a: The errors are imputed by the MICE algorithm. b: The errors in the original papers are in the 90% confidence level; we changed the errors to 1σ confidence level by multiplying by 0.995/1.645. c: The values are calculated using the spectral values in order to change the energy band. d: The unit is different from the original papers. e: The error is estimated as the central value multiplied by 0.1. f: We use the BASTE α peak value -1.1 as is common when α is not well constrained. g: We use the BASTE β peak value -2.2 as is common when β is not well constrained. h: The value in the original paper is in the rest frame; we divided the rest-frame value by $(1 + z)$ to get the observer-frame value. i: We changed the values into logarithm or from logarithm into the normal form. j: The values are calculated using other parameters. k: We convert the different metallicity calibrations into the Kobulnicky & Kewley (2004) calibrator using the method in Kewley & Ellison (2008). m: D_L is calculated using z with cosmology parameters from Planck Collaboration et al. (2016). The description of every parameter is in Section 2.

References. (1) Laskar et al. (2016); (2) Roberts et al. (2016); (3) Ricciarini et al. (2016); (4) Burns & Meegan (2016); (5) Cummings et al. (2016b); (6) https://swift.gsfc.nasa.gov/archive/grb_table/index.php; (7) Barthelmy et al. (2016c); (8) Ukwatta et al. (2016b); (9) Stamatikos et al. (2016a); (10) Sakamoto et al. (2016a); (11) Frederiks et al. (2016); (12) Palmer et al. (2016a); (13) Roberts (2016); (14) Mereghetti et al. (2016); (15) Markwardt et al. (2016a); (16) Lien et al. (2016b); (17) Krimm et al. (2016a); (18) Hui (2016); (19) Cummings et al. (2016a); (20) Barthelmy et al. (2016b); (21) Toelge & Hui (2016); (22) Ukwatta et al. (2016a); (23) Stamatikos et al. (2016b); (24) Sakamoto et al. (2016b); (25) Palmer et al. (2016b); (26) Ozawa et al. (2016); (27) von Kienlin et al. (2016); (28) Markwardt et al. (2016b); (29) Hui & Bissaldi (2016); (30) Lien et al. (2016c); (31) Krimm et al. (2016b); (32) Barthelmy et al. (2016e); (33) Barthelmy et al. (2016d); (34) Dado & Dar (2016); (35) Cummings et al. (2016c); (36) Barthelmy et al. (2016a); (37) Barthelmy et al. (2016f); (38) Ukwatta et al. (2016c); (39) Stamatikos et al. (2016c); (40) Palmer et al. (2016c); (41) Roberts & Burns (2016); (42) Nakahira et al. (2016); (43) Veres & Meegan (2016); (44) Palmer et al. (2016d); (45) Golenetskii et al. (2016a); (46) Yamada et al. (2016);

(47) Veres (2016); (48) Moriyama et al. (2016); (49) Veres et al. (2015b); (50) Lien et al. (2015e); (51) Krimm et al. (2015d); (52) Barthelmy et al. (2015g); (53) Bissaldi et al. (2015b); (54) Senuma et al. (2015); (55) Toelge & Bissaldi (2015); (56) Kawakubo et al. (2015); (57) Golenetskii et al. (2016b); (58) Yu (2015a); (59) Cummings et al. (2015e); (60) Barthelmy et al. (2015f); (61) Ukwatta et al. (2015d); (62) Stamatikos et al. (2015e); (63) Sakamoto et al. (2015b); (64)Stanbro (2015a); (65) von Kienlin (2015a); (66) Markwardt et al. (2015a); (67) Lien et al. (2015f); (68) Krimm et al. (2015e); (69) Cummings et al. (2015i); (70) Yoshida et al. (2015); (71) Stanbro & Meegan (2015); (72) Malesani et al. (2015); (73) Ukwatta et al. (2015a); (74) Tanvir et al. (2015a); (75) Stamatikos et al. (2015f); (76) Xu et al. (2015); (77) Sakamoto et al. (2015c); (78) Nappo et al. (2017); (79) Palmer et al. (2015d); (80) Markwardt et al. (2015i); (81) Lien et al. (2015g); (82) Krimm et al. (2015f); (83) Cummings et al. (2015f); (84) Barthelmy et al. (2015e); (85) Ukwatta et al. (2015e); (86) Stamatikos et al. (2015g); (87) Sakamoto et al. (2015d); (88) Roberts et al. (2015a); (89) Golenetskii et al. (2015a); (90) Augusto et al. (2016); (91) Palmer et al. (2015e); (92) Bissaldi (2015); (93) Markwardt et al. (2015c); (94) Zheng et al. (2009); (95) Lien et al. (2015h); (96) Krimm et al. (2015g); (97) Golenetskii et al. (2015b); (98) Roberts & Younes (2015a); (99) Cummings et al. (2015g); (100) Barthelmy et al. (2015h); (101) Ukwatta et al. (2015f); (102) Bissaldi & Burns (2015); (103) D'Elia et al. (2015); (104) Stamatikos et al. (2015h); (105) Roberts (2015a); (106) Yu & Burns (2015); (107) Sakamoto et al. (2015e); (108) Cano et al. (2017); (109) Palmer et al. (2015f); (110) Markwardt et al. (2015d); (111) Yu & Jenke (2015); (112) Jenke (2015a); (113) Krimm et al. (2015h); (114) Barthelmy et al. (2015i); (115) Ukwatta et al. (2015g); (116) Tanvir et al. (2015b); (117) Stamatikos et al. (2015d); (118) Younes (2015b); (119) Golenetskii et al. (2015c); (120) Veres et al. (2015a); (121) Palmer et al. (2015g); (122)Markwardt et al. (2015e); (123) Bissaldi et al. (2015a); (124) Lien et al. (2015i); (125) Lien et al. (2015j); (126) Krimm et al. (2015i); (127) Jenke (2015b); (128) Cummings et al. (2015h); (129) Barthelmy et al. (2015d); (130) Jenke (2015c); (131) Yu et al. (2015b); (132) Ukwatta et al. (2015h); (133) Stamatikos et al. (2015a); (134) Sakamoto et al. (2015a); (135) Golenetskii et al. (2015d); (136) Palmer et al. (2015b); (137) Roberts (2015b); (138) Cummings & Palmer (2015); (139) Markwardt et al. (2015f); (140) Yu et al. (2015d); (141) Lien et al. (2015a); (142) Yu (2015b); (143) Fujinuma et al. (2015); (144) de Ugarte Postigo et al. (2015); (145) Roberts et al. (2015b); (146) Lien et al. (2015b); (147) Younes (2015a); (148) Burns & Meegan (2015a); (149) Krimm et al. (2015a); (150) Roberts & Younes (2015b); (151) Zhang et al. (2014a); (152) Cummings et al. (2015b); (153) Baumgartner et al. (2015a); (154) Barthelmy et al. (2015a); (155) Siellez et al. (2016); (156) Ukwatta et al. (2015b); (157) Golenetskii et al. (2015e); (158) Deng et al. (2016); (159) Stamatikos et al. (2015b); (160) Sakamoto et al. (2015f); (161) Dichiara et al. (2016); (162) Zhang (2015); (163) Stanbro (2015b); (164) Palmer et al. (2015a); (165) von Kienlin (2015b); (166) Markwardt et al. (2015b); (167) Lien et al. (2015c); (168) Krimm et al. (2015b); (169) Cummings et al. (2015c); (170) Yu (2015c); (171) Baumgartner et al. (2015b); (172) Roberts & Stanbro (2015); (173) Barthelmy et al. (2015b); (174) Stamatikos et al. (2015c); (175) Gorbovskoy et al. (2016); (176) Burns & Meegan (2015b); (177) Sakamoto et al. (2015g); (178) Connaughton et al. (2015); (179) Markwardt et al. (2015g); (180) von Kienlin & Meegan (2015); (181) Mereghetti et al. (2015); (182) Krimm et al. (2015c); (183) Cummings et al. (2015a); (184) Baumgartner et al. (2015c); (185) Burns (2015a); (186) Barthelmy et al. (2015c); (187) Stamatikos et al. (2015i); (188) Burns & Yu (2015); (189) Ukwatta et al. (2015c); (190) Pelassa & Yu (2015); (191) Pelassa (2015); (192) Sakamoto et al. (2015h); (193) Palmer et al. (2015c); (194) Jenke & von Kienlin (2015); (195) Stanbro (2015c); (196) Golenetskii et al. (2015f); (197) Wiseman et al. (2015); (198) Markwardt et al. (2015h); (199) Sang et al. (2016); (200) Lien et al. (2015d); (201) von Kienlin & Burns (2015); (202) Burns (2015b); (203) Stanbro (2015d); (204) Stanbro (2015e); (205) Stanbro & Yu (2015); (206) Cummings et al. (2015d); (207) Xie et al. (2016); (208) Fong et al. (2015); (209) Stanbro (2015f); (210) Baumgartner et al. (2015d); (211) Cummings et al. (2014a); (212) Roberts (2014d); (213) Barthelmy et al. (2014a); (214) Jenke (2014a); (215) Jenke (2014b); (216) Ukwatta et al. (2014a); (217) Yu (2014a); (218) Ghirlanda et al. (2018); (219) Lin et al. (2016); (220) Stamatikos et al. (2014a); (221) Jenke et al. (2014); (222) Sakamoto et al. (2014a); (223) Palmer et al. (2014a); (224) Liu et al. (2015); (225) Burns (2014a); (226) Markwardt et al. (2014a); (227) Roberts (2014e); (228) Roberts (2014f); (229) Lien et al. (2014a); (230) Krimm et al. (2014a); (231) Cucchiara et al. (2015); (232) Jenke (2014c); (233) Cummings et al. (2014b); (234) Baumgartner et al. (2014a); (235) Cummings (2014a); (236) Zhang (2014a); (237) Barthelmy et al. (2014b); (238) Ukwatta et al. (2014b); (239) Roberts (2014g); (240) Roberts (2014h); (241) Xu et al. (2014); (242) Roberts (2014c); (243) Ruffini et al. (2016); (244) Stamatikos et al. (2014b); (245) Sakamoto et al. (2014b); (246) Palmer et al. (2014b); (247) Markwardt et al. (2014b); (248) Turpin et al. (2016); (249) Lien et al. (2014b); (250) von Kienlin (2014a); (251) Krimm et al. (2014b); (252) Roberts (2014a); (253) Cummings et al. (2014c); (254) Pelassa (2014a); (255) Baumgartner et al. (2014b); (256) von Kienlin & Meegan (2014); (257) Barthelmy et al. (2014c); (258) Ukwatta et al. (2014c); (259) Pelassa (2014b); (260) Stamatikos et al. (2014c); (261) Sakamoto et al. (2014c); (262) Zhang (2014b); (263) Golenetskii et al. (2014a); (264) Palmer et al. (2014c); (265) Troja et al. (2016); (266) Zhang (2014c); (267) Jenke (2014d); (268) Markwardt et al. (2014c); (269) von Kienlin (2014b); (270) Golenetskii et al. (2014b); (271) Lien et al. (2014c); (272) Krimm et al. (2014c); (273) Roberts (2014b); (274) Cummings et al. (2014d); (275) Roberts & Meegan (2014); (276) Roberts & Stanbro (2014); (277) Zhang (2014d); (278) Lipunov et al. (2016); (279) Pelassa (2014c); (280) Baumgartner et al. (2014c); (281) Stanbro (2014a); (282) Burns (2014b); (283) Barthelmy et al. (2014d); (284) Ukwatta et al. (2014d); (285) Cummings et al. (2014e); (286) Jenke & Yu (2014); (287) Stamatikos et al. (2014d); (288) Zhang (2014e); (289) Narayana Bhat et al. (2016); (290) Burns (2014c); (291) Sakamoto et al. (2014d); (292) Littlejohns et al. (2015); (293) Zhang (2014f); (294) Zhang (2014g); (295) Pescalli et al. (2016); (296) Cummings et al. (2014f); (297) Stamatikos et al. (2014e); (298) Younes et al. (2014b); (299) von Kienlin (2014c); (300) Younes & Meegan (2014); (301) Connaughton et al. (2014); (302) Palmer et al. (2014d); (303) Barthelmy et al. (2014e); (304) Markwardt et al. (2014d); (305) Golenetskii et al. (2014c); (306) Stanbro (2014b); (307) Krimm et al. (2014d); (308) Li et al. (2016); (309) Cano et al. (2015); (310) Cummings et al. (2014g); (311) Golenetskii et al. (2014d); (312) Cummings et al. (2014h); (313) Stanbro (2014c); (314) Golenetskii et al. (2014e); (315) Stanbro & Troja (2014); (316) Ukwatta et al. (2014e); (317) Stamatikos et al. (2014f); (318) Stamatikos et al. (2014g); (319) Melandri et al. (2015); (320) Palmer et al. (2014e); (321) Krühler et al. (2015); (322) Yu (2014b); (323) Yu (2014c); (324) Kopač et al. (2015); (325) Younes (2014a); (326) Krimm et al. (2014e); (327) Jenke (2014e); (328) Cummings (2014b); (329) Barthelmy et al. (2014f); (330) Ukwatta et al. (2014f); (331) Jenke & Fitzpatrick (2014); (332) Yu (2014d); (333) Cummings (2014c); (334) Stamatikos et al. (2014h); (335) Pelassa et al. (2014); (336) von Kienlin & Younes (2014); (337) Yu & von Kienlin (2014); (338) Golenetskii et al. (2014f); (339) Younes et al. (2014a); (340) Markwardt et al. (2014e); (341) Stanbro (2014d); (342) Stanbro (2014e); (343) Krimm et al. (2014f); (344) Golenetskii et al. (2014g); (345) Fitzpatrick & Stanbro (2014); (346) Cummings et al. (2014i); (347) Barthelmy et al. (2014g); (348) Ukwatta et al. (2014g); (349) Zhang (2014h); (350) Barthelmy et al. (2014h); (351) Stamatikos et al. (2014i); (352) Cummings et al. (2014j); (353) von Kienlin (2014d); (354) von Kienlin (2014e); (355) Palmer et al. (2014f); (356) Markwardt et al. (2014f); (357) Xiong (2014a); (358) Krimm et al. (2014g); (359) Greiner et al. (2015); (360) von Kienlin & Connaughton (2014); (361) Younes (2014b); (362) Xiong et al. (2014); (363) Xiong (2014b); (364) Baumgartner et al. (2014e); (365) von Kienlin & Bhat (2014); (366) Racusin et al. (2016); (367) Barthelmy et al. (2013a); (368) Stamatikos et al. (2013a); (369) Pelassa (2013a); (370) Golenetskii et al. (2014h); (371) von Kienlin & Meegan (2013a); (372) Sakamoto et al. (2013a); (373) Collazzi (2013a); (374) Yu (2013a); (375) von Kienlin (2013a); (376) Markwardt et al. (2013a); (377) Pelassa & Meegan (2013); (378) Golenetskii et al. (2013a); (379) Lien et al. (2013a); (380) Collazzi (2013b); (381) Krimm et al. (2013a); (382) Barthelmy et al. (2013b); (383) Fitzpatrick & Bhat (2013); (384) Barthelmy et al. (2013c); (385) Urata et al. (2015); (386) von Kienlin & Jenke (2013); (387) von Kienlin (2013b); (388) Zhang (2013a); (389) Barthelmy et al. (2013d); (390) Zhang (2013b); (391) Ukwatta et al. (2013a); (392) Fitzpatrick & Xiong (2013); (393) Jenke (2013a); (394) Xiong (2013a); (395) Golkhou & Butler (2014); (396) Sato et al. (2013); (397) von Kienlin & Meegan (2013b); (398) Cummings et al. (2013); (399) Palmer et al. (2013a); (400) Greiner et al. (2014); (401) Lien et al. (2013b); (402) Zhang et al. (2013a); (403) Xiong & Meegan (2013); (404) Baumgartner et al. (2013); (405) Cano et al. (2014); (406) Zhang et al. (2016a); (407) Beskin et al. (2015); (408) Collazzi (2013c); (409) Ukwatta et al. (2013b); (410) Golenetskii et al. (2013b); (411) Stamatikos et al. (2013b);

(412) Fitzpatrick & Younes (2013); (413) Golenetskii et al. (2013c); (414) Palmer et al. (2013b); (415) Markwardt et al. (2013c); (416) Lien et al. (2013c); (417) Yu et al. (2013); (418) Goldstein (2013a); (419) Barthelmy et al. (2013e); (420) Ukwatta et al. (2013c); (421) Golenetskii et al. (2013d); (422) Stamatikos et al. (2013c); (423) Foley & Meegan (2013); (424) Collazzi (2013d); (425) Fitzpatrick (2013); (426) Wang & Dai (2014); (427) Pelassa (2013b); (428) Contopoulos et al. (2014); (429) Stamatikos et al. (2013d); (430) Byrne (2013); (431) Sakamoto et al. (2013b); (432) Palmer et al. (2013c); (433) Byrne et al. (2013); (434) Barthelmy et al. (2013f); (435) Xiong (2013b); (436) Wang et al. (2016); (437) Golenetskii et al. (2013e); (438) Fitzpatrick & Burgess (2013); (439) Krimm et al. (2013b); (440) Yu et al. (2015c); (441) Yu (2013b); (442) Yu et al. (2015a); (443) Golenetskii et al. (2013f); (444) Collazzi (2013e); (445) Berger (2014); (446) Barthelmy et al. (2013g); (447) Krimm et al. (2013c); (448) Jeong et al. (2014); (449) Golenetskii et al. (2013g); (450) Barthelmy et al. (2013h); (451) Krimm & Cummings (2013); (452) Jenke (2013b); (453) Cummings & Krimm (2013); (454) Ukwatta et al. (2013d); (455) Sakamoto et al. (2013c); (456) Burgess et al. (2013); (457) von Kienlin (2013c); (458) Palmer et al. (2013d); (459) von Kienlin & Younes (2013); (460) Goldstein et al. (2016); (461) Song et al. (2016); (462) Gao et al. (2015b); (463) Japelj et al. (2014); (464) Niino et al. (2016); (465) von Kienlin (2013d); (466) Rau (2013); (467) Zhang et al. (2015a); (468) Krimm et al. (2013d); (469) Wei et al. (2014); (470) Serino et al. (2014); (471) Chaplin & Fitzpatrick (2013); (472) Barthelmy et al. (2013i); (473) Tierney (2013); (474) Golenetskii et al. (2013h); (475) Barthelmy et al. (2013j); (476) Barthelmy et al. (2013k); (477) D'Avanzo et al. (2014); (478) Norris et al. (2013); (479) Xiong & Chaplin (2013); (480) Pelassa (2013c); (481) Golenetskii et al. (2013i); (482) Yu & Xiong (2013); (483) Chaplin (2013a); (484) Chaplin (2013b); (485) Ukwatta et al. (2013e); (486) Goldstein (2013b); (487) Palmer et al. (2013e); (488) Pelassa (2013d); (489) Barthelmy et al. (2013l); (490) Golenetskii et al. (2013j); (491) Markwardt et al. (2013b); (492) Lü & Zhang (2014); (493) Baumgartner et al. (2012e); (494) Golenetskii et al. (2012w); (495) Liang et al. (2015); (496) Baumgartner et al. (2012e); (497) Heussaff et al. (2013); (498) Tierney (2012); (499) Golenetskii et al. (2012x); (500) Golenetskii et al. (2012y); (501) Golenetskii et al. (2012z); (502) Baumgartner et al. (2012f); (503) Baumgartner et al. (2012g); (504) Goldstein & Meegan (2012); (505) Kaneko et al. (2015); (506) Sakamoto et al. (2012a); (507) Ukwatta et al. (2012b); (508) Barthelmy et al. (2012l); (509) Pelassa (2012b); (510) Xiong et al. (2012); (511) Sakamoto et al. (2012d); (512) Palmer et al. (2012e); (513) Markwardt et al. (2012c); (514) Golenetskii et al. (2012aa); (515) Golenetskii et al. (2012f); (516) Barthelmy et al. (2012a); (517) Golenetskii et al. (2012b); (518) Pelassa (2012c); (519) Pelassa & Connaughton (2012); (520) Golenetskii et al. (2012d); (521) Gruber (2012b); (522) McGlynn (2012); (523) Golenetskii et al. (2012s); (524) Sakamoto et al. (2012b); (525) Golenetskii et al. (2012t); (526) Palmer et al. (2012d); (527) Xu et al. (2013); (528) Golenetskii et al. (2012v); (529) Barthelmy et al. (2012e); (530) Golenetskii et al. (2012u); (531) Barthelmy et al. (2012f); (532) Cummings et al. (2012a); (533) Barthelmy et al. (2012g); (534) Baumgartner et al. (2012d); (535) Barthelmy et al. (2012c); (536) Ukwatta et al. (2012c); (537) Golenetskii et al. (2012r); (538) Markwardt et al. (2012d); (539) Dereli et al. (2015); (540) Cummings et al. (2012b); (541) Baumgartner et al. (2012c); (542) von Kienlin et al. (2014); (543) Ukwatta et al. (2012d); (544) Golenetskii et al. (2012q); (545) Golenetskii et al. (2012p); (546) Barthelmy et al. (2012h); (547) Sakamoto et al. (2012e); (548) Golenetskii et al. (2012o); (549) Palmer et al. (2012c); (550) Golenetskii et al. (2012n); (551) Golenetskii et al. (2012ac); (552) Golenetskii et al. (2012m); (553) Markwardt et al. (2012b); (554) Gruber (2012a); (555) Cummings et al. (2012c); (556) Golenetskii et al. (2012l); (557) Baumgartner et al. (2012b); (558) Golenetskii et al. (2012ab); (559) Golenetskii et al. (2012k); (560) Golenetskii et al. (2012j); (561) Laskar et al. (2015); (562) Younes (2012); (563) Sakamoto et al. (2012c); (564) Collazzi (2012); (565) Palmer et al. (2012b); (566) Golenetskii et al. (2012i); (567) Markwardt et al. (2012a); (568) D'Elia et al. (2014); (569) Golenetskii et al. (2012h); (570) Golenetskii et al. (2012g); (571) Golenetskii et al. (2012e); (572) Barthelmy et al. (2012b); (573) Ukwatta et al. (2012a); (574) Stamatikos et al. (2012); (575) Palmer et al. (2012a); (576) Norris & Barthelmy (2012); (577) Pelassa (2012a); (578) Markwardt et al. (2012e); (579) Golenetskii et al. (2012c); (580) Barthelmy et al. (2012i); (581) Cummings et al. (2012d); (582) Barthelmy et al. (2012n); (583) Barthelmy et al. (2012j); (584) Baumgartner et al. (2012a); (585) Rau (2012); (586) Ukwatta et al. (2012e); (587) Bošnjak et al. (2014); (588) Barthelmy et al. (2012k); (589) Perley et al. (2016b); (590) Golenetskii et al. (2012a); (591) Barthelmy et al. (2012m); (592) Rau & Meegan (2012); (593) Golenetskii et al. (2011i); (594) Barthelmy et al. (2011e); (595) Wei et al. (2016); (596) Ukwatta et al. (2011d); (597) Stamatikos et al. (2011b); (598) Gao et al. (2016); (599) Kann et al. (2019); (600) Stratta et al. (2013); (601) Golenetskii et al. (2011h); (602) Markwardt et al. (2011a); (603) Barthelmy et al. (2011f); (604) Cummings et al. (2011b); (605) Margutti et al. (2012); (606) Baumgartner et al. (2011c); (607) Golenetskii et al. (2011g); (608) Tierney (2011); (609) Palmer et al. (2011c); (610) Barthelmy et al. (2011g); (611) Markwardt et al. (2011b); (612) Krimm et al. (2011b); (613) Sakamoto et al. (2011b); (614) Sakamoto et al. (2011e); (615) Cummings et al. (2011c); (616) Golenetskii et al. (2011f); (617) Barthelmy et al. (2011d); (618) Sparre et al. (2014); (619) Michałowski et al. (2015); (620) Greiner et al. (2016); (621) Barthelmy et al. (2011h); (622) Fitzpatrick (2011); (623) Frederiks et al. (2013); (624) Sakamoto et al. (2011c); (625) Golenetskii et al. (2011e); (626) Palmer et al. (2011b); (627) Golenetskii et al. (2011d); (628) Golenetskii et al. (2011c); (629) Tsutsui & Shigeyama (2013); (630) Ackermann et al. (2013); (631) Cummings et al. (2011d); (632) Baumgartner et al. (2011d); (633) Xiong (2011); (634) Baumgartner et al. (2011b); (635) Barthelmy et al. (2011i); (636) Ukwatta et al. (2011c); (637) Stamatikos et al. (2011a); (638) Golenetskii et al. (2011b); (639) Nava et al. (2012); (640) Melandri et al. (2012); (641) Allison et al. (2017); (642) Lin (2011); (643) Golenetskii et al. (2011j); (644) Cummings et al. (2011a); (645) Virgili et al. (2012); (646) Barthelmy et al. (2011c); (647) Ukwatta et al. (2011b); (648) Golenetskii et al. (2011a); (649) Palmer et al. (2011a); (650) Barthelmy et al. (2011b); (651) Markwardt et al. (2011c); (652) Krimm et al. (2011a); (653) Barthelmy et al. (2011j); (654) Cummings et al. (2011e); (655) Barthelmy et al. (2011a); (656) Baumgartner et al. (2011a); (657) Ukwatta et al. (2012f); (658) Ukwatta et al. (2011a); (659) Stamatikos et al. (2011c); (660) Sakamoto et al. (2011d); (661) von Kienlin (2011); (662) Cucchiara et al. (2011); (663) Chandra & Frail (2012); (664) Barthelmy et al. (2011k); (665) Cummings & Barthelmy (2011); (666) Stamatikos et al. (2011d); (667) Fermi Large Area Telescope Team et al. (2012); (668) Balázs et al. (2015); (669) Liu et al. (2016); (670) Kopač et al. (2012); (671) Tunnicliffe et al. (2014); (672) Foley (2010); (673) Frederiks (2010); (674) Baumgartner et al. (2010a); (675) Golenetskii et al. (2010c); (676) Barthelmy et al. (2010a); (677) Golenetskii et al. (2010b); (678) Gorbovskoy et al. (2012); (679) Sakamoto et al. (2010b); (680) Golenetskii et al. (2010a); (681) Krimm et al. (2010a); (682) Cummings et al. (2010b); (683) Baumgartner et al. (2010b); (684) Barthelmy et al. (2010b); (685) Ukwatta et al. (2010a); (686) Stamatikos et al. (2010a); (687) Sakamoto et al. (2010c); (688) Ghirlanda et al. (2012); (689) Barniol Duran (2014); (690) Geng et al. (2016); (691) Cummings et al. (2010a); (692) Barthelmy et al. (2010c); (693) von Kienlin (2010); (694) Sakamoto et al. (2010a); (695) Palmer et al. (2010a); (696) Ahlgren et al. (2015); (697) Markwardt et al. (2010); (698) Piranomonte et al. (2015); (699) Krimm et al. (2010b); (700) Barthelmy et al. (2010e); (701) Japelj et al. (2016); (702) Volnova et al. (2014); (703) Krühler et al. (2011); (704) Arcodia et al. (2016); (705) Cummings et al. (2010c); (706) Baumgartner et al. (2010c); (707) Afonso et al. (2010); (708) Stamatikos et al. (2010b); (709) Ripa (2011); (710) Cummings et al. (2010d); (711) Zhang et al. (2011); (712) Nava et al. (2011); (713) Levesque et al. (2010c); (714) Palmer et al. (2010b); (715) Greiner et al. (2011); (716) Baumgartner et al. (2010d); (717) Barthelmy et al. (2010d); (718) Sakamoto et al. (2010d); (719) Palmer et al. (2010c); (720) Yonetoku et al. (2010); (721) Sakamoto et al. (2011a); (722) Filgas et al. (2011); (723) Sakamoto et al. (2009); (724) Nemmen et al. (2012); (725) Lu et al. (2012b); (726) Wang et al. (2013); (727) Galli et al. (2013); (728) Robertson & Ellis (2012); (729) Guetta et al. (2011); (730) Butler et al. (2010); (731) Kopač et al. (2013); (732) Minaev et al. (2014); (733) Liang et al. (2009); (734) Qin & Chen (2013); (735) Zhang et al. (2009); (736) Krimm et al. (2009); (737) Perley et al. (2013); (738) Lü et al. (2012); (739) Lien et al. (2016a); (740) Dichiara et al. (2013b); (741) Nardini et al. (2011); (742) Li et al. (2012b); (743) Golkhou et al. (2015); (744) Vianello et al. (2009); (745) Kann et al. (2010); (746) Huja et al. (2009); (747) Thoene et al. (2008); (748) Bhat et al. (2012); (749) Xiao & Schaefer (2011); (750) Schady et al. (2011); (751) Krühler et al. (2009); (752) Ukwatta et al. (2010b); (753) Řípa et al. (2009); (754) Nava et al. (2008); (755) Perley et al. (2009); (756) Nardini et al. (2010); (757) Zheng et al. (2009); (758) Cenko et al. (2009); (759) Minaev et al. (2010); (760) Rossi et al. (2008); (761) Hjorth et al. (2012);

(762) Gehrels et al. (2008); (763) Nysewander et al. (2009); (764) Foley et al. (2008); (765) Xiao & Schaefer (2009b); (766) Graham & Fruchter (2013); (767) Kasliwal et al. (2008); (768) Schady et al. (2010); (769) Butler et al. (2007); (770) Perley et al. (2015); (771) Contini (2016); (772) Ghisellini et al. (2009); (773) Covino & Gotz (2016); (774) Gao & Dai (2010); (775) Savaglio et al. (2009); (776) Bellm et al. (2008); (777) Rizzuto et al. (2007); (778) Campisi & Li (2008); (779) Mosquera Cuesta et al. (2008); (780) Willingale et al. (2007b); (781) Schaefer (2007); (782) Rykoff et al. (2009); (783) Melandri et al. (2008); (784) Fong et al. (2010b); (785) De Laurentis et al. (2015); (786) Golenetskii et al. (2017); (787) Pélangeon et al. (2008); (788) Leibler & Berger (2010); (789) Collazzi & Schaefer (2008); (790) Xiao & Schaefer (2009a); (791) Levesque et al. (2010b); (792) Mannucci et al. (2011); (793) Tsutsui et al. (2013a); (794) Zaninoni et al. (2013); (795) Ghirlanda et al. (2007); (796) Guidorzi et al. (2016); (797) Tanvir et al. (2005); (798) Li et al. (2015); (799) Sakamoto et al. (2008); (800) Rau et al. (2005); (801) Guidorzi et al. (2005); (802) Friedman & Bloom (2005); (803) Sako et al. (2005); (804) Sakamoto et al. (2005); (805) Li et al. (2008); (806) Mazets et al. (2002); (807) Barraud et al. (2003); (808) Frontera (2004); (809) Frontera et al. (2009); (810) de Pasquale et al. (2006); (811) Guidorzi et al. (2011); (812) Atteia (2003); (813) Christensen et al. (2004); (814) https://gamma-ray.nsstc.nasa.gov/batse/grb/catalog/current/index.html; (815) Shahmoradi & Nemiroff (2010); (816) Goldstein et al. (2013); (817) Ashcraft & Schaefer (2007); (818) Ghirlanda et al. (2009); (819) Bloom et al. (2002); (820) Jimenez et al. (2001); (821) Kaneko et al. (2006); (822) Ramirez-Ruiz et al. (2002); (823) Smith et al. (2002); (824) Reichart et al. (2001); (825) Frail et al. (2001); (826) Schaefer (2003b); (827) Sokolov et al. (2001); (828) Simić & C. Popović (2012); (829) Fenimore & Ramirez-Ruiz (2000); (830) Svensson et al. (2010); (831) Bosnjak et al. (2006); (832) Postnov (2000); (833) Bloom et al. (2001); (834) Berger et al. (2003); (835) Fragile et al. (2004); (836) Amati et al. (2008); (837) Wei (2010); (838) Paciesas et al. (1999); (839) Lloyd-Ronning & Ramirez-Ruiz (2002); (840) Peng et al. (2012); (841) Preece et al. (2000); (842) Meegan et al. (1996); (843) Sazonov et al. (1998); (844) Hakkila et al. (2007); (845) Fishman et al. (1994); (846) Terekhov et al. (1994).

(This table is available in its entirety in machine-readable form.)

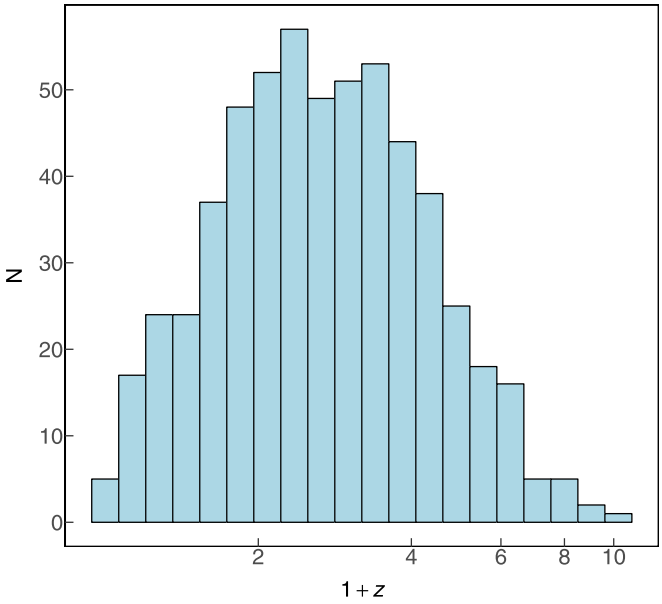

Figure 1. Histograms for $1+z$ as an example. The description of each parameter is given in Section 2.

(The complete figure set (58 images) is available.)

the basic information are available for every GRB. When we did not find the information, we left the place empty.

The prompt emission properties include z (redshift), $D_{\rm L}$ (luminosity distance, 10^{28} cm), T_{90}, T_{50}, $T_{\rm R45}$ (defined in Reichart et al. 2001), variability$_1$ (variability based on the Fenimore & Ramirez-Ruiz 2000 definition), variability$_2$ (variability based on the Reichart et al. 2001 definition), variability$_3$ (variability based on the Schaefer 2007 definition), $F_{\rm g}$ (fluence in the 20–2000 keV energy band, in units of 10^{-6} erg cm^{-2}), HR (hardness ratio between 100–2000 keV and 20–100 keV), $E_{\rm iso}$ (isotropic γ-ray energy in the rest-frame 1–10^4 keV energy band, in units of 10^{52} erg), $L_{\rm pk}$ (peak luminosity in the 1 s time bin in the rest-frame 1–10^4 keV energy band, in units of 10^{52} erg s^{-1}), $F_{\rm pk1}$ (peak energy flux in the 1 s time bin in the rest-frame 1–10^4 keV energy band, in units of 10^{-6} erg cm^{-2} s^{-1}), $F_{\rm pk2}$ (peak energy flux in the 64 ms time bin in the rest-frame 1–10^4 keV energy band, in units of 10^{-6} erg cm^{-2} s^{-1}), $F_{\rm pk3}$ (peak energy flux in the 256 ms time bin in the rest-frame 1–10^4 keV energy band, in units of 10^{-6} erg cm^{-2} s^{-1}), $F_{\rm pk4}$ (peak energy flux in the 1024 ms time bin in the rest-frame 1–10^4 keV energy band, in units of 10^{-6} erg cm^{-2} s^{-1}), $P_{\rm pk1}$ (peak photon flux in the 64 ms time bin in 10–1000 keV, in units of photons cm^{-2} s^{-1}), $P_{\rm pk2}$ (peak photon flux in the 256 ms time bin in 10–1000 keV, in units of photons cm^{-2} s^{-1}), $P_{\rm pk3}$ (peak photon flux in the 1024 ms time bin in 10–1000 keV, in units of photons cm^{-2} s^{-1}), $P_{\rm pk4}$ (peak photon flux in the 1 s time bin in 10–1000 keV, in units of photons cm^{-2} s^{-1}), $\alpha_{\rm Band}$ (low-energy spectral index of the Band model), $\beta_{\rm Band}$ (high-energy spectral index of the Band model), $E_{\rm p,Band}$ (spectral peak energy of the Band model, keV), $\alpha_{\rm cpl}$ (low-energy spectral index of the cutoff power-law (CPL) model), $E_{\rm p,cpl}$ (spectral peak energy of the CPL model, in units of keV), $\alpha_{\rm spl}$ (spectral index of simple power-law (SPL) model), $\theta_{\rm j}$ (jet-opening angle, in units of rad), spectral time lag (in units of ms MeV^{-1}), and Γ_0 (initial Lorentz factor). $P_{\rm pk}$ and $F_{\rm pk}$ have four time bins: 64 ms, 256 ms, 1024 ms, and 1 s. We use them as different parameters, because the data are from different instruments and different instruments have different energy bands and different sensitivities. In order to avoid the influence of the different energy bands, we corrected $P_{\rm pk}$ into the observer frame in the 10–1000 keV energy band and $F_{\rm pk}$ into the rest-frame 1–10^4 keV energy band using the method of Schaefer (2007) of four time bins. At the same time, using the same method, we changed all of the $F_{\rm g}$ into 20–2000 keV, HR into 100–2000/20–100 keV, $E_{\rm iso}$ into the rest-frame 1–10^4 keV energy band, and $L_{\rm pk}$ into the rest-frame 1–10^4 keV energy band. Further, we calculated a small part of $E_{\rm iso}$ also using the method of Schaefer (2007) with $F_{\rm g}$ and z. We provide different flags for different data calculations and corrections.

The afterglow properties include log $t_{\rm burst}$ (central engine active duration in logarithm, in units of s; defined in Zhang et al. 2014a), $t_{\rm pkX}$ (peak time in the X-ray LC, in units of s), $t_{\rm pkOpt}$ (peak time in the optical LC, s), $F_{\rm X11hr}$ (flux density in the X-ray band 11 hr after the trigger time, in units of Jy), $\beta_{\rm X11hr}$ (index in the X-ray band 11 hr after the trigger time), $F_{\rm Opt11hr}$ (flux density in the optical band 11 hr after the trigger time, Jy), $t_{\rm radio,pk}$ (peak time in the radio band, in units of s), and $F_{\rm radio,pk}$ (peak flux density in the radio band at 8.46 GHz, in units of Jy).

The host galaxy properties include the host galaxy offset (the distance from the GRB location to the center of its host galaxy, in units of kpc), metallicity (12 + log [O/H]), Mag (absolute magnitude in the AB system at the rest 3.6 μm wavelength), $N_{\rm H}$ (column density of hydrogen, in units of 10^{21} cm^{-2}), $A_{\rm V}$ (dust extinction), SFR (star formation rate, in units of $M_\odot$ yr^{-1}), log SSFR (specific star formation rate in logarithm, in units of Gyr^{-1}), Age (in units of Myr), and log Mass (stellar mass in

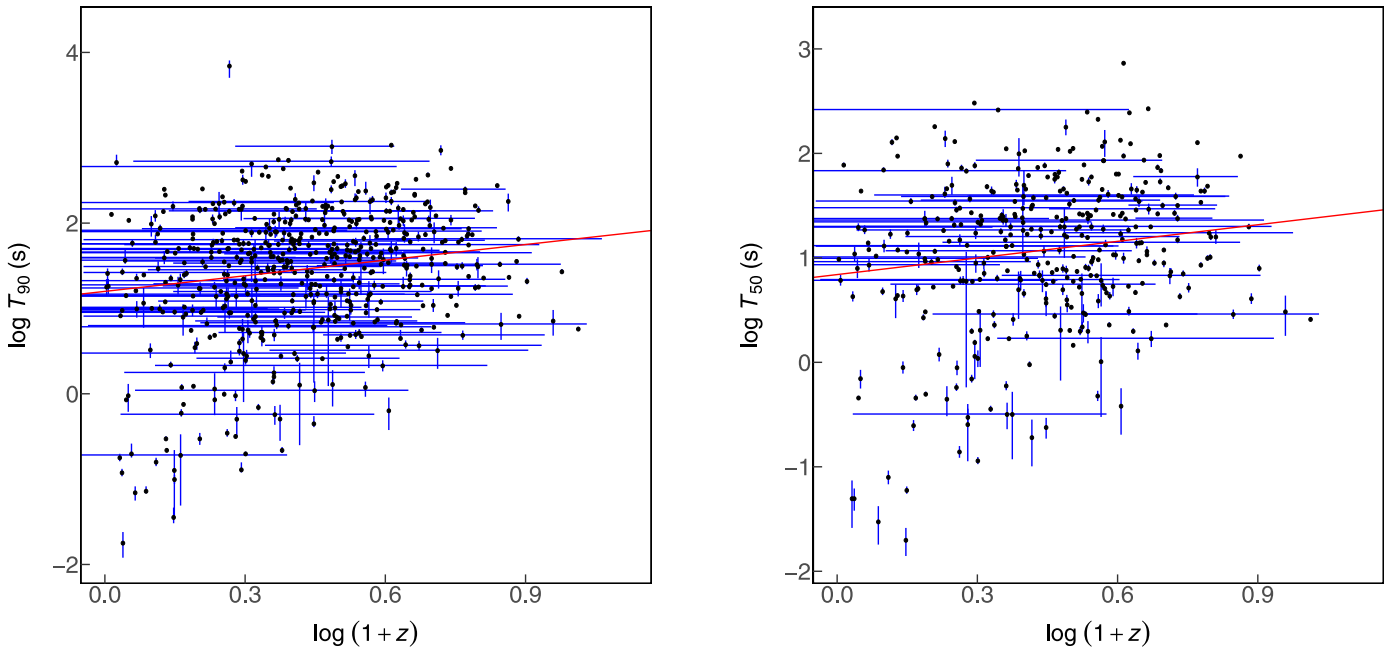

Figure 2. Scatter plots for two arbitrary parameters. The description of every parameter is defined in Section 2.
(The complete figure set (1475 images) is available.)

logarithm, in units of $M_{\odot}$). For metallicity, we converted different metallicity calibrations into the Kobulnicky & Kewley (2004) calibrator using the method given in Kewley & Ellison (2008).

We also changed 10 parameters from the observer frame to rest frame, including T_{90}, T_{50}, $T_{\rm R45}$, $E_{\rm p,Band}$, $E_{\rm p,cpl}$, spectral time lag, $\log t_{\rm burst}$, $t_{\rm pkX}$, $t_{\rm pkOpt}$, and $t_{\rm radio,pk}$. We use the label "i" to denote the parameters in the rest frame. We put the 10 rest-frame parameters as new parameters joining the statistics. However, we did not show the results for the same parameter, just in different frames, such as T_{90} and $T_{90,\rm i}$. In the table, we also did not include the 10 rest-frame parameters as they are easily obtained. When we collected the data from the literature, some data have different units for the same parameter. We convert them into the same units. For example, the units for $D_{\rm L}$ (luminosity distance) include 10^{28} cm, kpc, and others. In order to easily convert to erg for the $E_{\rm iso}$ calculation, we choose the unit 10^{28} cm for $D_{\rm L}$. The units of the parameters are all given in Table 1.

All of the information given above on the 6289 GRBs are collected in a machine-readable table. We put the first five samples in Table 1 as examples. In the machine-readable table, every GRB has the basic information and 46 parameter values. If the basic information is not available, we left it blank. If a parameter value is not available, we use "..." to denote this. For every available parameter value, we also put the relevant reference or flag (or both). For different situations, we use different flags. We introduce every flag one by one in the following. "a" means the errors are imputed by the MICE algorithm. The details of the error imputation are shown in Section 3. "b" means the errors in the original papers were in the 90% confidence level, and we convert the errors to the 1σ confidence level by multiplying by 0.995/1.645. "c" means the values are calculated using the spectral values in order to change the energy band to a uniform band, because for some parameters, the energy band is different for different instruments. In order to avoid the influence of different energy bands, we use the spectral values to correct the energy band of the four time bins of $P_{\rm pk}$ and $F_{\rm pk}$, $F_{\rm g}$, HR, $E_{\rm iso}$, and $L_{\rm pk}$. "d" means the units are different from the original papers. For example, the unit for $D_{\rm L}$ in Cano et al. (2014) is Mpc; we change it to 10^{28} cm. "e" means the error is estimated as the central value multiplied by 0.1. One can see Section 3 for more details. When it comes to spectral values, sometimes the spectral index cannot be constrained very well. We denote the BASTE α peak value -1.1, as is common, with flag "f," and the BASTE β peak value -2.2, as is common, with flag "g." Some values are in the rest frame; we change the values from the rest frame to the observer frame and denote these with flag "h." "i" means the values are converted into logarithm or from logarithm into the normal form. "j" means the values are calculated using other parameters. For example, almost half of the HRs are calculated from $F_{\rm g}$ and spectral values. "k" means we converted different metallicity calibrations into the Kobulnicky & Kewley (2004) calibrator using the method in Kewley & Ellison (2008). We found that the metallicity is different with different calibrators, so this step is necessary. "m" means the $D_{\rm L}$ is calculated using z with the cosmology parameters in Planck Collaboration et al. (2016). There is also a description in Table 1.

The data are from different works in the literature, the GCN, websites,[5] and calculations if it is not directly available and can be derived. The principle of data collection is as follows. We collect as many variables as possible. We only take certain values, which are mainly taken from the literature manually. Every data should be able to bedirected back to the original reference. The data should include error bars in 1σ. If the error is in another confidence, we convert the error into 1σ. If it is not available, we use the imputation method, which is shown in Section 3. For those data are shown in different literature, we choose the values in the following order (highest to lowerst priority): first, published papers (catalogs, data gatherings,

[5] Such as http://www.mpe.mpg.de/~jcg/grbgen.html.

other articles); second, GCNs; third, other websites; fourth, self-calculation if they can be obtained. For those data shown in ordinary published papers, the paper from the official team is in higher priority. Otherwise, the newer paper is of higher priority.

We excluded Fermi GRBs 120222A, 110920A, 110517A, and 101214A, because they have the same GRB names but two different trigger numbers (Narayana Bhat et al. 2016). This might be a mistake in the GRB names. For GRB 091024A, it triggered *Fermi*/GBM twice and triggered *Swift* once (Ukwatta et al. 2012f; Narayana Bhat et al. 2016). We set it as one GRB for the analysis. During the statistical study, we deleted some values with central values smaller than the error bars (which means the values on the lower side are not physical), because for some parameters, such as T_{90}, the lower limit must be greater than 0. If the central value is smaller than the error bar for T_{90}, the lower limit is smaller than 0. For example, in von Kienlin et al. (2014), the T_{90} of GRB 080719A is 16.128 ± 17.887 s; therefore, we did not include this. Note that we still put this kind of data in the table; we just did not include them in the statistics.

For the spectral parameters, the spectra are mainly fitted by three models: the Band model, CPL model, and SPL model (Li et al. 2016). The Band model is a smoothly joint broken power law with the definition (Band et al. 1993)

$$N(E) = \begin{cases} A\left(\frac{E}{100\ \mathrm{keV}}\right)^{\alpha} e^{-\frac{E}{E_0}}, & E < (\alpha - \beta)E_0, \\ A\left(\frac{E}{100\ \mathrm{keV}}\right)^{\beta}\left[\frac{(\alpha-\beta)E_0}{100\ \mathrm{keV}}\right]^{\alpha-\beta} e^{\beta-\alpha}, & E \geqslant (\alpha - \beta)E_0, \end{cases} \quad (1)$$

where α is the low-energy photon index, β is the high-energy photon index, A is the coefficient for normalization, E is the energy of the photons, and E_0 is the break energy. We mostly used E_p instead of E_0. E_p is the peak energy in the spectrum E^2N, $E_p = (2 + \alpha)E_0$. In the big table, we use α_{Band}, β_{Band} and $E_{p,\mathrm{Band}}$ as Band function spectral parameters, and α_{cpl} and $E_{p,\mathrm{cpl}}$ to mark CPL model spectrum parameters. The formula for the SPL model is $N(E) = AE^{\alpha_{\mathrm{spl}}}$.

Most of the data are taken from the following: (1) *Swift* lookup website,[6] with the number of selected data 1003; (2) "How long does a burst burst?" (Zhang et al. 2014a), with the number of selected data 354; (3) "Cosmic evolution of long GRB luminosity" (Deng et al. 2016), with the number of selected data 177; (4) "Effect of GRB spectra on the empirical luminosity correlations and the GRB Hubble diagram" (Lin et al. 2016), with the number of selected data 219; (5) "On the classification of GRBs and their occurrence rates" (Ruffini et al. 2016), with the number of selected data 571; (6) "The third *Fermi* GBM GRB catalog: the first six years" (Narayana Bhat et al. 2016), with the number of selected data 3702; (7) "A comparative study of long and short GRBs. I. Overlapping properties" (Li et al. 2016), with the number of selected data 786; (8) "GRB hosts through cosmic time. Very Large Telescope/X-Shooter emission-line spectroscopy of 96 γ-ray-burst-selected galaxies at $0.1 < z < 3.6$" (Krühler et al. 2015), with the number of selected data 107; (9) "Uncovering the intrinsic variability of GRBs" (Golkhou & Butler 2014), with the number of selected data 323; (10) "The E_{peak}–E_{iso} relation revisited with *Fermi* GRBs. Resolving a long-standing debate" (Heussaff et al. 2013), with the number of selected data 671; (11) "The second *Fermi* GBM GRB catalog: The first four years" (von Kienlin et al. 2014), with the number of selected data 2019; (12) "The spectral catalog of *INTEGRAL* GRBs. Results of the joint IBIS/SPI spectral analysis" (Bošnjak et al. 2014), with the number of selected data 138; (13) "The *Swift* GRB host galaxy legacy survey. II. Rest-frame near-IR luminosity distribution and evidence for a near-solar metallicity threshold" (Perley et al. 2016b), with the number of selected data 132; (14) "The dark bursts population in a complete sample of bright *Swift* long GRBs" (Melandri et al. 2012), with the number of selected data 107; (15) "A radio-selected sample of GRB afterglows" (Chandra & Frail 2012), with the number of selected data 347; (16) "Statistical analysis of the observable data of GRBs" (Ripa 2011), with the number of selected data 260; (17) "Spectral properties of 438 GRBs detected by *Fermi*/GBM" (Nava et al. 2011), with the number of selected data 694; (18) "Possible origins of dispersion of the peak energy–brightness correlations of GRBs" (Yonetoku et al. 2010), with the number of selected data 254; (19) "The cosmic rate, luminosity function and intrinsic correlations of long GRBs" (Butler et al. 2010), with the number of selected data 874; (20) "The updated spectral catalog of *INTEGRAL* GRBs" (Vianello et al. 2009), with the number of selected data 121; (21) "Redshift catalog for *Swift* long GRBs" (Xiao & Schaefer 2011), with the number of selected data 415; (22) "Search for GRB classes with the *RHESSI* satellite" (Řípa et al. 2009), with the number of selected data 323; (23) "Statistical studies of optically dark GRBs in the *Swift* era" (Zheng et al. 2009), with the number of selected data 271; (24) "Correlations of prompt and afterglow emission in *Swift* long and short GRBs" (Gehrels et al. 2008), with the number of selected data 209; (25) "A complete catalog of *Swift* GRB spectra and durations: Demise of a physical origin for pre-*Swift* high-energy Correlations" (Butler et al. 2007), with the number of selected data 1069; (26) "Intrinsic properties of a complete sample of *HETE*-2 GRBs. A measure of the GRB rate in the local universe" (Pélangeon et al. 2008), with the number of selected data 272; (27) "Global characteristics of X-ray flashes and X-ray rich GRBs observed by *HETE*-2" (Sakamoto et al. 2005), with the number of selected data 101; (28) "Konus catalog of SGRBs" (Mazets et al. 2002), with the number of selected data 128; (29) "The GRB catalog obtained with the GRB monitor aboard *BeppoSAX*" (Frontera et al. 2009), with the number of selected data 1619; (30) "Spectral catalog of bright GRBs detected with the *BeppoSAX*/GRBM" (Guidorzi et al. 2011), with the number of selected data 248; (31) BASTE current GRB catalog,[7] with the number of selected data 8983; (32) "Hardness as a spectral peak estimator for GRBs" (Shahmoradi & Nemiroff 2010), with the number of selected data 2128; (33) "The BATSE 5B GRB spectral catalog" (Goldstein et al. 2013), with the number of selected data 4764; (34) "Are there any redshift >8 GRBs in the BATSE catalog?" (Ashcraft & Schaefer 2007), with the number of selected data 110; (35) "Short versus long GRBs: spectra, energetics and luminosities" (Ghirlanda et al. 2009), with the number of selected data 139; (36) "The fourth BATSE GRB catalog (Revised)" (Paciesas et al. 1999), with the number of selected data 1049; (37) "On the spectral energy dependence of GRB variability" (Lloyd-Ronning & Ramirez-Ruiz 2002), with the number of selected data 159; and (38) "The third BATSE GRB

[6] https://swift.gsfc.nasa.gov/archive/grb_table/index.php

[7] https://gamma-ray.nsstc.nasa.gov/batse/grb/catalog/current/index.html

catalog" (Meegan et al. 1996), with the number of selected data 1380. A full reference list is given following Table 1.

3. Error Imputation

In the table, there are many incomplete data. There are especially many data just having central values without error bars. However, when we perform the statistics, we need to consider the uncertainty for each data. Therefore, we used the R package mice, which treats incomplete multivariate data by multiple imputation (Rubin 1987, 1996) by chained equations (MICE). Multiple imputation is a method for dealing with the problems of incomplete data. In the big table, many parameters have missing errors. For the first step in generating multiple imputations, we used the predictive mean matching (Little 1988) method. It is a general purpose, semiparametric imputation method of numeric-scale type. We did five times iterations for every missing error, and we set a threshold 0.25 for imputation. This means that the error of each parameter should have at least 25% information. If there is not enough information, the imputation may not be reliable. Then, we use three indicators to assess the imputation results: relative increased variance (RIV), fraction of missing information (FMI), and relative efficiency (RE; Rubin 1987, 1996). One can see the results in Table 2. However, there are some parameters for which we cannot impute the missing errors. For these, we use the 10% of the absolute central value as the error bars (Schaefer 2007). The errors of $t_{\rm pkX}$, $F_{\rm Opt11hr}$, Mag, log SSFR, Age, and $t_{\rm pkX,i}$ used the 10% of the absolute central value as the error bars. We do not impute the errors of z and $D_{\rm L}$, as the errors are relatively very small.

1. Relative increase in variance due to missing data r_m (RIV). It is the ratio of the between-imputation variance to the within-imputation variance of the five data sets, multiplied by the imputation time m. It stands for the increase in variance fraction, because due to missing data, the influence of the missing data is bigger when r_m is bigger. When r_m is smaller, it indicates that the influence of the change of m is smaller, that is to say, that missing data have a smaller influence on the data parameters, the imputation results are more stable, and the imputations are better. r_m is defined as
$$r_m = \frac{(1+\frac{1}{m})\sigma_{\rm B}{}^2}{\sigma_{\rm W}{}^2}, \quad (2)$$
where $\sigma_{\rm W}{}^2 = \frac{1}{m}\sum_{i=1}^{m}\sigma_{\rm i}{}^2$ is the within-imputation variance, $\sigma_{\rm B}{}^2 = \frac{1}{m-1}\sum_{i=1}^{m}(\hat{\theta}_{\rm i}-\hat{\theta})^2$ is the between-imputation variance, and $\hat{\theta}_{\rm i}$ is the mean of every complete data set, $\hat{\theta} = \frac{1}{m}\sum_{i=1}^{m}\hat{\theta}_{\rm i}$. $\sigma_{\rm W}$ stands for the mean of the variance of m data sets, and $\sigma_{\rm B}$ stands for the variance of the mean of m data sets.
2. Fraction of missing information γ_m (FMI). It stands for the influence of the missing data on the parameters (e.g., mean). If FMI is smaller, the imputation results are more stable:
$$\gamma_m = \frac{r_m + \frac{2}{v_m+3}}{r_m+1}, \quad (3)$$
where $v_m = (m-1)(1+\frac{1}{r_m}{}^2)$ is the derees of freedom.
3. Relative efficiency (RE). RE is a comprehensive analysis of RIV and FMI. It stands for the imputation fraction of missing information by MICE. If RE is bigger, the results are better:
$$\mathrm{RE} = \left(1+\frac{\gamma_m}{m}\right)^{-1}. \quad (4)$$

To analyze the imputed data and pooling analysis results, we use the mean of every imputed error bar. Because we also need to calculate some values and plot scatter plots with error bars, we cannot use five values for one error bar—we must get the best estimate for every imputed error bar, so we use the mean.

The imputation results are shown in Table 2. From the results, we can see that RIV and FMI are very close to 0, which means the imputation is stable. RE is very close to 1, which means the imputation efficiency is very high. We imputed almost all of the missing information. Therefore, the imputation is reliable.

4. Statistical Methods

4.1. Distributions of Each Parameter

We plotted the histograms for every parameter in the observer frame and for some parameters in the rest frame. Two histograms are shown in Figure 1. We made a figure set containing all figures—a total of 58 figures. Readers can see all the figures in the figure set accompanying Figure 1.

4.2. Scatter Plots between Two Arbitrary Parameters

We plotted the scatter plots between two arbitrary parameters when there are more than five points. We find that, with this large sample, we can also retain the relationships previously found. We removed the spectral lag value of GRB 060218, because it is an outlier (Foley et al. 2008). The two results are shown in Figure 2. We also made a figure set containing all the scatter plots. There are a total of 1475 plots.

4.3. Correlation Coefficients

The correlation coefficient is to measure the correlation between two parameters. There are four methods:

1. Pearson correlation coefficient (Pearson 1895). Suppose the two variables are $x_{\rm t}$ and $y_{\rm t}$, then
$$\gamma = \frac{\sum_{t=1}^{N}(x_{\rm t}-\bar{x})(y_{\rm t}-\bar{y})}{\sqrt{\sum_{t=1}^{N}(x_{\rm t}-\bar{x})^2}\sqrt{\sum_{t=1}^{N}(y_{\rm t}-\bar{y})^2}}, \quad (5)$$
where $\bar{x}$ is the mean of variable x, and $\bar{y}$ is the mean of variable y. The Pearson correlation coefficient is based on a normal distribution, so when the data is normally distributed, the Pearson correlation coefficient works very well.
2. Spearman correlation coefficient (Spearman 1987). This coefficient does not depend on the data distribution. It is a kind of rank measure:
$$\rho = \frac{n(\sum_{t=1}^{N}x_{\rm t}y_{\rm t}) - (\sum_{t=1}^{N}x_{\rm t})(\sum_{t=1}^{N}y_{\rm t})}{\sqrt{n(\sum_{t=1}^{N}x_{\rm t}^2) - \left(\sum_{t=1}^{N}x_{\rm t}\right)^2}\sqrt{n(\sum_{t=1}^{N}y_{\rm t}^2) - \left(\sum_{t=1}^{N}y_{\rm t}\right)^2}}, \quad (6)$$
3. Kendall τ correlation coefficient (Kendall 1938). This coefficient compares the order of two variables; it does

Table 2
Imputation Results

Parameters	RIV	FMI	RE	Parameters	RIV	FMI	RE
T_{901}	0.00000358	0.00000358	1	T_{902}	0.000126	0.000126	1
T_{501}	0.000143	0.000143	1	T_{502}	0.0000796	0.0000796	1
T_{R451}	0.0122	0.0122	0.998	T_{R452}	0.00172	0.00172	1
variability$_{11}$	0.0137	0.0136	0.997	variability$_{12}$	0.00491	0.0049	0.999
F_{g1}	0.0000144	0.0000144	1	F_{g2}	0.000317	0.000317	1
HR1	0.000454	0.000454	1	HR2	0.000354	0.000354	1
$E_{\gamma,iso1}$	0.00588	0.00587	0.999	$E_{\gamma,iso2}$	0.00071	0.00071	1
F_{pk11}	0.000259	0.000259	1	F_{pk12}	0.000901	0.000901	1
F_{pk21}	0.000324	0.000324	1	F_{pk22}	0.000849	0.000849	1
P_{pk11}	0.000205	0.000205	1	P_{pk12}	0.000274	0.000274	1
$-\alpha_{Band1}$	0.000911	0.000911	1	$-\alpha_{Band2}$	0.000289	0.000289	1
$-\beta_{Band1}$	0.0017	0.0017	1	$-\beta_{Band2}$	0.000599	0.000599	1
$E_{p,Band1}$	0.00176	0.00176	1	$E_{p,Band2}$	0.000471	0.000471	1
$-\alpha_{cpl1}$	0.00186	0.00185	1	$-\alpha_{cpl2}$	0.000343	0.000343	1
$E_{p,cpl1}$	0.00018	0.00018	1	$E_{p,cpl2}$	0.000244	0.000244	1
θ_{j1}	0.00547	0.00546	0.999	θ_{j2}	0.00924	0.0092	0.998
Γ_{01}	0.111	0.105	0.979	Γ_{02}	0.0273	0.0269	0.995
t_{pkOpt1}	0.044	0.043	0.991	t_{pkOpt2}	0.0147	0.0146	0.997
F_{X11hr1}	0.0131	0.0131	0.997	F_{X11hr2}	0.0388	0.038	0.992
$t_{radio,pk1}$	0.0197	0.0195	0.996	$t_{radio,pk2}$	0.0211	0.0209	0.996
$F_{radio,pk1}$	0.111	0.104	0.98	$F_{radio,pk2}$	0.0227	0.0224	0.996
offset1	0.0161	0.016	0.997	offset2	0.0119	0.0118	0.998
metallicity1	0.0569	0.0552	0.989	metallicity2	0.013	0.0129	0.997
N_{H1}	0.0016	0.0016	1	N_{H2}	0.00767	0.00764	0.998
A_{V1}	0.00734	0.00731	0.999	A_{V2}	0.0319	0.0313	0.994
SFR1	0.0231	0.0228	0.995	SFR2	0.0331	0.0325	0.994
log Mass1	0.0157	0.0156	0.997	log Mass2	0.0082	0.00816	0.998
$T_{90,i1}$	0.00311	0.0031	0.999	$T_{90,i2}$	0.0000847	0.0000847	1
$T_{50,i1}$	0.00634	0.00632	0.999	$T_{50,i2}$	0.000355	0.000355	1
$T_{R45,i1}$	0.00296	0.00296	0.999	$T_{R45,i2}$	0.00202	0.00202	1
$E_{p,Band,i1}$	0.00547	0.00546	0.999	$E_{p,Band,i2}$	0.0104	0.0104	0.998
$E_{p,cpl,i1}$	0.0061	0.00608	0.999	$E_{p,cpl,i2}$	0.00463	0.00462	0.999
$t_{pkOpt,i1}$	0.0237	0.0234	0.995	$t_{pkOpt,i2}$	0.0196	0.0194	0.996
$t_{radio,pk,i1}$	0.0416	0.0407	0.992	$t_{radio,pk,i2}$	0.0183	0.0182	0.996

Note. See Section 3 for the definitions of RIV, FMI, and RE. The description of every parameter is in Section 2.

Table 3
Correlation Coefficient and Correlation Ratio Results

Parameters	$\log(1+z)$ versus $\log D_L$	$\log(1+z)$ versus $\log T_{90}$	$\log(1+z)$ versus $\log T_{50}$	$\log(1+z)$ versus $\log T_{R45}$	$\log(1+z)$ versus variability$_1$
Pearson coefficient	0.76 ± 0.042	0.21 ± 0.022	0.18 ± 0.028	0.3 ± 0.019	0.0019 ± 0.05
Pearson p-value	1.7×10^{-8}	8.9×10^{-7}	7.6×10^{-4}	9×10^{-9}	9.8×10^{-1}
Spearman coefficient	0.91 ± 0.012	0.2 ± 0.016	0.17 ± 0.015	0.24 ± 0.013	0.066 ± 0.059
Spearman p-value	4.8×10^{-213}	2.5×10^{-6}	1.5×10^{-3}	3.9×10^{-6}	4.1×10^{-1}
Kendall coefficient	0.83 ± 0.011	0.13 ± 0.011	0.11 ± 0.01	0.17 ± 0.0088	0.04 ± 0.04
Kendall p-value	3×10^{-194}	2.8×10^{-6}	1.2×10^{-3}	3.7×10^{-6}	4.5×10^{-1}
Correlation ratio	0.091 ± 0.0067	0.66 ± 0.0041	0.51 ± 0.006	0.29 ± 0.0039	0.71 ± 0.044
Cosine similarity	0.88 ± 0.014	0.8 ± 0.02	0.77 ± 0.019	0.75 ± 0.007	0.3 ± 0.067

Note. Correlation coefficients and correlation ratio between two different parameters. The definitions are given in Section 4.3. We considered all the errors using MC method (Zou et al. 2018). All errors are in the 1σ confidence level. All the results are in a machine-readable table. The description of every parameter is given in Section 2.

(This table is available in its entirety in machine-readable form.)

not compare the values. It is also a kind of rank measure:

$$\tau = \frac{n_c - n_d}{1/2n(n-1)}, \tag{7}$$

where n is the length of the two variables, n_c is the number of concordant pairs, and n_d is the number of discordant pairs.

4. Cosine similarity (van Dongen & Enright 2012). Suppose the two variables are x_t and y_t. Then, the cosine similarity definition is

$$\cos\theta_{x,y} = \frac{\sum_{t=1}^{N} x_t y_t}{\sqrt{\sum_{t=1}^{N} x_t^2 \sum_{t=1}^{N} y_t^2}}, \tag{8}$$

When $\cos\theta_{x,y} = 1$, it means x_t and y_t are completely similar. When $\cos\theta_{x,y}$ is closer to 1, the two variables are very similar.

4.4. Correlation Ratio

Pearson correlation coefficients measure the linear correlation between two variables. But when it comes to nonlinear correlations, correlation coefficients do not work well. So, we need to use the correlation ratio (Fisher 1970) to measure the nonlinear correlation between different variables. The correlation ratio is a ratio of the statistical dispersion within individual categories to the dispersion across the entire population or sample, which is defined as the ratio of the standard deviation within individual categories to the standard deviation of the entire population or sample.

Suppose the variables are y_{xi}, where x means the category and i means the ith value for category x, and the number of categories x is n_x, then

$$\bar{y}_x = \frac{\sum_i y_{xi}}{n_x}, \tag{9}$$

$$\bar{y} = \frac{\sum_x n_x \bar{y}_x}{\sum_x n_x}, \tag{10}$$

where $\bar{y}_x$ is the mean of category x and $\bar{y}$ is the mean of the entire sample. The definition of the correlation ratio η is

$$\eta^2 = \frac{\sum_x n_x (\bar{y}_x - \bar{y})^2}{\sum_{x,i} (y_{xi} - \bar{y})^2}, \tag{11}$$

it is the ratio of the weighted variance of the category means to the variance of the whole sample. η is a value between 0 and 1; when η is closer to 1, the nonlinear correlation is stronger.

When the two parameters are available for at least five GRBs, we give the correlation coefficients and correlation ratio, and we exclude some trivial results. It means we removed the correlations between the rest frame and observer frame for the same parameters, such as the correlation between T_{90} and $T_{90,i}$. We have many results, so we just put the first five results in Table 3. One can find all the results in the accompanying machine-readable table. In Table 3, we give the results of the Pearson, Spearman, and Kendall τ coefficients, and the related p-values. We also considered all the error bars using MC method (Zou et al. 2018). The last two rows are the correlation ratio and cosine similarity with error bars, also using MC method. We analyzed the statistics between two arbitrary parameters in order to find remarkable correlations. In Section 5, we analyzed some interesting results and give some reasonable physical explanations. In this paper, we just analyzed the linear correlations. During the analyses, the Pearson, Spearman, and Kendall τ coefficients and the related p-values were the most important references for the linear correlations. When the hypothesis-testing p-value is smaller than 0.1, it means the correlation has a very high probability of being true. The sample selection biases are quite complicated (see, for examples, of the related discussion, Lloyd & Petrosian 1999; Lloyd et al. 2000a; Dainotti et al. 2013b, 2015a, 2015b). One should be cautious when considering the results. When the absolute values of the Pearson, Spearman, and Kendall τ coefficients are bigger, the correlation is stronger. For the cosine similarity, there is no hypothesis-testing, so it is just used to confirm the linear correlations. For the correlation ratio, we will analyze the nonlinear correlations in the future using this value.

4.5. Linear Regression of Two Parameters and Three Parameters

We performed the linear regression between two parameters and three parameters arbitrarily when the sample number is bigger than five. We also considered all the error bars using MC method (Zou et al. 2018). We excluded some trivial results. As an example, the first five linear regression results are shown in Tables 4 and 5, respectively. The full linear regression results are given in two machine-readable tables.

Table 4
Linear Regression Results between Two Parameters

y	x	b	a	Adjusted R^2
$\log 1+z$	$\log D_{\rm L}$	0.39 ± 0.014	0.22 ± 0.011	0.89
$\log D_{\rm L}$	$\log 1+z$	1.5 ± 0.19	-0.13 ± 0.083	0.89
$\log 1+z$	$\log T_{90}$	0.069 ± 0.0066	0.31 ± 0.012	0.064
$\log T_{90}$	$\log 1+z$	0.61 ± 0.098	1.2 ± 0.042	0.064
$\log 1+z$	$\log T_{50}$	0.058 ± 0.0069	0.36 ± 0.0078	0.049

Note. y is a dependent variable, x is an independent variable, b is the intercept of the linear model, a is the linear coefficient of x. The adjusted R^2 is used to measure the goodness of our regression model; it means the percentage of variance when considering the parameter freedom. All errors are in 1σ error bars. All of the results are in a machine -readable table. The description of every parameter is in Section 2.

(This table is available in its entirety in machine-readable form.)

Table 5
Linear Regression Results between Three Parameters

y	x_1	x_2	a_1	a_2	b	Adjusted R^2
log HR	$-\alpha_{\rm spl}$	log Age	-0.96 ± 0.23	-0.028 ± 0.096	2.3 ± 0.27	0.9997
$-\alpha_{\rm spl}$	log HR	log Age	-0.9 ± 0.23	0.0037 ± 0.098	2.2 ± 0.4	0.9997
$\log F_{\rm pk2}$	$\log F_{\rm pk3}$	$\log t_{\rm pkX,i}$	0.97 ± 0.44	0.014 ± 0.65	0.0071 ± 0.59	0.9991
$\log F_{\rm pk3}$	$\log F_{\rm pk2}$	$\log t_{\rm pkX,i}$	0.98 ± 0.44	0.077 ± 0.62	-0.13 ± 0.55	0.9991
$\log F_{\rm pk2}$	$\rm variability_2$	$\log F_{\rm pk3}$	0.25 ± 0.71	0.96 ± 0.08	0.025 ± 0.16	0.9989

Note. x_1 and x_2 are independent variables, and a_1 and a_2 are the linear coefficients of x_1 and x_2 respectively. y, b, and adjusted R^2 have the same meanings as in Table 4. All errors are in 1σ error bars. All of the results are in a machine-readable table. The description of every parameter is in Section 2.

(This table is available in its entirety in machine-readable form.)

In Table 4, y is a dependent variable, x is an independent variable, b is the intercept of the linear model, and a is the linear coefficient of x. The adjusted R^2 is used to measure the goodness of the regression model. It means the percentage of variance when considering the parameter freedom. We use the adjusted R^2 calculated using the central values as a representative. Because every time of MC, the adjusted R^2 does not change by much. In Table 5, x_1 and x_2 are independent variables, and a_1 and a_2 are the linear coefficients of x_1 and x_2, respectively. y, b, and adjusted R^2 have the same meanings as in Table 4. Readers can see Hron et al. (2012) for more details about the linear regression.

5. Remarkable Results between Two Parameters

In this section, we show some remarkable correlations between two parameters. The strategy of choosing the results are as follows. The correlation should have at least 10 GRBs. The adjusted R^2 should be bigger than 0.2, except in Section 5.1. The entire linear model and a have hypothesis-testing p-values smaller than 0.05. The Pearson, Spearman, and Kendall τ coefficients have at least one hypothesis-testing p-value smaller than 0.1. For the peak energy flux $F_{\rm pk}$ and peak photon flux $P_{\rm pk}$, both of them have four different time bins. If the $F_{\rm pk}$ correlates with the other parameters in all four time bins, we just showed the best time bin result. The best time bin result has the biggest adjusted R^2. $P_{\rm pk}$ is the same. The other results are all in machine-readable tables. Because some relations have been discovered before, we compared the differences between current and previous analyses. Readers can also refer to Table 6 for a clear comparison. We only show a portion of the results of this paper in this table. We provide all of the results in the figure sets and machine-readable tables, including our original data. If readers want to analyze them using other statistical methods, they can use our original data given in the machine-readable tables. One may notice that it is not only the correlations but also the non-existence of correlations among certain quantities that may reveal the underlying physics of GRBs.

5.1. Some Interesting Breaks

Interestingly, we found that there is a break in the $\log F_{\rm pk}$ and $-\alpha_{\rm spl}$ plots for all four time bins.

The correlation between $\log F_{\rm pk1}$ and $-\alpha_{\rm spl}$ is

$$\log F_{\rm pk1} = (-0.75 \pm 0.046) \times (-\alpha_{\rm spl}) + (1.1 \pm 0.083), \quad (12)$$

where $F_{\rm pk1}$ is the peak energy flux in the 1 s time bin in the rest-frame 1–10^4 keV energy band and is in units of 10^{-6} erg cm^{-2} s^{-1}. The adjusted R^2 is 0.3. The Pearson coefficient is -0.47 ± 0.028 with p-value 4.2×10^{-22}. The Spearman coefficient is -0.49 ± 0.024 with p-value 5.8×10^{-25}. The Kendall τ coefficient is -0.34 ± 0.018 with p-value 7.3×10^{-24}. The correlation ratio is 0.86 ± 0.0037. The cosine similarity is -0.37 ± 0.013. The scatter plot is in Figure 3.[8] The number of GRBs in the sample is 385.

The correlation between $\log F_{\rm pk2}$ and $-\alpha_{\rm spl}$ is

$$\log F_{\rm pk2} = (-0.46 \pm 0.036) \times (-\alpha_{\rm spl}) + (1.1 \pm 0.063), \quad (13)$$

where $F_{\rm pk2}$ is the peak energy flux in the 64 ms time bin in the rest-frame 1–10^4 keV energy band and is in units of 10^{-6} erg cm^{-2} s^{-1}.

[8] Note that all figures in this section are also listed in Figure Set 2.

Table 6
Differences between the Current and Previous Analyses

Reference	Correlations	Sample Number
Our result	$\log E_{\rm p,Band} = (0.24 \pm 0.011) \times \log E_{\rm iso} + (1.9 \pm 0.017)$	180
Amati et al. (2002)	$E_{\rm p,Band} \propto E_{\rm iso}^{0.52\pm0.06}$	12
Our result	$\log E_{\rm p,Band,i} = (0.35 \pm 0.011) \times \log E_{\rm iso} + (2.3 \pm 0.018)$	178
Amati et al. (2008)	$E_{\rm p,Band,i} \propto E_{\rm iso}^{0.57\pm0.01}$	70
Yonetoku et al. (2010)	$E_{\rm iso} = 10^{53.00\pm0.045} \times \left[\frac{E_{\rm p,Band,i}}{355\ {\rm keV}}\right]^{1.57\pm0.099}$	101
Demianski et al. (2017)	$\log\left(\frac{E_{\rm iso}}{1\ {\rm erg}}\right) = 1.75^{+0.18}_{-0.16} \times \log\left[\frac{E_{\rm p,Band,i}}{300\ {\rm keV}}\right] + (52.53 \pm 0.02)$	162
Our result	$\log L_{\rm pk} = (1.2 \pm 0.055) \times \log E_{\rm p,Band,i} + (-2.9 \pm 0.14)$	127
Yonetoku et al. (2004)	$\frac{L_{\rm pk}}{10^{52}\ {\rm erg\ s^{-1}}} = (2.34^{+2.29}_{-1.76}) \times 10^{-5}\left[\frac{E_{\rm p,Band,i}}{1\ {\rm keV}}\right]^{2\pm0.2}$	11
Yonetoku et al. (2010)	$L_{\rm pk} = 10^{52.43\pm0.037} \times \left[\frac{E_{\rm p,Band,i}}{355\ {\rm keV}}\right]^{1.60\pm0.082}$	101
Our result	$\log F_{\rm g} = (0.85 \pm 0.057) \times \log E_{\rm p,Band,i} + (-1 \pm 0.15)$	179
Lloyd et al. (2000a)	$F_{\rm g} \propto E_{\rm p,Band,i}^{0.28\pm0.04}$	5
Our result	$\log \Gamma_0 = (0.35 \pm 0.014) \times \log E_{\rm iso} + (1.9 \pm 0.018)$	51
Liang et al. (2010)	$\log \Gamma_0 = (0.269 \pm 0.002) \log E_{\rm iso,52} + (2.291 \pm 0.002)$	19
Lü et al. (2012)	$\log \Gamma_0 = (0.29 \pm 0.002) \log E_{\rm iso,52} + (1.96 \pm 0.002)$	38
Our result	$\log \Gamma_0 = (-0.49 \pm 0.011) \times \log t_{\rm pkOpt,i} + (3.2 \pm 0.026)$	45
Liang et al. (2010)	$\log \Gamma_0 = (-0.63 \pm 0.04) \times \log t_{\rm pkOpt,i} + (3.69 \pm 0.09)$	19

Note. Differences between the current and previous analyses of the four relations. Our sample number is obviously bigger than that in previous analyses.

The adjusted R^2 is 0.21. The Pearson coefficient is -0.37 ± 0.03 with p-value 1.8×10^{-17}. The Spearman coefficient is -0.55 ± 0.023 with p-value 8.8×10^{-41}. The Kendall τ coefficient is -0.39 ± 0.018 with p-value 3.2×10^{-38}. The correlation ratio is 0.81 ± 0.0045. The cosine similarity is 0.5 ± 0.018. The scatter plot is in Figure 4. The number of GRBs in the sample is 490.

The correlation between $\log F_{\rm pk3}$ and $-\alpha_{\rm spl}$ is

$$\log F_{\rm pk3} = (-0.37 \pm 0.032) \times (-\alpha_{\rm spl}) + (0.84 \pm 0.057), \quad (14)$$

where $F_{\rm pk3}$ is the peak energy flux in the 256 ms time bin in the rest-frame 1–10^4 keV energy band and is in units of $10^{-6}\,{\rm erg\,cm^{-2}\,s^{-1}}$. The adjusted R^2 is 0.17. The Pearson coefficient is -0.33 ± 0.031 with p-value 4.1×10^{-14}. The Spearman coefficient is -0.54 ± 0.024 with p-value 1.6×10^{-37}. The Kendall τ coefficient is -0.38 ± 0.018 with p-value 6.7×10^{-36}. The correlation ratio is 0.85 ± 0.0038. The cosine similarity is 0.33 ± 0.021. The scatter plot is in Figure 5. The number of GRBs in the sample is 487.

The correlation between $\log F_{\rm pk4}$ and $-\alpha_{\rm spl}$ is

$$\log F_{\rm pk4} = (-0.18 \pm 0.033) \times (-\alpha_{\rm spl}) + (0.22 \pm 0.059), \quad (15)$$

where $F_{\rm pk4}$ is the peak energy flux in the 1024 ms time bin in the rest-frame 1–10^4 keV energy band and is in units of $10^{-6}\,{\rm erg\,cm^{-2}\,s^{-1}}$. The adjusted R^2 is 0.055. The Pearson coefficient is -0.16 ± 0.032 with p-value 3.4×10^{-4}. The Spearman coefficient is -0.39 ± 0.027 with p-value 3.3×10^{-19}. The Kendall τ coefficient is -0.28 ± 0.02 with p-value 1.3×10^{-19}. The correlation ratio is 0.89 ± 0.004. The cosine similarity is -0.19 ± 0.018. The scatter plot is in Figure 6. The number of GRBs in the sample is 483.

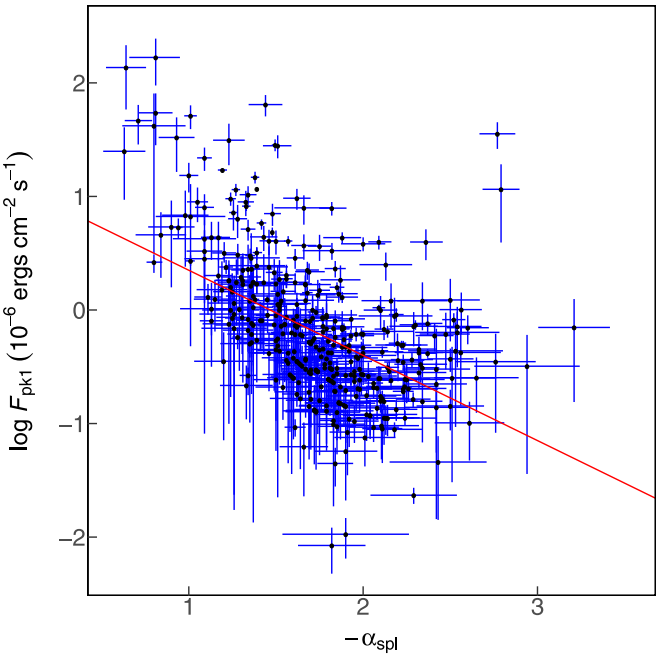

Figure 3. Scatter plot for $\log F_{\rm pk1}$ and $-\alpha_{\rm spl}$. The red line is our fit result. The formula for the red line is $\log F_{\rm pk1} = (-0.75 \pm 0.046) \times (-\alpha_{\rm spl}) + (1.1 \pm 0.083)$. The description of every parameter is in Section 2.

We also found a break in the log HR–log $F_{\rm pk2}$–$(-\alpha_{\rm spl})$ plot. In the other three time bins of $F_{\rm pk}$, there are also breaks. We just show the best one.

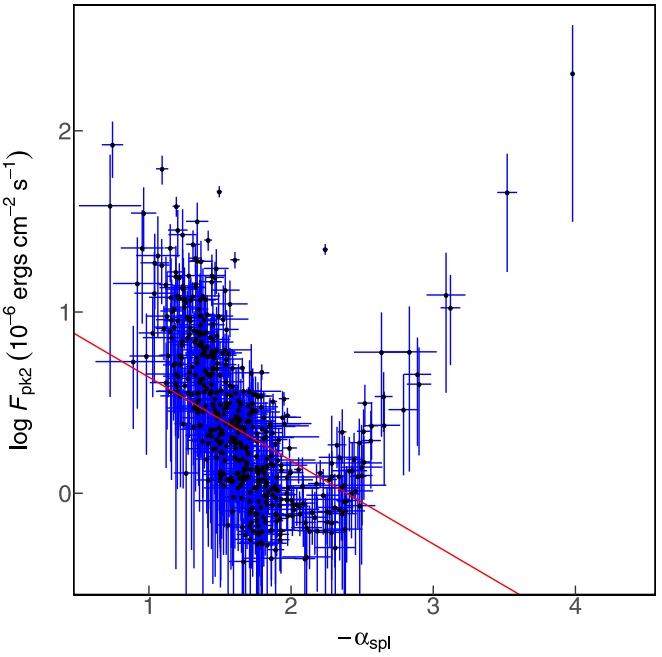

Figure 4. Scatter plot for $\log F_{pk2}$ and $-\alpha_{spl}$. The red line is our fit result. The formula for the red line is $\log F_{pk2} = (-0.46 \pm 0.036) \times (-\alpha_{spl}) + (1.1 \pm 0.063)$. The description of every parameter is in Section 2.

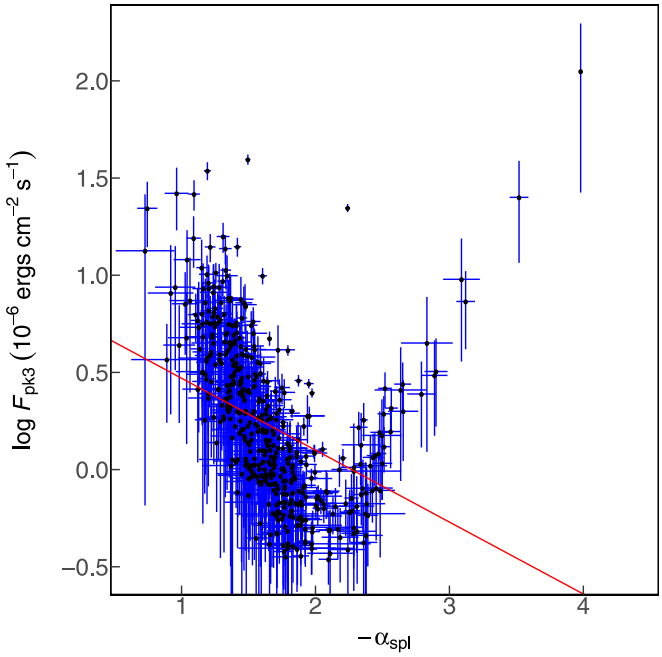

Figure 5. Scatter plot for $\log F_{pk3}$ and $-\alpha_{spl}$. The red line is our fit result. The formula for the red line is $\log F_{pk3} = (-0.37 \pm 0.032) \times (-\alpha_{spl}) + (0.84 \pm 0.057)$. The description of every parameter is in Section 2.

The log HR–log F_{pk2}–$(-\alpha_{spl})$ relation is

$$\log \mathrm{HR} = (0.17 \pm 0.036) \times \log F_{pk2} + (-0.9 \pm 0.039) \times (-\alpha_{spl}) + (2.2 \pm 0.075), \quad (16)$$

where F_{pk2} is the peak energy flux in the 64 ms time bin in the rest-frame 1–10^4 keV energy band and is in units of 10^{-6} erg cm^{-2} s^{-1}. The adjusted R^2 is 0.57. One can see Figure 85 for the scatter plot between these three parameters. The number of GRBs in the sample is 490.

It is not clear what causes these breaks. There are also weak signals in the P_{pk}–α_{spl} plot. It might be a selection effect, as there is no such effect in the L_{pk}–α_{spl} plot or in the F_g–α_{spl} plot. All corresponding figures can be found in the figure set.

5.2. Amati Relation

The Amati relation (Amati et al. 2002, 2008) is a widely known relation of GRBs.

The correlation between $\log E_{p,Band}$ and $\log E_{iso}$ is

$$\log E_{p,Band} = (0.24 \pm 0.011) \times \log E_{iso} + (1.9 \pm 0.017), \quad (17)$$

where $E_{p,Band}$ is in units of keV, E_{iso} is in units of 10^{52} erg and is in the rest-frame 1–10^4 keV energy band. In the Amati et al. (2002) initial data, the slope is 0.52 ± 0.06 with 12 GRBs. Here we have 180 GRBs. The adjusted R^2 is 0.26. The Pearson coefficient is 0.5 ± 0.021 with p-value 8.2×10^{-13}. The Spearman coefficient is 0.56 ± 0.019 with p-value 5.2×10^{-16}. The Kendall τ coefficient is 0.41 ± 0.014 with p-value 2.1×10^{-16}. The correlation ratio is 0.62 ± 0.0049. The cosine similarity is 0.75 ± 0.0055. It may be that GRBs with larger Γ_0 also have larger energy and peak energy (Ghirlanda et al. 2012), or an optically thin synchrotron shock model (Lloyd et al. 2000b). As

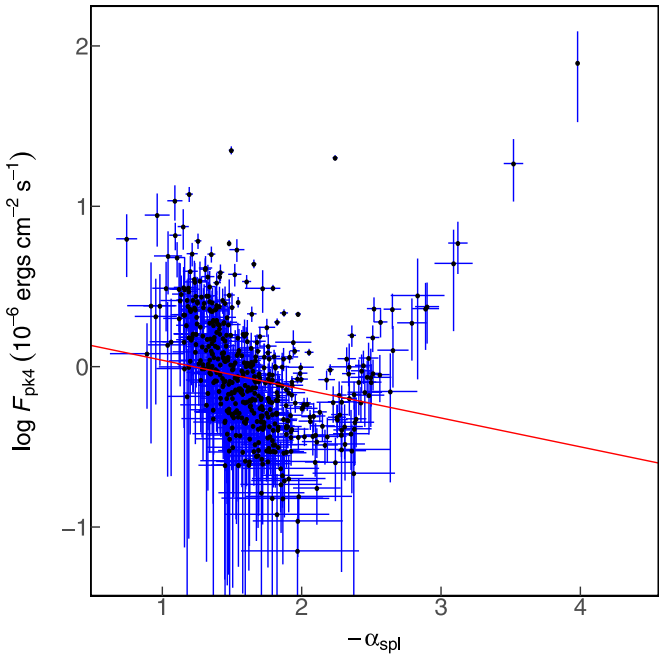

Figure 6. Scatter plot for $\log F_{pk4}$ and $-\alpha_{spl}$. The red line is our fit result. The formula for the red line is $\log F_{pk4} = (-0.18 \pm 0.033) \times (-\alpha_{spl}) + (0.22 \pm 0.059)$. The description of every parameter is in Section 2.

one can see in Section 5.6, the E_{iso} and peak energy both correlate with Γ_0. The scatter plot is in Figure 7. The number of GRBs in the sample is 180.

The correlation between $\log E_{p,Band,i}$ and $\log E_{iso}$ is

$$\log E_{p,Band,i} = (0.35 \pm 0.011) \times \log E_{iso} + (2.3 \pm 0.018). \quad (18)$$

In Amati et al. (2008), the slope is 0.57 ± 0.01 with 70 LGRBs and X-ray flares. We have 178 GRBs, where $E_{p,Band,i}$ is in units

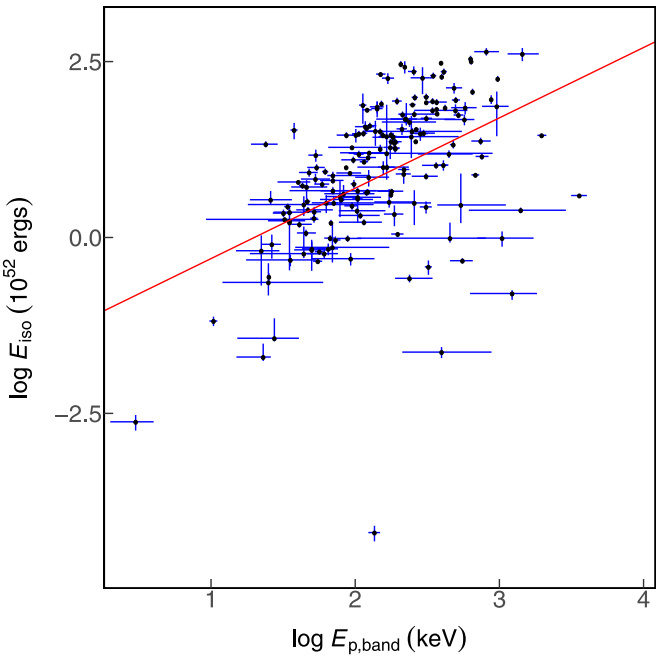

Figure 7. Scatter plot for $\log E_{\rm p,Band}$ and $\log E_{\rm iso}$. The red line is our fit result. The formula for the red line is $\log E_{\rm p,Band} = (0.24 \pm 0.011) \times \log E_{\rm iso} + (1.9 \pm 0.017)$. The description of every parameter is in Section 2.

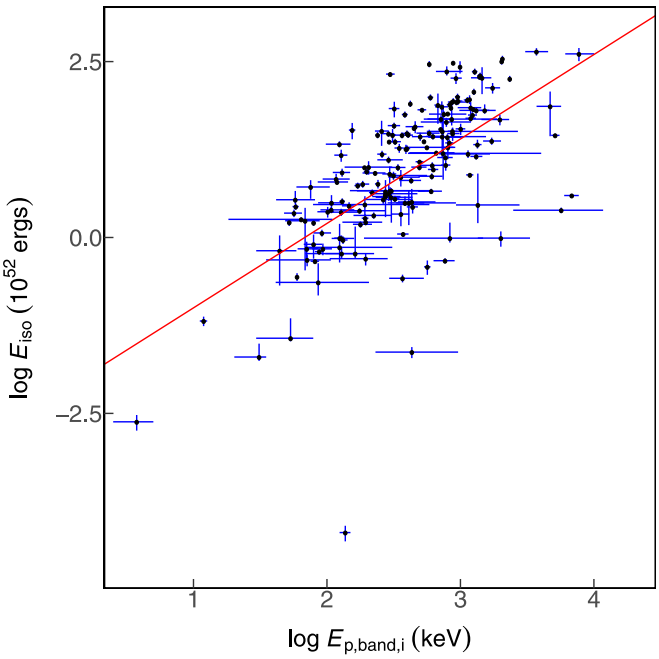

Figure 8. Scatter plot for $\log E_{\rm p,Band,i}$ and $\log E_{\rm iso}$. The red line is our fit result. The formula for the red line is $\log E_{\rm p,Band,i} = (0.35 \pm 0.011) \times \log E_{\rm iso} + (2.3 \pm 0.018)$. The description of every parameter is in Section 2.

of keV. $E_{\rm iso}$ is in units of 10^{52} erg and is in the rest-frame 1–10^4 keV energy band. The adjusted R^2 is 0.45. The Pearson coefficient is 0.65 ± 0.019 with p-value 7.2×10^{-23}. The Spearman coefficient is 0.69 ± 0.018 with p-value 4.9×10^{-26}. The Kendall τ coefficient is 0.51 ± 0.015 with p-value 3.1×10^{-24}. The correlation ratio is 0.72 ± 0.0038. The cosine similarity is 0.78 ± 0.0052. The scatter plot is in Figure 8. The number of GRBs in the sample is 178. The better correlation between $\log E_{\rm p,Band,i}$ and $\log E_{\rm iso}$ compared with $\log E_{\rm p,Band}$ and $\log E_{\rm iso}$ suggests this correlation is intrinsic. With enough data, one can investigate this relation within subgroups (Zhang et al. 2009; Qin & Chen 2013; Zou et al. 2018). A previous study gave $E_{\rm iso} = 10^{53.00\pm0.045} \times \left[\frac{E_{\rm p,Band,i}}{355\ {\rm keV}}\right]^{1.57\pm0.099}$ with 101 samples (Yonetoku et al. 2010), and $\log\left(\frac{E_{\rm iso}}{1\ {\rm erg}}\right) = 1.75^{+0.18}_{-0.16} \times \log\left[\frac{E_{\rm p,Band,i}}{300\ {\rm keV}}\right] + (52.53 \pm 0.02)$ with 162 samples (Demianski et al. 2017).

5.3. Some Correlations with L_{pk}

5.3.1. Yonetoku Relation

Yonetoku et al. (2004) found a correlation between the rest-frame peak energy and peak luminosity. We also found the $\log E_{\rm p,Band}$–$\log L_{\rm pk}$ and $\log E_{\rm p,Band,i}$–$\log L_{\rm pk}$ correlations.

The correlation between $\log L_{\rm pk}$ and $\log E_{\rm p,Band}$ is

$$\log L_{\rm pk} = (1 \pm 0.061) \times \log E_{\rm p,Band} + (-2 \pm 0.13), \quad (19)$$

where $L_{\rm pk}$ is in units of 10^{52} erg s^{-1} and in the 1–10^4 keV energy band. $E_{\rm p,Band}$ is in units of keV. The adjusted R^2 is 0.25. The Pearson coefficient is 0.49 ± 0.022 with p-value 3.2×10^{-9}. The Spearman coefficient is 0.52 ± 0.025 with p-value 1.5×10^{-10}. The Kendall τ coefficient is 0.37 ± 0.019 with p-value 4.9×10^{-10}. The correlation ratio is 0.8 ± 0.004. The cosine similarity is 0.33 ± 0.014. The scatter plot is in Figure 9. The number of GRBs in the sample is 130.

The correlation between $\log L_{\rm pk}$ and $\log E_{\rm p,Band,i}$ is

$$\log L_{\rm pk} = (1.2 \pm 0.055) \times \log E_{\rm p,Band,i} + (-2.9 \pm 0.14), \quad (20)$$

In Yonetoku et al. (2004), the slope is 1.94 ± 0.19 with 11 samples, where $L_{\rm pk}$ is in units of 10^{52} erg s^{-1} and in the 1–10^4 keV energy band. $E_{\rm p,Band,i}$ is in units of keV. The adjusted R^2 is 0.42. The Pearson coefficient is 0.63 ± 0.019 with p-value 4×10^{-15}. The Spearman coefficient is 0.64 ± 0.025 with p-value 4.3×10^{-16}. The Kendall τ coefficient is 0.47 ± 0.019 with p-value 7.5×10^{-15}. The correlation ratio is 0.85 ± 0.0031. The cosine similarity is 0.34 ± 0.013. The scatter plot is in Figure 10. The number of GRBs in the sample is 127. The rest-frame peak energy is also better correlated with the luminosity. Yonetoku et al. (2010) reanalyzed 101 GRBs and examined how the truncation of the detector sensitivity affects the Amati and Yonetoku relations. They conclude that these are surely intrinsic properties of GRBs. The result of Yonetoku et al. (2010) is $L_{\rm pk} = 10^{52.43\pm0.037} \times \left[\frac{E_{\rm p,Band,i}}{355\ {\rm keV}}\right]^{1.60\pm0.082}$ with 101 samples.

5.3.2. Other Correlations with $L_{\rm pk}$

The correlation between $\log L_{\rm pk}$ and log offset is

$$\log L_{\rm pk} = (-0.68 \pm 0.24) \times \log {\rm offset} + (-0.047 \pm 0.15), \quad (21)$$

where $L_{\rm pk}$ is in units of 10^{52} erg s^{-1} and in the 1–10^4 keV energy band. Host galaxy offset is in units of kpc. The adjusted R^2 is 0.22. The Pearson coefficient is -0.42 ± 0.092 with

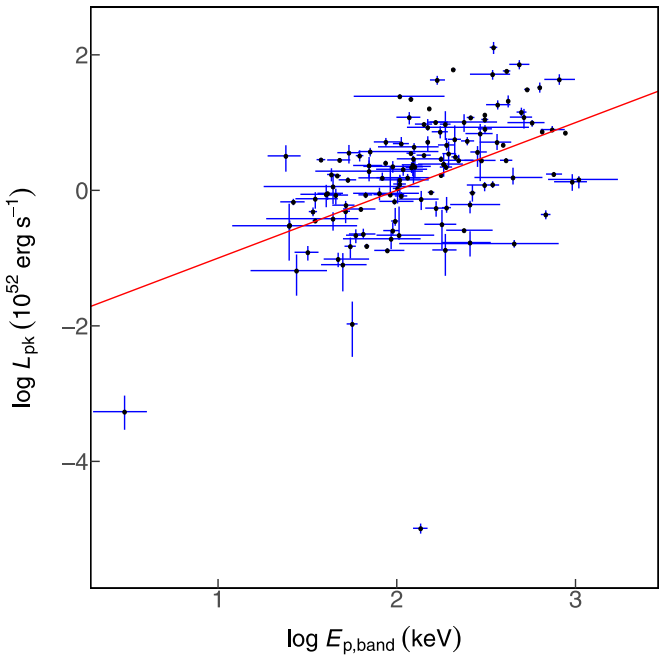

Figure 9. Scatter plot for $\log L_{pk}$ and $\log E_{p,Band}$. The red line is our fit result. The formula for the red line is $\log L_{pk} = (1 \pm 0.061) \times \log E_{p,Band} + (-2 \pm 0.13)$. The description of every parameter is in Section 2. The outlier with the lowest L_{pk} is GRB 980425B, as in Figure 10.

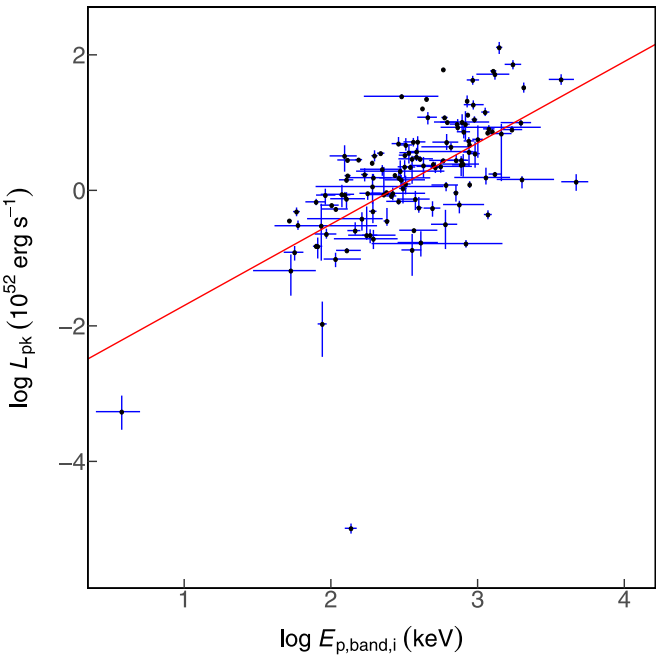

Figure 10. Scatter plot for $\log L_{pk}$ and $\log E_{p,Band,i}$. The red line is our fit result. The formula for the red line is $\log L_{pk} = (1.2 \pm 0.055) \times \log E_{p,Band,i} + (-2.9 \pm 0.14)$. The description of every parameter is in Section 2. There is an outlier in the plot with the lowest L_{pk}; this point is BATSE GRB 980425B, which is a well-known low-luminosity GRB.

p-value 3×10^{-2}. The Spearman coefficient is -0.44 ± 0.041 with p-value 2.2×10^{-2}. The Kendall τ coefficient is -0.31 ± 0.035 with p-value 2.3×10^{-2}. The correlation ratio is 0.42 ± 0.043. The cosine similarity is -0.5 ± 0.085. The scatter plot is in Figure 11. The number of GRBs in the sample is 27. As the SGRBs are located in the outer regions of the host galaxies and they are less luminous, this may cause the anticorrelation between L_{pk} and the offset.

The correlation between $\log L_{pk}$ and $\log t_{pkOpt}$ is

$$\log L_{pk} = (-0.74 \pm 0.04) \times \log t_{pkOpt} + (1.9 \pm 0.092), \quad (22)$$

where L_{pk} is in units of $10^{52}\,\mathrm{erg\,s^{-1}}$ and in the 1–10^4 keV energy band. t_{pkOpt} is in units of s. The adjusted R^2 is 0.26. The Pearson coefficient is -0.51 ± 0.023 with p-value 1.5×10^{-6}. The Spearman coefficient is -0.39 ± 0.033 with p-value 3.5×10^{-4}. The Kendall τ coefficient is -0.27 ± 0.024 with p-value 4×10^{-4}. The correlation ratio is 0.84 ± 0.0038. The cosine similarity is -0.067 ± 0.026. The scatter plot is in Figure 12. The number of GRBs in the sample is 80.

The correlation between $\log L_{pk}$ and $\log t_{pkOpt,i}$ is

$$\log L_{pk} = (-0.87 \pm 0.036) \times \log t_{pkOpt,i} + (1.8 \pm 0.069), \quad (23)$$

where L_{pk} is in units of $10^{52}\,\mathrm{erg\,s^{-1}}$ and in the 1–10^4 keV energy band. $t_{pkOpt,i}$ is in units of s. The adjusted R^2 is 0.4. The Pearson coefficient is -0.62 ± 0.019 with p-value 1.1×10^{-9}. The Spearman coefficient is -0.48 ± 0.031 with p-value 5.6×10^{-6}. The Kendall τ coefficient is -0.33 ± 0.023 with p-value 1.3×10^{-5}. The correlation ratio is 0.78 ± 0.0049. The cosine similarity is -0.13 ± 0.025. The scatter plot is in Figure 13. The number of GRBs in the sample is 80. This anticorrelation is mainly caused by the Lorentz factor, wherein a higher Lorentz factor corresponds to a shorter deceleration time, and consequently smaller $t_{pkOpt,i}$. We can also see that the rest-frame peak time is better correlated than the observational peak time with the luminosity.

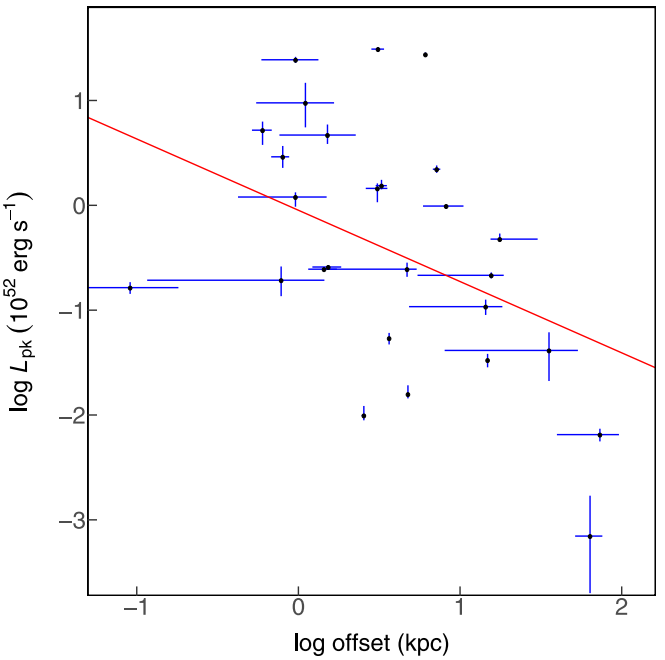

Figure 11. Scatter plot for $\log L_{pk}$ and log offset. The red line is our fit result. The formula for the red line is $\log L_{pk} = (-0.68 \pm 0.24) \times \log \mathrm{offset} + (-0.047 \pm 0.15)$. The description of every parameter is in Section 2.

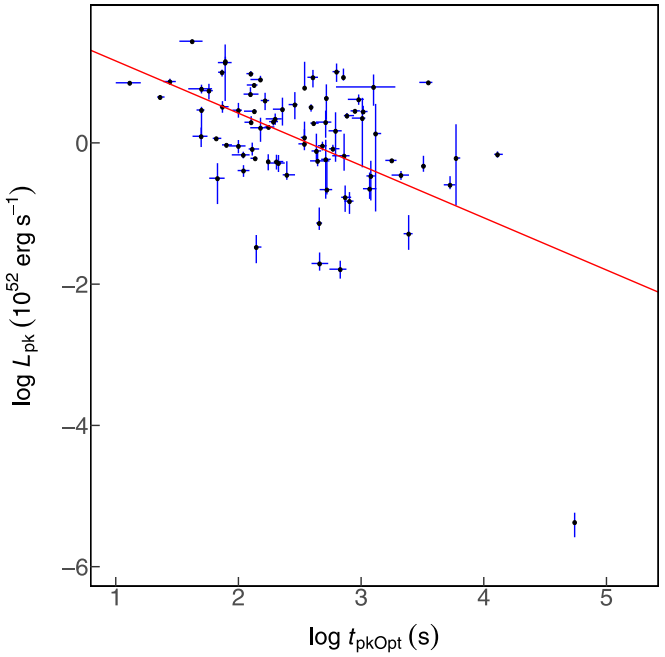

Figure 12. Scatter plot for $\log L_{pk}$ and $\log t_{pkOpt}$. The red line is our fit result. The formula for the red line is $\log L_{pk} = (-0.74 \pm 0.04) \times \log t_{pkOpt} + (1.9 \pm 0.092)$. The description of every parameter is in Section 2. The outlier is the low-luminosity GRB 060218A, which has the lowest L_{pk} in the plot.

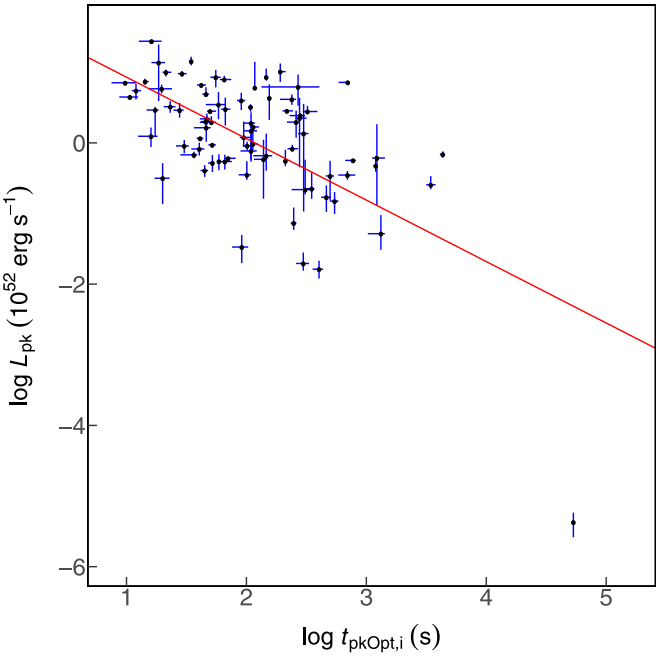

Figure 13. Scatter plot for $\log L_{pk}$ and $\log t_{pkOpt,i}$. The red line is our fit result. The formula for the red line is $\log L_{pk} = (-0.87 \pm 0.036) \times \log t_{pkOpt,i} + (1.8 \pm 0.069)$. The description of every parameter is in Section 2. The outlier is the low-luminosity GRB 060218A, which has the lowest L_{pk} in the plot.

5.4. Some Correlations with the Host Galaxy

We found that there are some correlations between the host galaxy parameters and redshift, and also with D_L. Mag especially has correlations with many parameters.

5.4.1. Some Correlations between Mag and the Other Parameters

The correlation between Mag and log Mass is

$$\text{Mag} = (-1.8 \pm 0.34) \times \log \text{Mass} + (-4 \pm 3.3), \quad (24)$$

where Mass is in units of $M_\odot$ and Mag is in units of magnitude. The adjusted R^2 is 0.84. The Pearson coefficient is -0.48 ± 0.077 with p-value 4.2×10^{-6}. The Spearman coefficient is -0.45 ± 0.083 with p-value 1.8×10^{-5}. The Kendall τ coefficient is -0.32 ± 0.061 with p-value 2.5×10^{-5}. The correlation ratio is 0.99 ± 0.00099. The cosine similarity is -0.99 ± 0.00091. The scatter plot is in Figure 14. The number of GRBs in the sample is 82. The luminosity of the host galaxy is positively related with its mass. It might be worth investigating the correlations for different types of galaxies, such as host galaxies of GRBs and supernovae, radio-loud galaxies, etc.

The correlation between Mag and log SFR is

$$\text{Mag} = (-1.8 \pm 0.41) \times \log \text{SFR} + (-19 \pm 0.51), \quad (25)$$

where SFR is in units of $M_\odot\,\text{yr}^{-1}$. Mag is in units of magnitude. The adjusted R^2 is 0.78. The Pearson coefficient is -0.56 ± 0.1 with p-value 7.1×10^{-4}. The Spearman coefficient is -0.5 ± 0.12 with p-value 3.1×10^{-3}. The Kendall τ coefficient is -0.36 ± 0.091 with p-value 3.6×10^{-3}. The correlation ratio is 0.98 ± 0.0032. The cosine similarity is -0.78 ± 0.027. The scatter plot is in Figure 15. The number of GRBs in the sample is 33. It might be more interesting to get the correlations for the specific SFR. However, those correlations are not obvious enough.

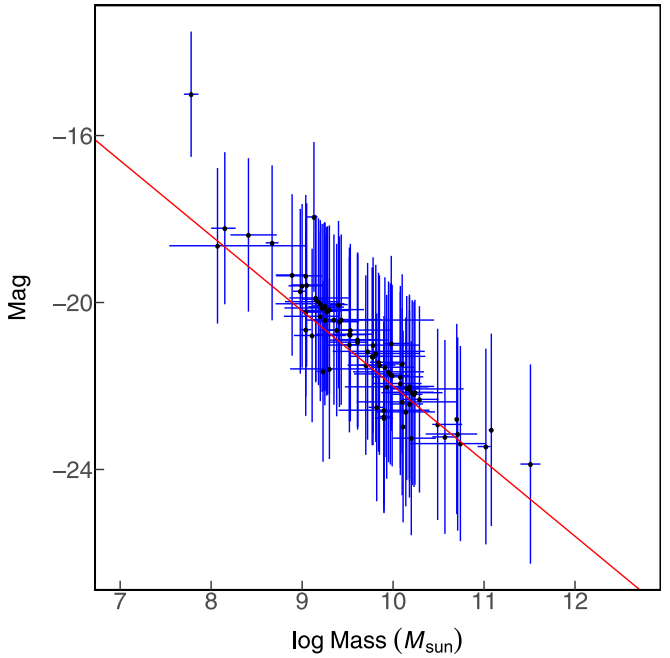

Figure 14. Scatter plot for Mag and log Mass. The red line is our fit result. The formula for the red line is $\text{Mag} = (-1.8 \pm 0.34) \times \log \text{Mass} + (-4 \pm 3.3)$. The description of every parameter is in Section 2.

The correlation between Mag and metallicity is

$$\text{Mag} = (-3.4 \pm 1.6) \times \text{metallicity} + (8.4 \pm 14), \quad (26)$$

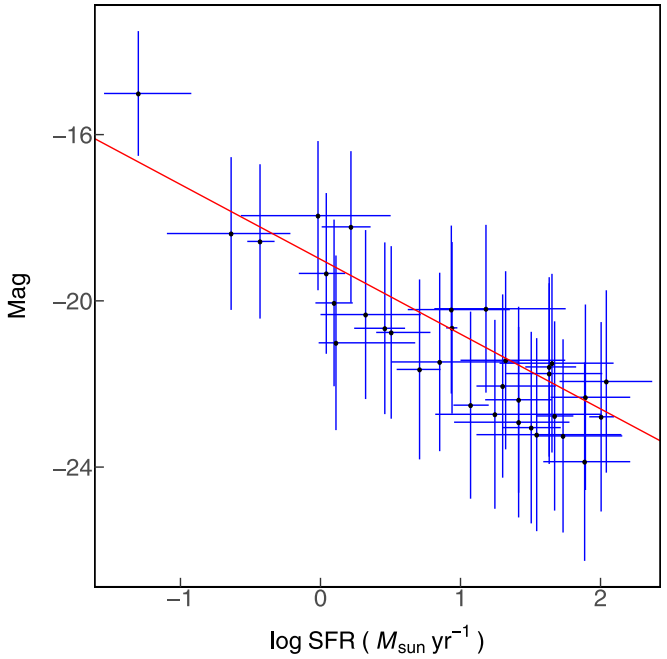

Figure 15. Scatter plot for Mag and log SFR. The red line is our fit result. The formula for the red line is Mag = $(-1.8 \pm 0.41) \times \log \mathrm{SFR} + (-19 \pm 0.51)$. The description of every parameter is in Section 2.

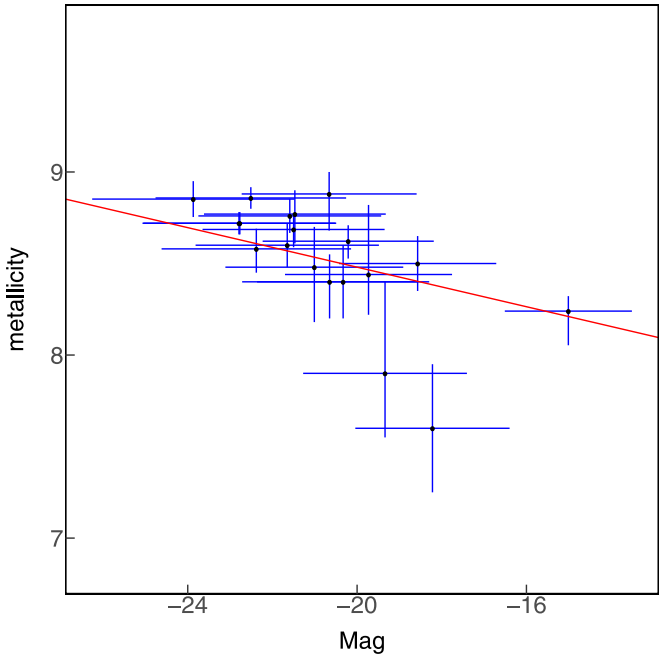

Figure 16. Scatter plot for Mag and metallicity. The red line is our fit result. The formula for the red line is Mag = $(-3.4 \pm 1.6) \times$ metallicity + (8.4 ± 14). The description of every parameter is in Section 2.

where Mag is in units of magnitude. The metallicity is the value of $12 + \log \mathrm{O/H}$. The adjusted R^2 is 0.41. The Pearson coefficient is -0.42 ± 0.15 with p-value 7.4×10^{-2}. The Spearman coefficient is -0.41 ± 0.17 with p-value 7.8×10^{-2}. The Kendall τ coefficient is -0.29 ± 0.13 with p-value 7.4×10^{-2}. The correlation ratio is 0.99 ± 0.0025. The cosine similarity is -0.99 ± 0.0022. The scatter plot is in Figure 16. The number of GRBs in the sample is 19. Metallicity indicates the star formation properties, and consequently, information on the progenitors of GRBs. However, the sample is not big enough, and the correlation is not very tight. One may not find much information from this correlation right now.

The correlation between Mag and $\log F_{\mathrm{Opt11hr}}$ is

$$\mathrm{Mag} = (0.73 \pm 0.3) \times \log F_{\mathrm{Opt11hr}} + (-17 \pm 1.5), \quad (27)$$

where F_{Opt11hr} is in units of Jy. Mag is in units of magnitude. The adjusted R^2 is 0.27. The Pearson coefficient is 0.27 ± 0.1 with p-value 3.3×10^{-2}. The Spearman coefficient is 0.23 ± 0.11 with p-value 7.3×10^{-2}. The Kendall τ coefficient is 0.16 ± 0.075 with p-value 6.9×10^{-2}. The correlation ratio is 0.97 ± 0.004. The cosine similarity is 0.98 ± 0.0028. The scatter plot is in Figure 17. The number of GRBs in the sample is 64. It is interesting that the magnitude of the host galaxy is related to the observed flux density of the afterglow. It is probably because the number density of the smaller galaxy is higher, and the luminosity at 11 hr is brighter.

The correlation between Mag and $\log D_{\mathrm{L}}$ is

$$\mathrm{Mag} = (-1.9 \pm 0.53) \times \log D_{\mathrm{L}} + (-20 \pm 0.37), \quad (28)$$

where D_{L} is in units of 10^{28} cm. Mag is in units of magnitude. The adjusted R^2 is 0.26. The Pearson coefficient is -0.3 ± 0.081 with p-value 6.9×10^{-3}. The Spearman coefficient is -0.2 ± 0.091

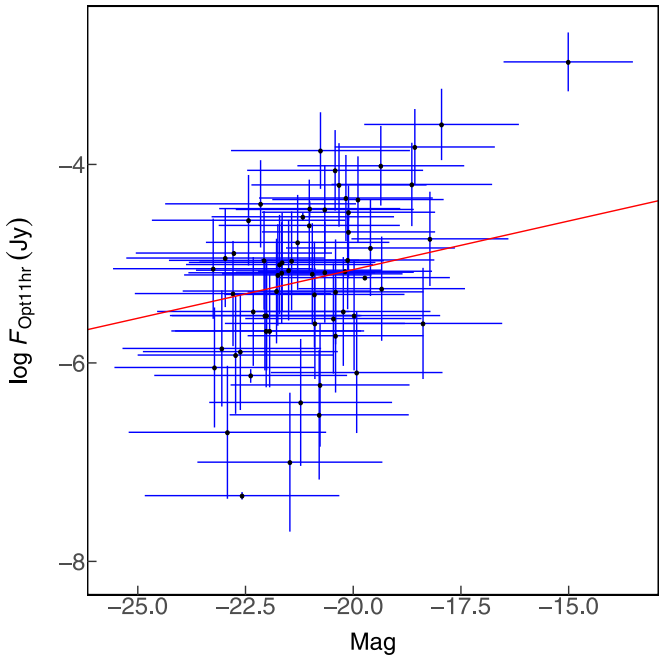

Figure 17. Scatter plot for Mag and $\log F_{\mathrm{Opt11hr}}$. The red line is our fit result. The formula for the red line is Mag = $(0.73 \pm 0.3) \times \log F_{\mathrm{Opt11hr}} + (-17 \pm 1.5)$. The description of every parameter is in Section 2.

with p-value 7.5×10^{-2}. The Kendall τ coefficient is -0.14 ± 0.064 with p-value 7.3×10^{-2}. The correlation ratio is 0.99 ± 0.002. The cosine similarity is -0.82 ± 0.0058. The scatter plot is in Figure 18. The number of GRBs in the sample is 81. This relation shows the observational selection effect on the data. Because of the flux limit of the observations, only bright galaxies can be observed in the far distance. The host galaxies observed are correlated to the distance.

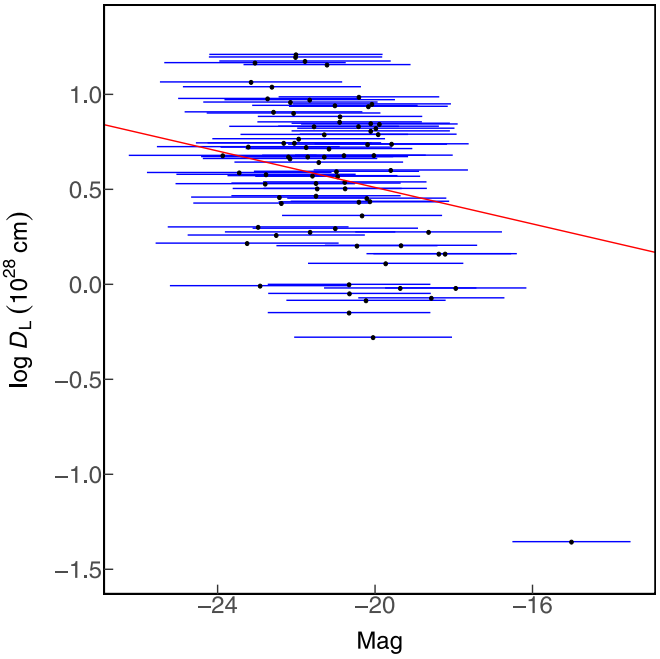

Figure 18. Scatter plot for Mag and $\log D_L$. The red line is our fit result. The formula for the red line is Mag $= (-1.9 \pm 0.53) \times \log D_L + (-20 \pm 0.37)$. The description of every parameter is in Section 2. The outlier is the low-luminosity GRB 060218A with the highest Mag and lowest D_L in the plot.

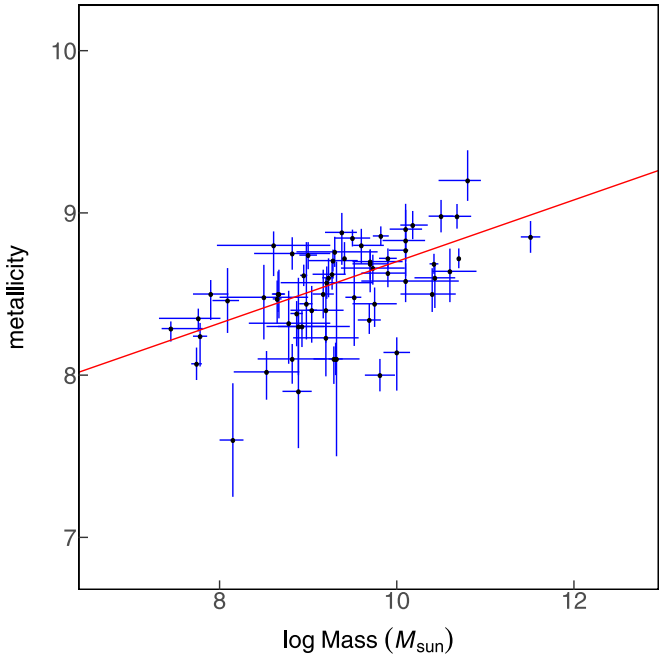

Figure 19. Scatter plot for metallicity and log Mass. The red line is our fit result. The formula for the red line is metallicity $= (0.19 \pm 0.025) \times$ log Mass $+ (6.8 \pm 0.24)$. The description of every parameter is in Section 2.

5.4.2. Some Other Correlations between Parameters Related to Host Galaxies

The correlation between metallicity and log Mass is

$$\text{metallicity} = (0.19 \pm 0.025) \times \log \text{Mass} + (6.8 \pm 0.24), \quad (29)$$

where the metallicity is the value of $12 + \log \text{O/H}$. Mass is in units of $M_\odot$. The adjusted R^2 is 0.3. The Pearson coefficient is 0.47 ± 0.054 with p-value 9.3×10^{-5}. The Spearman coefficient is 0.49 ± 0.057 with p-value 3.7×10^{-5}. The Kendall τ coefficient is 0.34 ± 0.043 with p-value 6.7×10^{-5}. The correlation ratio is 0.54 ± 0.022. The cosine similarity is 1 ± 0.00033. The scatter plot is in Figure 19. The number of GRBs in the sample is 64. The metallicity is positively correlated with the mass, which may indicate a history of merging of the galaxies. Arabsalmani et al. (2018) studied the mass–metallicity relation for GRB host galaxies and found that GRB-selected galaxies appear to track the mass–metallicity relation of star-forming galaxies but with an offset of 0.15 toward lower metallicities.

The correlation between log SFR and $\log(1 + z)$ is

$$\log \text{SFR} = (4.1 \pm 0.19) \times \log(1 + z) + (-0.59 \pm 0.051), \quad (30)$$

where SFR is in units of $M_\odot\ \text{yr}^{-1}$. The adjusted R^2 is 0.49. The Pearson coefficient is 0.69 ± 0.019 with p-value 1.3×10^{-14}. The Spearman coefficient is 0.69 ± 0.02 with p-value 4.8×10^{-15}. The Kendall τ coefficient is 0.49 ± 0.018 with p-value 1.6×10^{-12}. The correlation ratio is 0.24 ± 0.018. The cosine similarity is 0.76 ± 0.016. The scatter plot is in Figure 20. The number of GRBs in the sample is 96. This relation may indicate the history of the star formation. However, one should be cautious about the data selection effect.

The correlation between log SFR and $\log D_L$ is

$$\log \text{SFR} = (1.2 \pm 0.047) \times \log D_L + (0.43 \pm 0.025), \quad (31)$$

where SFR is in units of $M_\odot\ \text{yr}^{-1}$. D_L is in units of 10^{28} cm. The adjusted R^2 is 0.42. The Pearson coefficient is 0.64 ± 0.018 with p-value 3.2×10^{-12}. The Spearman coefficient is 0.66 ± 0.021 with p-value 2.1×10^{-13}. The Kendall τ coefficient is 0.46 ± 0.019 with p-value 2.1×10^{-11}. The correlation ratio is 0.29 ± 0.016. The cosine similarity is 0.69 ± 0.014. The scatter plot is in Figure 21. The number of GRBs in the sample is 96. This is similar to the SFR and $(1 + z)$ relation.

The correlation between log Mass and log SFR is

$$\log \text{Mass} = (0.62 \pm 0.041) \times \log \text{SFR} + (9.1 \pm 0.046), \quad (32)$$

where mass is in units of $M_\odot$. SFR is in units of $M_\odot\ \text{yr}^{-1}$. The adjusted R^2 is 0.54. The Pearson coefficient is 0.69 ± 0.034 with p-value 5.2×10^{-11}. The Spearman coefficient is 0.71 ± 0.034 with p-value 9.6×10^{-12}. The Kendall τ coefficient is 0.52 ± 0.032 with p-value 2×10^{-10}. The correlation ratio is 0.98 ± 0.0011. The cosine similarity is 0.57 ± 0.021. The scatter plot is in Figure 22. The number of GRBs in the sample is 69. It is natural that the more massive galaxy has a more intense total star formation rate. Notice that the index is 0.62 ± 0.041, which means less massive galaxies are more effective at forming stars per unit mass.

The correlation between $\log F_{\text{Opt11hr}}$ and log SFR is

$$\log F_{\text{Opt11hr}} = (-0.44 \pm 0.073) \times \log \text{SFR} + (-4.6 \pm 0.074), \quad (33)$$

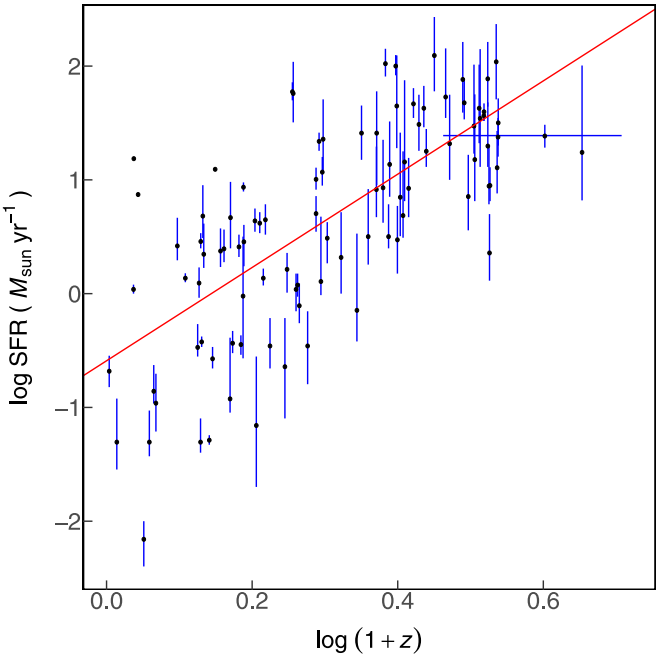

Figure 20. Scatter plot for log SFR and log(1 + z). The red line is our fit result. The formula for the red line is log SFR = (4.1 ± 0.19) × log(1 + z) + (−0.59 ± 0.051). The description of every parameter is in Section 2.

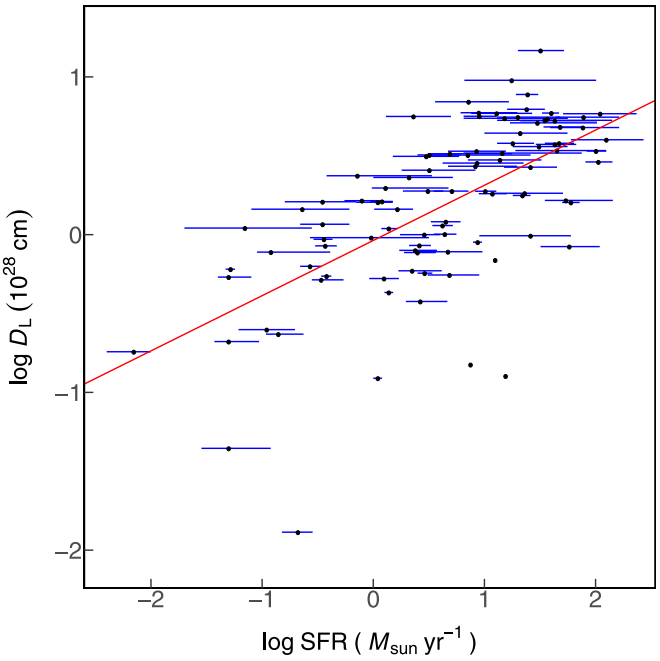

Figure 21. Scatter plot for log SFR and log D_L. The red line is our fit result. The formula for the red line is log SFR = (1.2 ± 0.047) × log D_L + (0.43 ± 0.025). The description of every parameter is in Section 2.

where $F_{Opt11hr}$ is in units of Jy. SFR is in units of $M_\odot$ yr^{-1}. The adjusted R^2 is 0.24. The Pearson coefficient is −0.43 ± 0.065 with p-value 1.7 × 10^{-3}. The Spearman coefficient is −0.43 ± 0.069 with p-value 1.6 × 10^{-3}. The Kendall τ coefficient is −0.29 ± 0.051 with p-value 2.3 × 10^{-3}. The correlation ratio is 0.94 ± 0.0042. The cosine similarity is −0.57 ± 0.03. The scatter plot is in Figure 23. The number of GRBs in the sample is 51. This correlation is related to the correlations given in Equations (32) and (27).

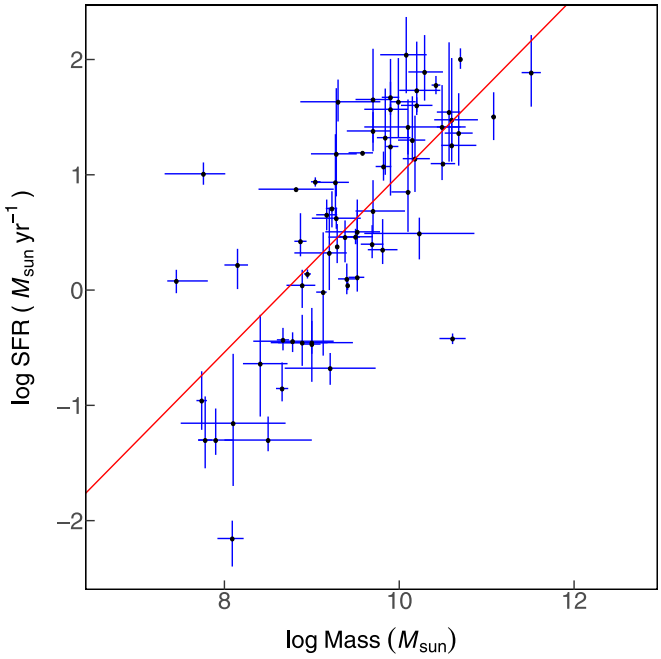

Figure 22. Scatter plot for log Mass and log SFR. The red line is our fit result. The formula for the red line is log Mass = (0.62 ± 0.041) × log SFR + (9.1 ± 0.046). The description of every parameter is in Section 2.

The correlation between log Age and log $E_{p,cpl}$ is

$$\log \text{Age} = (-0.69 \pm 0.19) \times \log E_{p,cpl} + (4.3 \pm 0.47), \quad (34)$$

where $E_{p,cpl}$ is in units of keV. Age is in units of Myr. The adjusted R^2 is 0.24. The Pearson coefficient is −0.39 ± 0.1 with p-value 2.2 × 10^{-2}. The Spearman coefficient is −0.39 ± 0.11 with p-value 1.9 × 10^{-2}. The Kendall τ coefficient is −0.27 ± 0.077 with p-value 2.1 × 10^{-2}. The correlation ratio is 0.24 ± 0.049. The cosine similarity is 0.92 ± 0.0086. The scatter plot is in Figure 24. The number of GRBs in the sample is 35.

The correlation between log Age and log $E_{p,cpl,i}$ is

$$\log \text{Age} = (-0.81 \pm 0.16) \times \log E_{p,cpl,i} + (4.8 \pm 0.43), \quad (35)$$

where Age is in units of Myr. $E_{p,cpl,i}$ is in units of keV. The adjusted R^2 is 0.39. The Pearson coefficient is −0.5 ± 0.087 with p-value 2.1 × 10^{-3}. The Spearman coefficient is −0.51 ± 0.094 with p-value 1.8 × 10^{-3}. The Kendall τ coefficient is −0.36 ± 0.071 with p-value 2.3 × 10^{-3}. The correlation ratio is 0.069 ± 0.042. The cosine similarity is 0.91 ± 0.0086. The scatter plot is in Figure 24. The number of GRBs in the sample is 35. This interesting correlation might be counterevidence for the two origins of GRBs. SGRBs are from mergers of double compact objects, which need a longer time for evolution, and consequently, are in older galaxies. SGRBs are harder in spectrum, and the peak energy $E_{p,cpl,i}$ should be higher. Therefore, the age should be positively correlated to the peak energy, while Equation (35) shows the contrary.

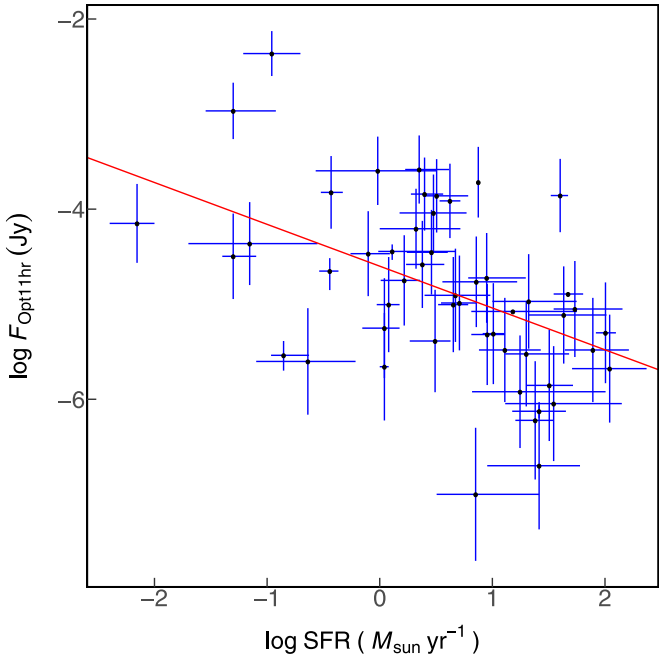

Figure 23. Scatter plot for $\log F_{\rm Opt11hr}$ and log SFR. The red line is our fit result. The formula for the red line is $\log F_{\rm Opt11hr} = (-0.44 \pm 0.073) \times \log {\rm SFR} + (-4.6 \pm 0.074)$. The description of every parameter is in Section 2.

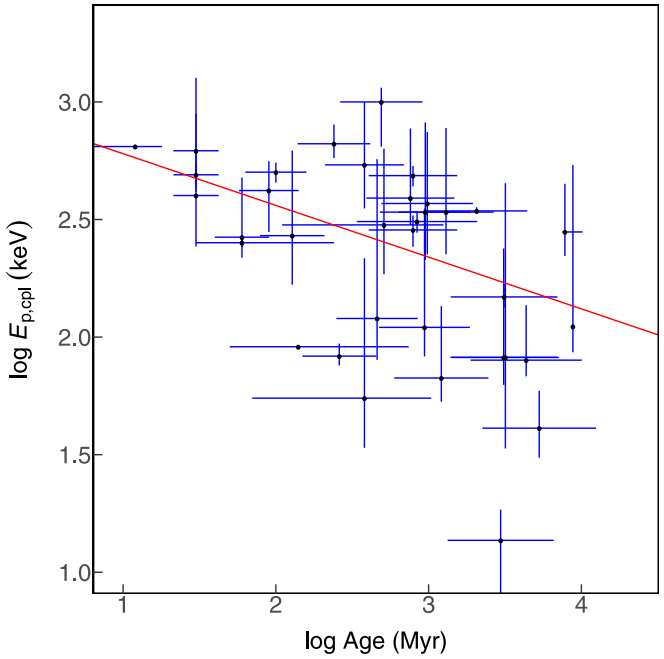

Figure 24. Scatter plot for log Age and $\log E_{\rm p,cpl}$. The red line is our fit result. The formula for the red line is $\log {\rm Age} = (-0.69 \pm 0.19) \times \log E_{\rm p,cpl} + (4.3 \pm 0.47)$. The description of every parameter is in Section 2.

5.5. Correlations about HR

5.5.1. Correlations with HR

The correlation between $-\alpha_{\rm spl}$ and log HR is

$$(-\alpha_{\rm spl}) = (-0.55 \pm 0.021) \times \log {\rm HR} + (2.1 \pm 0.017), \quad (36)$$

and the adjusted R^2 is 0.69. The Pearson coefficient is -0.73 ± 0.016 with p-value 1.6×10^{-148}. The Spearman coefficient is -0.78 ± 0.011 with p-value 1.9×10^{-176}. The Kendall τ coefficient is -0.6 ± 0.01 with p-value 8.4×10^{-158}. The correlation ratio is 0.71 ± 0.0043. The cosine similarity is 0.59 ± 0.0093. The scatter plot is in Figure 36. The number of GRBs in the sample is 874. This just shows the consistency of the spectrum. The outliers and the width show that the HR itself is not good enough to present information on the spectrum. All correlations in this section show similar information.

The correlation between $\log E_{\rm p,cpl}$ and log HR is

$$\log E_{\rm p,cpl} = (0.54 \pm 0.013) \times \log {\rm HR} + (2.1 \pm 0.0084), \quad (37)$$

where $E_{\rm p,cpl}$ is in units of keV. The adjusted R^2 is 0.65. The Pearson coefficient is 0.69 ± 0.014 with p-value 3.8×10^{-211}. The Spearman coefficient is 0.78 ± 0.0094 with p-value 6.5×10^{-305}. The Kendall τ coefficient is 0.61 ± 0.0083 with p-value 1.1×10^{-267}. The correlation ratio is 0.86 ± 0.0023. The cosine similarity is 0.67 ± 0.008. The scatter plot is in Figure 27. The number of GRBs in the sample is 1469.

The correlation between $\log E_{\rm p,cpl,i}$ and log HR is

$$\log E_{\rm p,cpl,i} = (0.55 \pm 0.036) \times \log {\rm HR} + (2.6 \pm 0.018), \quad (38)$$

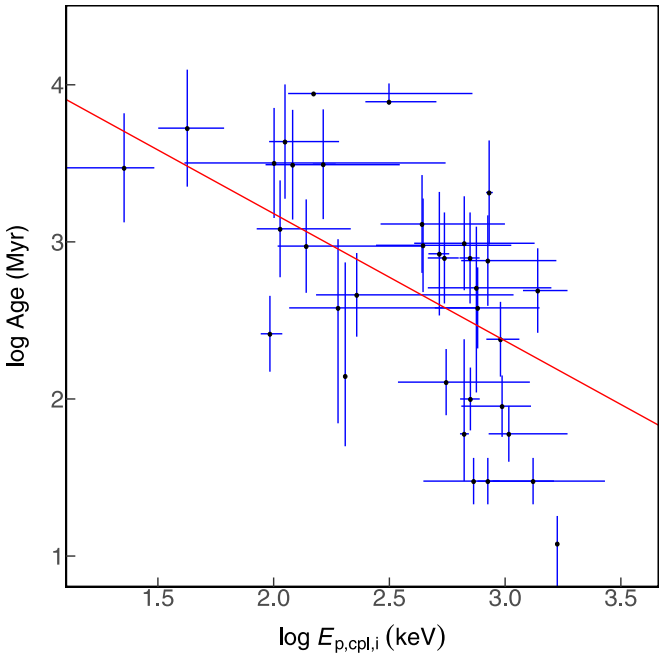

Figure 25. Scatter plot for log Age and $\log E_{\rm p,cpl,i}$. The red line is our fit result. The formula for the red line is $\log {\rm Age} = (-0.81 \pm 0.16) \times \log E_{\rm p,cpl,i} + (4.8 \pm 0.43)$. The description of every parameter is in Section 2.

where $E_{\rm p,cpl,i}$ is in units of keV. The adjusted R^2 is 0.6. The Pearson coefficient is 0.63 ± 0.03 with p-value 4.3×10^{-27}. The Spearman coefficient is 0.68 ± 0.028 with p-value 1.9×10^{-32}. The Kendall τ coefficient is 0.49 ± 0.023 with p-value 2.2×10^{-28}. The correlation ratio is 0.93 ± 0.0032. The cosine similarity is 0.38 ± 0.026. The scatter plot is in Figure 28. The number of GRBs in the sample is 229.

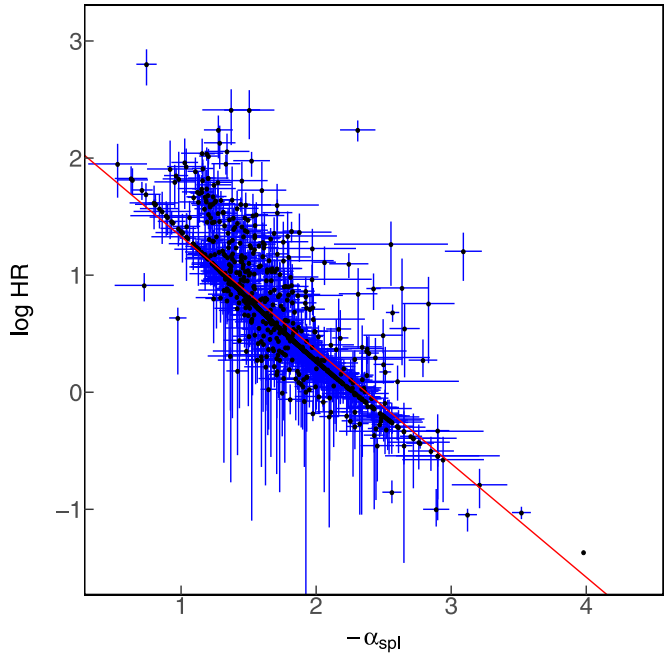

Figure 26. Scatter plot for $-\alpha_{spl}$ and log HR. The red line is our fit result. The formula for the red line is $(-\alpha_{spl}) = (-0.55 \pm 0.021) \times \log \mathrm{HR} + (2.1 \pm 0.017)$. The description of every parameter is in Section 2.

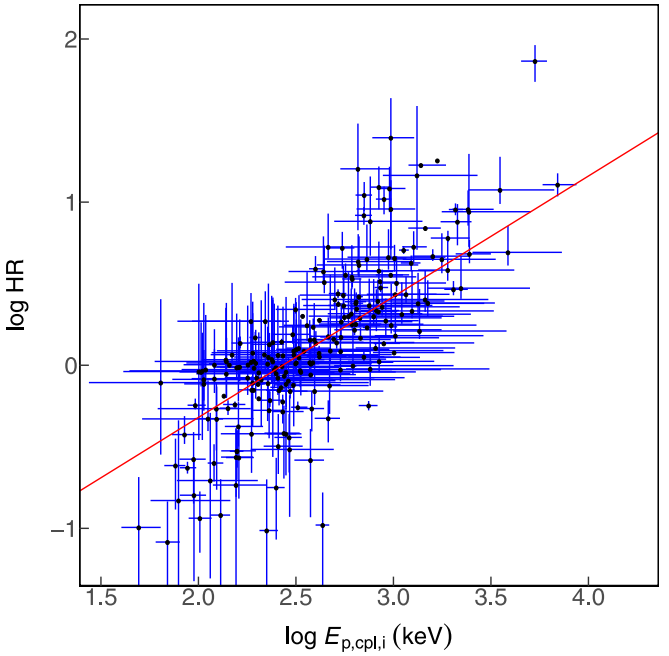

Figure 28. Scatter plot for $\log E_{p,cpl,i}$ and log HR. The red line is our fit result. The formula for the red line is $\log E_{p,cpl,i} = (0.55 \pm 0.036) \times \log \mathrm{HR} + (2.6 \pm 0.018)$. The description of every parameter is in Section 2.

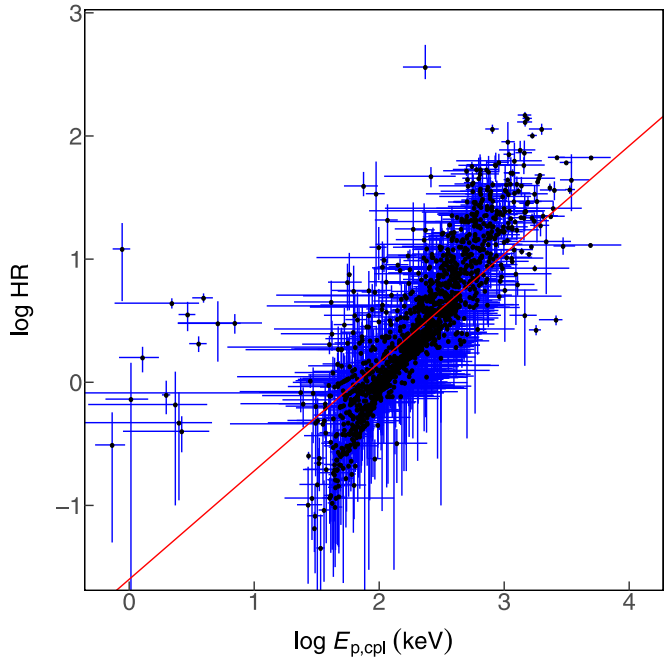

Figure 27. Scatter plot for $\log E_{p,cpl}$ and log HR. The red line is our fit result. The formula for the red line is $\log E_{p,cpl} = (0.54 \pm 0.013) \times \log \mathrm{HR} + (2.1 \pm 0.0084)$. The description of every parameter is in Section 2.

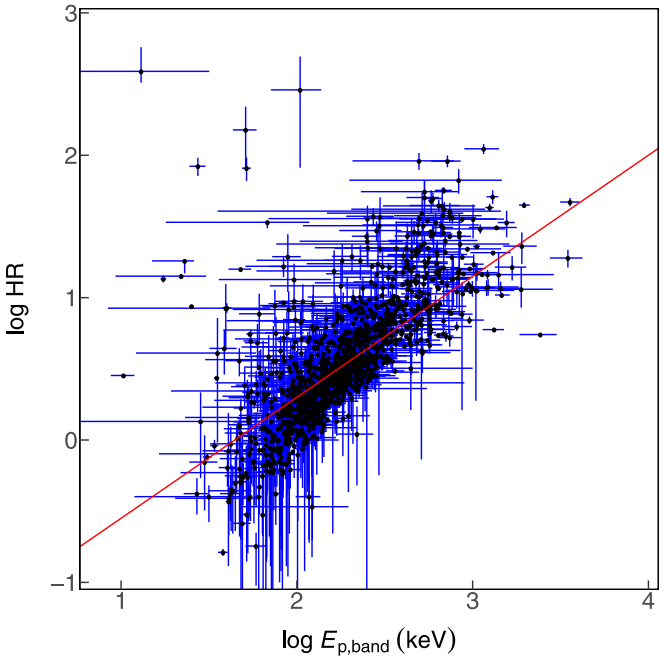

Figure 29. Scatter plot for $\log E_{p,Band}$ and log HR. The red line is our fit result. The formula for the red line is $\log E_{p,Band} = (0.47 \pm 0.017) \times \log \mathrm{HR} + (2 \pm 0.01)$. The description of every parameter is in Section 2.

The correlation between $\log E_{p,Band}$ and log HR is

$$\log E_{p,Band} = (0.47 \pm 0.017) \times \log \mathrm{HR} + (2 \pm 0.01), \quad (39)$$

where $E_{p,Band}$ is in units of keV. The adjusted R^2 is 0.51. The Pearson coefficient is 0.63 ± 0.017 with p-value 5.2×10^{-149}. The Spearman coefficient is 0.72 ± 0.01 with p-value 2.3×10^{-214}. The Kendall τ coefficient is 0.56 ± 0.0081 with p-value 5.9×10^{-207}. The correlation ratio is 0.9 ± 0.0021. The cosine similarity is 0.81 ± 0.0079. The scatter plot is in Figure 29. The number of GRBs in the sample is 1332.

The correlation between $\log E_{p,Band,i}$ and log HR is

$$\log E_{p,Band,i} = (0.58 \pm 0.066) \times \log \mathrm{HR} + (2.4 \pm 0.041), \quad (40)$$

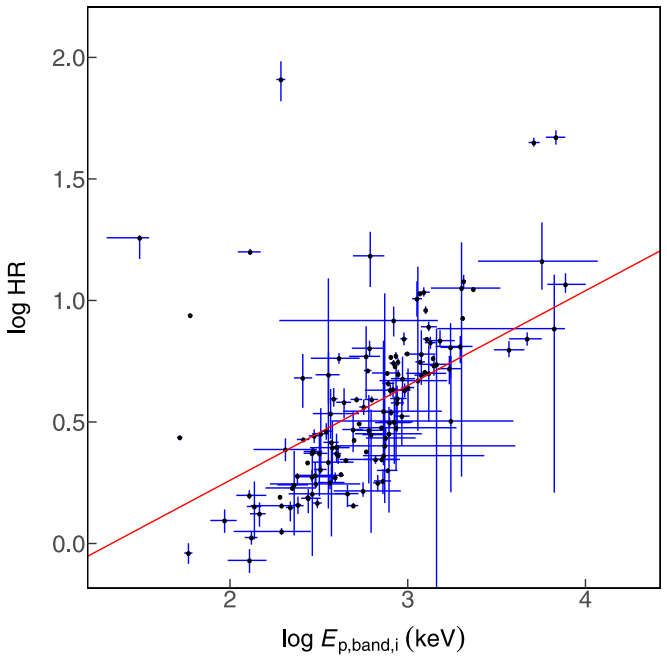

Figure 30. Scatter plot for $\log E_{\rm p,Band,i}$ and log HR. The red line is our fit result. The formula for the red line is $\log E_{\rm p,Band,i} = (0.58 \pm 0.066) \times \log {\rm HR} + (2.4 \pm 0.041)$. The description of every parameter is in Section 2.

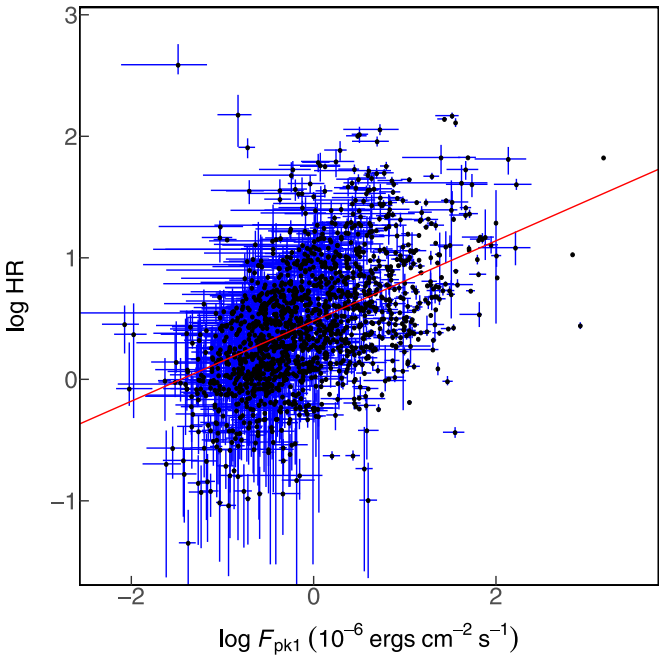

Figure 31. Scatter plot for $\log F_{\rm pk1}$ and log HR. The red line is our fit result. The formula for the red line is $\log F_{\rm pk1} = (0.6 \pm 0.017) \times \log {\rm HR} + (-0.34 \pm 0.0094)$. The description of every parameter is in Section 2.

where $E_{\rm p,Band,i}$ is in units of keV. The adjusted R^2 is 0.3. The Pearson coefficient is 0.48 ± 0.045 with p-value 4.6×10^{-9}. The Spearman coefficient is 0.6 ± 0.035 with p-value 1.4×10^{-14}. The Kendall τ coefficient is 0.47 ± 0.028 with p-value 4×10^{-16}. The correlation ratio is 0.94 ± 0.0025. The cosine similarity is 0.87 ± 0.013. The scatter plot is in Figure 30. The number of GRBs in the sample is 136.

5.5.2. Correlations between Parameters Related with HR or Peak Energies

The correlation between $\log F_{\rm pk1}$ and log HR is

$$\log F_{\rm pk1} = (0.6 \pm 0.017) \times \log {\rm HR} + (-0.34 \pm 0.0094), \quad (41)$$

where $F_{\rm pk1}$ is the peak energy flux in the 1 s time bin in the rest-frame 1–10^4 keV energy band and is in units of 10^{-6} erg cm^{-2} s^{-1}. The adjusted R^2 is 0.26. The Pearson coefficient is 0.45 ± 0.011 with p-value 3.9×10^{-75}. The Spearman coefficient is 0.47 ± 0.01 with p-value 7.9×10^{-83}. The Kendall τ coefficient is 0.33 ± 0.0073 with p-value 4.2×10^{-79}. The correlation ratio is 0.37 ± 0.0044. The cosine similarity is 0.29 ± 0.011. The scatter plot is in Figure 31. The number of GRBs in the sample is 1494. Although there is a correlation, one could say that it is just a weak tendency.

Mallozzi et al. (1995) found a correlation between the mean peak energies and the 256 ms peak photon flux $P_{\rm pk2}$. After accumulating more data, we found that $P_{\rm pk2}$ and the peak energy, except for $P_{\rm pk4}$ and $E_{\rm p,Band}$, have no obvious correlation with adjusted R^2 smaller than 0.1.

The correlation between $\log E_{\rm p,Band}$ and $\log P_{\rm pk4}$ is

$$\log E_{\rm p,Band} = (0.28 \pm 0.03) \times \log P_{\rm pk4} + (1.8 \pm 0.033), \quad (42)$$

where $P_{\rm pk4}$ is the peak photon flux in the 1 s time bin in 10–1000 keV and is in units of photons cm^{-2} s^{-1}. $E_{\rm p,Band}$ is in units of keV. The adjusted R^2 is 0.19. The Pearson coefficient is 0.4 ± 0.032 with p-value 1.9×10^{-8}. The Spearman coefficient is 0.46 ± 0.024 with p-value 4.5×10^{-11}. The Kendall τ coefficient is 0.31 ± 0.017 with p-value 3.4×10^{-10}. The correlation ratio is 0.71 ± 0.0087. The cosine similarity is 0.81 ± 0.017. The scatter plot is in Figure 32. The number of GRBs in the sample is 181. As one can see from the figure, even this relation is not very tight. One would say there is not much correlation between the peak energies in spectra and peak photon fluxes in LCs.

Conversely, we found a tighter correlation between the peak energy flux and peak energy. The peak energy flux can be calculated from the peak photon flux, so this correlation is natural.

The correlation between $\log E_{\rm p,cpl}$ and $\log F_{\rm pk1}$ is

$$\log E_{\rm p,cpl} = (0.31 \pm 0.012) \times \log F_{\rm pk1} + (2.3 \pm 0.0067), \quad (43)$$

where $F_{\rm pk1}$ is the peak energy flux in the 1 s time bin in the rest-frame 1–10^4 keV energy band and is in units of 10^{-6} erg cm^{-2} s^{-1}. $E_{\rm p,cpl}$ is in units of keV. The adjusted R^2 is 0.33. The Pearson coefficient is 0.48 ± 0.018 with p-value 1.7×10^{-43}. The Spearman coefficient is 0.47 ± 0.018 with p-value 1.6×10^{-42}. The Kendall τ coefficient is 0.33 ± 0.013 with p-value 3.4×10^{-42}. The correlation ratio is 0.9 ± 0.0014. The cosine similarity is -0.22 ± 0.0083. The

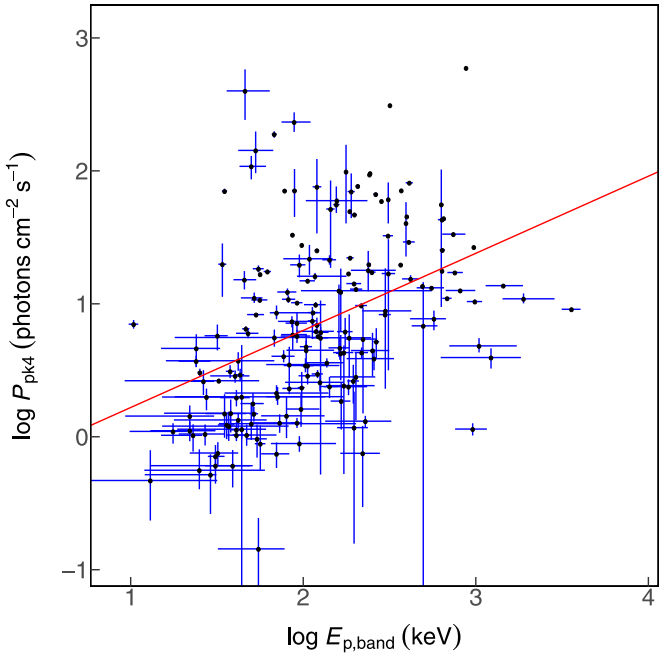

Figure 32. Scatter plot for $\log E_{\rm p,Band}$ and $\log P_{\rm pk4}$. The red line is our fit result. The formula for the red line is $\log E_{\rm p,Band} = (0.28 \pm 0.03) \times \log P_{\rm pk4} + (1.8 \pm 0.033)$. The description of every parameter is in Section 2.

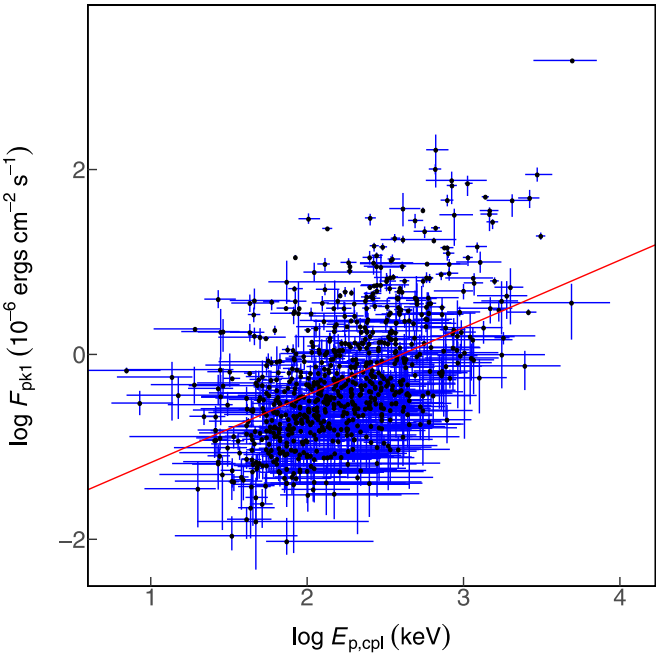

Figure 33. Scatter plot for $\log E_{\rm p,cpl}$ and $\log F_{\rm pk1}$. The red line is our fit result. The formula for the red line is $\log E_{\rm p,cpl} = (0.31 \pm 0.012) \times \log F_{\rm pk1} + (2.3 \pm 0.0067)$. The description of every parameter is in Section 2.

scatter plot is in Figure 33. The number of GRBs in the sample is 749.

The correlation between $\log E_{\rm p,Band}$ and $\log F_{\rm pk2}$ is

$$\log E_{\rm p,Band} = (0.28 \pm 0.012) \times \log F_{\rm pk2} + (2.2 \pm 0.0049), \quad (44)$$

where $F_{\rm pk2}$ is the peak energy flux in the 64 ms time bin in the rest-frame 1–10^4 keV energy band and is in units of 10^{-6} erg cm^{-2} s^{-1}. $E_{\rm p,Band}$ is in units of keV. The adjusted R^2 is 0.33. The Pearson coefficient is 0.5 ± 0.015 with p-value 1.1×10^{-73}. The Spearman coefficient is 0.52 ± 0.012 with p-value 6.7×10^{-81}. The Kendall τ coefficient is 0.36 ± 0.009 with p-value 1.5×10^{-75}. The correlation ratio is 0.89 ± 0.0024. The cosine similarity is 0.4 ± 0.015. The scatter plot is in Figure 34. The number of GRBs in the sample is 1168. One can see from these two figures that the data are still widely distributed. What's more, as the flux is the energy of the photons multiplied by the number of photons, the flux contains information from the spectrum. Therefore, these two correlations do not reveal more information.

5.6. Correlations with the Lorentz Factor Γ_0

The correlation between $\log \Gamma_0$ and $\log E_{\rm iso}$ is

$$\log \Gamma_0 = (0.35 \pm 0.014) \times \log E_{\rm iso} + (1.9 \pm 0.018), \quad (45)$$

where $E_{\rm iso}$ is in units of 10^{52} erg and in the rest-frame 1–10^4 keV energy band. The adjusted R^2 is 0.58. The Pearson coefficient is 0.75 ± 0.016 with p-value 1.9×10^{-10}. The Spearman coefficient is 0.68 ± 0.02 with p-value 4.4×10^{-8}. The Kendall τ coefficient is 0.52 ± 0.019 with p-value 9.5×10^{-8}. The correlation ratio is 0.67 ± 0.0065. The cosine similarity is 0.79 ± 0.013. The scatter plot is in Figure 35. The number of GRBs in the sample is 51. Previous studies gave $\log \Gamma_0 = (0.269 \pm 0.002) \log E_{\rm iso,52} + (2.291 \pm 0.002)$ with 19 samples (Liang et al. 2010) and $\log \Gamma_0 = (0.29 \pm 0.002) \log E_{\rm iso,52} + (1.96 \pm 0.002)$ with 38 samples (Lü et al. 2012), which are shown here for comparison.[9] The positive correlation shows that stronger burstsare likely to produce faster ejecta, which might reveal the acceleration mechanism of the central engine.

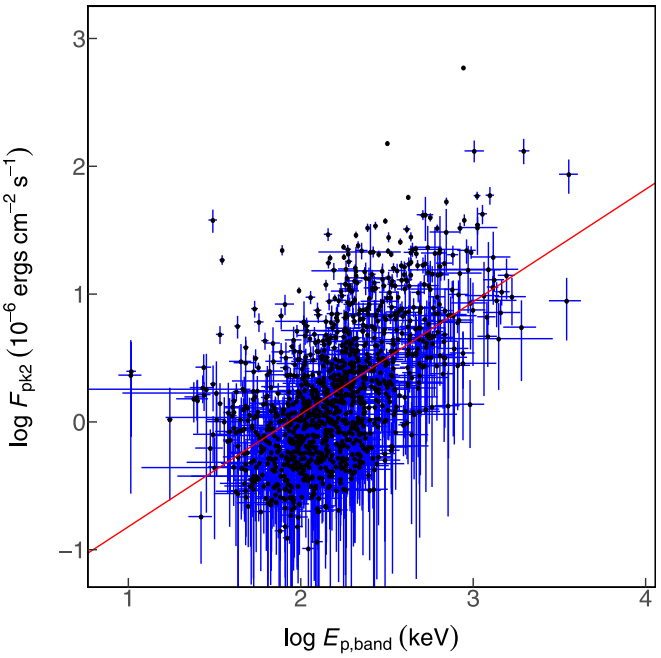

Figure 34. Scatter plot for $\log E_{\rm p,Band}$ and $\log F_{\rm pk2}$. The red line is our fit result. The formula for the red line is $\log E_{\rm p,Band} = (0.28 \pm 0.012) \times \log F_{\rm pk2} + (2.2 \pm 0.0049)$. The description of every parameter is in Section 2.

[9] Note that the notation $Q_x \equiv Q/10^x$ is used throughout this paper, and it is in cgs units by default if they are not defined explicitly.

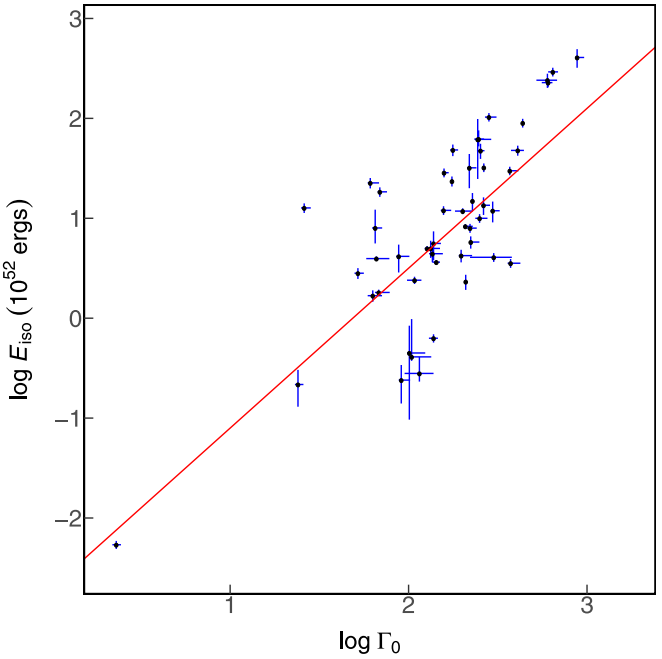

Figure 35. Scatter plot for $\log \Gamma_0$ and $\log E_{\rm iso}$. The red line is our fit result. The formula for the red line is $\log \Gamma_0 = (0.35 \pm 0.014) \times \log E_{\rm iso} + (1.9 \pm 0.018)$. The description of every parameter is in Section 2. The outlier is GRB 060218A.

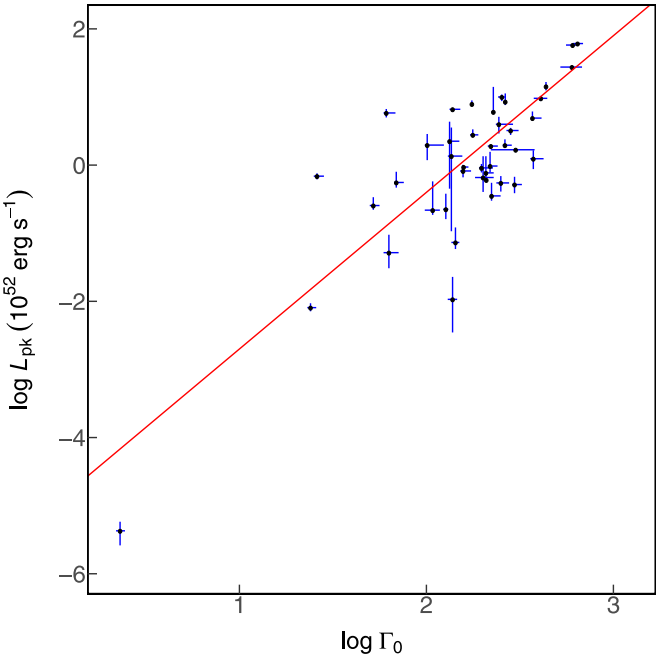

Figure 36. Scatter plot for $\log \Gamma_0$ and $\log L_{\rm pk}$. The red line is our fit result. The formula for the red line is $\log \Gamma_0 = (0.29 \pm 0.011) \times \log L_{\rm pk} + (2.2 \pm 0.01)$. The description of every parameter is in Section 2. The outlier is GRB 060218A with lowest $L_{\rm pk}$ and Γ_0.

The correlation between $\log \Gamma_0$ and $\log L_{\rm pk}$ is

$$\log \Gamma_0 = (0.29 \pm 0.011) \times \log L_{\rm pk} + (2.2 \pm 0.01), \quad (46)$$

where $L_{\rm pk}$ is in units of $10^{52}\,{\rm erg\,s^{-1}}$ and is in the 1–10^4 keV energy band. The adjusted R^2 is 0.66. The Pearson coefficient is 0.81 ± 0.015 with p-value 1.1×10^{-10}. The Spearman coefficient is 0.63 ± 0.031 with p-value 7×10^{-6}. The Kendall τ coefficient is 0.47 ± 0.027 with p-value 1×10^{-5}. The correlation ratio is 0.77 ± 0.0061. The cosine similarity is 0.16 ± 0.026. The scatter plot is in Figure 36. The number of GRBs in the sample is 42. A previous study gave $\log \Gamma_0 = (0.28 \pm 0.002) \log L_{\rm iso,52} + (2.39 \pm 0.003)$ with 38 samples (Lü et al. 2012). This correlation is related to Equation (45).

The correlation between $\log \Gamma_0$ and $\log t_{\rm pkOpt,i}$ is

$$\log \Gamma_0 = (-0.49 \pm 0.011) \times \log t_{\rm pkOpt,i} + (3.2 \pm 0.026), \quad (47)$$

where $t_{\rm pkOpt,i}$ is in units of s. The adjusted R^2 is 0.66. The Pearson coefficient is -0.81 ± 0.011 with p-value 1.5×10^{-11}. The Spearman coefficient is -0.64 ± 0.019 with p-value 2.6×10^{-6}. The Kendall τ coefficient is -0.48 ± 0.019 with p-value 3.5×10^{-6}. The correlation ratio is 0.019 ± 0.0085. The cosine similarity is 0.9 ± 0.0016. The scatter plot is in Figure 37. The number of GRBs in the sample is 45. A previous study gave $\log \Gamma_0 = (-0.63 \pm 0.04) \times \log t_{\rm pkOpt,i} + (3.69 \pm 0.09)$ with 19 samples (Liang et al. 2010; note that two of them are the peak times in X-rays). The anticorrelation mainly reveals how the GRB jets are decelerated by the circumburst environment. Noticing that the deceleration time is also related to the profile of the density of the environment, the correlation here might not be very tight.

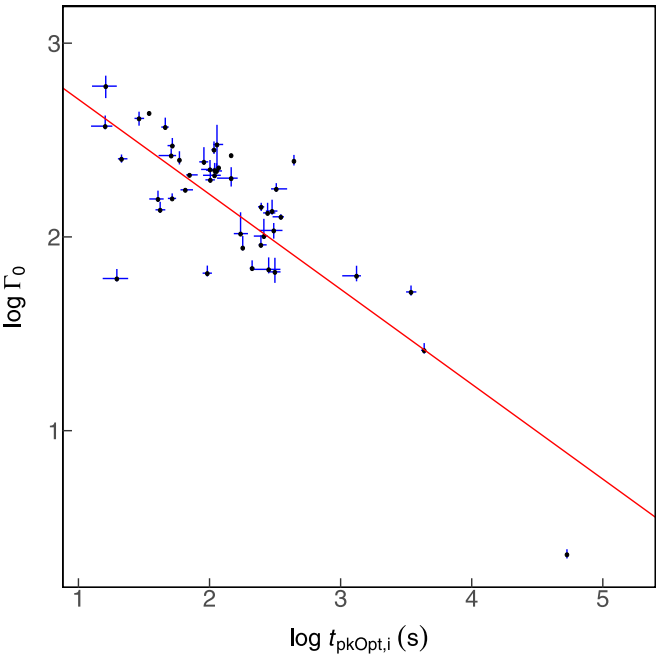

Figure 37. Scatter plot for $\log \Gamma_0$ and $\log t_{\rm pkOpt,i}$. The red line is our fit result. The formula for the red line is $\log \Gamma_0 = (-0.49 \pm 0.011) \times \log t_{\rm pkOpt,i} + (3.2 \pm 0.026)$. The description of every parameter is in Section 2. The outlier is GRB 060218A.

The correlation between $\log \Gamma_0$ and $\log t_{\rm pkOpt}$ is

$$\log \Gamma_0 = (-0.48 \pm 0.012) \times \log t_{\rm pkOpt} + (3.4 \pm 0.033), \quad (48)$$

where $t_{\rm pkOpt}$ is in units of s. The adjusted R^2 is 0.56. The Pearson coefficient is -0.75 ± 0.012 with p-value 3.4×10^{-9}. The Spearman coefficient is -0.59 ± 0.022 with p-value

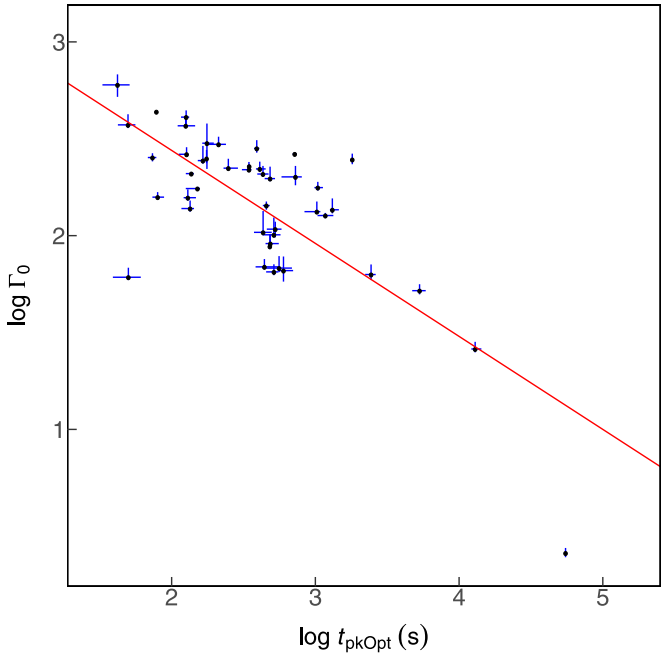

Figure 38. Scatter plot for $\log \Gamma_0$ and $\log t_{\rm pkOpt}$. The red line is our fit result. The formula for the red line is $\log \Gamma_0 = (-0.48 \pm 0.012) \times \log t_{\rm pkOpt} + (3.4 \pm 0.033)$. The description of every parameter is in Section 2. The outlier is GRB 060218A.

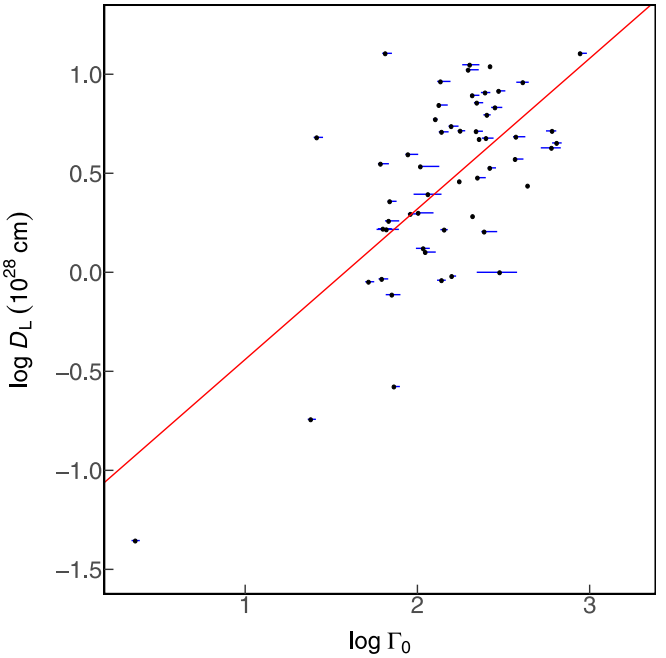

Figure 39. Scatter plot for $\log \Gamma_0$ and $\log D_{\rm L}$. The red line is our fit result. The formula for the red line is $\log \Gamma_0 = (0.58 \pm 0.0095) \times \log D_{\rm L} + (1.9 \pm 0.0074)$. The description of every parameter is in Section 2. The outlier is GRB 060218A.

2.4×10^{-5}. The Kendall τ coefficient is -0.44 ± 0.021 with p-value 1.8×10^{-5}. The correlation ratio is 0.38 ± 0.0084. The cosine similarity is 0.93 ± 0.0012. The scatter plot is in Figure 38. The number of GRBs in the sample is 45. This correlation is clearly worse than the previous one shown in Equation (47), which has the redshift correction. It implies that the correlation between Γ_0 and $t_{\rm pkOpt,i}$ is intrinsic, and the time dilation due to redshift goes against the correlation.

The correlation between $\log \Gamma_0$ and $\log D_{\rm L}$ is

$$\log \Gamma_0 = (0.58 \pm 0.0095) \times \log D_{\rm L} + (1.9 \pm 0.0074), \quad (49)$$

where $D_{\rm L}$ is in units of 10^{28} cm. The adjusted R^2 is 0.43. The Pearson coefficient is 0.67 ± 0.01 with p-value 2.6×10^{-8}. The Spearman coefficient is 0.5 ± 0.019 with p-value 9.6×10^{-5}. The Kendall τ coefficient is 0.35 ± 0.014 with p-value 1.5×10^{-4}. The correlation ratio is 0.89 ± 0.00096. The cosine similarity is 0.78 ± 0.0014. The scatter plot is in Figure 39. The number of GRBs in the sample is 55. The dependence on distance indicates observational bias that the low-Γ_0 GRBs might not be observable at longer distance. The other possibility is that the GRBs that exploded earlier do have higher Γ_0.

The correlation between $\log \Gamma_0$ and $\log t_{\rm radio,pk}$ is

$$\log \Gamma_0 = (1.5 \pm 0.14) \times \log t_{\rm radio,pk} + (-6.5 \pm 0.81), \quad (50)$$

where $t_{\rm radio,pk}$ is in units of s. The adjusted R^2 is 0.39. The Pearson coefficient is 0.64 ± 0.05 with p-value 2.4×10^{-2}. The Spearman coefficient is 0.49 ± 0.086 with p-value 0.11. The Kendall τ coefficient is 0.37 ± 0.081 with p-value 0.1. The correlation ratio is 0.96 ± 0.0013. The cosine similarity is 0.97 ± 0.0013. The scatter plot is in Figure 40. The number of GRBs in the sample is 12. Interestingly, unlike Equation (47), Γ_0 here is positively correlated with $t_{\rm radio,pk}$. As $t_{\rm radio,pk}$ does not represent the deceleration time, a higher Γ_0 may correspond to higher kinetic energy, and the radio emission lasts longer.

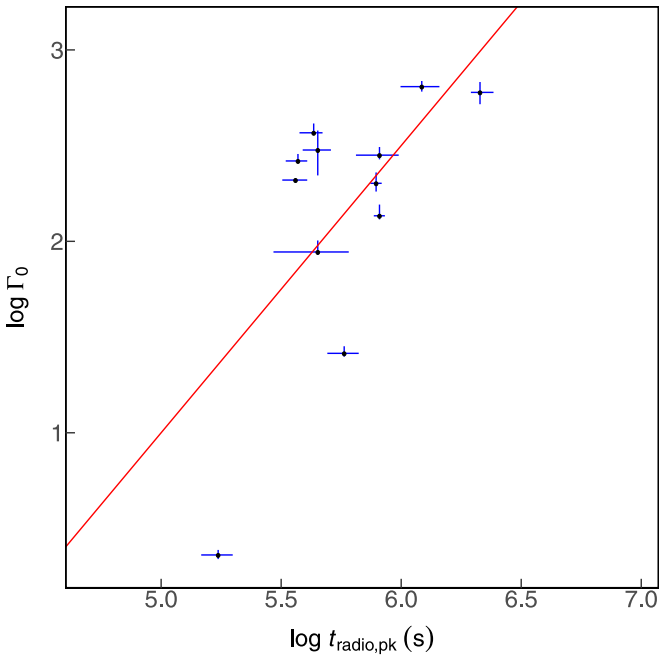

Figure 40. Scatter plot for $\log \Gamma_0$ and $\log t_{\rm radio,pk}$. The red line is our fit result. The formula for the red line is $\log \Gamma_0 = (1.5 \pm 0.14) \times \log t_{\rm radio,pk} + (-6.5 \pm 0.81)$. The description of every parameter is in Section 2.

The correlation between $\log \Gamma_0$ and $\log E_{\rm p,cpl,i}$ is

$$\log \Gamma_0 = (0.52 \pm 0.084) \times \log E_{\rm p,cpl,i} + (0.71 \pm 0.22), \quad (51)$$

where $E_{\rm p,cpl,i}$ is in units of keV. The adjusted R^2 is 0.31. The Pearson coefficient is 0.53 ± 0.061 with p-value 9.9×10^{-3}.

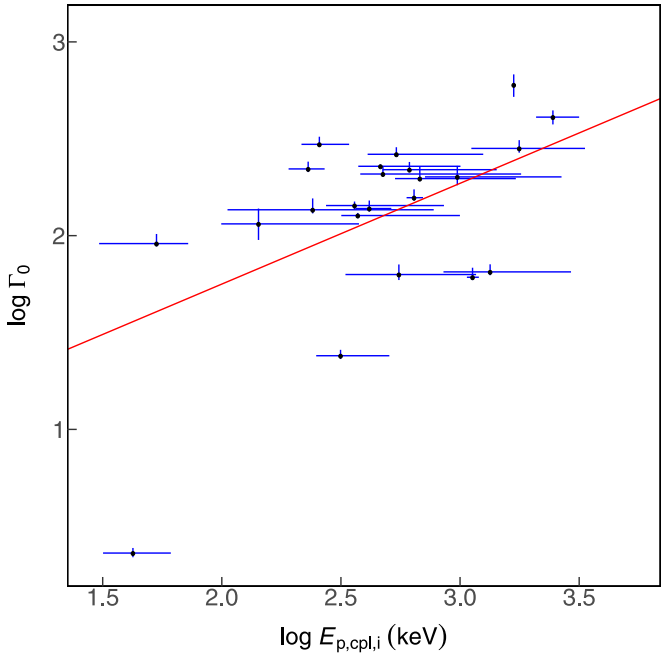

Figure 41. Scatter plot for log Γ_0 and log $E_{\rm p,cpl,i}$. The red line is our fit result. The formula for the red line is $\log \Gamma_0 = (0.52 \pm 0.084) \times \log E_{\rm p,cpl,i} + (0.71 \pm 0.22)$. The description of every parameter is in Section 2.

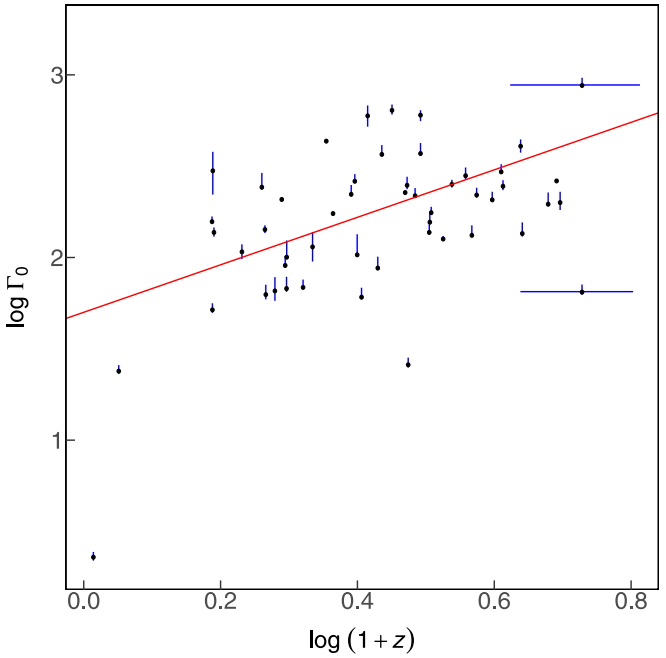

Figure 42. Scatter plot for log Γ_0 and $\log(1+z)$. The red line is our fit result. The formula for the red line is $\log \Gamma_0 = (1.3 \pm 0.071) \times \log(1+z) + (1.7 \pm 0.03)$. The description of every parameter is in Section 2. The outlier is GRB 060218A.

The Spearman coefficient is 0.38 ± 0.087 with p-value 7.7×10^{-2}. The Kendall τ coefficient is 0.27 ± 0.07 with p-value 6.8×10^{-2}. The correlation ratio is 0.52 ± 0.031. The cosine similarity is 0.98 ± 0.0028. The scatter plot is in Figure 41. The number of GRBs in the sample is 23. As Γ_0 is related to $E_{\rm iso}$ (as shown in Equation (45)), and $E_{\rm iso}$ is related to $E_{\rm p}$ (as shown in Equation (17)), it is not surprising that Γ_0 is related to $E_{\rm p}$.

The correlation between log Γ_0 and $\log(1+z)$ is

$$\log \Gamma_0 = (1.3 \pm 0.071) \times \log(1+z) + (1.7 \pm 0.03), \quad (52)$$

the adjusted R^2 is 0.25. The Pearson coefficient is 0.52 ± 0.024 with p-value 9.8×10^{-5}. The Spearman coefficient is 0.42 ± 0.026 with p-value 2.3×10^{-3}. The Kendall τ coefficient is 0.29 ± 0.018 with p-value 2.9×10^{-3}. The correlation ratio is 0.94 ± 0.0011. The cosine similarity is 0.95 ± 0.0026. The scatter plot is in Figure 42. The number of GRBs in the sample is 51. This might be a selection effect, that farther GRBs can be observed only if they are stronger and have faster jets. Otherwise, this may indicate that the properties of GRBs evolve with cosmic time. This relation is intrinsically the same as that shown in Equation (49).

The correlation between log Γ_0 and log Mass is

$$\log \Gamma_0 = (0.3 \pm 0.052) \times \log \text{Mass} + (-0.71 \pm 0.49), \quad (53)$$

where Mass is in units of $M_\odot$. The adjusted R^2 is 0.25. The Pearson coefficient is 0.52 ± 0.058 with p-value 3.3×10^{-2}. The Spearman coefficient is 0.35 ± 0.1 with p-value 0.17. The Kendall τ coefficient is 0.26 ± 0.078 with p-value 0.14. The correlation ratio is 0.98 ± 0.0029. The cosine similarity is 0.98 ± 0.0017. The scatter plot is in Figure 43. The number of GRBs in the sample is 17. This weak correlation may imply that stronger GRBs are harbored in more massive host galaxies.

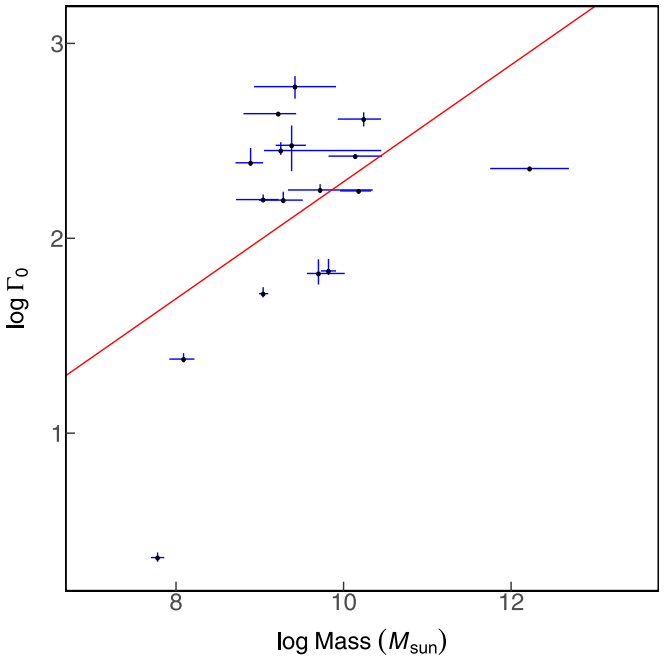

Figure 43. Scatter plot for log Γ_0 and log Mass. The red line is our fit result. The formula for the red line is $\log \Gamma_0 = (0.3 \pm 0.052) \times \log \text{Mass} + (-0.71 \pm 0.49)$. The description of every parameter is in Section 2. The outlier is GRB 060218A.

5.7. Some Correlations with t_{pkX}

$t_{\rm pkX}$ is the peak time in the X-ray LC. It is often taken as the time of the ejecta deceleration by the circumburst medium. It

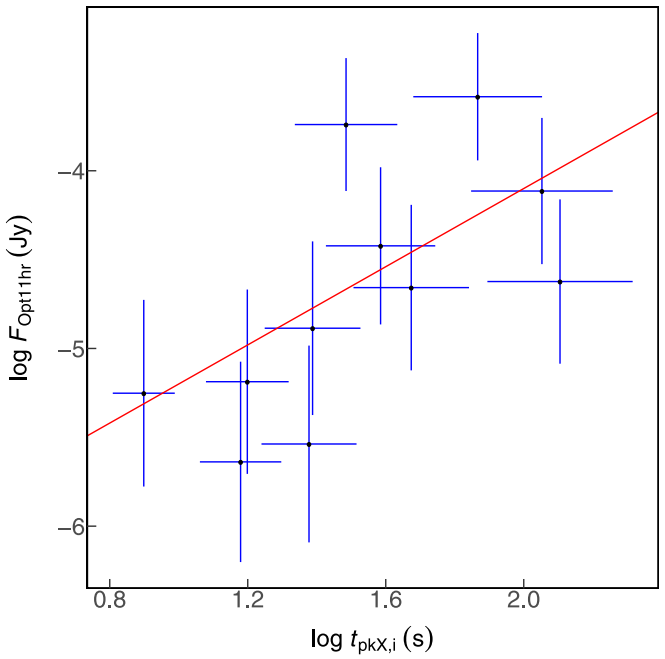

Figure 44. Scatter plot for $\log F_{\rm Opt11hr}$ and $\log t_{\rm pkX,i}$. The red line is our fit result. The formula for the red line is $\log F_{\rm Opt11hr} = (1.1 \pm 0.44) \times \log t_{\rm pkX,i} + (-6.3 \pm 0.71)$. The description of every parameter is in Section 2.

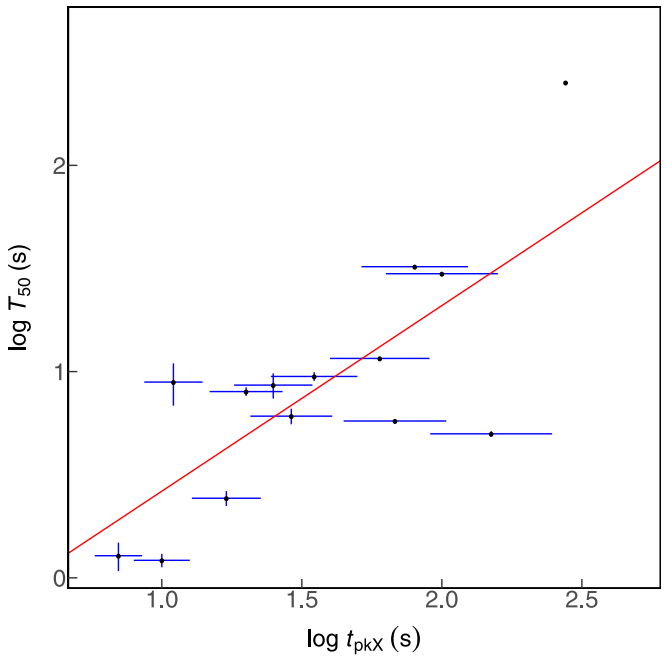

Figure 45. Scatter plot for $\log T_{50}$ and $\log t_{\rm pkX}$. The red line is our fit result. The formula for the red line is $\log T_{50} = (0.9 \pm 0.12) \times \log t_{\rm pkX} + (-0.48 \pm 0.17)$. The description of every parameter is in Section 2.

mainly reveals information on the initial Lorentz factor and the number density of the circumburst medium.

The correlation between $\log F_{\rm Opt11hr}$ and $\log t_{\rm pkX,i}$ is

$$\log F_{\rm Opt11hr} = (1.1 \pm 0.44) \times \log t_{\rm pkX,i} + (-6.3 \pm 0.71), \quad (54)$$

where $F_{\rm Opt11hr}$ is in units of Jy. $t_{\rm pkX,i}$ is in units of s. The adjusted R^2 is 0.36. The Pearson coefficient is 0.5 ± 0.17 with p-value 0.11. The Spearman coefficient is 0.54 ± 0.18 with p-value 8.9×10^{-2}. The Kendall τ coefficient is 0.39 ± 0.15 with p-value 0.1. The correlation ratio is 0.98 ± 0.0049. The cosine similarity is -0.94 ± 0.014. The scatter plot is in Figure 44. The number of GRBs in the sample is 11. As the afterglow fades after the deceleration time, and the deceleration time is generally shorter than 11 hr, as shown in Figure 44, the optical afterglow might be brighter if it is closer to the deceleration time. Therefore, $F_{\rm Opt11hr}$ is roughly proportional to $t_{\rm pkX,i}$.

The correlation between $\log T_{50}$ and $\log t_{\rm pkX}$ is

$$\log T_{50} = (0.9 \pm 0.12) \times \log t_{\rm pkX} + (-0.48 \pm 0.17), \quad (55)$$

where T_{50} is in units of s. $t_{\rm pkX}$ is in units of s. The adjusted R^2 is 0.57. The Pearson coefficient is 0.74 ± 0.058 with p-value 2.4×10^{-3}. The Spearman coefficient is 0.6 ± 0.076 with p-value 2.2×10^{-2}. The Kendall τ coefficient is 0.47 ± 0.074 with p-value 1.9×10^{-2}. The correlation ratio is 0.52 ± 0.023. The cosine similarity is 0.93 ± 0.0085. The scatter plot is in Figure 45. The number of GRBs in the sample is 14. The duration is positively correlated with the deceleration time, which may indicate that the luminosity of the GRBs remain consistent, and that the longer duration sustains the ejecta decelerated at a later time. However, as can be seen from the figure, this relation far from being a tight correlation.

5.8. Some Correlations with $\rm F_g$

The γ-ray fluence $F_{\rm g}$ is related to several other parameters of GRBs. However, $F_{\rm g}$ is just an observational property, and it is highly affected by the distance compared with the more intrinsic quantities like the luminosity and the total energy. Therefore, correlations with $F_{\rm g}$ cannot directly reveal intrinsic properties. One should try to seek correlations between intrinsic properties. As $F_{\rm g}$ is one of the easiest quantities to obtain, we still list the correlations in the following. One might be able to get clues from these correlations.

The correlation between $\log F_{\rm g}$ and $\log T_{50}$ is

$$\log F_{\rm g} = (0.48 \pm 0.0051) \times \log T_{50} + (0.13 \pm 0.0057), \quad (56)$$

where $F_{\rm g}$ is in units of 10^{-6} erg cm^{-2} and in the 20–2000 keV energy band. T_{50} is in units of s. The adjusted R^2 is 0.3. The Pearson coefficient is 0.53 ± 0.0044 with p-value 6.2×10^{-211}. The Spearman coefficient is 0.53 ± 0.0032 with p-value 6.3×10^{-212}. The Kendall τ coefficient is 0.37 ± 0.0023 with p-value 5.7×10^{-195}. The correlation ratio is 0.15 ± 0.0021. The cosine similarity is 0.69 ± 0.0039. The scatter plot is in Figure 46. The number of GRBs in the sample is 2916. One can find two subgroups in the figure, which are defined as SGRBs and LGRBs.

The correlation between $\log F_{\rm g}$ and $\log F_{\rm X11hr}$ is

$$\log F_{\rm g} = (0.47 \pm 0.018) \times \log F_{\rm X11hr} + (4.1 \pm 0.14), \quad (57)$$

where $F_{\rm g}$ is in units of 10^{-6} erg cm^{-2} and in the 20–2000 keV energy band. $F_{\rm X11hr}$ is in units of Jy. The adjusted R^2 is 0.29. The Pearson coefficient is 0.52 ± 0.017 with p-value 6.7×10^{-18}. The Spearman coefficient is 0.57 ± 0.016 with p-value 2.1×10^{-22}. The Kendall τ coefficient is 0.4 ± 0.013 with p-value 2.2×10^{-20}. The correlation ratio is 0.98 ± 0.00041.

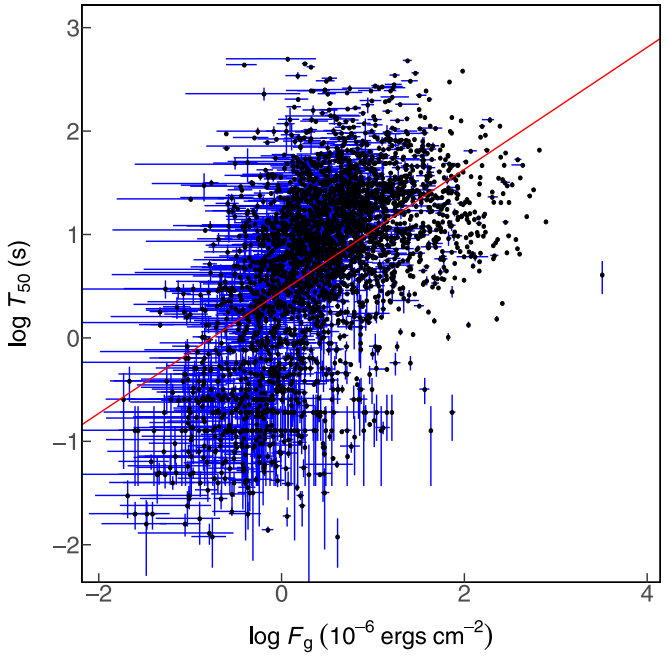

Figure 46. Scatter plot for $\log F_g$ and $\log T_{50}$. The red line is our fit result. The formula for the red line is $\log F_g = (0.48 \pm 0.0051) \times \log T_{50} + (0.13 \pm 0.0057)$. The description of every parameter is in Section 2.

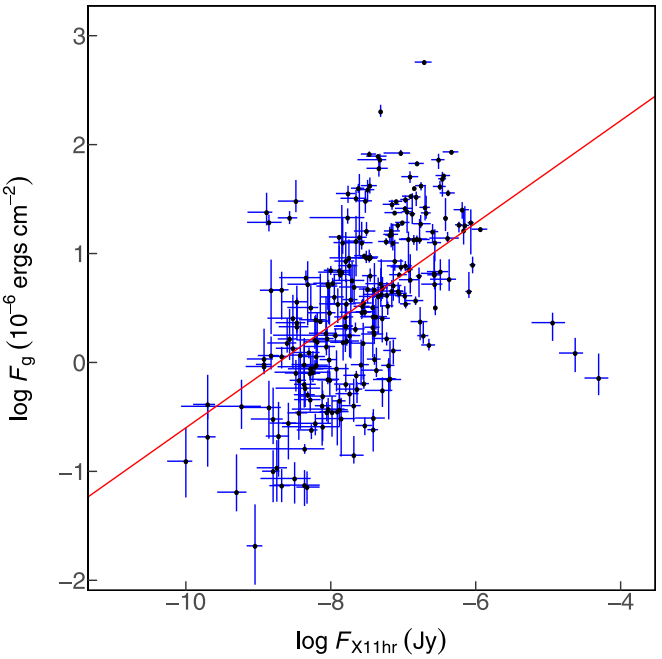

Figure 47. Scatter plot for $\log F_g$ and $\log F_{X11hr}$. The red line is our fit result. The formula for the red line is $\log F_g = (0.47 \pm 0.018) \times \log F_{X11hr} + (4.1 \pm 0.14)$. The description of every parameter is in Section 2. GRB 060804, GRB 050916, and GRB 060719A are outliers, having the highest F_{X11hr}.

The cosine similarity is -0.51 ± 0.012. The scatter plot is in Figure 47. The number of GRBs in the sample is 239.

The correlation between $\log F_g$ and $\log T_{R45,i}$ is

$$\log F_g = (0.69 \pm 0.015) \times \log T_{R45,i} + (0.45 \pm 0.0097), \quad (58)$$

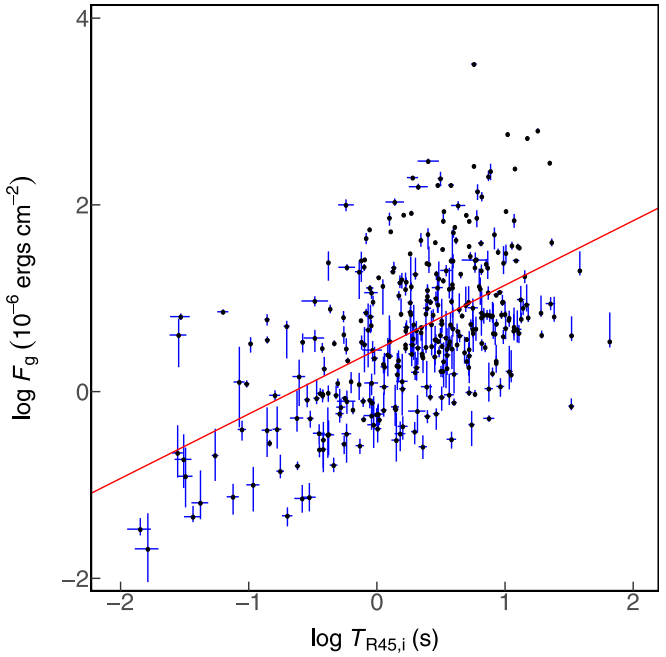

Figure 48. Scatter plot for $\log F_g$ and $\log T_{R45,i}$. The red line is our fit result. The formula for the red line is $\log F_g = (0.69 \pm 0.015) \times \log T_{R45,i} + (0.45 \pm 0.0097)$. The description of every parameter is in Section 2.

where F_g is in units of 10^{-6} erg cm^{-2} and in the 20–2000 keV energy band. $T_{R45,i}$ is in units of s. The adjusted R^2 is 0.28. The Pearson coefficient is 0.53 ± 0.0089 with p-value 1.3×10^{-25}. The Spearman coefficient is 0.48 ± 0.0089 with p-value 5×10^{-21}. The Kendall τ coefficient is 0.33 ± 0.0068 with p-value 5.6×10^{-20}. The correlation ratio is 0.24 ± 0.0053. The cosine similarity is 0.64 ± 0.0064. The scatter plot is in Figure 48. The number of GRBs in the sample is 337. Interestingly, the clustering effect in this figure is not obvious compared with Figure 46.

Lloyd et al. (2000a) found a correlation between F_g and $E_{p,Band}$, and also mentioned a correlation between F_g and $E_{p,Band,i}$. They explained that this correlation is due to an intrinsic relation between the burst rest-frame peak energy and the total radiated energy. They also found that the internal shock model is consistent with their interpretation of the correlation, but not the external shock.

The correlation between $\log F_g$ and $\log E_{p,Band,i}$ is

$$\log F_g = (0.85 \pm 0.057) \times \log E_{p,Band,i} + (-1 \pm 0.15), \quad (59)$$

where F_g is in units of 10^{-6} erg cm^{-2} and in the 20–2000 keV energy band. $E_{p,Band,i}$ is in units of keV. The adjusted R^2 is 0.26. The Pearson coefficient is 0.49 ± 0.027 with p-value 2.4×10^{-12}. The Spearman coefficient is 0.51 ± 0.022 with p-value 1.8×10^{-13}. The Kendall τ coefficient is 0.35 ± 0.016 with p-value 1.9×10^{-12}. The correlation ratio is 0.71 ± 0.0047. The cosine similarity is 0.85 ± 0.0072. The scatter plot is in Figure 49. The number of GRBs in the sample is 179.

The correlation between $\log F_g$ and $\log T_{90,i}$ is

$$\log F_g = (0.55 \pm 0.012) \times \log T_{90,i} + (0.11 \pm 0.016), \quad (60)$$

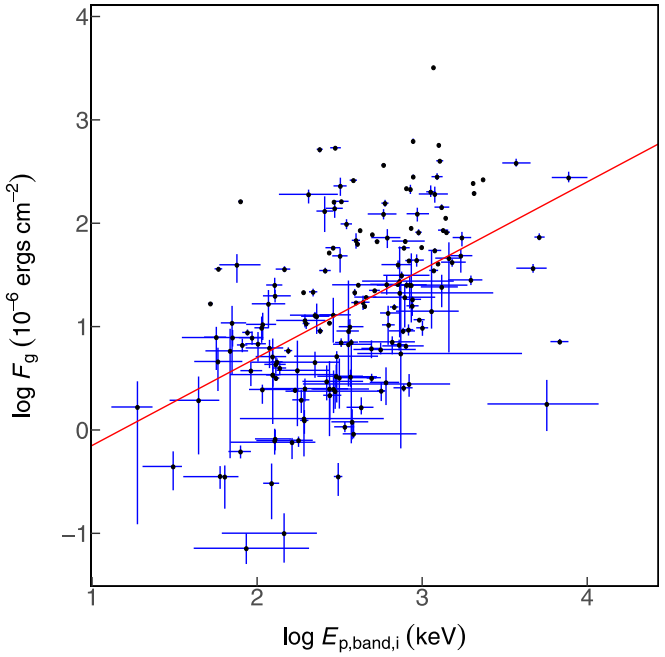

Figure 49. Scatter plot for $\log F_g$ and $\log E_{p,Band,i}$. The red line is our fit result. The formula for the red line is $\log F_g = (0.85 \pm 0.057) \times \log E_{p,Band,i} + (-1 \pm 0.15)$. The description of every parameter is in Section 2.

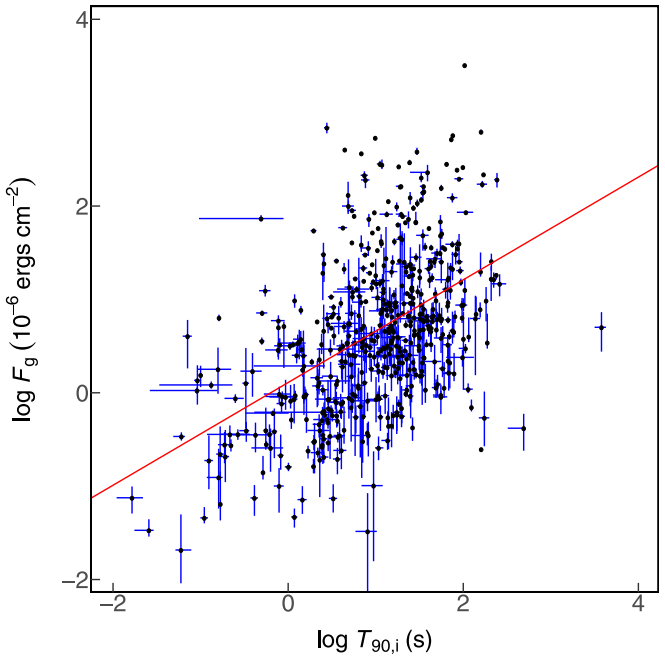

Figure 50. Scatter plot for $\log F_g$ and $\log T_{90,i}$. The red line is our fit result. The formula for the red line is $\log F_g = (0.55 \pm 0.012) \times \log T_{90,i} + (0.11 \pm 0.016)$. The description of every parameter is in Section 2.

where F_g is in units of 10^{-6} erg cm^{-2} and in the 20–2000 keV energy band. $T_{90,i}$ is in units of s. The adjusted R^2 is 0.24. The Pearson coefficient is 0.48 ± 0.009 with p-value 6.9×10^{-32}. The Spearman coefficient is 0.48 ± 0.0081 with p-value 3.2×10^{-31}. The Kendall τ coefficient is 0.33 ± 0.006 with p-value 2.5×10^{-29}. The correlation ratio is 0.21 ± 0.0043. The cosine similarity is 0.72 ± 0.0063. The scatter plot is in Figure 50. The number of GRBs in the sample is 526.

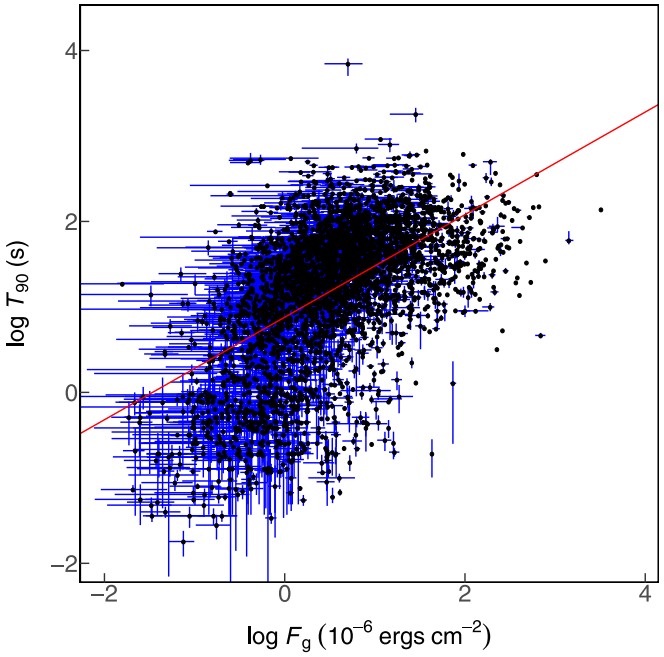

Figure 51. Scatter plot for $\log F_g$ and $\log T_{90}$. The red line is our fit result. The formula for the red line is $\log F_g = (0.5 \pm 0.0049) \times \log T_{90} + (-0.083 \pm 0.0075)$. The description of every parameter is in Section 2.

The correlation between $\log F_g$ and $\log T_{90}$ is

$$\log F_g = (0.5 \pm 0.0049) \times \log T_{90} + (-0.083 \pm 0.0075), \quad (61)$$

where T_{90} is in units of s. F_g is in units of 10^{-6} erg cm^{-2} and is in the 20–2000 keV energy band. The adjusted R^2 is 0.32. The Pearson coefficient is 0.55 ± 0.004 with p-value 2.5×10^{-276}. The Spearman coefficient is 0.55 ± 0.0029 with p-value 8.2×10^{-281}. The Kendall τ coefficient is 0.38 ± 0.0022 with p-value 1.5×10^{-257}. The correlation ratio is 0.38 ± 0.0018. The cosine similarity is 0.72 ± 0.0036. The scatter plot is in Figure 51. The number of GRBs in the sample is 3532. Comparing with Figure 50, the clustering effect is much more obvious in Figure 51. However, the rest-frame duration should be more intrinsic. It could be a puzzle. Notice that the sample number in Figure 50 is much lower, which might make the clustering effect less obvious.

The correlation between $\log F_g$ and $\log P_{pk3}$ is

$$\log F_g = (1 \pm 0.02) \times \log P_{pk3} + (-0.096 \pm 0.015), \quad (62)$$

where F_g is in units of 10^{-6} erg cm^{-2} and in the 20–2000 keV energy band. P_{pk3} is the peak photon flux in the 1024 ms time bin in 10–1000 keV and is in units of photons cm^{-2} s^{-1}. The adjusted R^2 is 0.48. The Pearson coefficient is 0.65 ± 0.0073 with p-value 3.8×10^{-304}. The Spearman coefficient is 0.64 ± 0.0049 with p-value 3×10^{-289}. The Kendall τ coefficient is 0.46 ± 0.004 with p-value 7.7×10^{-263}. The correlation ratio is 0.064 ± 0.0032. The cosine similarity is 0.77 ± 0.0052. The scatter plot is in Figure 52. The number of GRBs in the sample is 2531. It is quite natural that the fluence F_g is proportional to peak photon numbers P_{pk}. There are similar relations that are not shown here.

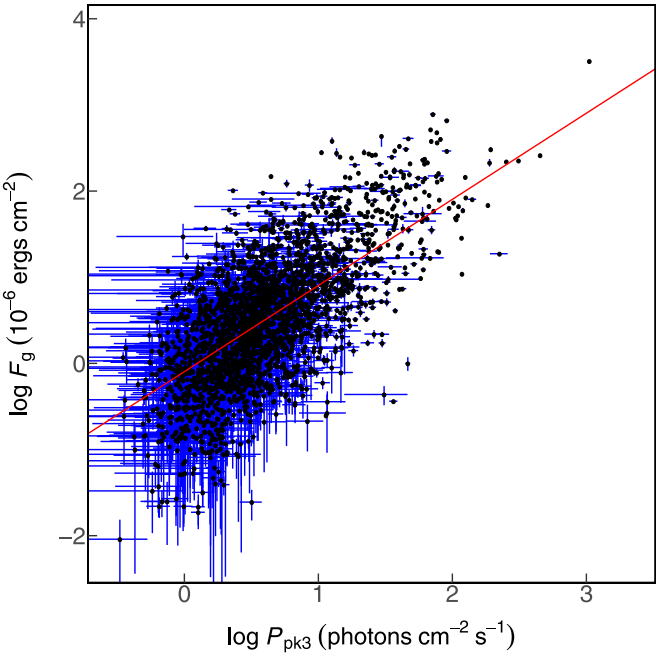

Figure 52. Scatter plot for $\log F_g$ and $\log P_{pk3}$. The red line is our fit result. The formula for the red line is $\log F_g = (1 \pm 0.02) \times \log P_{pk3} + (-0.096 \pm 0.015)$. The description of every parameter is in Section 2.

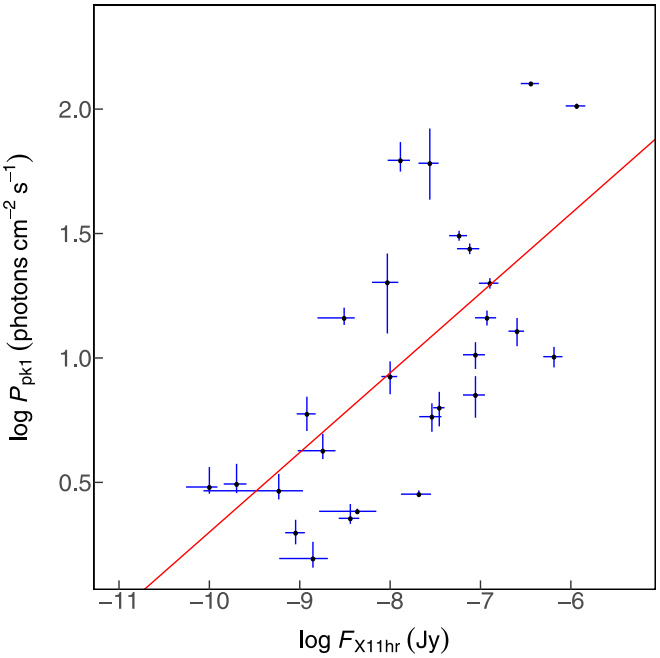

Figure 53. Scatter plot for $\log F_{X11hr}$ and $\log P_{pk1}$. The red line is our fit result. The formula for the red line is $\log F_{X11hr} = (1.4 \pm 0.086) \times \log P_{pk1} + (-9.2 \pm 0.1)$. The description of every parameter is in Section 2.

5.9. Some Correlations with F_{X11hr}

The correlation between $\log F_{X11hr}$ and $\log P_{pk1}$ is

$$\log F_{X11hr} = (1.4 \pm 0.086) \times \log P_{pk1} + (-9.2 \pm 0.1), \quad (63)$$

where F_{X11hr} is in units of Jy. P_{pk1} is the peak photon flux in the 64 ms time bin in 10–1000 keV and is in units of photons cm^{-2} s^{-1}. The adjusted R^2 is 0.44. The Pearson coefficient is 0.66 ± 0.026 with p-value 1.8×10^{-4}. The Spearman coefficient is 0.68 ± 0.03 with p-value 1.1×10^{-4}. The Kendall τ coefficient is 0.47 ± 0.027 with p-value 5.8×10^{-4}. The correlation ratio is 0.98 ± 0.0012. The cosine similarity is -0.83 ± 0.0054. The scatter plot is in Figure 53. The number of GRBs in the sample is 27.

The correlation between $\log F_{X11hr}$ and $\log F_{pk2}$ is

$$\log F_{X11hr} = (0.93 \pm 0.13) \times \log F_{pk2} + (-8.1 \pm 0.063), \quad (64)$$

where F_{pk2} is the peak energy flux in the 64 ms time bin in the rest-frame 1–10^4 keV energy band and is in units of 10^{-6} erg cm^{-2} s^{-1}. F_{X11hr} is in units of Jy. The adjusted R^2 is 0.33. The Pearson coefficient is 0.55 ± 0.063 with p-value 3.8×10^{-3}. The Spearman coefficient is 0.57 ± 0.066 with p-value 2.4×10^{-3}. The Kendall τ coefficient is 0.39 ± 0.054 with p-value 5.1×10^{-3}. The correlation ratio is 0.98 ± 0.0016. The cosine similarity is -0.3 ± 0.068. The scatter plot is in Figure 54. The number of GRBs in the sample is 26.

5.10. Some Correlations with $F_{Opt11hr}$

$\log F_{X11hr}$ and $\log F_{Opt11hr}$ have a remarkable linear correlation, but it is not very strong. The hypothesis-testing p-values of the entire formula, the linear coefficient a, and the Pearson,

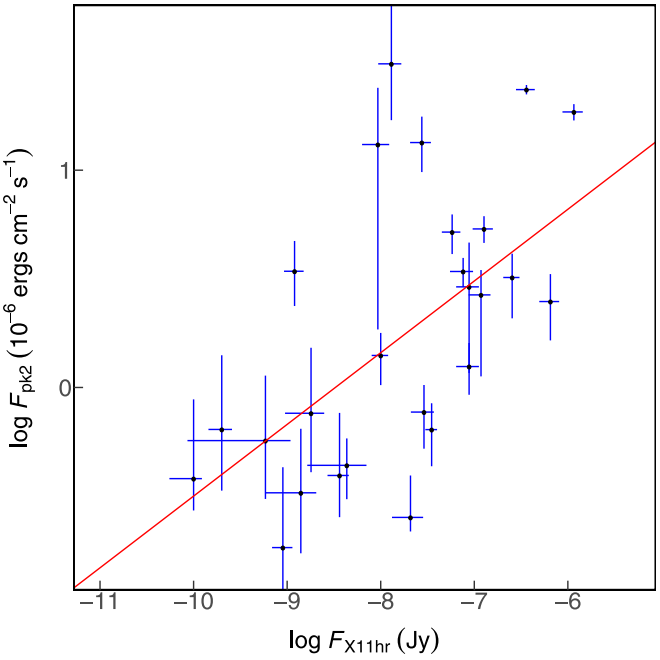

Figure 54. Scatter plot for $\log F_{X11hr}$ and $\log F_{pk2}$. The red line is our fit result. The formula for the red line is $\log F_{X11hr} = (0.93 \pm 0.13) \times \log F_{pk2} + (-8.1 \pm 0.063)$. The description of every parameter is in Section 2.

Spearman, and Kendall τ coefficients are all smaller than 0.05. The Pearson coefficient is 0.25 ± 0.033 with p-value 6.5×10^{-5}. The Spearman coefficient is 0.27 ± 0.036 with p-value 1.3×10^{-5}. The Kendall τ coefficient is 0.18 ± 0.025 with p-value 1.2×10^{-5}. The adjusted R^2 is 0.08. Because $\log F_{X11hr}$ is correlated with $\log P_{pk1}$ and $\log F_{pk2}$, $\log F_{Opt11hr}$ should have similar results.

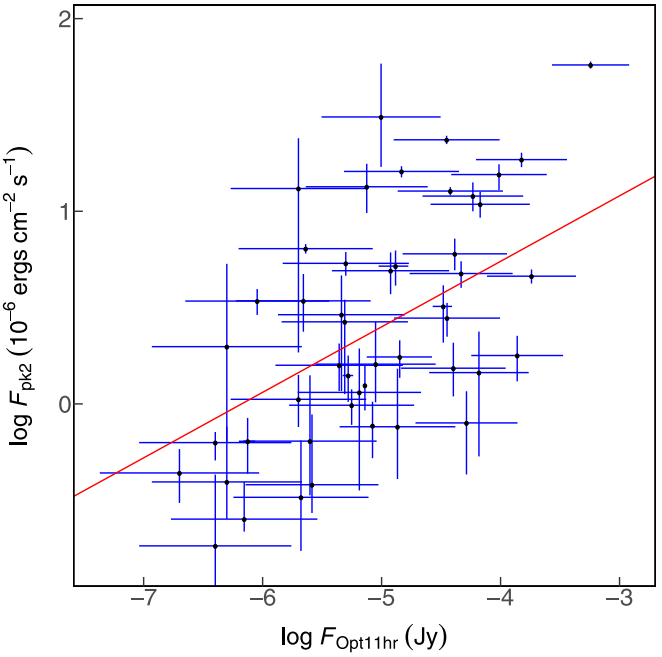

Figure 55. Scatter plot for $\log F_{\rm Opt11hr}$ and $\log F_{\rm pk2}$. The red line is our fit result. The formula for the red line is $\log F_{\rm Opt11hr} = (0.76 \pm 0.14) \times \log F_{\rm pk2} + (-5.4 \pm 0.095)$. The description of every parameter is in Section 2.

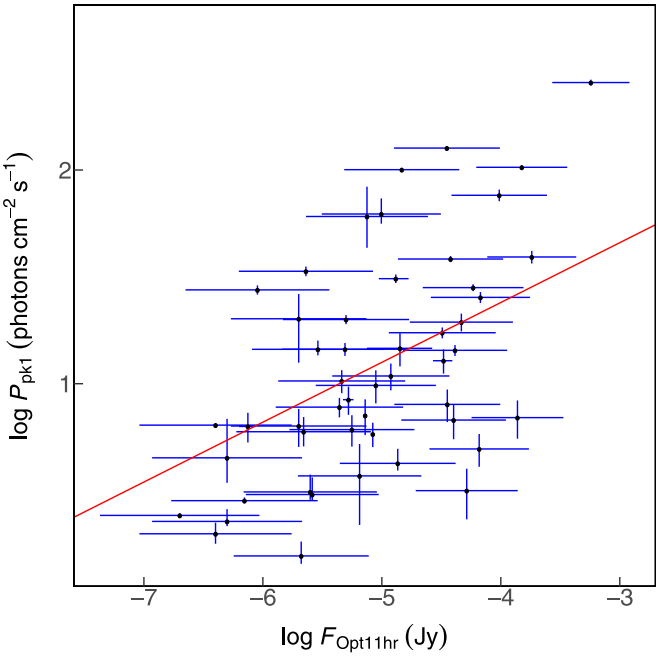

Figure 56. Scatter plot for $\log F_{\rm Opt11hr}$ and $\log P_{\rm pk1}$. The red line is our fit result. The formula for the red line is $\log F_{\rm Opt11hr} = (0.88 \pm 0.14) \times \log P_{\rm pk1} + (-6 \pm 0.17)$. The description of every parameter is in Section 2.

The correlation between $\log F_{\rm Opt11hr}$ and $\log F_{\rm pk2}$ is

$$\log F_{\rm Opt11hr} = (0.76 \pm 0.14) \times \log F_{\rm pk2} + (-5.4 \pm 0.095), \quad (65)$$

where $F_{\rm pk2}$ is the peak energy flux in the 64 ms time bin in the rest-frame 1–10^4 keV energy band and is in units of 10^{-6} erg cm^{-2} s^{-1}. $F_{\rm Opt11hr}$ is in units of Jy. The adjusted R^2 is 0.36. The Pearson coefficient is 0.51 ± 0.075 with p-value 2.5×10^{-4}. The Spearman coefficient is 0.49 ± 0.077 with p-value 4.5×10^{-4}. The Kendall τ coefficient is 0.35 ± 0.058 with p-value 5.3×10^{-4}. The correlation ratio is 0.96 ± 0.0038. The cosine similarity is -0.46 ± 0.043. The scatter plot is in Figure 55. The number of GRBs in the sample is 48.

The correlation between $\log F_{\rm Opt11hr}$ and $\log P_{\rm pk1}$ is

$$\log F_{\rm Opt11hr} = (0.88 \pm 0.14) \times \log P_{\rm pk1} + (-6 \pm 0.17), \quad (66)$$

where $F_{\rm Opt11hr}$ is in units of Jy. $P_{\rm pk1}$ is the peak photon flux in the 64 ms time bin in 10–1000 keV and is in units of photons cm^{-2} s^{-1}. The adjusted R^2 is 0.32. The Pearson coefficient is 0.49 ± 0.065 with p-value 2.8×10^{-4}. The Spearman coefficient is 0.46 ± 0.07 with p-value 8.2×10^{-4}. The Kendall τ coefficient is 0.33 ± 0.053 with p-value 8×10^{-4}. The correlation ratio is 0.97 ± 0.0029. The cosine similarity is -0.85 ± 0.008. The scatter plot is in Figure 56. The number of GRBs in the sample is 50.

5.11. Some Correlations with $F_{radio,pk}$

The correlation between $\log F_{\rm radio,pk}$ and $\log F_{\rm Opt11hr}$ is

$$\log F_{\rm radio,pk} = (0.26 \pm 0.039) \times \log F_{\rm Opt11hr} + (-2.4 \pm 0.17), \quad (67)$$

where $F_{\rm Opt11hr}$ is in units of Jy. $F_{\rm radio,pk}$ is in units of Jy. The adjusted R^2 is 0.32. The Pearson coefficient is 0.47 ± 0.059 with p-value 1.3×10^{-4}. The Spearman coefficient is 0.41 ± 0.071 with p-value 1.3×10^{-3}. The Kendall τ coefficient is 0.28 ± 0.052 with p-value 1.4×10^{-3}. The correlation ratio is 0.56 ± 0.028. The cosine similarity is 0.99 ± 0.002. The scatter plot is in Figure 57. The number of GRBs in the sample is 60.

The correlation between $\log F_{\rm radio,pk}$ and log SSFR is

$$\log F_{\rm radio,pk} = (0.44 \pm 0.027) \times \log {\rm SSFR} + (-3.4 \pm 0.013), \quad (68)$$

where $F_{\rm radio,pk}$ is in units of Jy. log SSFR is in units of Gyr^{-1}. The adjusted R^2 is 0.34. The Pearson coefficient is 0.6 ± 0.018 with p-value 3.9×10^{-4}. The Spearman coefficient is 0.74 ± 0.021 with p-value 2.3×10^{-6}. The Kendall τ coefficient is 0.54 ± 0.019 with p-value 2×10^{-5}. The correlation ratio is 0.94 ± 0.0024. The cosine similarity is 0.023 ± 0.018. The scatter plot is in Figure 58. The number of GRBs in the sample is 31.

5.12. Some Correlations with α_{spl}

The correlation between $\log P_{\rm pk3}$ and $-\alpha_{\rm spl}$ is

$$\log P_{\rm pk3} = (0.4 \pm 0.023) \times (-\alpha_{\rm spl}) + (-0.37 \pm 0.036), \quad (69)$$

where $P_{\rm pk3}$ is the peak photon flux in the 1024 ms time bin in 10–1000 keV and is in units of photons cm^{-2} s^{-1}. The adjusted R^2 is 0.29. The Pearson coefficient is 0.46 ± 0.028 with p-value 7.4×10^{-27}. The Spearman coefficient is 0.49 ± 0.021 with p-value 2.2×10^{-31}. The Kendall τ coefficient is 0.35 ± 0.015 with p-value 6.5×10^{-31}. The correlation ratio is

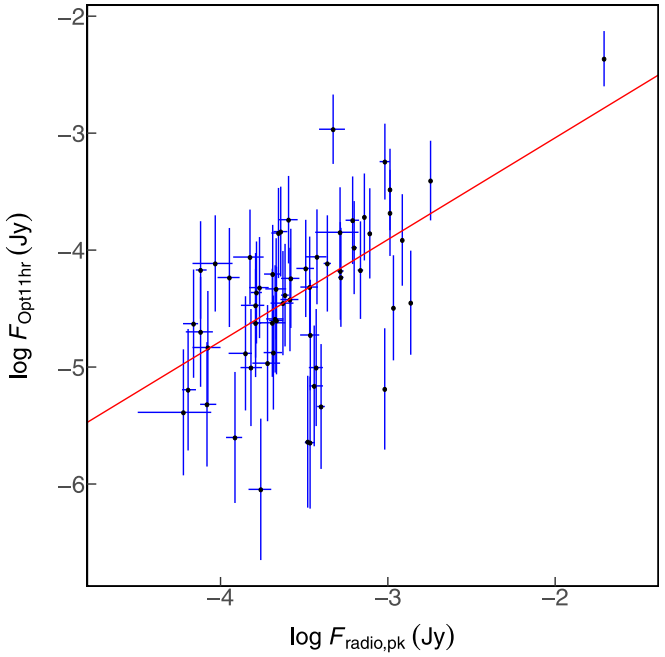

Figure 57. Scatter plot for $\log F_{\rm radio,pk}$ and $\log F_{\rm Opt11hr}$. The red line is our fit result. The formula for the red line is $\log F_{\rm radio,pk} = (0.26 \pm 0.039) \times \log F_{\rm Opt11hr} + (-2.4 \pm 0.17)$. The description of every parameter is in Section 2. The outlier is GRB 030329A, having the highest $\log F_{\rm radio,pk}$ and $\log F_{\rm Opt11hr}$.

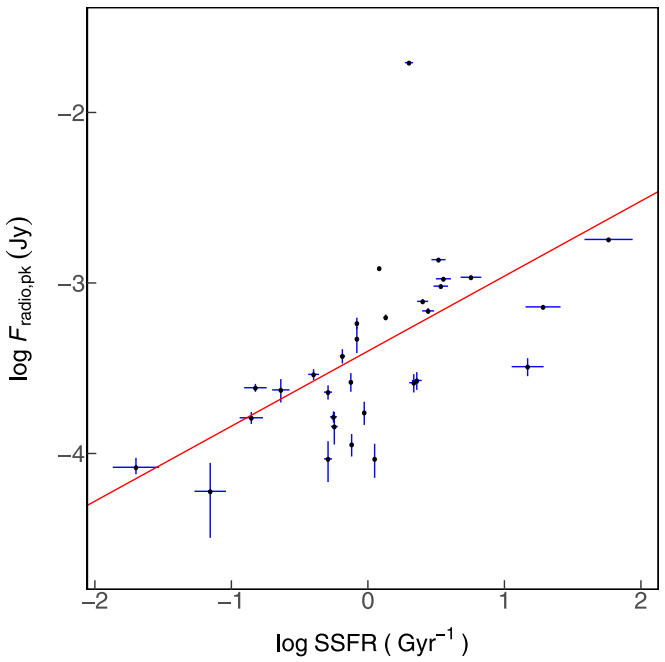

Figure 58. Scatter plot for $\log F_{\rm radio,pk}$ and log SSFR. The red line is our fit result. The formula for the red line is $\log F_{\rm radio,pk} = (0.44 \pm 0.027) \times \log {\rm SSFR} + (-3.4 \pm 0.013)$. The description of every parameter is in Section 2. The outlier is GRB 030329A with highest $\log F_{\rm radio,pk}$.

0.87 ± 0.0027. The cosine similarity is 0.7 ± 0.018. The scatter plot is in Figure 59. The number of GRBs in the sample is 488. This might be a selection effect, wherein those GRBs with steep spectra (larger $-\alpha_{\rm spl}$) can only be observed if they are strong, i.e., high peak photon flux.

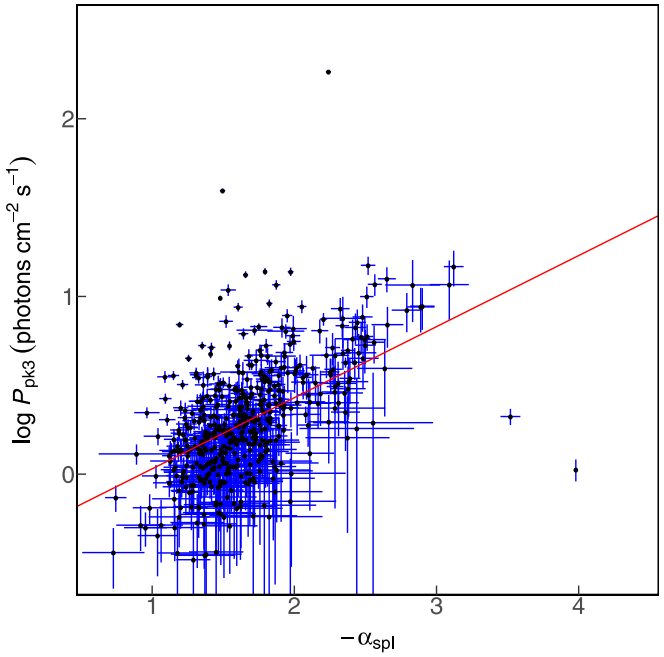

Figure 59. Scatter plot for $\log P_{\rm pk3}$ and $(-\alpha_{\rm spl})$. The red line is our fit result. The formula for the red line is $\log P_{\rm pk3} = (0.4 \pm 0.023) \times (-\alpha_{\rm spl}) + (-0.37 \pm 0.036)$. The description of every parameter is in Section 2.

The correlation between $\beta_{\rm X11hr}$ and $-\alpha_{\rm spl}$ is

$$\beta_{\rm X11hr} = (0.72 \pm 0.24) \times (-\alpha_{\rm spl}) + (0.43 \pm 0.42), \quad (70)$$

and the adjusted R^2 is 0.43. The Pearson coefficient is 0.53 ± 0.14 with p-value 3.3×10^{-2}. The Spearman coefficient is 0.52 ± 0.14 with p-value 3.7×10^{-2}. The Kendall τ coefficient is 0.39 ± 0.11 with p-value 3.1×10^{-2}. The correlation ratio is 0.12 ± 0.081. The cosine similarity is 0.96 ± 0.015. The scatter plot is in Figure 60. The number of GRBs in the sample is 16. It shows that those GRBs with steeper spectra in the prompt emission stage also have steeper spectra in the afterglow stage; even the main emitting energy bands are different. It is likely that the emission in these two stages share the same radiation mechanism, and with the cooling of the ejecta, the radiation bands shift from γ-rays to X-rays.

The correlation between log HR and $-\alpha_{\rm spl}$ is

$$\log {\rm HR} = (-0.97 \pm 0.023) \times (-\alpha_{\rm spl}) + (2.3 \pm 0.039), \quad (71)$$

and the adjusted R^2 is 0.69. The Pearson coefficient is -0.73 ± 0.016 with p-value 1.6×10^{-148}. The Spearman coefficient is -0.78 ± 0.011 with p-value 1.9×10^{-176}. The Kendall τ coefficient is -0.6 ± 0.01 with p-value 8.4×10^{-158}. The correlation ratio is 0.71 ± 0.0043. The cosine similarity is 0.59 ± 0.0093. The scatter plot is in Figure 61. The number of GRBs in the sample is 874. One can see a double linear relation in the figure. This may indicate that classification is important before correlation analysis.

Because $\beta_{\rm X11hr}$ and $P_{\rm pk3}$ are both correlated with $\alpha_{\rm spl}$, and $P_{\rm pk3}$ and $P_{\rm pk4}$ are also correlated, $\beta_{\rm X11hr}$ and $P_{\rm pk4}$ are naturally correlated.

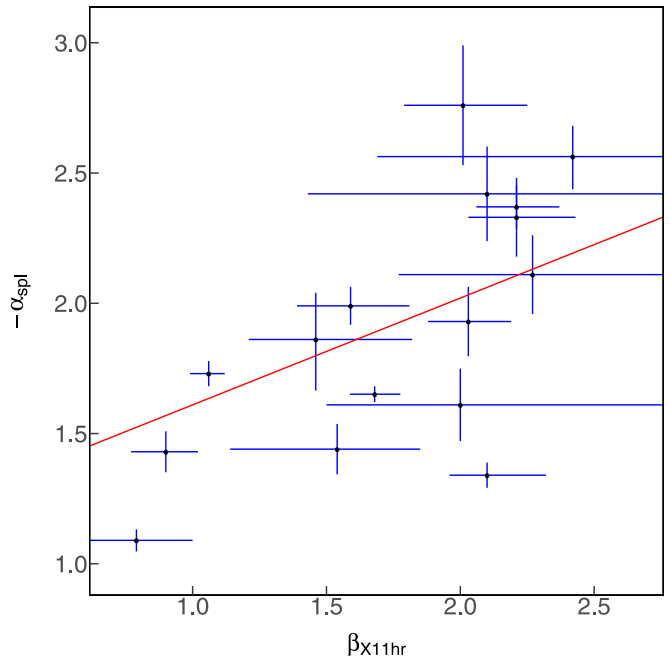

Figure 60. Scatter plot for β_{X11hr} and $(-\alpha_{spl})$. The red line is our fit result. The formula for the red line is $\beta_{X11hr} = (0.72 \pm 0.24) \times (-\alpha_{spl}) + (0.43 \pm 0.42)$. The description of every parameter is in Section 2.

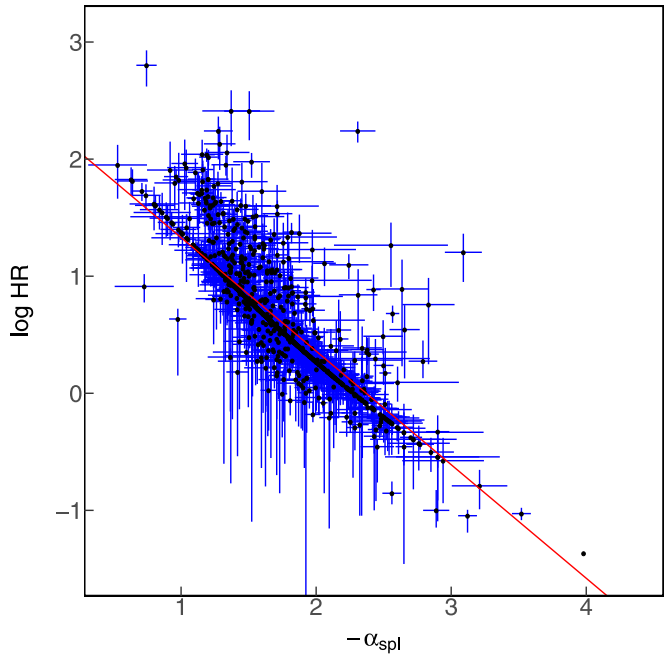

Figure 61. Scatter plot for log HR and $-\alpha_{spl}$. The red line is our fit result. The formula for the red line is $\log \mathrm{HR} = (-0.97 \pm 0.023) \times (-\alpha_{spl}) + (2.3 \pm 0.039)$. The description of every parameter is in Section 2.

The correlation between $\log P_{pk4}$ and β_{X11hr} is

$$\log P_{pk4} = (-0.32 \pm 0.047) \times \beta_{X11hr} + (1.2 \pm 0.087), \quad (72)$$

where P_{pk4} is the peak photon flux in the 1 s time bin in 10–1000 keV and is in units of photons $\mathrm{cm}^{-2}\,\mathrm{s}^{-1}$. The adjusted R^2 is 0.29. The Pearson coefficient is -0.44 ± 0.058 with p-value 1.5×10^{-8}. The Spearman coefficient is -0.48 ± 0.037

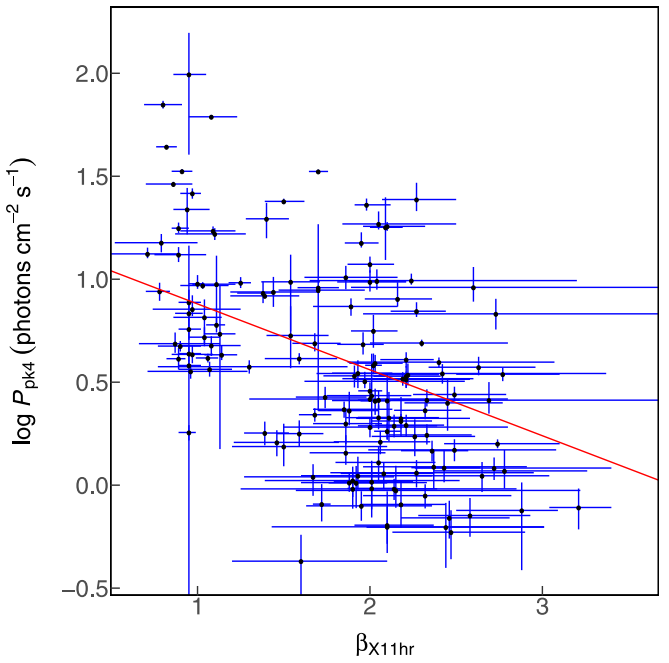

Figure 62. Scatter plot for $\log P_{pk4}$ and β_{X11hr}. The red line is our fit result. The formula for the red line is $\log P_{pk4} = (-0.32 \pm 0.047) \times \beta_{X11hr} + (1.2 \pm 0.087)$. The description of every parameter is in Section 2.

with p-value 4.4×10^{-10}. The Kendall τ coefficient is -0.33 ± 0.028 with p-value 2.9×10^{-9}. The correlation ratio is 0.72 ± 0.012. The cosine similarity is 0.6 ± 0.018. The scatter plot is in Figure 62. The number of GRBs in the sample is 151.

5.13. Correlations with Host Galaxy Offset

The correlation between $\log F_{Opt11hr}$ and log offset is

$$\log F_{Opt11hr} = (-0.48 \pm 0.21) \times \log \mathrm{offset} + (-5 \pm 0.16), \quad (73)$$

where $F_{Opt11hr}$ is in units of Jy. The host galaxy offset is in units of kpc. The adjusted R^2 is 0.28. The Pearson coefficient is -0.39 ± 0.13 with p-value 4.3×10^{-2}. The Spearman coefficient is -0.46 ± 0.12 with p-value 1.6×10^{-2}. The Kendall τ coefficient is -0.32 ± 0.085 with p-value 1.8×10^{-2}. The correlation ratio is 0.96 ± 0.01. The cosine similarity is -0.6 ± 0.12. The scatter plot is in Figure 63. The number of GRBs in the sample is 27.

The correlation between $\log T_{50,i}$ and log offset is

$$\log T_{50,i} = (-0.74 \pm 0.2) \times \log \mathrm{offset} + (0.33 \pm 0.19), \quad (74)$$

where the host galaxy offset is in units of kpc. $T_{50,i}$ is in units of s. The adjusted R^2 is 0.4. The Pearson coefficient is -0.56 ± 0.076 with p-value 2.6×10^{-3}. The Spearman coefficient is -0.58 ± 0.05 with p-value 1.4×10^{-3}. The Kendall τ coefficient is -0.42 ± 0.042 with p-value 2.2×10^{-3}. The correlation ratio is 0.46 ± 0.05. The cosine similarity is -0.54 ± 0.043. The scatter plot is in Figure 64. The number of GRBs in the sample is 27. This is consistent with the classification of LGRBs and SGRBs: as SGRBs are thought to

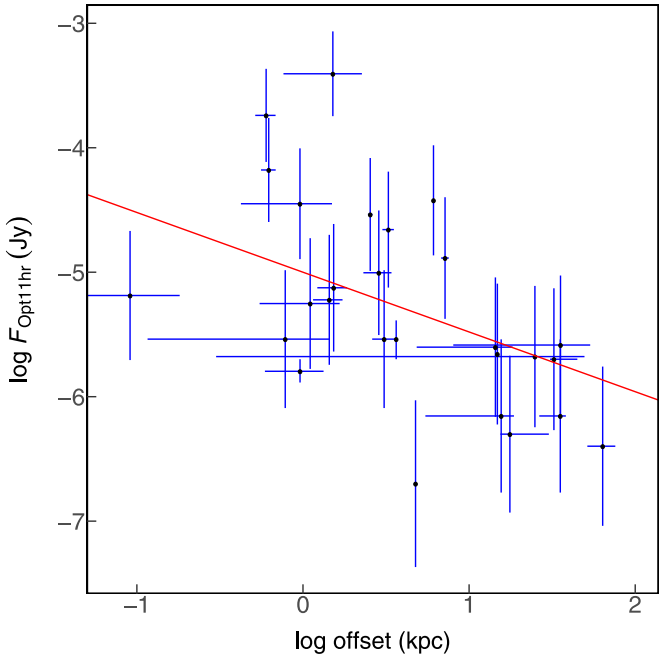

Figure 63. Scatter plot for log $F_{\rm Opt11hr}$ and log offset. The red line is our fit result. The formula for the red line is $\log F_{\rm Opt11hr} = (-0.48 \pm 0.21) \times$ log offset $+ (-5 \pm 0.16)$. The description of every parameter is in Section 2.

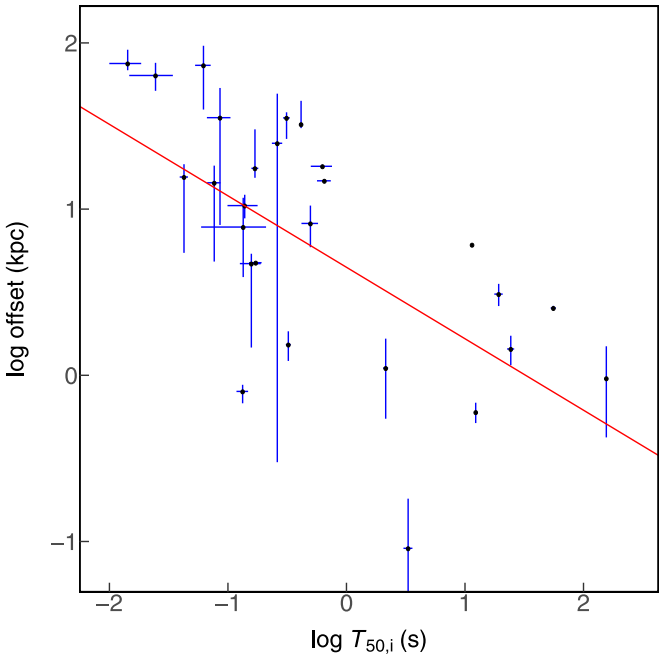

Figure 64. Scatter plot for log $T_{50,i}$ and log offset. The red line is our fit result. The formula for the red line is $\log T_{50,i} = (-0.74 \pm 0.2) \times$ log offset $+$ (0.33 ± 0.19). The description of every parameter is in Section 2.

occur farther from the center of the host galaxies, $T_{50,i}$ and the offset are therefore anticorrelated.

The correlation between spectral lag and log offset is

$$\text{spectral lag} = (-582 \pm 289) \times \log \text{offset} + (735 \pm 276), \quad (75)$$

where the spectral time lag is in units of ms MeV^{-1}. The host galaxy offset is in units of kpc. The adjusted R^2 is 0.35. The

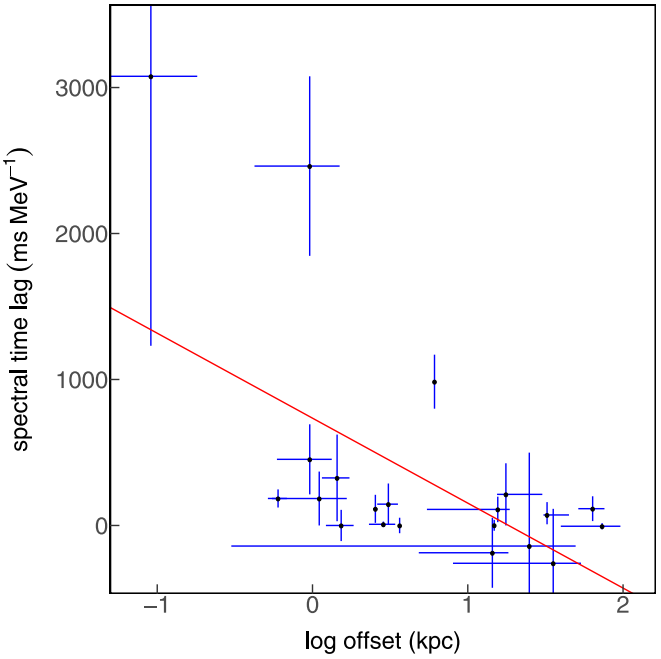

Figure 65. Scatter plot for spectral lag and log offset. The red line is our fit result. The formula for the red line is spectral lag $= (-582 \pm 289) \times$ log offset $+ (735 \pm 276)$. The description of every parameter is in Section 2.

Pearson coefficient is -0.53 ± 0.19 with p-value 1.4×10^{-2}. The Spearman coefficient is -0.41 ± 0.15 with p-value 6.5×10^{-2}. The Kendall τ coefficient is -0.3 ± 0.11 with p-value 6.1×10^{-2}. The correlation ratio is 0.28 ± 0.051. The cosine similarity is -0.17 ± 0.18. The scatter plot is in Figure 65. The number of GRBs in the sample is 21.

The correlation between rest-frame spectral lag and log offset is

$$\text{rest-frame spectral lag} = (-306 \pm 154) \times \log \text{offset} + (396 \pm 151), \quad (76)$$

where rest-frame spectral lag is in units of ms MeV^{-1}. The host galaxy offset is in units of kpc. The adjusted R^2 is 0.35. The Pearson coefficient is -0.53 ± 0.19 with p-value 1.6×10^{-2}. The Spearman coefficient is -0.35 ± 0.15 with p-value 0.12. The Kendall τ coefficient is -0.25 ± 0.11 with p-value 0.12. The correlation ratio is 0.29 ± 0.05. The cosine similarity is -0.17 ± 0.19. The scatter plot is in Figure 66. The number of GRBs in the sample is 20. This may also come from the difference between LGRBs and SGRBs. SGRBs are thought to have smaller spectral lags. Given the large scatter, one may not get much information from it.

5.14. Some Correlations with $t_{radio,pk}$

The correlation between the rest-frame spectral lag and log $t_{\rm radio,pk,i}$ is

$$\text{rest-frame spectral lag} = (1998 \pm 431) \times \log t_{\rm radio,pk,i} + (-10118 \pm 2304), \quad (77)$$

where the rest-frame spectral lag is in units of ms MeV^{-1}. $t_{\rm radio,pk,i}$ is in units of s. The adjusted R^2 is 0.34. The Pearson coefficient is 0.53 ± 0.072 with p-value 1.3×10^{-3}. The Spearman coefficient is 0.38 ± 0.076 with p-value 2.7×10^{-2}.

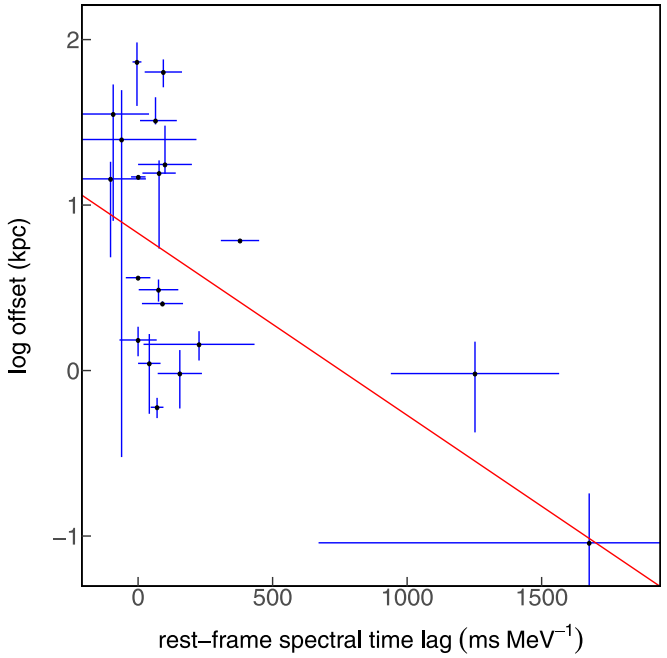

Figure 66. Scatter plot for rest-frame spectral lag and log offset. The red line is our fit result. The formula for the red line is rest-frame spectral lag = $(-306 \pm 154) \times$ log offset + (396 ± 151). The description of every parameter is in Section 2.

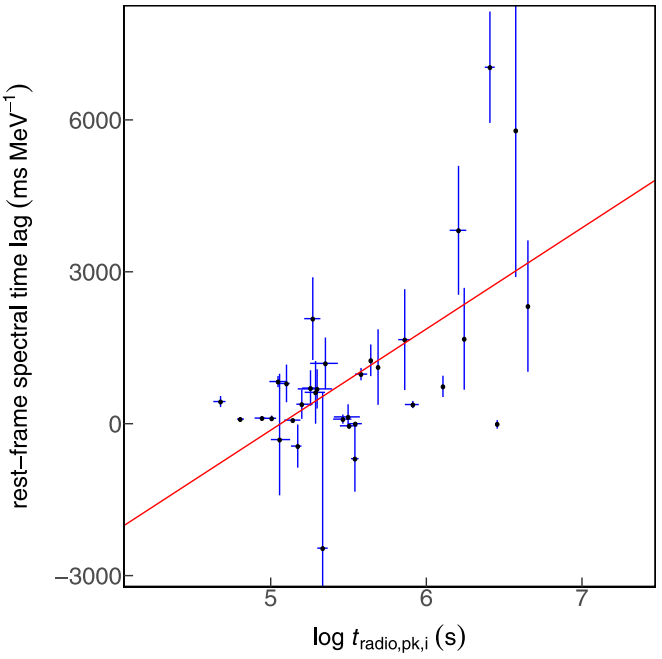

Figure 67. Scatter plot for the rest-frame spectral lag and log $t_{\rm radio,pk,i}$. The red line is our fit result. The formula for the red line is rest-frame spectral lag = $(1998 \pm 431) \times \log t_{\rm radio,pk,i} + (-10118 \pm 2304)$. The description of every parameter is in Section 2.

The Kendall τ coefficient is 0.27 ± 0.056 with p-value 2.6×10^{-2}. The correlation ratio is 0.33 ± 0.061. The cosine similarity is 0.48 ± 0.075. The scatter plot is in Figure 67. The number of GRBs in the sample is 33. This is an interesting correlation. The spectral lag is a quantity of the prompt emission, although its physical origin is still not clear. The peak time of the radio emission $t_{\rm radio,pk}$ is a quantity of the late afterglow. The spectral lag might be related to the radiation mechanism, while $t_{\rm radio,pk}$ is more likely related to the total energy and the environment. They are not likely to be related to each other. The reason for this correlation is not clear.

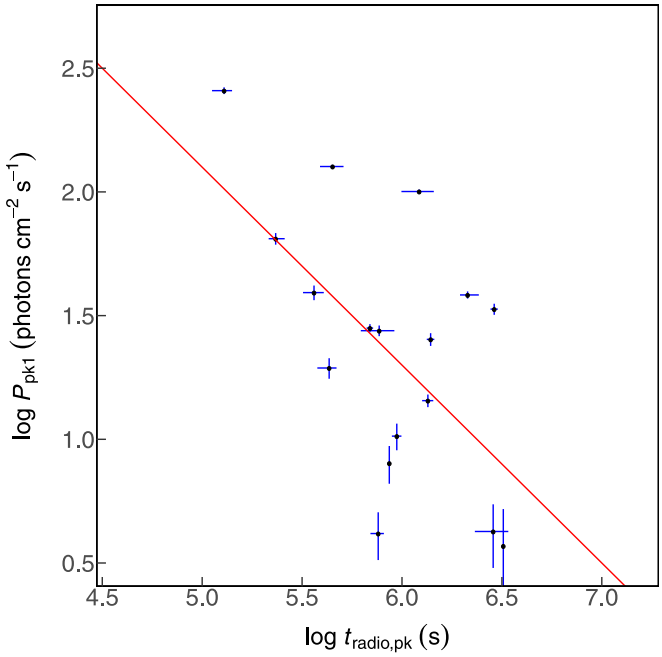

Figure 68. Scatter plot for log $P_{\rm pk1}$ and log $t_{\rm radio,pk}$. The red line is our fit result. The formula for the red line is $\log P_{\rm pk1} = (-0.8 \pm 0.066) \times \log t_{\rm radio,pk} + (6.1 \pm 0.38)$. The description of every parameter is in Section 2.

The correlation between log $P_{\rm pk1}$ and log $t_{\rm radio,pk}$ is

$$\log P_{\rm pk1} = (-0.8 \pm 0.066) \times \log t_{\rm radio,pk} + (6.1 \pm 0.38), \quad (78)$$

where $P_{\rm pk1}$ is the peak photon flux in the 64 ms time bin in 10–1000 keV and is in units of photons cm^{-2} s^{-1}. $t_{\rm radio,pk}$ is in units of s. The adjusted R^2 is 0.31. The Pearson coefficient is -0.59 ± 0.032 with p-value 1.3×10^{-2}. The Spearman coefficient is -0.5 ± 0.044 with p-value 4.2×10^{-2}. The Kendall τ coefficient is -0.36 ± 0.035 with p-value 4.8×10^{-2}. The correlation ratio is 0.98 ± 0.0011. The cosine similarity is 0.92 ± 0.0077. The scatter plot is in Figure 68. The number of GRBs in the sample is 17.

The correlation between log $F_{\rm pk2}$ and log $t_{\rm radio,pk}$ is

$$\log F_{\rm pk2} = (-0.79 \pm 0.11) \times \log t_{\rm radio,pk} + (5.4 \pm 0.63), \quad (79)$$

where $F_{\rm pk2}$ is the peak energy flux in the 64 ms time bin in the rest-frame 1–10^4 keV energy band and is in units of 10^{-6} erg cm^{-2} s^{-1}. $t_{\rm radio,pk}$ is in units of s. The adjusted R^2 is 0.27. The Pearson coefficient is -0.54 ± 0.049 with p-value 2.5×10^{-2}. The Spearman coefficient is -0.41 ± 0.049 with p-value 0.11. The Kendall τ coefficient is -0.3 ± 0.043 with p-value 9.9×10^{-2}. The correlation ratio is 0.98 ± 0.002. The cosine similarity is 0.77 ± 0.044. The scatter plot is in Figure 69. The number of GRBs in the sample is 17.

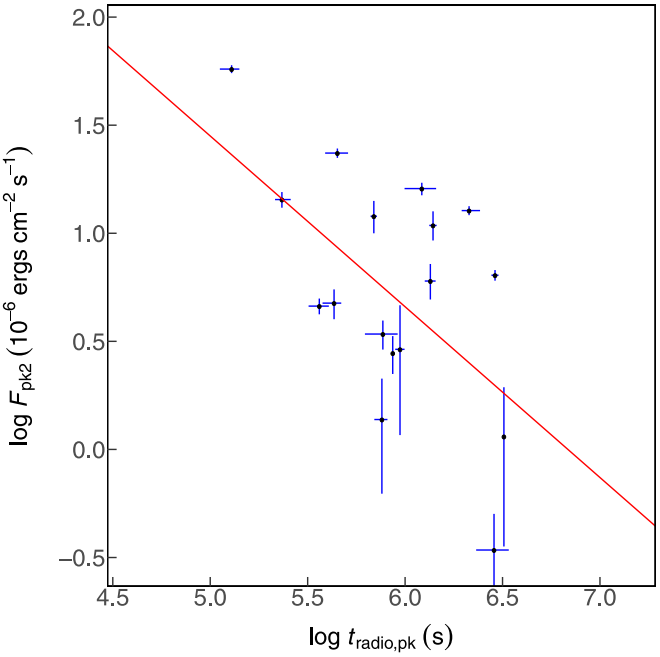

Figure 69. Scatter plot for $\log F_{\rm pk2}$ and $\log t_{\rm radio,pk}$. The red line is our fit result. The formula for the red line is $\log F_{\rm pk2} = (-0.79 \pm 0.11) \times \log t_{\rm radio,pk} + (5.4 \pm 0.63)$. The description of every parameter is in Section 2.

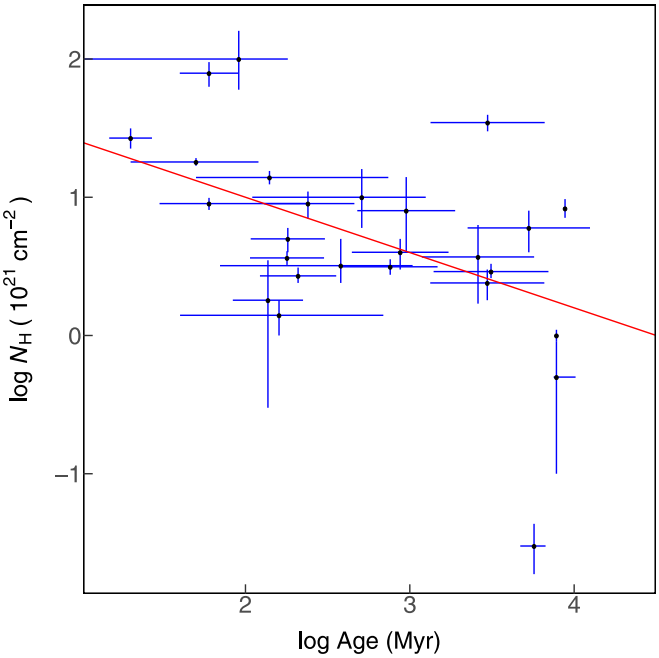

Figure 70. Scatter plot for $\log N_{\rm H}$ and log Age. The red line is our fit result. The formula for the red line is $\log N_{\rm H} = (-0.4 \pm 0.075) \times \log {\rm Age} + (1.8 \pm 0.21)$. The description of every parameter is in Section 2.

5.15. Correlations with N_H

The correlation between $\log N_{\rm H}$ and log Age is

$$\log N_{\rm H} = (-0.4 \pm 0.075) \times \log {\rm Age} + (1.8 \pm 0.21), \quad (80)$$

where $N_{\rm H}$ is in units of 10^{21} cm^{-2}. Age is in units of Myr. The adjusted R^2 is 0.25. The Pearson coefficient is -0.49 ± 0.077 with p-value 1.2×10^{-2}. The Spearman coefficient is -0.45 ± 0.083 with p-value 2.2×10^{-2}. The Kendall τ coefficient is -0.32 ± 0.067 with p-value 2.1×10^{-2}. The correlation ratio is 0.78 ± 0.034. The cosine similarity is 0.53 ± 0.055. The scatter plot is in Figure 70. The number of GRBs in the sample is 26. This may reveal a property of the evolution of host galaxies in that more material has been formed into stars for the older galaxies.

The correlation between $\log N_{\rm H}$ and log SFR is

$$\log N_{\rm H} = (0.33 \pm 0.052) \times \log {\rm SFR} + (0.47 \pm 0.049), \quad (81)$$

where $N_{\rm H}$ is in units of 10^{21} cm^{-2}. The SFR is in units of $M_\odot$ yr^{-1}. The adjusted R^2 is 0.31. The Pearson coefficient is 0.55 ± 0.056 with p-value 5.6×10^{-4}. The Spearman coefficient is 0.52 ± 0.056 with p-value 1.3×10^{-3}. The Kendall τ coefficient is 0.37 ± 0.046 with p-value 1.6×10^{-3}. The correlation ratio is 0.03 ± 0.022. The cosine similarity is 0.71 ± 0.034. The scatter plot is in Figure 71. The number of GRBs in the sample is 36. It is clear that in a star-forming galaxy, the material must be rich. Consequently, the column density of hydrogen is high.

The correlation between $\log N_{\rm H}$ and $\log F_{\rm pk4}$ is

$$\log N_{\rm H} = (-0.43 \pm 0.037) \times \log F_{\rm pk4} + (0.89 \pm 0.041), \quad (82)$$

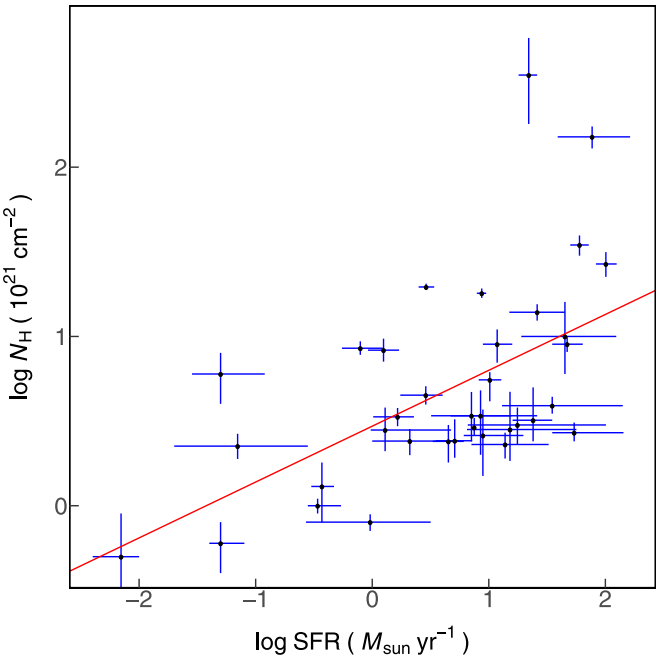

Figure 71. Scatter plot for $\log N_{\rm H}$ and log SFR. The red line is our fit result. The formula for the red line is $\log N_{\rm H} = (0.33 \pm 0.052) \times \log {\rm SFR} + (0.47 \pm 0.049)$. The description of every parameter is in Section 2.

where $F_{\rm pk4}$ is the peak energy flux in the 1024 ms time bin in the rest-frame 1–10^4 keV energy band and is in units of 10^{-6} erg cm^{-2} s^{-1}. $N_{\rm H}$ is in units of 10^{21} cm^{-2}. The adjusted R^2 is 0.35. The Pearson coefficient is -0.58 ± 0.055 with p-value 3.1×10^{-3}. The Spearman coefficient is -0.58 ± 0.078 with p-value 3×10^{-3}. The Kendall τ coefficient is -0.43 ± 0.061 with p-value 3.4×10^{-3}. The correlation ratio

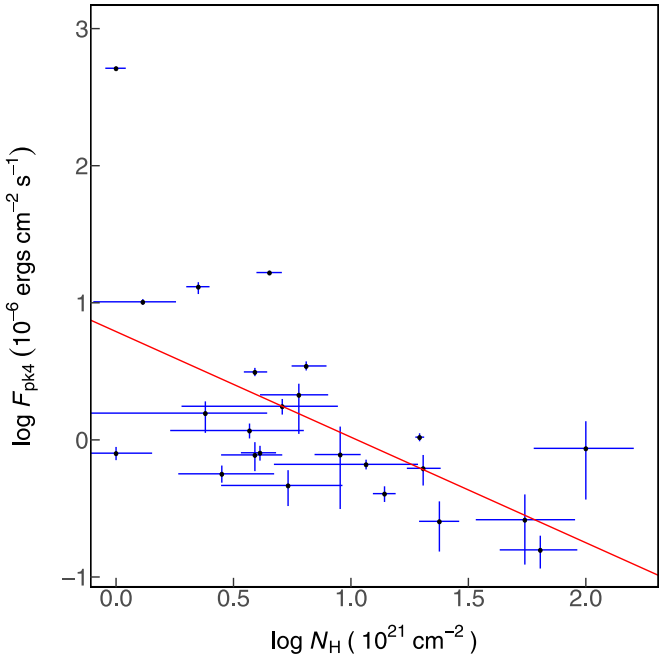

Figure 72. Scatter plot for $\log N_{\rm H}$ and $\log F_{\rm pk4}$. The red line is our fit result. The formula for the red line is $\log N_{\rm H} = (-0.43 \pm 0.037) \times \log F_{\rm pk4} + (0.89 \pm 0.041)$. The description of every parameter is in Section 2.

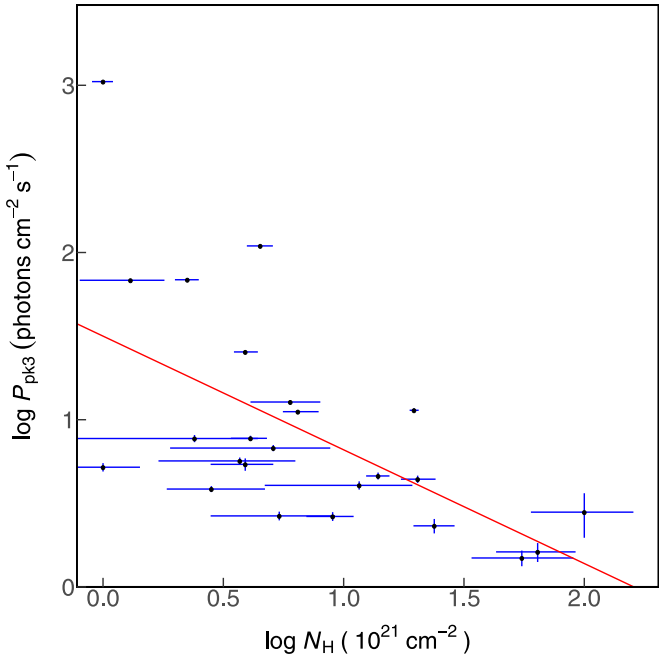

Figure 73. Scatter plot for $\log N_{\rm H}$ and $\log P_{\rm pk3}$. The red line is our fit result. The formula for the red line is $\log N_{\rm H} = (-0.51 \pm 0.038) \times \log P_{\rm pk3} + (1.3 \pm 0.065)$. The description of every parameter is in Section 2.

is 0.45 ± 0.027. The cosine similarity is -0.16 ± 0.05. The scatter plot is in Figure 72. The number of GRBs in the sample is 24.

The correlation between $\log N_{\rm H}$ and $\log P_{\rm pk3}$ is

$$\log N_{\rm H} = (-0.51 \pm 0.038) \times \log P_{\rm pk3} + (1.3 \pm 0.065), \quad (83)$$

where $P_{\rm pk3}$ is the peak photon flux in the 1024 ms time bin in 10–1000 keV and is in units of photons cm^{-2} s^{-1}. $N_{\rm H}$ is in units of 10^{21} cm^{-2}. The adjusted R^2 is 0.36. The Pearson coefficient is -0.59 ± 0.049 with p-value 2.7×10^{-3}. The Spearman coefficient is -0.61 ± 0.058 with p-value 1.5×10^{-3}. The Kendall τ coefficient is -0.45 ± 0.05 with p-value 2.1×10^{-3}. The correlation ratio is 0.1 ± 0.031. The cosine similarity is 0.49 ± 0.026. The scatter plot is in Figure 73. The number of GRBs in the sample is 24.

5.16. Correlations with the Age of the Host Galaxies

The correlation between log Age and $\log t_{\rm burst,i}$ is

$$\log \text{Age} = (0.61 \pm 0.12) \times \log t_{\rm burst,i} + (1 \pm 0.33), \quad (84)$$

where the Age is in units of Myr. $t_{\rm burst,i}$ is in units of s. The adjusted R^2 is 0.3. The Pearson coefficient is 0.54 ± 0.093 with p-value 2×10^{-2}. The Spearman coefficient is 0.69 ± 0.094 with p-value 1.6×10^{-3}. The Kendall τ coefficient is 0.51 ± 0.08 with p-value 3.5×10^{-3}. The correlation ratio is 0.044 ± 0.032. The cosine similarity is 0.96 ± 0.0073. The scatter plot is in Figure 74. The number of GRBs in the sample is 18. $t_{\rm burst,i}$ indicates the active timescale of the GRB central engine. It is unclear why older host galaxies contain GRBs with longer activity.

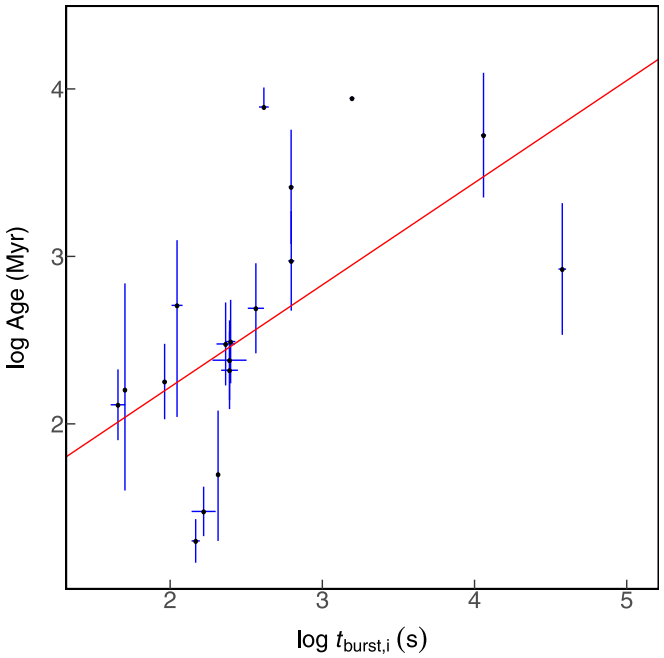

Figure 74. Scatter plot for log Age and $\log t_{\rm burst,i}$. The red line is our fit result. The formula for the red line is $\log \text{Age} = (0.61 \pm 0.12) \times \log t_{\rm burst,i} + (1 \pm 0.33)$. The description of every parameter is in Section 2.

The correlation between log Age and log SFR is

$$\log \text{Age} = (-0.38 \pm 0.059) \times \log \text{SFR} + (3.2 \pm 0.065), \quad (85)$$

where the SFR is in units of $M_\odot\,{\rm yr}^{-1}$. Age is in units of Myr. The adjusted R^2 is 0.28. The Pearson coefficient is -0.5 ± 0.067 with p-value 6.4×10^{-3}. The Spearman coefficient is -0.49 ± 0.079 with p-value 7.6×10^{-3}. The Kendall τ coefficient is

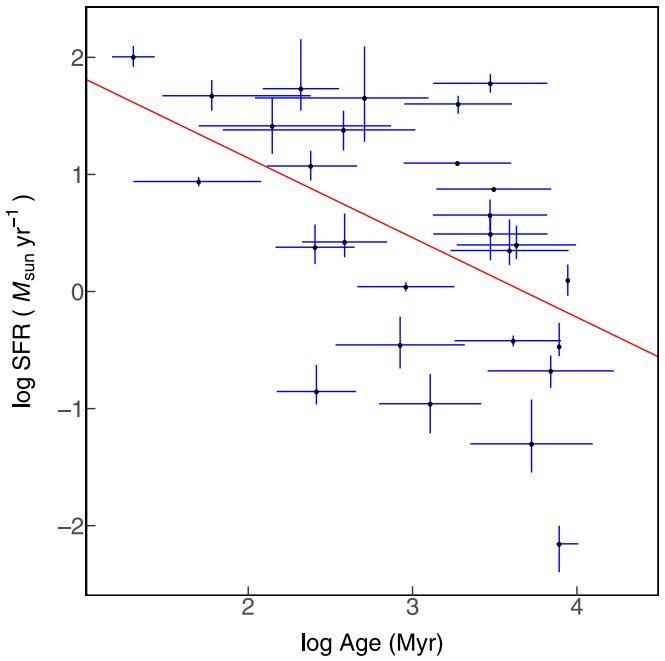

Figure 75. Scatter plot for log Age and log SFR. The red line is our fit result. The formula for the red line is $\log \mathrm{Age} = (-0.38 \pm 0.059) \times \log \mathrm{SFR} + (3.2 \pm 0.065)$. The description of every parameter is in Section 2.

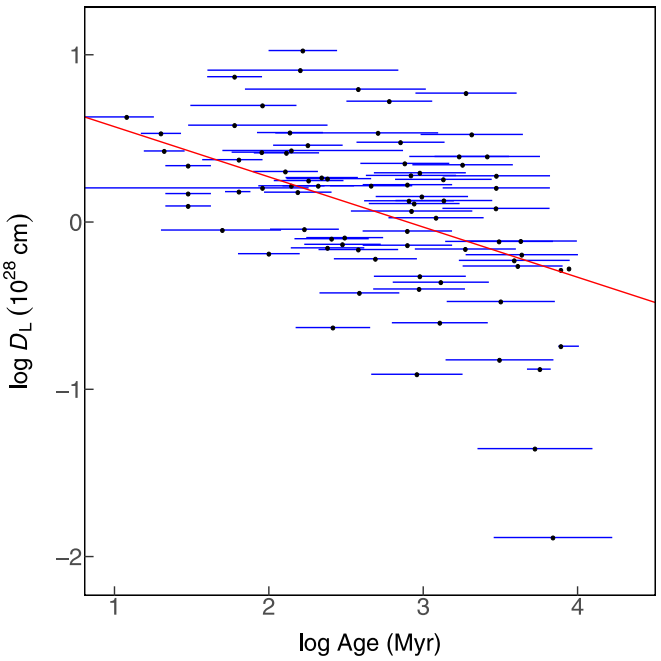

Figure 76. Scatter plot for log Age and $\log D_{\rm L}$. The red line is our fit result. The formula for the red line is $\log \mathrm{Age} = (-0.75 \pm 0.078) \times \log D_{\rm L} + (2.7 \pm 0.036)$. The description of every parameter is in Section 2.

-0.35 ± 0.062 with p-value 9.1×10^{-3}. The correlation ratio is 0.8 ± 0.014. The cosine similarity is 0.27 ± 0.035. The scatter plot is in Figure 75. The number of GRBs in the sample is 28. It is natural that star formation is more active in a younger galaxy. The correlation between the age and the SFR is evidence of this.

The correlation between log Age and $\log D_{\rm L}$ is

$$\log \mathrm{Age} = (-0.75 \pm 0.078) \times \log D_{\rm L} + (2.7 \pm 0.036), \quad (86)$$

where $D_{\rm L}$ is in units of 10^{28} cm. Age is in units of Myr. The adjusted R^2 is 0.26. The Pearson coefficient is -0.3 ± 0.081 with p-value 6.9×10^{-3}. The Spearman coefficient is -0.2 ± 0.091 with p-value 7.5×10^{-2}. The Kendall τ coefficient is -0.14 ± 0.064 with p-value 7.3×10^{-2}. The correlation ratio is 0.99 ± 0.002. The cosine similarity is -0.82 ± 0.0058. The scatter plot is in Figure 76. The number of GRBs in the sample is 82.

The correlation between log Age and $\log(1+z)$ is

$$\log \mathrm{Age} = (-2 \pm 0.38) \times \log(1+z) + (3.2 \pm 0.11), \quad (87)$$

where the age is in units of Myr. The adjusted R^2 is 0.22. The Pearson coefficient is -0.39 ± 0.059 with p-value 3×10^{-4}. The Spearman coefficient is -0.43 ± 0.049 with p-value 5.5×10^{-5}. The Kendall τ coefficient is -0.29 ± 0.035 with p-value 9.9×10^{-5}. The correlation ratio is 0.91 ± 0.011. The cosine similarity is 0.76 ± 0.03. The scatter plot is in Figure 77. The number of GRBs in the sample is 82. It is similar to that shown in Equation (86). It is quite reasonable that the farther galaxy is younger. However, the relation between the age of the host galaxies and the redshift is not exact because of the cosmological evolution. Considering the large scatter, it is hard to infer special information on the GRB host galaxies from the general evolution of the universe.

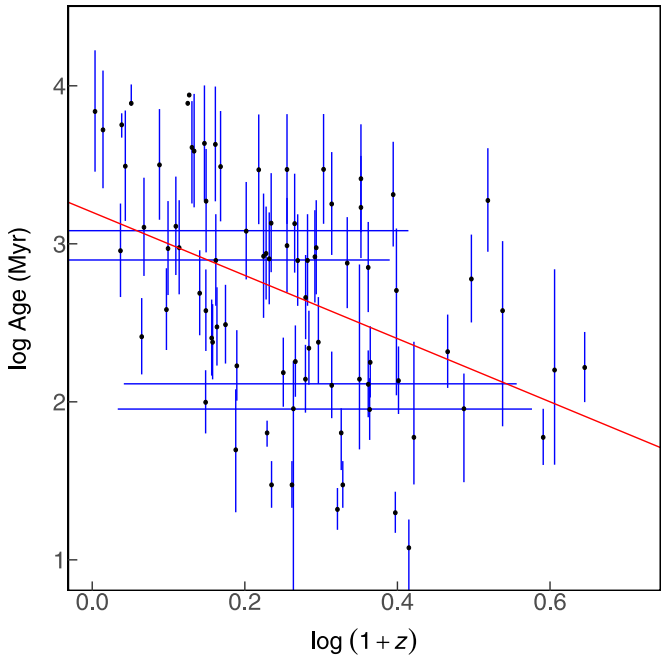

Figure 77. Scatter plot for log Age and $\log(1+z)$. The red line is our fit result. The formula for the red line is $\log \mathrm{Age} = (-2 \pm 0.38) \times \log(1+z) + (3.2 \pm 0.11)$. The description of every parameter is in Section 2.

Age also correlates with $E_{\rm p,cpl}$ and $E_{\rm p,cpl,i}$. We have shown the two correlations in Section 5.6.

5.17. Some Correlations with $L_{radio,pk}$

There might be quite a few derivative quantities that have a stronger correlation with other properties. We show an example of a derivative quantity in this section. We calculated the radio luminosity $L_{\rm radio,pk}$ in rest-frame 8.46 GHz. The formula is

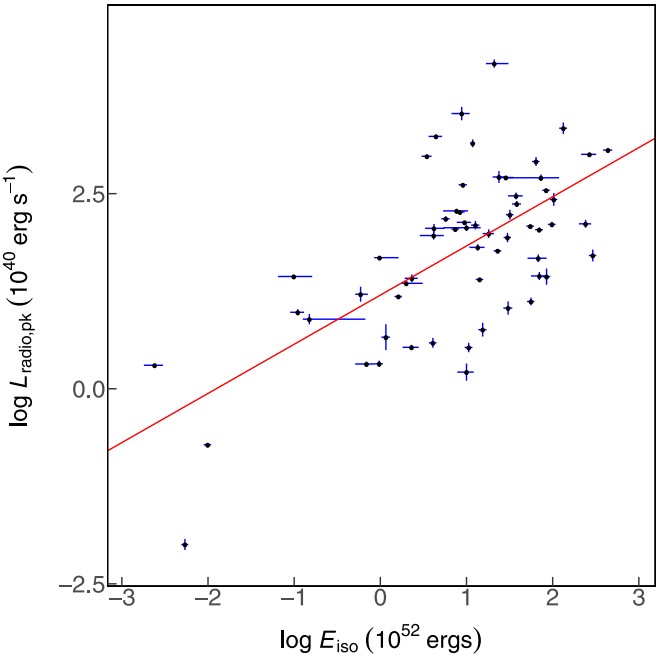

Figure 78. Scatter plot for $\log L_{\rm radio,pk}$ and $\log E_{\rm iso}$. The red line is our fit result. The formula for the red line is $\log L_{\rm radio,pk} = (0.63 \pm 0.013) \times \log E_{\rm iso} + (1.2 \pm 0.019)$. The description of every parameter is in Section 2.

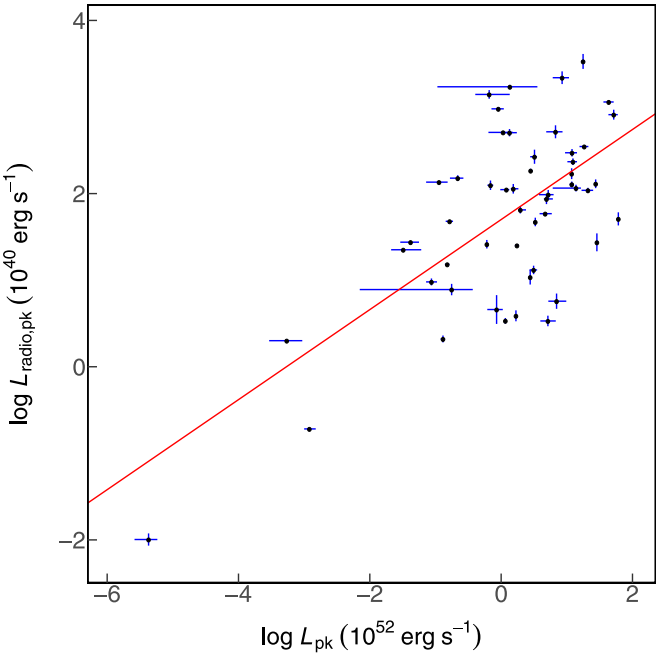

Figure 79. Scatter plot for $\log L_{\rm radio,pk}$ and $\log L_{\rm pk}$. The red line is our fit result. The formula for the red line is $\log L_{\rm radio,pk} = (0.52 \pm 0.025) \times \log L_{\rm pk} + (1.7 \pm 0.018)$. The description of every parameter is in Section 2.

$L_{\rm radio,pk} = 4\pi D_{\rm L}^2 \times F_{\rm radio,pk} \times (1+z) \times 8.46$ GHz. The unit of $L_{\rm radio,pk}$ is 10^{40} erg s^{-1}. We also found some interesting results.

The correlation between $\log L_{\rm radio,pk}$ and $\log E_{\rm iso}$ is

$$\log L_{\rm radio,pk} = (0.63 \pm 0.013) \times \log E_{\rm iso} + (1.2 \pm 0.019), \quad (88)$$

where $L_{\rm radio,pk}$ is in rest-frame 8.46 GHz and in units of 10^{40} erg s^{-1}. $E_{\rm iso}$ is in units of 10^{52} erg and in the rest-frame 1–10^4 keV energy band. The adjusted R^2 is 0.41. The Pearson coefficient is 0.64 ± 0.0094 with p-value 2.2×10^{-8}. The Spearman coefficient is 0.52 ± 0.015 with p-value 1.5×10^{-5}. The Kendall τ coefficient is 0.37 ± 0.013 with p-value 2.6×10^{-5}. The correlation ratio is 0.37 ± 0.0057. The cosine similarity is 0.81 ± 0.0067. The scatter plot is in Figure 78. The number of GRBs in the sample is 61. The peak times of the radio emission are often very late. The peak radio luminosity mainly represents the total kinetic energy and environment, while the isotropic equivalent γ-ray energy $E_{\rm iso}$ is also positively correlated to the total kinetic energy, although it is usually assumed that they are proportional by an efficiency factor. Therefore, the correlation between $L_{\rm radio,pk}$ and $E_{\rm iso}$ is expected. As the data are largely scattered, the actual power-law index between them is not clear. With the accumulated data and classification, the indices might change.

The correlation between $\log L_{\rm radio,pk}$ and $\log L_{\rm pk}$ is

$$\log L_{\rm radio,pk} = (0.52 \pm 0.025) \times \log L_{\rm pk} + (1.7 \pm 0.018), \quad (89)$$

where $L_{\rm radio,pk}$ is in rest-frame 8.46 GHz and in units of 10^{40} erg s^{-1}. $L_{\rm pk}$ is in units of 10^{52} erg s^{-1} and in the 1–10^4 keV energy band. The adjusted R^2 is 0.45. The Pearson coefficient is 0.67 ± 0.023 with p-value 9.1×10^{-8}. The Spearman coefficient is 0.45 ± 0.029 with p-value 8.2×10^{-4}. The Kendall τ coefficient is 0.32 ± 0.021 with p-value 8.9×10^{-4}. The correlation ratio is 0.57 ± 0.0055. The cosine similarity is 0.4 ± 0.027. The scatter plot is in Figure 79. The number of GRBs in the sample is 51. This relation is similar to Equation (88).

The correlation between $\log L_{\rm radio,pk}$ and log SFR is

$$\log L_{\rm radio,pk} = (0.63 \pm 0.092) \times \log {\rm SFR} + (0.43 \pm 0.073), \quad (90)$$

where $L_{\rm radio,pk}$ is in rest-frame 8.46 GHz and in units of 10^{40} erg s^{-1}. SFR is in units of $M_\odot$ yr^{-1}. The adjusted R^2 is 0.25. The Pearson coefficient is 0.53 ± 0.057 with p-value 4×10^{-2}. The Spearman coefficient is 0.37 ± 0.06 with p-value 0.17. The Kendall τ coefficient is 0.25 ± 0.052 with p-value 0.18. The correlation ratio is 0.13 ± 0.03. The cosine similarity is 0.64 ± 0.054. The scatter plot is in Figure 80. The number of GRBs in the sample is 15. This relation may reveal the dependence of the radio afterglow and the environment of the GRBs. A higher star formation rate region implies a higher number density of the environment.

The correlation between $\log L_{\rm radio,pk}$ and log Age is

$$\log L_{\rm radio,pk} = (-0.61 \pm 0.16) \times \log {\rm Age} + (2.9 \pm 0.48), \quad (91)$$

where $L_{\rm radio,pk}$ is in rest-frame 8.46 GHz and is in units of 10^{40} erg s^{-1}. Age is in units of Myr. The adjusted R^2 is 0.21. The Pearson coefficient is -0.43 ± 0.085 with p-value 3.4×10^{-2}. The Spearman coefficient is -0.44 ± 0.099 with p-value 3.1×10^{-2}. The Kendall τ coefficient is -0.31 ± 0.077 with p-value 3.3×10^{-2}. The correlation ratio is 0.66 ± 0.038. The cosine similarity is 0.64 ± 0.024. The scatter plot is in Figure 81. The number of GRBs in the sample is 24. As shown

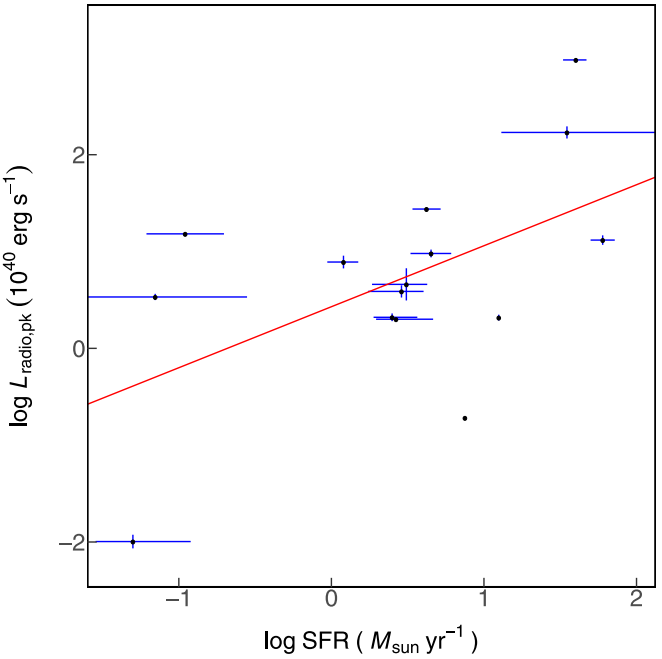

Figure 80. Scatter plot for $\log L_{\rm radio,pk}$ and log SFR. The red line is our fit result. The formula for the red line is $\log L_{\rm radio,pk} = (0.63 \pm 0.092) \times \log {\rm SFR} + (0.43 \pm 0.073)$. The description of every parameter is in Section 2.

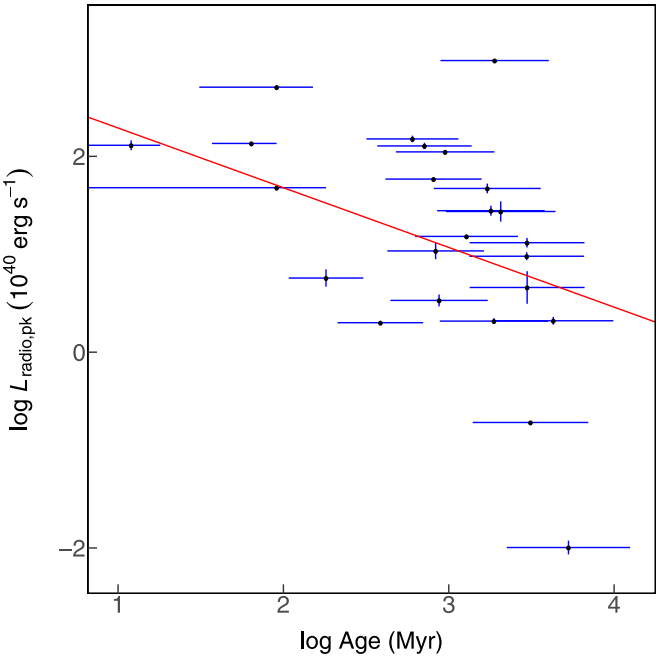

Figure 81. Scatter plot for $\log L_{\rm radio,pk}$ and log Age. The red line is our fit result. The formula for the red line is $\log L_{\rm radio,pk} = (-0.61 \pm 0.16) \times \log {\rm Age} + (2.9 \pm 0.48)$. The description of every parameter is in Section 2.

in Equation (90), higher radio luminosity corresponds to more active star formation. In Equation (85), a higher star formation rate corresponds to a younger host galaxy. These two relations are derive from Equation (91).

The correlation between $\log L_{\rm radio,pk}$ and $\log E_{\rm p,Band,i}$ is

$$\log L_{\rm radio,pk} = (0.86 \pm 0.054) \times \log E_{\rm p,Band,i} + (-0.48 \pm 0.14), \quad (92)$$

where $L_{\rm radio,pk}$ is in rest-frame 8.46 GHz and is in units of 10^{40} erg s^{-1}. $E_{\rm p,Band,i}$ is in units of keV. The adjusted R^2 is 0.32. The Pearson coefficient is 0.57 ± 0.027 with p-value 2.6×10^{-4}. The Spearman coefficient is 0.5 ± 0.037 with p-value 1.8×10^{-3}. The Kendall τ coefficient is 0.35 ± 0.031 with p-value 2.5×10^{-3}. The correlation ratio is 0.51 ± 0.011. The cosine similarity is 0.93 ± 0.0032. The scatter plot is in Figure 82. The number of GRBs in the sample is 36. This relation might be from the Amati relation. As a higher peak energy corresponds to a higher total energy of the GRBs, it also leads to brighter radio luminosity.

The correlation between $\log L_{\rm radio,pk}$ and $\log E_{\rm p,cpl,i}$ is

$$\log L_{\rm radio,pk} = (1.5 \pm 0.2) \times \log E_{\rm p,cpl,i} + (-2.2 \pm 0.55), \quad (93)$$

where $L_{\rm radio,pk}$ is in rest-frame 8.46 GHz and is in units of 10^{40} erg s^{-1}. $E_{\rm p,cpl,i}$ is in units of keV. The adjusted R^2 is 0.42. The Pearson coefficient is 0.65 ± 0.057 with p-value 2.1×10^{-3}. The Spearman coefficient is 0.57 ± 0.077 with p-value 8.7×10^{-3}. The Kendall τ coefficient is 0.42 ± 0.064 with p-value 9.4×10^{-3}. The correlation ratio is 0.31 ± 0.018. The cosine similarity is 0.88 ± 0.0075. The scatter plot is in Figure 83. The number of GRBs in the sample is 20. It is similar to Equation (92).

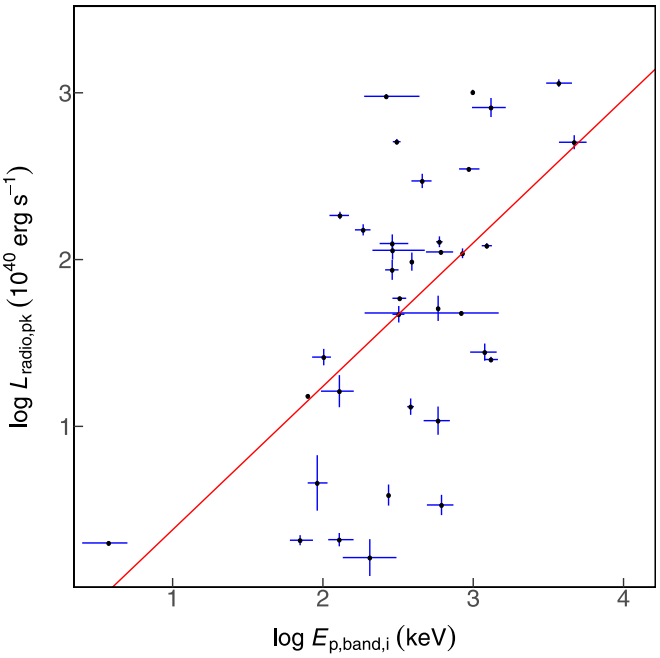

Figure 82. Scatter plot for $\log L_{\rm radio,pk}$ and $\log E_{\rm p,Band,i}$. The red line is our fit result. The formula for the red line is $\log L_{\rm radio,pk} = (0.86 \pm 0.054) \times \log E_{\rm p,Band,i} + (-0.48 \pm 0.14)$. The description of every parameter is in Section 2.

The correlation between $\log L_{\rm radio,pk}$ and rest-frame spectral lag is

$$\log L_{\rm radio,pk} = (-0.00023 \pm 0.000048) \times \text{rest-frame spectral lag} + (2 \pm 0.063), \quad (94)$$

where $L_{\rm radio,pk}$ is in rest-frame 8.46 GHz and is in units of 10^{40} erg s^{-1}. Rest-frame spectral lag is in units of ms MeV^{-1}.

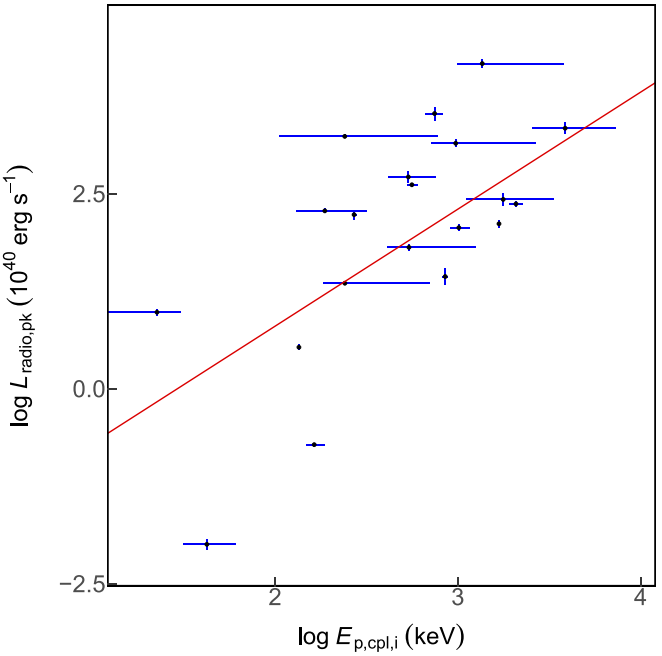

Figure 83. Scatter plot for $\log L_{\rm radio,pk}$ and $\log E_{\rm p,cpl,i}$. The red line is our fit result. The formula for the red line is $\log L_{\rm radio,pk} = (1.5 \pm 0.2) \times \log E_{\rm p,cpl,i} + (-2.2 \pm 0.55)$. The description of every parameter is in Section 2.

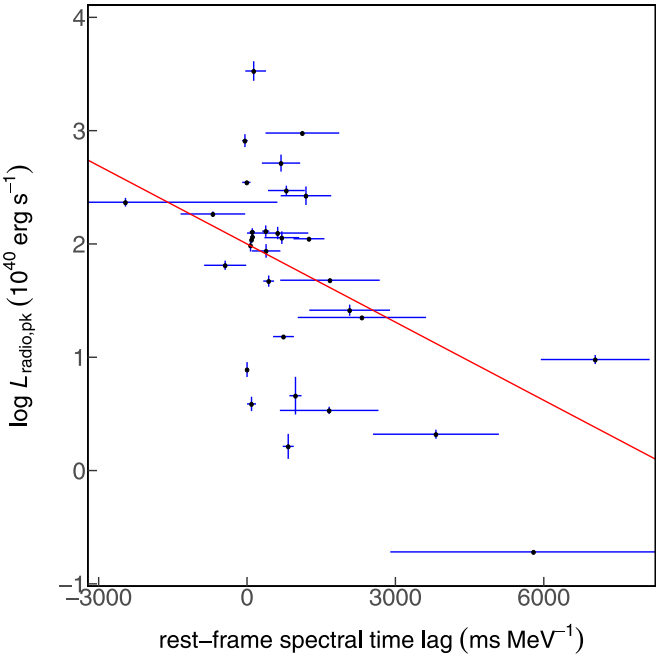

Figure 84. Scatter plot for $\log L_{\rm radio,pk}$ and rest-frame spectral lag. The red line is our fit result. The formula for the red line is $\log L_{\rm radio,pk} = (-0.00023 \pm 0.000048) \times$ the rest-frame spectral lag $+ (2 \pm 0.063)$. The description of every parameter is in Section 2.

The adjusted R^2 is 0.29. The Pearson coefficient is -0.49 ± 0.089 with p-value 4.2×10^{-3}. The Spearman coefficient is -0.4 ± 0.081 with p-value 2.2×10^{-2}. The Kendall τ coefficient is -0.28 ± 0.06 with p-value 2.3×10^{-2}. The correlation ratio is 0.34 ± 0.06. The cosine similarity is 0.2 ± 0.078. The scatter plot is in Figure 84. The number of GRBs in the sample is 32. It is also quite puzzling why the radio luminosity is related to the spectral lag.

6. Remarkable Results for Three Parameters

In this section, we analyze some good correlations among three parameters. First, the correlation should include at least 10 GRBs. The adjusted R^2 should also be bigger than 0.2. The entire linear model, and a_1 and a_2 should have hypothesis-testing p-values smaller than 0.05. The peak energy flux $F_{\rm pk}$ and peak photon flux $P_{\rm pk}$ both have four different time bins. If the $F_{\rm pk}$ in four time bins correlates in another time bin with the same parameter, we just showed the best time bin result. It is the same for $P_{\rm pk}$. All results are in machine-readable tables. In the following, we will show all of the remarkable results in order of increasing sample numbers. We just show the figures with the remarkable results; the total number is 361. We provide all 361 figures in the figure set and show the first 6 figures in Figure 85.

The $\log \Gamma_0$–$(-\alpha_{\rm Band})$–$\beta_{\rm X11hr}$ formula is

$$\log \Gamma_0 = (-0.39 \pm 0.09) \times (-\alpha_{\rm Band}) + (-0.59 \pm 0.14) \times \beta_{\rm X11hr} + (3.4 \pm 0.21), \quad (95)$$

and the adjusted R^2 is 0.6552. The number of GRBs in the sample is 10.

The log SSFR–log Mass–$\log t_{\rm pkX,i}$ formula is

$$\log {\rm SSFR} = (-0.47 \pm 0.14) \times \log {\rm Mass} + (-0.76 \pm 0.18) \times \log t_{\rm pkX,i} + (5.5 \pm 1.3), \quad (96)$$

where log SSFR is in units of Gyr^{-1}. Mass is in units of $M_\odot$. $t_{\rm pkX,i}$ is in units of s. The adjusted R^2 is 0.6759. The number of GRBs in the sample is 10.

The $\log t_{\rm pkX,i}$–log SSFR–$\log T_{90,i}$ formula is

$$\log t_{\rm pkX,i} = (-0.31 \pm 0.13) \times \log {\rm SSFR} + (0.84 \pm 0.18) \times \log T_{90,i} + (0.53 \pm 0.22), \quad (97)$$

where $t_{\rm pkX,i}$ is in units of s. log SSFR is in units of Gyr^{-1}. $T_{90,i}$ is in units of s. The adjusted R^2 is 0.7597. The number of GRBs in the sample is 10.

The log Age–$\log N_{\rm H}$–$\log t_{\rm burst,i}$ formula is

$$\log {\rm Age} = (-0.87 \pm 0.25) \times \log N_{\rm H} + (1 \pm 0.2) \times \log t_{\rm burst,i} + (0.78 \pm 0.59), \quad (98)$$

where Age is in units of Myr. $N_{\rm H}$ is in units of 10^{21} cm^{-2}. $t_{\rm burst,i}$ is in units of s. The adjusted R^2 is 0.681. The number of GRBs in the sample is 10.

The $(-\beta_{\rm Band})$–log offset–log Age formula is

$$(-\beta_{\rm Band}) = (0.65 \pm 0.61) \times \log {\rm offset} + (-0.42 \pm 0.49) \times \log {\rm Age} + (3.5 \pm 1.3), \quad (99)$$

where host galaxy offset is in units of kpc. Age is in units of Myr. The adjusted R^2 is 0.5508. The number of GRBs in the sample is 10.

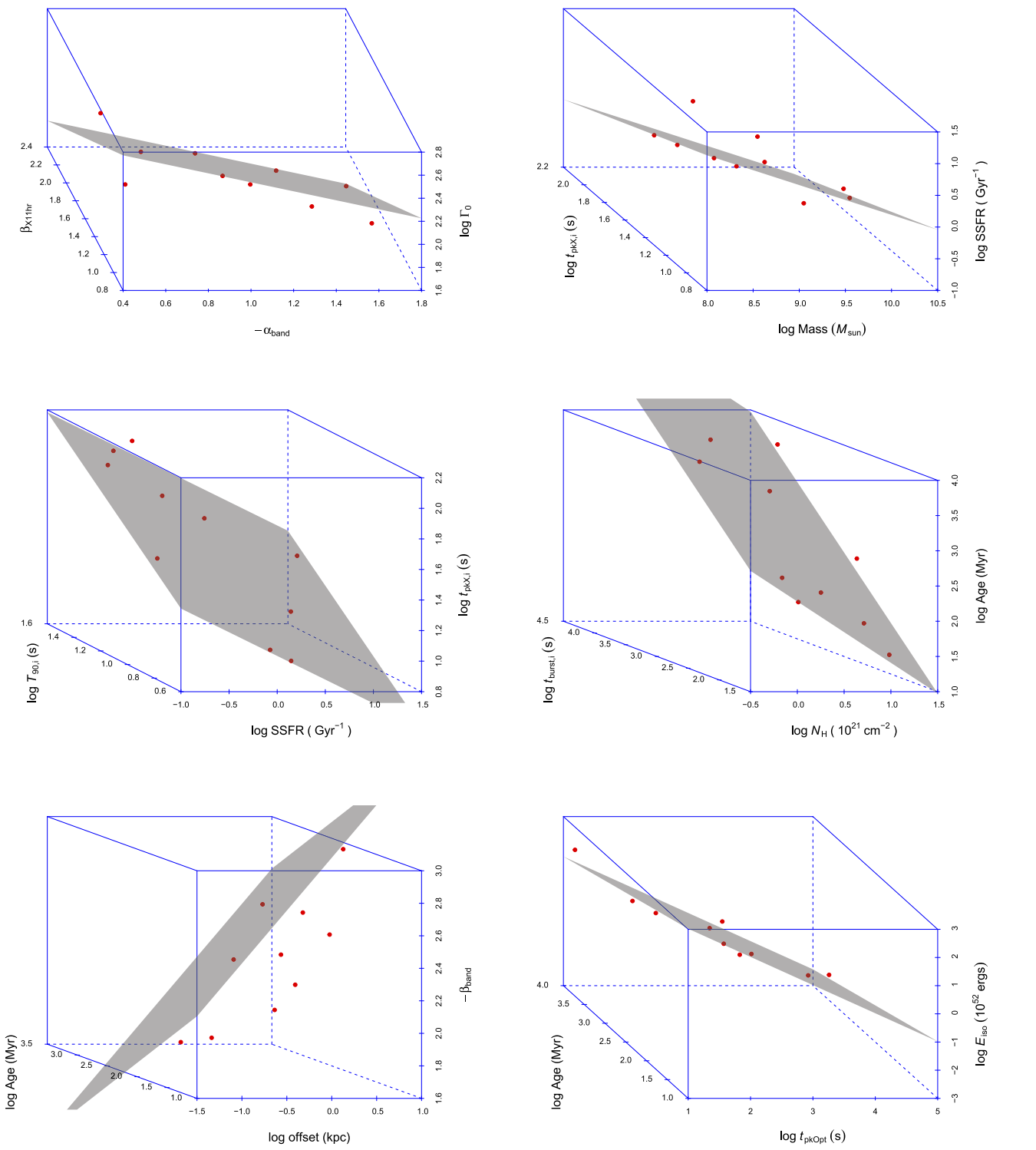

Figure 85. The scatter plots among three parameters. The gray plane in every plot is our fitted result. All results can be found in the machine-readable tables. The description of every parameter is in Section 2.

(The complete figure set (388 images) is available.)

The $\log E_{\rm iso}$–$\log t_{\rm pkOpt}$–log Age formula is

$$\log E_{\rm iso} = (-1 \pm 0.05) \times \log t_{\rm pkOpt} + (-0.48 \pm 0.061) \times \log {\rm Age} + (4.5 \pm 0.22), \quad (100)$$

where $E_{\rm iso}$ is in units of 10^{52} erg and in the rest-frame 1–10^4 keV energy band. $t_{\rm pkOpt}$ is in units of s. Age is in units of Myr. The adjusted R^2 is 0.9079. The number of GRBs in the sample is 10.

The $\log \Gamma_0$–$\log L_{\rm radio,pk}$–$\log T_{\rm R45}$ formula is

$$\log \Gamma_0 = (0.33 \pm 0.012) \times \log L_{\rm radio,pk} + (-0.96 \pm 0.086) \times \log T_{\rm R45} + (2.6 \pm 0.11), \quad (101)$$

where $L_{\rm radio,pk}$ is in rest-frame 8.46 GHz, and the unit is $10^{40}\,{\rm erg\,s^{-1}}$. $T_{\rm R45}$ is in units of s. The adjusted R^2 is 0.6438. The number of GRBs in the sample is 10.

The $\beta_{\rm X11hr}$–$(-\alpha_{\rm spl})$–log Mass formula is

$$\beta_{\rm X11hr} = (0.68 \pm 0.16) \times (-\alpha_{\rm spl}) + (0.24 \pm 0.068) \times \log {\rm Mass} + (-1.9 \pm 0.76), \quad (102)$$

where Mass is in units of $M_\odot$. The adjusted R^2 is 0.5919. The number of GRBs in the sample is 11.

The $\log E_{\rm p,cpl}$–log HR–$\log t_{\rm pkX}$ formula is

$$\log E_{\rm p,cpl} = (0.59 \pm 0.1) \times \log {\rm HR} + (0.15 \pm 0.11) \times \log t_{\rm pkX} + (1.8 \pm 0.19), \quad (103)$$

where $E_{\rm p,cpl}$ is in units of keV. $t_{\rm pkX}$ is in units of s. The adjusted R^2 is 0.9356. The number of GRBs in the sample is 11.

The $\log E_{\rm iso}$–$\log t_{\rm burst,i}$–$\log t_{\rm radio,pk,i}$ formula is

$$\log E_{\rm iso} = (-1.1 \pm 0.047) \times \log t_{\rm burst,i} + (-1.6 \pm 0.2) \times \log t_{\rm radio,pk,i} + (12 \pm 1.1), \quad (104)$$

where $E_{\rm iso}$ is in units of 10^{52} erg and in the rest-frame 1–10^4 keV energy band. $t_{\rm burst,i}$ is in units of s. $t_{\rm radio,pk,i}$ is in units of s. The adjusted R^2 is 0.6305. The number of GRBs in the sample is 11.

The $\log F_{\rm radio,pk}$–$\log t_{\rm burst,i}$–$\log t_{\rm radio,pk,i}$ formula is

$$\log F_{\rm radio,pk} = (0.24 \pm 0.026) \times \log t_{\rm burst,i} + (0.66 \pm 0.055) \times \log t_{\rm radio,pk,i} + (-7.7 \pm 0.31), \quad (105)$$

where $F_{\rm radio,pk}$ is in units of Jy. $t_{\rm burst,i}$ is in units of s. $t_{\rm radio,pk,i}$ is in units of s. The adjusted R^2 is 0.4834. The number of GRBs in the sample is 11.

The $\beta_{\rm X11hr}$–$\log P_{\rm pk2}$–log SSFR formula is

$$\beta_{\rm X11hr} = (-0.57 \pm 0.13) \times \log P_{\rm pk2} + (-0.55 \pm 0.12) \times \log {\rm SSFR} + (2.1 \pm 0.22), \quad (106)$$

where $P_{\rm pk2}$ is the peak photon flux in the 256 ms time bin in 10–1000 keV and is in units of photons $\rm cm^{-2}\,s^{-1}$. log SSFR is in units of $\rm Gyr^{-1}$. The adjusted R^2 is 0.6811. The number of GRBs in the sample is 11.

The $\log \Gamma_0$–$\log t_{\rm radio,pk}$–$\log T_{\rm 50,i}$ formula is

$$\log \Gamma_0 = (1.3 \pm 0.12) \times \log t_{\rm radio,pk} + (-0.74 \pm 0.068) \times \log T_{\rm 50,i} + (-4.5 \pm 0.73), \quad (107)$$

where $t_{\rm radio,pk}$ is in units of s. $T_{\rm 50,i}$ is in units of s. The adjusted R^2 is 0.6372. The number of GRBs in the sample is 11.

The log Mass–$\log T_{90}$–$\log t_{\rm pkX}$ formula is

$$\log {\rm Mass} = (-2.3 \pm 0.36) \times \log T_{90} + (1.7 \pm 0.37) \times \log t_{\rm pkX} + (9.7 \pm 0.88), \quad (108)$$

where Mass is in units of $M_\odot$. T_{90} is in units of s. $t_{\rm pkX}$ is in units of s. The adjusted R^2 is 0.7206. The number of GRBs in the sample is 11.

The $\log L_{\rm pk}$–$\log L_{\rm radio,pk}$–$\log t_{\rm burst}$ formula is

$$\log L_{\rm pk} = (0.91 \pm 0.07) \times \log L_{\rm radio,pk} + (-0.98 \pm 0.24) \times \log t_{\rm burst} + (0.68 \pm 0.7), \quad (109)$$

where $L_{\rm pk}$ is in units of $10^{52}\,{\rm erg\,s^{-1}}$ and in the 1–10^4 keV energy band. $L_{\rm radio,pk}$ is in rest-frame 8.46 GHz and is in units of $10^{40}\,{\rm erg\,s^{-1}}$. $t_{\rm burst}$ is in units of s. The adjusted R^2 is 0.8403. The number of GRBs in the sample is 11.

The rest-frame spectral lag–$\log L_{\rm radio,pk}$–$\log E_{\rm p,cpl}$ formula is

$$\text{rest-frame spectral lag} = (-1263 \pm 580) \times \log L_{\rm radio,pk} + (-2816 \pm 951) \times \log E_{\rm p,cpl} + (10058 \pm 2111), \quad (110)$$

where the rest-frame spectral lag is in units of $\rm ms\,MeV^{-1}$. $L_{\rm radio,pk}$ is in rest-frame 8.46 GHz and in units of $10^{40}\,{\rm erg\,s^{-1}}$. $E_{\rm p,cpl}$ is in units of keV. The adjusted R^2 is 0.7246. The number of GRBs in the sample is 11.

The $\log \Gamma_0$–$\log L_{\rm radio,pk}$–$\log t_{\rm pkOpt}$ formula is

$$\log \Gamma_0 = (0.15 \pm 0.015) \times \log L_{\rm radio,pk} + (-0.57 \pm 0.023) \times \log t_{\rm pkOpt} + (3.4 \pm 0.093), \quad (111)$$

where $L_{\rm radio,pk}$ is in rest-frame 8.46 GHz and in units of $10^{40}\,{\rm erg\,s^{-1}}$. $t_{\rm pkOpt}$ is in units of s. The adjusted R^2 is 0.9562. The number of GRBs in the sample is 11.

The $\log E_{\rm iso}$–$\log \Gamma_0$–$\log F_{\rm radio,pk}$ formula is

$$\log E_{\rm iso} = (1.2 \pm 0.094) \times \log \Gamma_0 + (-2.2 \pm 0.35) \times \log F_{\rm radio,pk} + (-9.7 \pm 1.2), \quad (112)$$

where $E_{\rm iso}$ is in units of 10^{52} erg and in the rest-frame 1–10^4 keV energy band. $F_{\rm radio,pk}$ is in units of Jy. The adjusted R^2 is 0.8299. The number of GRBs in the sample is 12.

The $\log F_{\rm g}$–$\log \Gamma_0$–$\log t_{\rm radio,pk,i}$ formula is

$$\log F_{\rm g} = (0.64 \pm 0.08) \times \log \Gamma_0 + (1.8 \pm 0.24) \times \log t_{\rm radio,pk,i} + (-9.9 \pm 1.2), \quad (113)$$

where $F_{\rm g}$ is in units of $10^{-6}\,{\rm erg\,cm^{-2}}$ and in the 20–2000 keV energy band. $t_{\rm radio,pk,i}$ is in units of s. The adjusted R^2 is 0.7167. The number of GRBs in the sample is 12.

The Mag–$\log F_{\rm Opt11hr}$–metallicity formula is

$$\rm Mag = (1.1 \pm 0.64) \times \log F_{Opt11hr} + (-2.4 \pm 1.8) \times metallicity + (5.5 \pm 15), \quad (114)$$

where Mag is in units of magnitude. $F_{\rm Opt11hr}$ is in units of Jy. The metallicity is the value of $12 + \log {\rm O/H}$. The adjusted R^2 is 0.5847. The number of GRBs in the sample is 13.

The $\log L_{\rm pk}$–log offset–$\log E_{\rm p,cpl,i}$ formula is

$$\log L_{\rm pk} = (-0.94 \pm 0.26) \times \log \text{offset} + (1.1 \pm 0.33) \times \log E_{\rm p,cpl,i} + (-3.2 \pm 0.86), \quad (115)$$

where $L_{\rm pk}$ is in units of $10^{52}\,{\rm erg\,s^{-1}}$ and in the 1–10^4 keV energy band. The host galaxy offset is in units of kpc. $E_{\rm p,cpl,i}$ is in units of keV. The adjusted R^2 is 0.4724. The number of GRBs in the sample is 13.

The $\log t_{\rm pkX}$–$\log T_{50}$–log HR formula is

$$\log t_{\rm pkX} = (0.59 \pm 0.057) \times \log T_{50} + (0.44 \pm 0.11) \times \log \text{HR} + (0.81 \pm 0.083), \quad (116)$$

where $t_{\rm pkX}$ is in units of s. T_{50} is in units of s. The adjusted R^2 is 0.7483. The number of GRBs in the sample is 13.

The $\log F_{\rm pk3}$–$\log T_{90}$–$\log F_{\rm X11hr}$ formula is

$$\log F_{\rm pk3} = (-1 \pm 0.15) \times \log T_{90} + (0.54 \pm 0.063) \times \log F_{\rm X11hr} + (5.5 \pm 0.41), \quad (117)$$

where $F_{\rm pk3}$ is the peak energy flux in the 256 ms time bin in the rest-frame 1–10^4 keV energy band and is in units of $10^{-6}\,{\rm erg\,cm^{-2}\,s^{-1}}$. T_{90} is in units of s. $F_{\rm X11hr}$ is in units of Jy. The adjusted R^2 is 0.7421. The number of GRBs in the sample is 13.

The $\log P_{\rm pk2}$–$\log T_{90}$–$\log F_{\rm X11hr}$ formula is

$$\log P_{\rm pk2} = (-0.97 \pm 0.12) \times \log T_{90} + (0.46 \pm 0.047) \times \log F_{\rm X11hr} + (5.7 \pm 0.31), \quad (118)$$

where $P_{\rm pk2}$ is the peak photon flux in the 256 ms time bin in 10–1000 keV and is in units of photons $\rm cm^{-2}\,s^{-1}$. T_{90} is in units of s. $F_{\rm X11hr}$ is in units of Jy. The adjusted R^2 is 0.65. The number of GRBs in the sample is 13.

The $(-\alpha_{\rm spl})$–variability$_1$–$\log F_{\rm X11hr}$ formula is

$$(-\alpha_{\rm spl}) = (0.48 \pm 0.76) \times \text{variability}_1 + (-0.23 \pm 0.062) \times \log F_{\rm X11hr} + (0.44 \pm 0.48), \quad (119)$$

where $F_{\rm X11hr}$ is in units of Jy. The adjusted R^2 is 0.4567. The number of GRBs in the sample is 13.

The $\log F_{\rm pk2}$–$(-\beta_{\rm Band})$–$\log t_{\rm radio,pk}$ formula is

$$\log F_{\rm pk2} = (0.46 \pm 0.1) \times (-\beta_{\rm Band}) + (-0.68 \pm 0.13) \times \log t_{\rm radio,pk} + (3.7 \pm 0.67), \quad (120)$$

where $F_{\rm pk2}$ is the peak energy flux in the 64 ms time bin in the rest-frame 1–10^4 keV energy band and is in units of $10^{-6}\,{\rm erg\,cm^{-2}\,s^{-1}}$. $t_{\rm radio,pk}$ is in units of s. The adjusted R^2 is 0.499. The number of GRBs in the sample is 14.

The $(-\beta_{\rm Band})$–$\log F_{\rm pk2}$–$\log F_{\rm radio,pk}$ formula is

$$(-\beta_{\rm Band}) = (0.64 \pm 0.16) \times \log F_{\rm pk2} + (-0.83 \pm 0.21) \times \log F_{\rm radio,pk} + (-1 \pm 0.7), \quad (121)$$

where $F_{\rm pk2}$ is the peak energy flux in the 64 ms time bin in the rest-frame 1–10^4 keV energy band and is in units of $10^{-6}\,{\rm erg\,cm^{-2}\,s^{-1}}$. $F_{\rm radio,pk}$ is in units of Jy. The adjusted R^2 is 0.6076. The number of GRBs in the sample is 14.

The log HR–$\log F_{\rm pk3}$–log Age formula is

$$\log \text{HR} = (0.39 \pm 0.035) \times \log F_{\rm pk3} + (-0.24 \pm 0.065) \times \log \text{Age} + (1.2 \pm 0.19), \quad (122)$$

where $F_{\rm pk3}$ is the peak energy flux in the 256 ms time bin in the rest-frame 1–10^4 keV energy band and is in units of $10^{-6}\,{\rm erg\,cm^{-2}\,s^{-1}}$. Age is in units of Myr. The adjusted R^2 is 0.5974. The number of GRBs in the sample is 14.

The $\log t_{\rm pkOpt}$–$\log L_{\rm pk}$–log SSFR formula is

$$\log t_{\rm pkOpt} = (-0.47 \pm 0.014) \times \log L_{\rm pk} + (0.69 \pm 0.042) \times \log \text{SSFR} + (2.2 \pm 0.025), \quad (123)$$

where $t_{\rm pkOpt}$ is in units of s. $L_{\rm pk}$ is in units of $10^{52}\,{\rm erg\,s^{-1}}$ and in the 1–10^4 keV energy band. log SSFR is in units of $\rm Gyr^{-1}$. The adjusted R^2 is 0.8097. The number of GRBs in the sample is 14.

The $\log t_{\rm pkOpt,i}$–Mag–$\log N_{\rm H}$ formula is

$$\log t_{\rm pkOpt,i} = (0.14 \pm 0.058) \times \text{Mag} + (0.74 \pm 0.19) \times \log N_{\rm H} + (4.9 \pm 1.2), \quad (124)$$

where $t_{\rm pkOpt,i}$ is in units of s. Mag is in units of magnitude. $N_{\rm H}$ is in units of $10^{21}\,{\rm cm^{-2}}$. The adjusted R^2 is 0.4411. The number of GRBs in the sample is 14.

The $(-\beta_{\rm Band})$–$\log P_{\rm pk1}$–$\log F_{\rm radio,pk}$ formula is

$$(-\beta_{\rm Band}) = (0.59 \pm 0.13) \times \log P_{\rm pk1} + (-0.73 \pm 0.2) \times \log F_{\rm radio,pk} + (-0.99 \pm 0.61), \quad (125)$$

where $P_{\rm pk1}$ is the peak photon flux in the 64 ms time bin in 10–1000 keV and is in units of photons $\rm cm^{-2}\,s^{-1}$. $F_{\rm radio,pk}$ is in units of Jy. The adjusted R^2 is 0.5843. The number of GRBs in the sample is 14.

The log HR–$\log P_{\rm pk2}$–log Age formula is

$$\log \text{HR} = (0.38 \pm 0.039) \times \log P_{\rm pk2} + (-0.26 \pm 0.077) \times \log \text{Age} + (1 \pm 0.21), \quad (126)$$

where $P_{\rm pk2}$ is the peak photon flux in the 256 ms time bin in 10–1000 keV and is in units of photons $\rm cm^{-2}\,s^{-1}$. Age is in units of Myr. The adjusted R^2 is 0.3174. The number of GRBs in the sample is 14.

The $\log L_{\rm pk}$–$\log L_{\rm radio,pk}$–$\log t_{\rm pkOpt}$ formula is

$$\log L_{\rm pk} = (0.62 \pm 0.068) \times \log L_{\rm radio,pk} + (-0.99 \pm 0.089) \times \log t_{\rm pkOpt} + (1.3 \pm 0.28), \quad (127)$$

where $L_{\rm pk}$ is in units of $10^{52}\,{\rm erg\,s^{-1}}$ and in the 1–10^4 keV energy band. $L_{\rm radio,pk}$ is in rest-frame 8.46 GHz and is in units of $10^{40}\,{\rm erg\,s^{-1}}$. $t_{\rm pkOpt}$ is in units of s. The adjusted R^2 is 0.8128. The number of GRBs in the sample is 14.

The log Age–log θ_j–log N_H formula is

$$\log \mathrm{Age} = (0.94 \pm 0.3) \times \log \theta_j + (-0.82 \pm 0.32) \times \log N_H + (4.5 \pm 0.37), \quad (128)$$

where Age is in units of Myr. θ_j is in units of rad. N_H is in units of $10^{21}\,\mathrm{cm}^{-2}$. The adjusted R^2 is 0.3373. The number of GRBs in the sample is 15.

The log F_g–$(-\alpha_{spl})$–log N_H formula is

$$\log F_g = (-1.2 \pm 0.2) \times (-\alpha_{spl}) + (0.39 \pm 0.089) \times \log N_H + (2.3 \pm 0.37), \quad (129)$$

where F_g is in units of $10^{-6}\,\mathrm{erg\,cm}^{-2}$ and in the 20–2000 keV energy band. N_H is in units of $10^{21}\,\mathrm{cm}^{-2}$. The adjusted R^2 is 0.5037. The number of GRBs in the sample is 16.

The log F_{pk2}–log $E_{p,cpl}$–log F_{X11hr} formula is

$$\log F_{pk2} = (0.87 \pm 0.29) \times \log E_{p,cpl} + (0.35 \pm 0.099) \times \log F_{X11hr} + (0.81 \pm 0.7), \quad (130)$$

where F_{pk2} is the peak energy flux in the 64 ms time bin in the rest-frame 1–10^4 keV energy band and is in units of $10^{-6}\,\mathrm{erg\,cm}^{-2}\,\mathrm{s}^{-1}$. $E_{p,cpl}$ is in units of keV. F_{X11hr} is in units of Jy. The adjusted R^2 is 0.6483. The number of GRBs in the sample is 16.

The log Γ_0–log F_g–log Mass formula is

$$\log \Gamma_0 = (0.57 \pm 0.035) \times \log F_g + (0.25 \pm 0.038) \times \log \mathrm{Mass} + (-1.1 \pm 0.35), \quad (131)$$

where F_g is in units of $10^{-6}\,\mathrm{erg\,cm}^{-2}$ and in the 20–2000 keV energy band. Mass is in units of $M_\odot$. The adjusted R^2 is 0.6784. The number of GRBs in the sample is 16.

The $(-\alpha_{Band})$–variability$_3$–log P_{pk4} formula is

$$(-\alpha_{Band}) = (-21 \pm 12) \times \mathrm{variability}_3 + (0.12 \pm 0.045) \times \log P_{pk4} + (1.2 \pm 0.099), \quad (132)$$

where P_{pk4} is the peak photon flux in the 1 s time bin in 10–1000 keV and is in units of photons $\mathrm{cm}^{-2}\,\mathrm{s}^{-1}$. The adjusted R^2 is 0.4653. The number of GRBs in the sample is 16.

The log $E_{p,cpl,i}$–log $L_{radio,pk}$–A_V formula is

$$\log E_{p,cpl,i} = (0.28 \pm 0.036) \times \log L_{radio,pk} + (-0.42 \pm 0.13) \times A_V + (2.4 \pm 0.091), \quad (133)$$

where $E_{p,cpl,i}$ is in units of keV. $L_{radio,pk}$ is in rest-frame 8.46 GHz and in units of $10^{40}\,\mathrm{erg\,s}^{-1}$. The adjusted R^2 is 0.5624. The number of GRBs in the sample is 16.

The log F_g–$(-\alpha_{spl})$–log F_{X11hr} formula is

$$\log F_g = (-0.67 \pm 0.16) \times (-\alpha_{spl}) + (0.43 \pm 0.078) \times \log F_{X11hr} + (4.6 \pm 0.57), \quad (134)$$

where F_g is in units of $10^{-6}\,\mathrm{erg\,cm}^{-2}$ and in the 20–2000 keV energy band. F_{X11hr} is in units of Jy. The adjusted R^2 is 0.4784. The number of GRBs in the sample is 17.

The log Γ_0–log F_{pk1}–log Mass formula is

$$\log \Gamma_0 = (0.37 \pm 0.028) \times \log F_{pk1} + (0.23 \pm 0.045) \times \log \mathrm{Mass} + (-0.22 \pm 0.43), \quad (135)$$

where F_{pk1} is the peak energy flux in the 1 s time bin in the rest-frame 1–10^4 keV energy band and is in units of $10^{-6}\,\mathrm{erg\,cm}^{-2}\,\mathrm{s}^{-1}$. Mass is in units of $M_\odot$. The adjusted R^2 is 0.4798. The number of GRBs in the sample is 17.

The log$(1+z)$–log F_{pk2}–log $F_{radio,pk}$ formula is

$$\log(1+z) = (-0.13 \pm 0.025) \times \log F_{pk2} + (-0.29 \pm 0.027) \times \log F_{radio,pk} + (-0.47 \pm 0.11), \quad (136)$$

where F_{pk2} is the peak energy flux in the 64 ms time bin in the rest-frame 1–10^4 keV energy band and is in units of $10^{-6}\,\mathrm{erg\,cm}^{-2}\,\mathrm{s}^{-1}$. $F_{radio,pk}$ is in units of Jy. The adjusted R^2 is 0.6147. The number of GRBs in the sample is 17.

The log $t_{radio,pk}$–log $F_{radio,pk}$–log $t_{pkOpt,i}$ formula is

$$\log t_{radio,pk} = (-0.56 \pm 0.063) \times \log F_{radio,pk} + (-0.2 \pm 0.021) \times \log t_{pkOpt,i} + (4.2 \pm 0.22), \quad (137)$$

where $t_{radio,pk}$ is in units of s. $F_{radio,pk}$ is in units of Jy. $t_{pkOpt,i}$ is in units of s. The adjusted R^2 is 0.3468. The number of GRBs in the sample is 17.

The log D_L–log Γ_0–log Mass formula is

$$\log D_L = (0.73 \pm 0.05) \times \log \Gamma_0 + (0.2 \pm 0.041) \times \log \mathrm{Mass} + (-3.1 \pm 0.31), \quad (138)$$

where D_L is in units of 10^{28} cm. Mass is in units of $M_\odot$. The adjusted R^2 is 0.7751. The number of GRBs in the sample is 17.

The spectral lag–log $t_{burst,i}$–log $t_{pkOpt,i}$ formula is

$$\mathrm{spectral\ lag} = (3801 \pm 940) \times \log t_{burst,i} + (4028 \pm 1142) \times \log t_{pkOpt,i} + (-13854 \pm 3488), \quad (139)$$

where spectral time lag is in units of $\mathrm{ms\,MeV}^{-1}$. $t_{burst,i}$ is in units of s. $t_{pkOpt,i}$ is in units of s. The adjusted R^2 is 0.4456. The number of GRBs in the sample is 17.

The log Γ_0–log θ_j–log $E_{p,cpl,i}$ formula is

$$\log \Gamma_0 = (-0.64 \pm 0.11) \times \log \theta_j + (0.63 \pm 0.13) \times \log E_{p,cpl,i} + (-0.35 \pm 0.35), \quad (140)$$

where θ_j is in units of rad. $E_{p,cpl,i}$ is in units of keV. The adjusted R^2 is 0.6444. The number of GRBs in the sample is 17.

The log $L_{radio,pk}$–log T_{90}–log $t_{pkOpt,i}$ formula is

$$\log L_{radio,pk} = (1.6 \pm 0.11) \times \log T_{90} + (-1 \pm 0.033) \times \log t_{pkOpt,i} + (1.3 \pm 0.2), \quad (141)$$

where $L_{radio,pk}$ is in rest-frame 8.46 GHz and in units of $10^{40}\,\mathrm{erg\,s}^{-1}$. T_{90} is in units of s. $t_{pkOpt,i}$ is in units of s. The adjusted R^2 is 0.5211. The number of GRBs in the sample is 17.

The $\log E_{\rm iso}$–$\log L_{\rm radio,pk}$–$\log t_{\rm pkOpt,i}$ formula is

$$\log E_{\rm iso} = (0.36 \pm 0.019) \times \log L_{\rm radio,pk} + (-0.51 \pm 0.03) \times \log t_{\rm pkOpt,i} + (1.3 \pm 0.097), \quad (142)$$

where $E_{\rm iso}$ is in units of 10^{52} erg and in the rest-frame 1–10^4 keV energy band. $L_{\rm radio,pk}$ is in rest-frame 8.46 GHz and is in units of 10^{40} erg s^{-1}. $t_{\rm pkOpt,i}$ is in units of s. The adjusted R^2 is 0.6016. The number of GRBs in the sample is 17.

The $\log T_{\rm R45}$–$\log F_{\rm X11hr}$–$\log t_{\rm radio,pk,i}$ formula is

$$\log T_{\rm R45} = (-0.41 \pm 0.044) \times \log F_{\rm X11hr} + (-0.75 \pm 0.07) \times \log t_{\rm radio,pk,i} + (1.9 \pm 0.3), \quad (143)$$

where $T_{\rm R45}$ is in units of s. $F_{\rm X11hr}$ is in units of Jy. $t_{\rm radio,pk,i}$ is in units of s. The adjusted R^2 is 0.3888. The number of GRBs in the sample is 18.

The $(-\beta_{\rm Band})$–$\log P_{\rm pk1}$–log SSFR formula is

$$(-\beta_{\rm Band}) = (0.12 \pm 0.27) \times \log P_{\rm pk1} + (-0.75 \pm 0.57) \times \log {\rm SSFR} + (2.4 \pm 0.63), \quad (144)$$

where $P_{\rm pk1}$ is the peak photon flux in the 64 ms time bin in 10–1000 keV and is in units of photons cm^{-2} s^{-1}. log SSFR is in units of Gyr^{-1}. The adjusted R^2 is 0.4079. The number of GRBs in the sample is 18.

The $\log t_{\rm radio,pk,i}$–$\log T_{50}$–log SSFR formula is

$$\log t_{\rm radio,pk,i} = (-0.44 \pm 0.018) \times \log T_{50} + (0.43 \pm 0.025) \times \log {\rm SSFR} + (6.3 \pm 0.025), \quad (145)$$

where $t_{\rm radio,pk,i}$ is in units of s. T_{50} is in units of s. log SSFR is in units of Gyr^{-1}. The adjusted R^2 is 0.6841. The number of GRBs in the sample is 18.

The $\log \theta_{\rm j}$–variability$_3$–$\log N_{\rm H}$ formula is

$$\log \theta_{\rm j} = (24 \pm 5.3) \times {\rm variability}_3 + (0.28 \pm 0.057) \times \log N_{\rm H} + (-1.7 \pm 0.078), \quad (146)$$

where $\theta_{\rm j}$ is in units of rad. $N_{\rm H}$ is in units of 10^{21} cm^{-2}. The adjusted R^2 is 0.4522. The number of GRBs in the sample is 18.

The metallicity–$(-\alpha_{\rm cpl})$–$\beta_{\rm X11hr}$ formula is

$${\rm metallicity} = (-0.13 \pm 0.066) \times (-\alpha_{\rm cpl}) + (0.1 \pm 0.064) \times \beta_{\rm X11hr} + (8.6 \pm 0.13), \quad (147)$$

where metallicity is the value of 12 + log O/H. The adjusted R^2 is 0.3058. The number of GRBs in the sample is 19.

The $\log E_{\rm p,cpl,i}$–log HR–$\log t_{\rm radio,pk,i}$ formula is

$$\log E_{\rm p,cpl,i} = (0.64 \pm 0.099) \times \log {\rm HR} + (-0.31 \pm 0.12) \times \log t_{\rm radio,pk,i} + (4.4 \pm 0.67), \quad (148)$$

where $E_{\rm p,cpl,i}$ is in units of keV. $t_{\rm radio,pk,i}$ is in units of s. The adjusted R^2 is 0.6582. The number of GRBs in the sample is 19.

The $\log L_{\rm pk}$–$\log t_{\rm pkOpt}$–Mag formula is

$$\log L_{\rm pk} = (-1.3 \pm 0.14) \times \log t_{\rm pkOpt} + (-0.22 \pm 0.06) \times {\rm Mag} + (-1.1 \pm 1.3), \quad (149)$$

where $L_{\rm pk}$ is in units of 10^{52} erg s^{-1} and in the 1–10^4 keV energy band. $t_{\rm pkOpt}$ is in units of s. Mag is in units of magnitude. The adjusted R^2 is 0.9072. The number of GRBs in the sample is 19.

The Mag–log(1 + z)–metallicity formula is

$${\rm Mag} = (-12 \pm 4.5) \times \log(1+z) + (-1.7 \pm 1.6) \times {\rm metallicity} + (-2.5 \pm 13), \quad (150)$$

where Mag is in units of magnitude. The metallicity is the value of 12 + log O/H. The adjusted R^2 is 0.7636. The number of GRBs in the sample is 19.

The $\log L_{\rm radio,pk}$–$\log F_{\rm Opt11hr}$–$\log E_{\rm p,cpl,i}$ formula is

$$\log L_{\rm radio,pk} = (-0.75 \pm 0.19) \times \log F_{\rm Opt11hr} + (1.4 \pm 0.23) \times \log E_{\rm p,cpl,i} + (-5.1 \pm 0.95), \quad (151)$$

where $L_{\rm radio,pk}$ is in rest-frame 8.46 GHz and is in units of 10^{40} erg s^{-1}. $F_{\rm Opt11hr}$ is in units of Jy. $E_{\rm p,cpl,i}$ is in units of keV. The adjusted R^2 is 0.6282. The number of GRBs in the sample is 19.

The $\log F_{\rm pk3}$–$A_{\rm V}$–log SSFR formula is

$$\log F_{\rm pk3} = (-0.57 \pm 0.14) \times A_{\rm V} + (-0.48 \pm 0.076) \times \log {\rm SSFR} + (1.2 \pm 0.13), \quad (152)$$

where $F_{\rm pk3}$ is the peak energy flux in the 256 ms time bin in the rest-frame 1–10^4 keV energy band and is in units of 10^{-6} erg cm^{-2} s^{-1}. log SSFR is in units of Gyr^{-1}. The adjusted R^2 is 0.363. The number of GRBs in the sample is 20.

The $\log F_{\rm Opt11hr}$–$(-\alpha_{\rm cpl})$–$\log \Gamma_0$ formula is

$$\log F_{\rm Opt11hr} = (0.34 \pm 0.24) \times (-\alpha_{\rm cpl}) + (-0.56 \pm 0.19) \times \log \Gamma_0 + (-3.8 \pm 0.49), \quad (153)$$

where $F_{\rm Opt11hr}$ is in units of Jy. The adjusted R^2 is 0.3106. The number of GRBs in the sample is 20.

The $\log \Gamma_0$–$\log F_{\rm Opt11hr}$–$\log E_{\rm p,cpl,i}$ formula is

$$\log \Gamma_0 = (-0.23 \pm 0.079) \times \log F_{\rm Opt11hr} + (0.61 \pm 0.098) \times \log E_{\rm p,cpl,i} + (-0.59 \pm 0.43), \quad (154)$$

where $F_{\rm Opt11hr}$ is in units of Jy. $E_{\rm p,cpl,i}$ is in units of keV. The adjusted R^2 is 0.5677. The number of GRBs in the sample is 20.

The $\log D_{\rm L}$–$\log F_{\rm radio,pk}$–$\log E_{\rm p,cpl,i}$ formula is

$$\log D_{\rm L} = (-0.72 \pm 0.092) \times \log F_{\rm radio,pk} + (0.6 \pm 0.088) \times \log E_{\rm p,cpl,i} + (-3.7 \pm 0.37), \quad (155)$$

where $D_{\rm L}$ is in units of 10^{28} cm. $F_{\rm radio,pk}$ is in units of Jy. $E_{\rm p,cpl,i}$ is in units of keV. The adjusted R^2 is 0.5231. The number of GRBs in the sample is 20.

The log SFR–log HR–$(-\alpha_{\rm spl})$ formula is

$$\log {\rm SFR} = (-0.17 \pm 0.98) \times \log {\rm HR} + (-0.59 \pm 1) \times (-\alpha_{\rm spl}) + (1.9 \pm 2.3), \quad (156)$$

where SFR is in units of $M_\odot\,{\rm yr}^{-1}$. The adjusted R^2 is 0.2678. The number of GRBs in the sample is 20.

The log SFR–Mag–log $E_{\rm p,cpl,i}$ formula is

$$\log {\rm SFR} = (-0.16 \pm 0.055) \times {\rm Mag} + (0.78 \pm 0.4) \times \log E_{\rm p,cpl,i} + (-4.3 \pm 1.1), \quad (157)$$

where SFR is in units of $M_\odot\,{\rm yr}^{-1}$. Mag is in units of magnitude. $E_{\rm p,cpl,i}$ is in units of keV. The adjusted R^2 is 0.8205. The number of GRBs in the sample is 20.

The log SFR–log$(1+z)$–$(-\alpha_{\rm spl})$ formula is

$$\log {\rm SFR} = (3.5 \pm 0.4) \times \log(1+z) + (-0.49 \pm 0.13) \times (-\alpha_{\rm spl}) + (0.49 \pm 0.23), \quad (158)$$

where SFR is in units of $M_\odot\,{\rm yr}^{-1}$. The adjusted R^2 is 0.4955. The number of GRBs in the sample is 20.

The log $E_{\rm iso}$–log $L_{\rm radio,pk}$–log $E_{\rm p,cpl}$ formula is

$$\log E_{\rm iso} = (0.56 \pm 0.03) \times \log L_{\rm radio,pk} + (1 \pm 0.17) \times \log E_{\rm p,cpl} + (-2.5 \pm 0.35), \quad (159)$$

where $E_{\rm iso}$ is in units of 10^{52} erg and in the rest-frame 1–10^4 keV energy band. $L_{\rm radio,pk}$ is in rest-frame 8.46 GHz and in units of $10^{40}\,{\rm erg\,s^{-1}}$. $E_{\rm p,cpl}$ is in units of keV. The adjusted R^2 is 0.7599. The number of GRBs in the sample is 20.

The log $T_{90,\rm i}$–log $L_{\rm radio,pk}$–$(-\alpha_{\rm cpl})$ formula is

$$\log T_{90,\rm i} = (-0.18 \pm 0.046) \times \log L_{\rm radio,pk} + (0.67 \pm 0.25) \times (-\alpha_{\rm cpl}) + (0.83 \pm 0.33), \quad (160)$$

where $T_{90,\rm i}$ is in units of s. $L_{\rm radio,pk}$ is in rest-frame 8.46 GHz and is in units of $10^{40}\,{\rm erg\,s^{-1}}$. The adjusted R^2 is 0.3241. The number of GRBs in the sample is 20.

The log $t_{\rm pkOpt}$–log $E_{\rm p,Band}$–log $t_{\rm burst}$ formula is

$$\log t_{\rm pkOpt} = (-0.58 \pm 0.097) \times \log E_{\rm p,Band} + (0.5 \pm 0.027) \times \log t_{\rm burst} + (2.4 \pm 0.2), \quad (161)$$

where $t_{\rm pkOpt}$ is in units of s. $E_{\rm p,Band}$ is in units of keV. $t_{\rm burst}$ is in units of s. The adjusted R^2 is 0.2739. The number of GRBs in the sample is 21.

The log $P_{\rm pk1}$–log $F_{\rm g}$–metallicity formula is

$$\log P_{\rm pk1} = (0.44 \pm 0.027) \times \log F_{\rm g} + (0.87 \pm 0.24) \times {\rm metallicity} + (-6.6 \pm 2.1), \quad (162)$$

where $P_{\rm pk1}$ is the peak photon flux in the 64 ms time bin in 10–1000 keV and is in units of photons $\rm cm^{-2}\,s^{-1}$. $F_{\rm g}$ is in units of $10^{-6}\,{\rm erg\,cm^{-2}}$ and in the 20–2000 keV energy band. The metallicity is the value of 12 + log O/H. The adjusted R^2 is 0.5787. The number of GRBs in the sample is 21.

The spectral lag–log$(1+z)$–log $F_{\rm pk3}$ formula is

$$\text{spectral lag} = (-28190 \pm 4027) \times \log(1+z) + (-8125 \pm 1343) \times \log F_{\rm pk3} + (17758 \pm 2296), \quad (163)$$

where spectral time lag is in units of $\rm ms\,MeV^{-1}$. $F_{\rm pk3}$ is the peak energy flux in the 256 ms time bin in the rest-frame 1–10^4 keV energy band and is in units of $10^{-6}\,{\rm erg\,cm^{-2}\,s^{-1}}$. The adjusted R^2 is 0.4887. The number of GRBs in the sample is 21.

The spectral lag–log$(1+z)$–log $P_{\rm pk2}$ formula is

$$\text{spectral lag} = (-26436 \pm 3596) \times \log(1+z) + (-7866 \pm 1114) \times \log P_{\rm pk2} + (22841 \pm 2772), \quad (164)$$

where spectral time lag is in units of $\rm ms\,MeV^{-1}$. $P_{\rm pk2}$ is the peak photon flux in the 256 ms time bin in 10–1000 keV and is in units of photons $\rm cm^{-2}\,s^{-1}$. The adjusted R^2 is 0.3876. The number of GRBs in the sample is 21.

The log $F_{\rm radio,pk}$–$(-\alpha_{\rm Band})$–log Mass formula is

$$\log F_{\rm radio,pk} = (0.58 \pm 0.16) \times (-\alpha_{\rm Band}) + (-0.3 \pm 0.077) \times \log {\rm Mass} + (-1.1 \pm 0.81), \quad (165)$$

where $F_{\rm radio,pk}$ is in units of Jy. Mass is in units of $M_\odot$. The adjusted R^2 is 0.434. The number of GRBs in the sample is 22.

The log $F_{\rm pk2}$–$(-\alpha_{\rm cpl})$–log $F_{\rm Opt11hr}$ formula is

$$\log F_{\rm pk2} = (-0.48 \pm 0.17) \times (-\alpha_{\rm cpl}) + (0.23 \pm 0.11) \times \log F_{\rm Opt11hr} + (1.9 \pm 0.59), \quad (166)$$

where $F_{\rm pk2}$ is the peak energy flux in the 64 ms time bin in the rest-frame 1–10^4 keV energy band and is in units of $10^{-6}\,{\rm erg\,cm^{-2}\,s^{-1}}$. $F_{\rm Opt11hr}$ is in units of Jy. The adjusted R^2 is 0.3327. The number of GRBs in the sample is 22.

The log SFR–metallicity–log Age formula is

$$\log {\rm SFR} = (1.3 \pm 0.38) \times {\rm metallicity} + (-0.64 \pm 0.12) \times \log {\rm Age} + (-9.1 \pm 3.3), \quad (167)$$

where SFR is in units of $M_\odot\,{\rm yr}^{-1}$. The metallicity is the value of 12 + log O/H. Age is in units of Myr. The adjusted R^2 is 0.4076. The number of GRBs in the sample is 22.

The Mag–log $N_{\rm H}$–log $E_{\rm p,cpl,i}$ formula is

$${\rm Mag} = (-1.5 \pm 0.89) \times \log N_{\rm H} + (-1.2 \pm 0.96) \times \log E_{\rm p,cpl,i} + (-17 \pm 2.5), \quad (168)$$

where Mag is in units of magnitude. $N_{\rm H}$ is in units of $10^{21}\,{\rm cm^{-2}}$. $E_{\rm p,cpl,i}$ is in units of keV. The adjusted R^2 is 0.2554. The number of GRBs in the sample is 22.

The log $E_{\rm iso}$–log offset–log $E_{\rm p,cpl,i}$ formula is

$$\log E_{\rm iso} = (-0.8 \pm 0.21) \times \log {\rm offset} + (1.3 \pm 0.3) \times \log E_{\rm p,cpl,i} + (-3.7 \pm 0.82), \quad (169)$$

where $E_{\rm iso}$ is in units of 10^{52} erg and in the rest-frame 1–10^4 keV energy band. The host galaxy offset is in units of

kpc. $E_{\rm p,cpl,i}$ is in units of keV. The adjusted R^2 is 0.5009. The number of GRBs in the sample is 22.

The Mag–log SFR–log $t_{\rm burst,i}$ formula is

$$\begin{aligned}{\rm Mag} = &(-1.5 \pm 0.54) \times \log {\rm SFR} + (0.68 \pm 0.65) \\ &\times \log t_{\rm burst,i} + (-21 \pm 2),\end{aligned} \tag{170}$$

where Mag is in units of magnitude. SFR is in units of $M_\odot\,{\rm yr}^{-1}$. $t_{\rm burst,i}$ is in units of s. The adjusted R^2 is 0.8763. The number of GRBs in the sample is 22.

The $\log F_{\rm radio,pk}$–$\log(1+z)$–variability$_1$ formula is

$$\begin{aligned}\log F_{\rm radio,pk} = &(-0.74 \pm 0.13) \times \log(1+z) \\ &+ (-0.75 \pm 0.87) \times {\rm variability}_1 \\ &+ (-3.2 \pm 0.053),\end{aligned} \tag{171}$$

where $F_{\rm radio,pk}$ is in units of Jy. The adjusted R^2 is 0.286. The number of GRBs in the sample is 22.

The $\log T_{\rm R45,i}$–$\log L_{\rm radio,pk}$–log SSFR formula is

$$\begin{aligned}\log T_{\rm R45,i} = &(-0.19 \pm 0.011) \times \log L_{\rm radio,pk} \\ &+ (0.3 \pm 0.026) \times \log {\rm SSFR} \\ &+ (0.61 \pm 0.016),\end{aligned} \tag{172}$$

where $T_{\rm R45,i}$ is in units of s. $L_{\rm radio,pk}$ is in rest-frame 8.46 GHz and in units of $10^{40}\,{\rm erg\,s^{-1}}$. log SSFR is in units of ${\rm Gyr}^{-1}$. The adjusted R^2 is 0.2284. The number of GRBs in the sample is 23.

The $\log F_{\rm X11hr}$–$\log F_{\rm pk2}$–$\beta_{\rm X11hr}$ formula is

$$\begin{aligned}\log F_{\rm X11hr} = &(0.65 \pm 0.13) \times \log F_{\rm pk2} \\ &+ (-0.94 \pm 0.17) \times \beta_{\rm X11hr} \\ &+ (-6.5 \pm 0.25),\end{aligned} \tag{173}$$

where $F_{\rm X11hr}$ is in units of Jy. $F_{\rm pk2}$ is the peak energy flux in the 64 ms time bin in the rest-frame 1–10^4 keV energy band and is in units of $10^{-6}\,{\rm erg\,cm^{-2}\,s^{-1}}$. The adjusted R^2 is 0.6052. The number of GRBs in the sample is 23.

The $\log E_{\rm iso}$–$\log \Gamma_0$–$\log E_{\rm p,cpl,i}$ formula is

$$\begin{aligned}\log E_{\rm iso} = &(1.3 \pm 0.11) \times \log \Gamma_0 \\ &+ (0.83 \pm 0.17) \times \log E_{\rm p,cpl,i} + (-4.3 \pm 0.3),\end{aligned} \tag{174}$$

where $E_{\rm iso}$ is in units of $10^{52}\,{\rm erg}$ and in the rest-frame 1–10^4 keV energy band. $E_{\rm p,cpl,i}$ is in units of keV. The adjusted R^2 is 0.9021. The number of GRBs in the sample is 23.

The $\log E_{\rm p,Band,i}$–log HR–log SFR formula is

$$\begin{aligned}\log E_{\rm p,Band,i} = &(1.1 \pm 0.14) \times \log {\rm HR} \\ &+ (0.11 \pm 0.026) \times \log {\rm SFR} \\ &+ (2 \pm 0.081),\end{aligned} \tag{175}$$

where $E_{\rm p,Band,i}$ is in units of keV. SFR is in units of $M_\odot\,{\rm yr}^{-1}$. The adjusted R^2 is 0.6949. The number of GRBs in the sample is 23.

The Mag–log HR–$\log E_{\rm p,Band,i}$ formula is

$$\begin{aligned}{\rm Mag} = &(2.7 \pm 2.1) \times \log {\rm HR} + (-2.4 \pm 1.4) \\ &\times \log E_{\rm p,Band,i} + (-16 \pm 3.4),\end{aligned} \tag{176}$$

where Mag is in units of magnitude. $E_{\rm p,Band,i}$ is in units of keV. The adjusted R^2 is 0.3913. The number of GRBs in the sample is 23.

The log offset–$\log T_{50}$–$\log P_{\rm pk4}$ formula is

$$\begin{aligned}\log {\rm offset} = &(-0.32 \pm 0.044) \times \log T_{50} \\ &+ (-0.35 \pm 0.19) \times \log P_{\rm pk4} + (1.1 \pm 0.17),\end{aligned} \tag{177}$$

where the host galaxy offset is in units of kpc. T_{50} is in units of s. $P_{\rm pk4}$ is the peak photon flux in the 1 s time bin in 10–1000 keV and is in units of photons $\rm cm^{-2}\,s^{-1}$. The adjusted R^2 is 0.4552. The number of GRBs in the sample is 23.

The $\log T_{90}$–variability$_2$–$\log E_{\rm p,cpl,i}$ formula is

$$\begin{aligned}\log T_{90} = &(3.5 \pm 0.93) \times {\rm variability}_2 + (0.36 \pm 0.13) \\ &\times \log E_{\rm p,cpl,i} + (0.18 \pm 0.38),\end{aligned} \tag{178}$$

where T_{90} is in units of s. $E_{\rm p,cpl,i}$ is in units of keV. The adjusted R^2 is 0.3912. The number of GRBs in the sample is 23.

The $\log E_{\rm iso}$–$\log L_{\rm radio,pk}$–variability$_3$ formula is

$$\begin{aligned}\log E_{\rm iso} = &(0.33 \pm 0.037) \times \log L_{\rm radio,pk} \\ &+ (58 \pm 7.7) \times {\rm variability}_3 + (0.1 \pm 0.094),\end{aligned} \tag{179}$$

where $E_{\rm iso}$ is in units of $10^{52}\,{\rm erg}$ and in the rest-frame 1–10^4 keV energy band. $L_{\rm radio,pk}$ is in rest-frame 8.46 GHz and in units of $10^{40}\,{\rm erg\,s^{-1}}$. The adjusted R^2 is 0.3608. The number of GRBs in the sample is 24.

The Mag–$(-\beta_{\rm Band})$–$\log F_{\rm Opt11hr}$ formula is

$$\begin{aligned}{\rm Mag} = &(0.48 \pm 0.85) \times (-\beta_{\rm Band}) \\ &+ (0.54 \pm 0.47) \times \log F_{\rm Opt11hr} + (-20 \pm 3.4),\end{aligned} \tag{180}$$

where Mag is in units of magnitude. $F_{\rm Opt11hr}$ is in units of Jy. The adjusted R^2 is 0.3541. The number of GRBs in the sample is 24.

The $\log P_{\rm pk1}$–$\log F_{\rm g}$–$\log N_{\rm H}$ formula is

$$\begin{aligned}\log P_{\rm pk1} = &(0.44 \pm 0.016) \times \log F_{\rm g} \\ &+ (-0.28 \pm 0.043) \times \log N_{\rm H} \\ &+ (0.93 \pm 0.042),\end{aligned} \tag{181}$$

where $P_{\rm pk1}$ is the peak photon flux in the 64 ms time bin in 10–1000 keV and is in units of photons $\rm cm^{-2}\,s^{-1}$. $F_{\rm g}$ is in units of $10^{-6}\,{\rm erg\,cm^{-2}}$ and in the 20–2000 keV energy band. $N_{\rm H}$ is in units of $10^{21}\,{\rm cm^{-2}}$. The adjusted R^2 is 0.6225. The number of GRBs in the sample is 24.

The $\log t_{\rm pkOpt}$–$\log N_{\rm H}$–$\log t_{\rm burst,i}$ formula is

$$\begin{aligned}\log t_{\rm pkOpt} = &(0.52 \pm 0.08) \times \log N_{\rm H} \\ &+ (0.45 \pm 0.028) \times \log t_{\rm burst,i} + (1.1 \pm 0.092),\end{aligned} \tag{182}$$

where $t_{\rm pkOpt}$ is in units of s. $N_{\rm H}$ is in units of $10^{21}\,{\rm cm^{-2}}$. $t_{\rm burst,i}$ is in units of s. The adjusted R^2 is 0.3136. The number of GRBs in the sample is 24.

The $\log F_{\rm Opt11hr}$–log SFR–$\log t_{\rm burst,i}$ formula is

$$\begin{aligned}\log F_{\rm Opt11hr} = &(-0.28 \pm 0.11) \times \log {\rm SFR} \\ &+ (0.56 \pm 0.14) \times \log t_{\rm burst,i} + (-6.1 \pm 0.41),\end{aligned} \tag{183}$$

where $F_{\rm Opt11hr}$ is in units of Jy. SFR is in units of $M_\odot\,{\rm yr}^{-1}$. $t_{\rm burst,i}$ is in units of s. The adjusted R^2 is 0.4728. The number of GRBs in the sample is 24.

The $\log F_{\rm pk3}$–$\log(1+z)$–$\log N_{\rm H}$ formula is

$$\log F_{\rm pk3} = (-1.5 \pm 0.24) \times \log(1+z) + (-0.5 \pm 0.12) \times \log N_{\rm H} + (1.3 \pm 0.078), \quad (184)$$

where $F_{\rm pk3}$ is the peak energy flux in the 256 ms time bin in the rest-frame 1–10^4 keV energy band and is in units of $10^{-6}\,{\rm erg\,cm^{-2}\,s^{-1}}$. $N_{\rm H}$ is in units of $10^{21}\,{\rm cm^{-2}}$. The adjusted R^2 is 0.4391. The number of GRBs in the sample is 24.

The log SFR–$\log F_{\rm Opt11hr}$–$\log N_{\rm H}$ formula is

$$\log {\rm SFR} = (-0.47 \pm 0.12) \times \log F_{\rm Opt11hr} + (1.2 \pm 0.22) \times \log N_{\rm H} + (-2.3 \pm 0.55), \quad (185)$$

where SFR is in units of $M_\odot\,{\rm yr}^{-1}$. $F_{\rm Opt11hr}$ is in units of Jy. $N_{\rm H}$ is in units of $10^{21}\,{\rm cm^{-2}}$. The adjusted R^2 is 0.5387. The number of GRBs in the sample is 25.

The $A_{\rm V}$–$\log F_{\rm pk4}$–$(-\alpha_{\rm cpl})$ formula is

$$A_{\rm V} = (1 \pm 0.16) \times \log F_{\rm pk4} + (-0.72 \pm 0.2) \times (-\alpha_{\rm cpl}) + (1.7 \pm 0.23), \quad (186)$$

where $F_{\rm pk4}$ is the peak energy flux in the 1024 ms time bin in the rest-frame 1–10^4 keV energy band and is in units of $10^{-6}\,{\rm erg\,cm^{-2}\,s^{-1}}$. The adjusted R^2 is 0.2497. The number of GRBs in the sample is 25.

The Mag–$\log L_{\rm pk}$–$(-\beta_{\rm Band})$ formula is

$${\rm Mag} = (-0.68 \pm 0.79) \times \log L_{\rm pk} + (0.5 \pm 0.77) \times (-\beta_{\rm Band}) + (-22 \pm 1.8), \quad (187)$$

where Mag is in units of magnitude. $L_{\rm pk}$ is in units of $10^{52}\,{\rm erg\,s^{-1}}$ and in the 1–10^4 keV energy band. The adjusted R^2 is 0.227. The number of GRBs in the sample is 25.

The $\log F_{\rm Opt11hr}$–log Mass–$\log t_{\rm pkOpt,i}$ formula is

$$\log F_{\rm Opt11hr} = (-0.27 \pm 0.092) \times \log {\rm Mass} + (0.43 \pm 0.11) \times \log t_{\rm pkOpt,i} + (-2.9 \pm 0.97), \quad (188)$$

where $F_{\rm Opt11hr}$ is in units of Jy. Mass is in units of $M_\odot$. $t_{\rm pkOpt,i}$ is in units of s. The adjusted R^2 is 0.3158. The number of GRBs in the sample is 25.

The $A_{\rm V}$–$\log P_{\rm pk3}$–$(-\alpha_{\rm cpl})$ formula is

$$A_{\rm V} = (1.2 \pm 0.19) \times \log P_{\rm pk3} + (-0.75 \pm 0.2) \times (-\alpha_{\rm cpl}) + (0.74 \pm 0.25), \quad (189)$$

where $P_{\rm pk3}$ is the peak photon flux in the 1024 ms time bin in 10–1000 keV and is in units of photons $\,{\rm cm^{-2}\,s^{-1}}$. The adjusted R^2 is 0.2262. The number of GRBs in the sample is 25.

The $\log N_{\rm H}$–$\log T_{90}$–$\log F_{\rm pk2}$ formula is

$$\log N_{\rm H} = (0.45 \pm 0.057) \times \log T_{90} + (-0.43 \pm 0.055) \times \log F_{\rm pk2} + (0.23 \pm 0.099), \quad (190)$$

where $N_{\rm H}$ is in units of $10^{21}\,{\rm cm^{-2}}$. T_{90} is in units of s. $F_{\rm pk2}$ is the peak energy flux in the 64 ms time bin in the rest-frame 1–10^4 keV energy band and is in units of $10^{-6}\,{\rm erg\,cm^{-2}\,s^{-1}}$. The adjusted R^2 is 0.4444. The number of GRBs in the sample is 25.

The rest-frame spectral lag–variability$_3$–$\log\theta_{\rm j}$ formula is

$${\rm rest\text{-}frame\ spectral\ lag} = (-54909 \pm 24240) \times {\rm variability}_3 + (1590 \pm 590) \times \log\theta_{\rm j} + (3315 \pm 906), \quad (191)$$

where rest-frame spectral lag is in units of $\,{\rm ms\,MeV^{-1}}$. $\theta_{\rm j}$ is in units of rad. The adjusted R^2 is 0.4137. The number of GRBs in the sample is 25.

The log SFR–$A_{\rm V}$–log Age formula is

$$\log {\rm SFR} = (0.43 \pm 0.16) \times A_{\rm V} + (-0.77 \pm 0.11) \times \log {\rm Age} + (2.5 \pm 0.33), \quad (192)$$

where SFR is in units of $M_\odot\,{\rm yr}^{-1}$. Age is in units of Myr. The adjusted R^2 is 0.4286. The number of GRBs in the sample is 26.

The $\log N_{\rm H}$–log Age–$\log T_{90,\rm i}$ formula is

$$\log N_{\rm H} = (-0.41 \pm 0.071) \times \log {\rm Age} + (0.41 \pm 0.054) \times \log T_{90,\rm i} + (1.2 \pm 0.22), \quad (193)$$

where $N_{\rm H}$ is in units of $10^{21}\,{\rm cm^{-2}}$. Age is in units of Myr. $T_{90,\rm i}$ is in units of s. The adjusted R^2 is 0.4491. The number of GRBs in the sample is 26.

The log Age–$\log E_{\rm iso}$–$\log N_{\rm H}$ formula is

$$\log {\rm Age} = (-0.21 \pm 0.062) \times \log E_{\rm iso} + (-0.51 \pm 0.16) \times \log N_{\rm H} + (3.1 \pm 0.094), \quad (194)$$

where Age is in units of Myr. $E_{\rm iso}$ is in units of 10^{52} erg and in the rest-frame 1–10^4 keV energy band. $N_{\rm H}$ is in units of $10^{21}\,{\rm cm^{-2}}$. The adjusted R^2 is 0.3666. The number of GRBs in the sample is 26.

The log Age–$\log(1+z)$–$\log N_{\rm H}$ formula is

$$\log {\rm Age} = (-2.7 \pm 0.58) \times \log(1+z) + (-0.41 \pm 0.17) \times \log N_{\rm H} + (3.8 \pm 0.11), \quad (195)$$

where Age is in units of Myr. $N_{\rm H}$ is in units of $10^{21}\,{\rm cm^{-2}}$. The adjusted R^2 is 0.5434. The number of GRBs in the sample is 26.

The $\log T_{90,\rm i}$–$\beta_{\rm X11hr}$–log offset formula is

$$\log T_{90,\rm i} = (-0.6 \pm 0.17) \times \beta_{\rm X11hr} + (-0.55 \pm 0.16) \times \log {\rm offset} + (1.6 \pm 0.31), \quad (196)$$

where $T_{90,\rm i}$ is in units of s. The host galaxy offset is in units of kpc. The adjusted R^2 is 0.4588. The number of GRBs in the sample is 27.

The $\log T_{50}$–$\log F_{\rm g}$–log offset formula is

$$\log T_{50} = (0.56 \pm 0.067) \times \log F_{\rm g} + (-0.49 \pm 0.15) \times \log {\rm offset} + (0.29 \pm 0.14), \quad (197)$$

where T_{50} is in units of s. F_g is in units of 10^{-6} erg cm^{-2} and in the 20–2000 keV energy band. The host galaxy offset is in units of kpc. The adjusted R^2 is 0.5799. The number of GRBs in the sample is 27.

The $\log F_{\rm Opt11hr}$–$\log F_{\rm pk2}$–$A_{\rm V}$ formula is

$$\log F_{\rm Opt11hr} = (0.63 \pm 0.2) \times \log F_{\rm pk2} + (-0.4 \pm 0.2) \times A_{\rm V} + (-4.9 \pm 0.2), \quad (198)$$

where $F_{\rm Opt11hr}$ is in units of Jy. $F_{\rm pk2}$ is the peak energy flux in the 64 ms time bin in the rest-frame 1–10^4 keV energy band and is in units of 10^{-6} erg cm^{-2} s^{-1}. The adjusted R^2 is 0.406. The number of GRBs in the sample is 27.

The $\log F_{\rm g}$–$\log F_{\rm X11hr}$–log Age formula is

$$\log F_{\rm g} = (0.72 \pm 0.073) \times \log F_{\rm X11hr} + (-0.43 \pm 0.098) \times \log {\rm Age} + (7.1 \pm 0.57), \quad (199)$$

where $F_{\rm g}$ is in units of 10^{-6} erg cm^{-2} and in the 20–2000 keV energy band. $F_{\rm X11hr}$ is in units of Jy. Age is in units of Myr. The adjusted R^2 is 0.6765. The number of GRBs in the sample is 27.

The Mag–$\log L_{\rm pk}$–log SFR formula is

$$\mathrm{Mag} = (-0.54 \pm 0.38) \times \log L_{\rm pk} + (-1.5 \pm 0.56) \times \log {\rm SFR} + (-20 \pm 0.71), \quad (200)$$

where Mag is in units of magnitude. $L_{\rm pk}$ is in units of 10^{52} erg s^{-1} and in the 1–10^4 keV energy band. SFR is in units of $M_\odot$ yr^{-1}. The adjusted R^2 is 0.837. The number of GRBs in the sample is 27.

The $\log F_{\rm Opt11hr}$–metallicity–log Age formula is

$$\log F_{\rm Opt11hr} = (-1.3 \pm 0.42) \times \mathrm{metallicity} + (0.55 \pm 0.17) \times \log {\rm Age} + (4.9 \pm 3.7), \quad (201)$$

where $F_{\rm Opt11hr}$ is in units of Jy. The metallicity is the value of $12 + \log {\rm O/H}$. Age is in units of Myr. The adjusted R^2 is 0.471. The number of GRBs in the sample is 27.

The log Mass–log offset–log Age formula is

$$\log \mathrm{Mass} = (0.42 \pm 0.15) \times \log \mathrm{offset} + (0.69 \pm 0.15) \times \log {\rm Age} + (7.9 \pm 0.37), \quad (202)$$

where Mass is in units of $M_\odot$. The host galaxy offset is in units of kpc. Age is in units of Myr. The adjusted R^2 is 0.6363. The number of GRBs in the sample is 27.

The log SFR–log Age–log Mass formula is

$$\log {\rm SFR} = (-0.49 \pm 0.092) \times \log {\rm Age} + (0.8 \pm 0.092) \times \log \mathrm{Mass} + (-5.6 \pm 0.98), \quad (203)$$

where SFR is in units of $M_\odot$ yr^{-1}. Age is in units of $M_\odot$. The adjusted R^2 is 0.6711. The number of GRBs in the sample is 28.

The $\log T_{90}$–$\beta_{\rm X11hr}$–log offset formula is

$$\log T_{90} = (-0.62 \pm 0.18) \times \beta_{\rm X11hr} + (-0.62 \pm 0.17) \times \log \mathrm{offset} + (2 \pm 0.32), \quad (204)$$

where T_{90} is in units of s. The host galaxy offset is in units of kpc. The adjusted R^2 is 0.5046. The number of GRBs in the sample is 28.

The log Mass–$\log E_{\rm p,Band}$–log SFR formula is

$$\log \mathrm{Mass} = (0.45 \pm 0.1) \times \log E_{\rm p,Band} + (0.61 \pm 0.064) \times \log {\rm SFR} + (8.2 \pm 0.21), \quad (205)$$

where Mass is in units of $M_\odot$. $E_{\rm p,Band}$ is in units of keV. SFR is in units of $M_\odot$ yr^{-1}. The adjusted R^2 is 0.5525. The number of GRBs in the sample is 28.

The $\log F_{\rm Opt11hr}$–$\log F_{\rm pk2}$–$\beta_{\rm X11hr}$ formula is

$$\log F_{\rm Opt11hr} = (0.67 \pm 0.18) \times \log F_{\rm pk2} + (-0.41 \pm 0.21) \times \beta_{\rm X11hr} + (-5 \pm 0.3), \quad (206)$$

where $F_{\rm Opt11hr}$ is in units of Jy. $F_{\rm pk2}$ is the peak energy flux in the 64 ms time bin in the rest-frame 1–10^4 keV energy band and is in units of 10^{-6} erg cm^{-2} s^{-1}. The adjusted R^2 is 0.4429. The number of GRBs in the sample is 28.

The $\log F_{\rm g}$–$\log \Gamma_0$–$\log F_{\rm X11hr}$ formula is

$$\log F_{\rm g} = (0.51 \pm 0.05) \times \log \Gamma_0 + (0.37 \pm 0.056) \times \log F_{\rm X11hr} + (2.5 \pm 0.43), \quad (207)$$

where $F_{\rm g}$ is in units of 10^{-6} erg cm^{-2} and in the 20–2000 keV energy band. $F_{\rm X11hr}$ is in units of Jy. The adjusted R^2 is 0.2285. The number of GRBs in the sample is 28.

The log Mass–$\log P_{\rm pk1}$–log Age formula is

$$\log \mathrm{Mass} = (-0.55 \pm 0.1) \times \log P_{\rm pk1} + (0.52 \pm 0.096) \times \log {\rm Age} + (9.2 \pm 0.25), \quad (208)$$

where Mass is in units of $M_\odot$. $P_{\rm pk1}$ is the peak photon flux in the 64 ms time bin in 10–1000 keV and is in units of photons cm^{-2} s^{-1}. Age is in units of Myr. The adjusted R^2 is 0.3665. The number of GRBs in the sample is 28.

The log HR–$(-\alpha_{\rm Band})$–$\log F_{\rm radio,pk}$ formula is

$$\log {\rm HR} = (-0.51 \pm 0.087) \times (-\alpha_{\rm Band}) + (0.29 \pm 0.07) \times \log F_{\rm radio,pk} + (2.1 \pm 0.28), \quad (209)$$

where $F_{\rm radio,pk}$ is in units of Jy. The adjusted R^2 is 0.4247. The number of GRBs in the sample is 29.

The log Mass–$(-\beta_{\rm Band})$–metallicity formula is

$$\log \mathrm{Mass} = (-0.24 \pm 0.18) \times (-\beta_{\rm Band}) + (0.89 \pm 0.26) \times \mathrm{metallicity} + (2.3 \pm 2.3), \quad (210)$$

where Mass is in units of $M_\odot$. The metallicity is the value of $12 + \log {\rm O/H}$. The adjusted R^2 is 0.2659. The number of GRBs in the sample is 29.

The spectral lag–$\log F_{\rm pk2}$–$\log T_{\rm R45,i}$ formula is

$$\text{spectral lag} = (-4955 \pm 1139) \times \log F_{\rm pk2} + (4402 \pm 716) \times \log T_{\rm R45,i} + (4946 \pm 784), \quad (211)$$

where the spectral time lag is in units of ms $\rm MeV^{-1}$. $F_{\rm pk2}$ is the peak energy flux in the 64 ms time bin in the rest-frame $1–10^4$ keV energy band and is in units of 10^{-6} erg $\rm cm^{-2}$ $\rm s^{-1}$. $T_{\rm R45,i}$ is in units of s. The adjusted R^2 is 0.2428. The number of GRBs in the sample is 29.

The $\log F_{\rm Opt11hr}$–$\log F_{\rm pk3}$–$\log T_{\rm 50,i}$ formula is

$$\log F_{\rm Opt11hr} = (0.69 \pm 0.14) \times \log F_{\rm pk3} + (0.49 \pm 0.15) \times \log T_{\rm 50,i} + (-5.4 \pm 0.15), \quad (212)$$

where $F_{\rm Opt11hr}$ is in units of Jy. $F_{\rm pk3}$ is the peak energy flux in the 256 ms time bin in the rest-frame $1–10^4$ keV energy band and is in units of 10^{-6} erg $\rm cm^{-2}$ $\rm s^{-1}$. $T_{\rm 50,i}$ is in units of s. The adjusted R^2 is 0.3968. The number of GRBs in the sample is 29.

The log Mass–metallicity–$\log E_{\rm p,Band,i}$ formula is

$$\log \text{Mass} = (0.82 \pm 0.22) \times \text{metallicity} + (0.55 \pm 0.1) \times \log E_{\rm p,Band,i} + (1.1 \pm 1.9), \quad (213)$$

where Mass is in units of $M_\odot$. The metallicity is the value of $12 + \log \rm O/H$. $E_{\rm p,Band,i}$ is in units of keV. The adjusted R^2 is 0.2796. The number of GRBs in the sample is 29.

The $\log F_{\rm Opt11hr}$–$\log P_{\rm pk2}$–$\log T_{\rm 50,i}$ formula is

$$\log F_{\rm Opt11hr} = (0.61 \pm 0.15) \times \log P_{\rm pk2} + (0.5 \pm 0.15) \times \log T_{\rm 50,i} + (-5.8 \pm 0.23), \quad (214)$$

where $F_{\rm Opt11hr}$ is in units of Jy. $P_{\rm pk2}$ is the peak photon flux in the 256 ms time bin in 10–1000 keV and is in units of photons $\rm cm^{-2}$ $\rm s^{-1}$. $T_{\rm 50,i}$ is in units of s. The adjusted R^2 is 0.2895. The number of GRBs in the sample is 29.

The Mag–$\log D_{\rm L}$–$(-\beta_{\rm Band})$ formula is

$$\text{Mag} = (-1.4 \pm 1.1) \times \log D_{\rm L} + (0.38 \pm 0.69) \times (-\beta_{\rm Band}) + (-21 \pm 1.9), \quad (215)$$

where Mag is in units of magnitude. $D_{\rm L}$ is in units of 10^{28} cm. The adjusted R^2 is 0.2703. The number of GRBs in the sample is 30.

The $\log t_{\rm pkOpt,i}$–$\log E_{\rm p,cpl}$–$\log F_{\rm Opt11hr}$ formula is

$$\log t_{\rm pkOpt,i} = (-0.66 \pm 0.15) \times \log E_{\rm p,cpl} + (0.32 \pm 0.1) \times \log F_{\rm Opt11hr} + (4.9 \pm 0.52), \quad (216)$$

where $t_{\rm pkOpt,i}$ is in units of s. $E_{\rm p,cpl}$ is in units of keV. $F_{\rm Opt11hr}$ is in units of Jy. The adjusted R^2 is 0.3993. The number of GRBs in the sample is 30.

The Mag–$\log T_{90}$–$(-\beta_{\rm Band})$ formula is

$$\text{Mag} = (-1.3 \pm 0.95) \times \log T_{90} + (0.48 \pm 0.67) \times (-\beta_{\rm Band}) + (-20 \pm 2.4), \quad (217)$$

where Mag is in units of magnitude. T_{90} is in units of s. The adjusted R^2 is 0.3291. The number of GRBs in the sample is 30.

The $\log \Gamma_0$–$\log \theta_{\rm j}$–$\log T_{\rm 50,i}$ formula is

$$\log \Gamma_0 = (-0.45 \pm 0.077) \times \log \theta_{\rm j} + (-0.35 \pm 0.031) \times \log T_{\rm 50,i} + (2 \pm 0.12), \quad (218)$$

where $\theta_{\rm j}$ is in units of rad. $T_{\rm 50,i}$ is in units of s. The adjusted R^2 is 0.2545. The number of GRBs in the sample is 30.

The $\log P_{\rm pk3}$–$\log(1+z)$–$\log t_{\rm pkOpt}$ formula is

$$\log P_{\rm pk3} = (-2.6 \pm 0.047) \times \log(1+z) + (-0.45 \pm 0.017) \times \log t_{\rm pkOpt} + (3.1 \pm 0.039), \quad (219)$$

where $P_{\rm pk3}$ is the peak photon flux in the 1024 ms time bin in 10–1000 keV and is in units of photons $\rm cm^{-2}$ $\rm s^{-1}$. $t_{\rm pkOpt}$ is in units of s. The adjusted R^2 is 0.5827. The number of GRBs in the sample is 30.

The Mag–$\log(1+z)$–$(-\beta_{\rm Band})$ formula is

$$\text{Mag} = (-3.4 \pm 2.3) \times \log(1+z) + (0.36 \pm 0.69) \times (-\beta_{\rm Band}) + (-20 \pm 2.1), \quad (220)$$

where Mag is in units of magnitude. The adjusted R^2 is 0.3315. The number of GRBs in the sample is 30.

The $\log L_{\rm pk}$–$\log L_{\rm radio,pk}$–$\log E_{\rm p,Band}$ formula is

$$\log L_{\rm pk} = (0.36 \pm 0.048) \times \log L_{\rm radio,pk} + (1.2 \pm 0.13) \times \log E_{\rm p,Band} + (-2.9 \pm 0.25), \quad (221)$$

where $L_{\rm pk}$ is in units of 10^{52} erg $\rm s^{-1}$ and in the $1–10^4$ keV energy band. $L_{\rm radio,pk}$ is in rest-frame 8.46 GHz and in units of 10^{40} erg $\rm s^{-1}$. $E_{\rm p,Band}$ is in units of keV. The adjusted R^2 is 0.5213. The number of GRBs in the sample is 30.

The log Mass–$\log L_{\rm radio,pk}$–log SSFR formula is

$$\log \text{Mass} = (0.36 \pm 0.07) \times \log L_{\rm radio,pk} + (-0.52 \pm 0.18) \times \log \text{SSFR} + (9 \pm 0.086), \quad (222)$$

where Mass is in units of $M_\odot$. $L_{\rm radio,pk}$ is in rest-frame 8.46 GHz and in units of 10^{40} erg $\rm s^{-1}$. log SSFR is in units of $\rm Gyr^{-1}$. The adjusted R^2 is 0.3256. The number of GRBs in the sample is 30.

The $\log(1+z)$–$\log \Gamma_0$–$\log N_{\rm H}$ formula is

$$\log(1+z) = (0.25 \pm 0.016) \times \log \Gamma_0 + (0.13 \pm 0.021) \times \log N_{\rm H} + (-0.2 \pm 0.036), \quad (223)$$

where $N_{\rm H}$ is in units of 10^{21} $\rm cm^{-2}$. The adjusted R^2 is 0.481. The number of GRBs in the sample is 31.

The Mag–log SSFR–log Mass formula is

$$\mathrm{Mag} = (-0.95 \pm 0.76) \times \log \mathrm{SSFR} + (-1.9 \pm 0.47) \times \log \mathrm{Mass} + (-2.2 \pm 4.5), \quad (224)$$

where Mag is in units of magnitude. log SSFR is in units of Gyr^{-1}. Mass is in units of $M_\odot$. The adjusted R^2 is 0.8329. The number of GRBs in the sample is 31.

The $\log t_{\mathrm{pkOpt,i}}$–$\log F_{\mathrm{Opt11hr}}$–$\log N_{\mathrm{H}}$ formula is

$$\log t_{\mathrm{pkOpt,i}} = (0.51 \pm 0.095) \times \log F_{\mathrm{Opt11hr}} + (0.38 \pm 0.11) \times \log N_{\mathrm{H}} + (4.2 \pm 0.43), \quad (225)$$

where $t_{\mathrm{pkOpt,i}}$ is in units of s. F_{Opt11hr} is in units of Jy. N_{H} is in units of $10^{21}\,\mathrm{cm}^{-2}$. The adjusted R^2 is 0.4855. The number of GRBs in the sample is 32.

The log SFR–$\log N_{\mathrm{H}}$–log Mass formula is

$$\log \mathrm{SFR} = (0.58 \pm 0.16) \times \log N_{\mathrm{H}} + (0.66 \pm 0.11) \times \log \mathrm{Mass} + (-5.9 \pm 0.98), \quad (226)$$

where SFR is in units of $M_\odot\,\mathrm{yr}^{-1}$. N_{H} is in units of $10^{21}\,\mathrm{cm}^{-2}$. Mass is in units of $M_\odot$. The adjusted R^2 is 0.6262. The number of GRBs in the sample is 32.

The $\log L_{\mathrm{pk}}$–$\log P_{\mathrm{pk4}}$–$\log F_{\mathrm{radio,pk}}$ formula is

$$\log L_{\mathrm{pk}} = (0.8 \pm 0.089) \times \log P_{\mathrm{pk4}} + (-1.3 \pm 0.097) \times \log F_{\mathrm{radio,pk}} + (-5.4 \pm 0.38), \quad (227)$$

where L_{pk} is in units of $10^{52}\,\mathrm{erg\,s}^{-1}$ and in the 1–10^4 keV energy band. P_{pk4} is the peak photon flux in the 1 s time bin in 10–1000 keV and is in units of photons $\mathrm{cm}^{-2}\,\mathrm{s}^{-1}$. $F_{\mathrm{radio,pk}}$ is in units of Jy. The adjusted R^2 is 0.2764. The number of GRBs in the sample is 32.

The $(-\alpha_{\mathrm{Band}})$–$\mathrm{variability}_3$–$A_{\mathrm{V}}$ formula is

$$(-\alpha_{\mathrm{Band}}) = (-15 \pm 6.8) \times \mathrm{variability}_3 + (-0.13 \pm 0.068) \times A_{\mathrm{V}} + (1.3 \pm 0.097), \quad (228)$$

and the adjusted R^2 is 0.2283. The number of GRBs in the sample is 32.

The rest-frame spectral lag–$\log L_{\mathrm{radio,pk}}$–$\log t_{\mathrm{radio,pk}}$ formula is

$$\text{rest-frame spectral lag} = (-1029 \pm 290) \times \log L_{\mathrm{radio,pk}} + (1663 \pm 355) \times \log t_{\mathrm{radio,pk}} + (-7091 \pm 1663), \quad (229)$$

where the rest-frame spectral lag is in units of $\mathrm{ms\,MeV}^{-1}$. $L_{\mathrm{radio,pk}}$ is in rest-frame 8.46 GHz and in units of $10^{40}\,\mathrm{erg\,s}^{-1}$. $t_{\mathrm{radio,pk}}$ is in units of s. The adjusted R^2 is 0.4842. The number of GRBs in the sample is 32.

The $\log L_{\mathrm{radio,pk}}$–$A_{\mathrm{V}}$–$\log E_{\mathrm{p,Band,i}}$ formula is

$$\log L_{\mathrm{radio,pk}} = (-0.31 \pm 0.083) \times A_{\mathrm{V}} + (0.72 \pm 0.056) \times \log E_{\mathrm{p,Band,i}} + (0.11 \pm 0.17), \quad (230)$$

where $L_{\mathrm{radio,pk}}$ is in rest-frame 8.46 GHz and in units of $10^{40}\,\mathrm{erg\,s}^{-1}$. $E_{\mathrm{p,Band,i}}$ is in units of keV. The adjusted R^2 is 0.4928. The number of GRBs in the sample is 32.

The log HR–$\log E_{\mathrm{p,cpl}}$–log Age formula is

$$\log \mathrm{HR} = (0.79 \pm 0.18) \times \log E_{\mathrm{p,cpl}} + (-0.15 \pm 0.07) \times \log \mathrm{Age} + (-1 \pm 0.54), \quad (231)$$

where $E_{\mathrm{p,cpl}}$ is in units of keV. Age is in units of Myr. The adjusted R^2 is 0.9192. The number of GRBs in the sample is 33.

The $\log F_{\mathrm{Opt11hr}}$–log HR–$\log P_{\mathrm{pk2}}$ formula is

$$\log F_{\mathrm{Opt11hr}} = (0.65 \pm 0.21) \times \log \mathrm{HR} + (0.66 \pm 0.15) \times \log P_{\mathrm{pk2}} + (-5.9 \pm 0.2), \quad (232)$$

where F_{Opt11hr} is in units of Jy. P_{pk2} is the peak photon flux in the 256 ms time bin in 10–1000 keV and is in units of photons $\mathrm{cm}^{-2}\,\mathrm{s}^{-1}$. The adjusted R^2 is 0.2795. The number of GRBs in the sample is 33.

The Mag–log SFR–log Mass formula is

$$\mathrm{Mag} = (-0.85 \pm 0.66) \times \log \mathrm{SFR} + (-1.3 \pm 0.73) \times \log \mathrm{Mass} + (-7.4 \pm 6.5), \quad (233)$$

where Mag is in units of magnitude. SFR is in units of $M_\odot\,\mathrm{yr}^{-1}$. Mass is in units of $M_\odot$. The adjusted R^2 is 0.8705. The number of GRBs in the sample is 33.

The $\log L_{\mathrm{radio,pk}}$–$A_{\mathrm{V}}$–log Mass formula is

$$\log L_{\mathrm{radio,pk}} = (-0.24 \pm 0.066) \times A_{\mathrm{V}} + (0.5 \pm 0.088) \times \log \mathrm{Mass} + (-3.1 \pm 0.82) \quad (234)$$

where $L_{\mathrm{radio,pk}}$ is in rest-frame 8.46 GHz and in units of $10^{40}\,\mathrm{erg\,s}^{-1}$. Mass is in units of $M_\odot$. The adjusted R^2 is 0.2234. The number of GRBs in the sample is 34.

The $\log L_{\mathrm{pk}}$–β_{X11hr}–$\log t_{\mathrm{pkOpt,i}}$ formula is

$$\log L_{\mathrm{pk}} = (-0.39 \pm 0.1) \times \beta_{\mathrm{X11hr}} + (-0.46 \pm 0.05) \times \log t_{\mathrm{pkOpt,i}} + (1.7 \pm 0.13), \quad (235)$$

where L_{pk} is in units of $10^{52}\,\mathrm{erg\,s}^{-1}$ and in the 1–10^4 keV energy band. $t_{\mathrm{pkOpt,i}}$ is in units of s. The adjusted R^2 is 0.2613. The number of GRBs in the sample is 34.

The log Age–$\log E_{\mathrm{iso}}$–$(-\alpha_{\mathrm{cpl}})$ formula is

$$\log \mathrm{Age} = (-0.27 \pm 0.047) \times \log E_{\mathrm{iso}} + (0.48 \pm 0.18) \times (-\alpha_{\mathrm{cpl}}) + (2.1 \pm 0.19), \quad (236)$$

where Age is in units of Myr. E_{iso} is in units of 10^{52} erg and in the rest-frame 1–10^4 keV energy band. The adjusted R^2 is 0.4063. The number of GRBs in the sample is 34.

The $\log P_{\mathrm{pk1}}$–$\log L_{\mathrm{pk}}$–$\log F_{\mathrm{Opt11hr}}$ formula is

$$\log P_{\mathrm{pk1}} = (0.22 \pm 0.028) \times \log L_{\mathrm{pk}} + (0.21 \pm 0.049) \times \log F_{\mathrm{Opt11hr}} + (2.2 \pm 0.24), \quad (237)$$

where P_{pk1} is the peak photon flux in the 64 ms time bin in 10–1000 keV and is in units of photons $\mathrm{cm}^{-2}\,\mathrm{s}^{-1}$. L_{pk} is in units of $10^{52}\,\mathrm{erg\,s}^{-1}$ and in the 1–10^4 keV energy band.

$F_{\rm Opt11hr}$ is in units of Jy. The adjusted R^2 is 0.4753. The number of GRBs in the sample is 34.

The $\log F_{\rm g}$–variability$_3$–$\log T_{50,\rm i}$ formula is

$$\log F_{\rm g} = (59 \pm 13) \times \text{variability}_3 + (0.45 \pm 0.053) \times \log T_{50,\rm i} + (0.16 \pm 0.11), \quad (238)$$

where $F_{\rm g}$ is in units of $10^{-6}\,{\rm erg\,cm^{-2}}$ and in the 20–2000 keV energy band. $T_{50,\rm i}$ is in units of s. The adjusted R^2 is 0.388. The number of GRBs in the sample is 34.

The log Age–$\log D_{\rm L}$–$\log E_{\rm p,cpl}$ formula is

$$\log \text{Age} = (-0.83 \pm 0.14) \times \log D_{\rm L} + (-0.5 \pm 0.18) \times \log E_{\rm p,cpl} + (3.9 \pm 0.43), \quad (239)$$

where Age is in units of Myr. $D_{\rm L}$ is in units of 10^{28} cm. $E_{\rm p,cpl}$ is in units of keV. The adjusted R^2 is 0.4641. The number of GRBs in the sample is 35.

The rest-frame spectral lag–$\log D_{\rm L}$–log SFR formula is

$$\text{rest-frame spectral lag} = (-9353 \pm 1291) \times \log D_{\rm L} + (2618 \pm 725) \times \log \text{SFR} + (2406 \pm 525), \quad (240)$$

where rest-frame spectral lag is in units of ms MeV^{-1}. $D_{\rm L}$ is in units of 10^{28} cm. SFR is in units of $M_\odot\,{\rm yr^{-1}}$. The adjusted R^2 is 0.384. The number of GRBs in the sample is 35.

The log SFR–$\log E_{\rm iso}$–$\log N_{\rm H}$ formula is

$$\log \text{SFR} = (0.35 \pm 0.052) \times \log E_{\rm iso} + (0.83 \pm 0.094) \times \log N_{\rm H} + (-0.033 \pm 0.088), \quad (241)$$

where SFR is in units of $M_\odot\,{\rm yr^{-1}}$. $E_{\rm iso}$ is in units of 10^{52} erg and in the rest-frame 1–10^4 keV energy band. $N_{\rm H}$ is in units of $10^{21}\,{\rm cm^{-2}}$. The adjusted R^2 is 0.4156. The number of GRBs in the sample is 35.

The Mag–$\log F_{\rm Opt11hr}$–$\log E_{\rm p,cpl,i}$ formula is

$$\text{Mag} = (0.89 \pm 0.41) \times \log F_{\rm Opt11hr} + (-1.2 \pm 0.83) \times \log E_{\rm p,cpl,i} + (-13 \pm 2.7), \quad (242)$$

where Mag is in units of magnitude. $F_{\rm Opt11hr}$ is in units of Jy. $E_{\rm p,cpl,i}$ is in units of keV. The adjusted R^2 is 0.4763. The number of GRBs in the sample is 35.

The $(-\alpha_{\rm cpl})$–$\log T_{90}$–log Age formula is

$$(-\alpha_{\rm cpl}) = (0.15 \pm 0.045) \times \log T_{90} + (0.2 \pm 0.083) \times \log \text{Age} + (0.35 \pm 0.2), \quad (243)$$

where T_{90} is in units of s. Age is in units of Myr. The adjusted R^2 is 0.2569. The number of GRBs in the sample is 35.

The Mag–$\log \theta_{\rm j}$–log Mass formula is

$$\text{Mag} = (0.61 \pm 0.76) \times \log \theta_{\rm j} + (-1.8 \pm 0.5) \times \log \text{Mass} + (-2.7 \pm 4.7), \quad (244)$$

where Mag is in units of magnitude. $\theta_{\rm j}$ is in units of rad. Mass is in units of $M_\odot$. The adjusted R^2 is 0.878. The number of GRBs in the sample is 35.

The log Age–$\log(1+z)$–$\log E_{\rm p,cpl}$ formula is

$$\log \text{Age} = (-2 \pm 0.63) \times \log(1+z) + (-0.6 \pm 0.19) \times \log E_{\rm p,cpl} + (4.6 \pm 0.44), \quad (245)$$

where Age is in units of Myr. $E_{\rm p,cpl}$ is in units of keV. The adjusted R^2 is 0.4777. The number of GRBs in the sample is 35.

The log Age–$\log(1+z)$–$(-\alpha_{\rm cpl})$ formula is

$$\log \text{Age} = (-2.2 \pm 0.64) \times \log(1+z) + (0.45 \pm 0.2) \times (-\alpha_{\rm cpl}) + (2.8 \pm 0.28), \quad (246)$$

where Age is in units of Myr. The adjusted R^2 is 0.4567. The number of GRBs in the sample is 35.

The log SFR–$\log D_{\rm L}$–$\log N_{\rm H}$ formula is

$$\log \text{SFR} = (1.3 \pm 0.12) \times \log D_{\rm L} + (0.7 \pm 0.083) \times \log N_{\rm H} + (-0.061 \pm 0.081), \quad (247)$$

where SFR is in units of $M_\odot\,{\rm yr^{-1}}$. $D_{\rm L}$ is in units of 10^{28} cm. $N_{\rm H}$ is in units of $10^{21}\,{\rm cm^{-2}}$. The adjusted R^2 is 0.6648. The number of GRBs in the sample is 36.

The $\log \Gamma_0$–$\log F_{\rm g}$–$\log F_{\rm Opt11hr}$ formula is

$$\log \Gamma_0 = (0.26 \pm 0.028) \times \log F_{\rm g} + (-0.21 \pm 0.06) \times \log F_{\rm Opt11hr} + (0.94 \pm 0.27), \quad (248)$$

where $F_{\rm g}$ is in units of $10^{-6}\,{\rm erg\,cm^{-2}}$ and in the 20–2000 keV energy band. $F_{\rm Opt11hr}$ is in units of Jy. The adjusted R^2 is 0.3764. The number of GRBs in the sample is 36.

The $\log \Gamma_0$–$\log F_{\rm pk1}$–$\log F_{\rm Opt11hr}$ formula is

$$\log \Gamma_0 = (0.2 \pm 0.027) \times \log F_{\rm pk1} + (-0.2 \pm 0.063) \times \log F_{\rm Opt11hr} + (1.3 \pm 0.29), \quad (249)$$

where $F_{\rm pk1}$ is the peak energy flux in the 1 s time bin in the rest-frame 1–10^4 keV energy band and is in units of $10^{-6}\,{\rm erg\,cm^{-2}\,s^{-1}}$. $F_{\rm Opt11hr}$ is in units of Jy. The adjusted R^2 is 0.3141. The number of GRBs in the sample is 36.

The $\log E_{\rm p,Band}$–variability$_3$–$\log T_{90,\rm i}$ formula is

$$\log E_{\rm p,Band} = (23 \pm 5) \times \text{variability}_3 + (0.2 \pm 0.046) \times \log T_{90,\rm i} + (1.7 \pm 0.085), \quad (250)$$

where $E_{\rm p,Band}$ is in units of keV. $T_{90,\rm i}$ is in units of s. The adjusted R^2 is 0.287. The number of GRBs in the sample is 36.

The log SFR–$\log(1+z)$–$\log N_{\rm H}$ formula is

$$\log \text{SFR} = (4.1 \pm 0.42) \times \log(1+z) + (0.73 \pm 0.082) \times \log N_{\rm H} + (-1.1 \pm 0.12), \quad (251)$$

where SFR is in units of $M_\odot\,{\rm yr^{-1}}$. $N_{\rm H}$ is in units of $10^{21}\,{\rm cm^{-2}}$. The adjusted R^2 is 0.6871. The number of GRBs in the sample is 36.

The $\log E_{\rm p,Band,i}$–$\log L_{\rm radio,pk}$–$\log T_{90}$ formula is

$$\log E_{\rm p,Band,i} = (0.32 \pm 0.023) \times \log L_{\rm radio,pk} + (0.37 \pm 0.036) \times \log T_{90} + (1.4 \pm 0.072), \quad (252)$$

where $E_{\rm p,Band,i}$ is in units of keV. $L_{\rm radio,pk}$ is in rest-frame 8.46 GHz and in units of $10^{40}\,{\rm erg\,s^{-1}}$. T_{90} is in units of s. The adjusted R^2 is 0.4479. The number of GRBs in the sample is 36.

The $\log E_{\rm iso}$–$\log L_{\rm radio,pk}$–$\log E_{\rm p,Band}$ formula is

$$\log E_{\rm iso} = (0.43 \pm 0.039) \times \log L_{\rm radio,pk} + (1.3 \pm 0.11) \times \log E_{\rm p,Band} + (-2.5 \pm 0.21), \quad (253)$$

where $E_{\rm iso}$ is in units of $10^{52}\,{\rm erg}$ and in the rest-frame 1–10^4 keV energy band. $L_{\rm radio,pk}$ is in rest-frame 8.46 GHz and in units of $10^{40}\,{\rm erg\,s^{-1}}$. $E_{\rm p,Band}$ is in units of keV. The adjusted R^2 is 0.6844. The number of GRBs in the sample is 36.

The Mag–$A_{\rm V}$–$\log E_{\rm p,cpl,i}$ formula is

$$\mathrm{Mag} = (-0.59 \pm 0.45) \times A_{\rm V} + (-1.1 \pm 0.81) \times \log E_{\rm p,cpl,i} + (-18 \pm 2.2), \quad (254)$$

where Mag is in units of magnitude. $E_{\rm p,cpl,i}$ is in units of keV. The adjusted R^2 is 0.2498. The number of GRBs in the sample is 37.

The $\log F_{\rm g}$–$\log E_{\rm p,Band}$–$\log t_{\rm radio,pk}$ formula is

$$\log F_{\rm g} = (1.3 \pm 0.12) \times \log E_{\rm p,Band} + (-0.54 \pm 0.091) \times \log t_{\rm radio,pk} + (1.7 \pm 0.67), \quad (255)$$

where $F_{\rm g}$ is in units of $10^{-6}\,{\rm erg\,cm^{-2}}$ and in the 20–2000 keV energy band. $E_{\rm p,Band}$ is in units of keV. $t_{\rm radio,pk}$ is in units of s. The adjusted R^2 is 0.404. The number of GRBs in the sample is 37.

The $\log F_{\rm Opt11hr}$–$\log F_{\rm radio,pk}$–$\log T_{\rm R45,i}$ formula is

$$\log F_{\rm Opt11hr} = (0.84 \pm 0.14) \times \log F_{\rm radio,pk} + (0.48 \pm 0.16) \times \log T_{\rm R45,i} + (-1.6 \pm 0.51), \quad (256)$$

where $F_{\rm Opt11hr}$ is in units of Jy. $F_{\rm radio,pk}$ is in units of Jy. $T_{\rm R45,i}$ is in units of s. The adjusted R^2 is 0.4266. The number of GRBs in the sample is 37.

The $\log F_{\rm radio,pk}$–log HR–$\log T_{50,i}$ formula is

$$\log F_{\rm radio,pk} = (0.34 \pm 0.05) \times \log \mathrm{HR} + (0.18 \pm 0.023) \times \log T_{50,i} + (-3.9 \pm 0.029), \quad (257)$$

where $F_{\rm radio,pk}$ is in units of Jy. $T_{50,i}$ is in units of s. The adjusted R^2 is 0.255. The number of GRBs in the sample is 37.

The $\log L_{\rm pk}$–$\mathrm{variability}_1$–$(-\alpha_{\rm Band})$ formula is

$$\log L_{\rm pk} = (4.3 \pm 2.3) \times \mathrm{variability}_1 + (-0.95 \pm 0.51) \times (-\alpha_{\rm Band}) + (1.1 \pm 0.54), \quad (258)$$

where $L_{\rm pk}$ is in units of $10^{52}\,{\rm erg\,s^{-1}}$ and in the 1–10^4 keV energy band. The adjusted R^2 is 0.2743. The number of GRBs in the sample is 37.

The $\log F_{\rm pk3}$–$\log E_{\rm p,cpl}$–$\log t_{\rm burst}$ formula is

$$\log F_{\rm pk3} = (0.35 \pm 0.12) \times \log E_{\rm p,cpl} + (-0.25 \pm 0.035) \times \log t_{\rm burst} + (-0.23 \pm 0.27), \quad (259)$$

where $F_{\rm pk3}$ is the peak energy flux in the 256 ms time bin in the rest-frame 1–10^4 keV energy band and is in units of $10^{-6}\,{\rm erg\,cm^{-2}\,s^{-1}}$. $E_{\rm p,cpl}$ is in units of keV. $t_{\rm burst}$ is in units of s. The adjusted R^2 is 0.2004. The number of GRBs in the sample is 38.

The $\log T_{90}$–$\log F_{\rm g}$–log offset formula is

$$\log T_{90} = (0.65 \pm 0.039) \times \log F_{\rm g} + (-0.39 \pm 0.094) \times \log \mathrm{offset} + (0.47 \pm 0.082), \quad (260)$$

where T_{90} is in units of s. $F_{\rm g}$ is in units of $10^{-6}\,{\rm erg\,cm^{-2}}$ and in the 20–2000 keV energy band. Host galaxy offset is in units of kpc. The adjusted R^2 is 0.6172. The number of GRBs in the sample is 38.

The $\log(1+z)$–$\log P_{\rm pk4}$–$\log F_{\rm radio,pk}$ formula is

$$\log(1+z) = (-0.11 \pm 0.019) \times \log P_{\rm pk4} + (-0.24 \pm 0.031) \times \log F_{\rm radio,pk} + (-0.33 \pm 0.12), \quad (261)$$

where $P_{\rm pk4}$ is the peak photon flux in the 1 s time bin in 10–1000 keV and is in units of photons $\mathrm{cm^{-2}\,s^{-1}}$. $F_{\rm radio,pk}$ is in units of Jy. The adjusted R^2 is 0.3862. The number of GRBs in the sample is 38.

The $\log P_{\rm pk1}$–$\mathrm{variability}_1$–$(-\alpha_{\rm cpl})$ formula is

$$\log P_{\rm pk1} = (-1.7 \pm 0.91) \times \mathrm{variability}_1 + (0.57 \pm 0.074) \times (-\alpha_{\rm cpl}) + (0.54 \pm 0.09), \quad (262)$$

where $P_{\rm pk1}$ is the peak photon flux in the 64 ms time bin in 10–1000 keV and is in units of photons $\mathrm{cm^{-2}\,s^{-1}}$. The adjusted R^2 is 0.4813. The number of GRBs in the sample is 38.

The $\log L_{\rm pk}$–$\mathrm{variability}_2$–$(-\alpha_{\rm Band})$ formula is

$$\log L_{\rm pk} = (4.9 \pm 1.3) \times \mathrm{variability}_2 + (-0.59 \pm 0.38) \times (-\alpha_{\rm Band}) + (0.19 \pm 0.48), \quad (263)$$

where $L_{\rm pk}$ is in units of $10^{52}\,{\rm erg\,s^{-1}}$ and in the 1–10^4 keV energy band. The adjusted R^2 is 0.2358. The number of GRBs in the sample is 38.

The $\log L_{\rm pk}$–$\mathrm{variability}_3$–$\log \theta_{\rm j}$ formula is

$$\log L_{\rm pk} = (47 \pm 6.9) \times \mathrm{variability}_3 + (-0.97 \pm 0.12) \times \log \theta_{\rm j} + (-1.3 \pm 0.17), \quad (264)$$

where $L_{\rm pk}$ is in units of $10^{52}\,{\rm erg\,s^{-1}}$ and in the 1–10^4 keV energy band. $\theta_{\rm j}$ is in units of rad. The adjusted R^2 is 0.3097. The number of GRBs in the sample is 38.

The $\log L_{\rm radio,pk}$–$\log T_{50}$–$\log L_{\rm pk}$ formula is

$$\log L_{\rm radio,pk} = (0.44 \pm 0.038) \times \log T_{50} + (0.61 \pm 0.029) \times \log L_{\rm pk} + (1.2 \pm 0.052), \quad (265)$$

where $L_{\rm radio,pk}$ is in rest-frame 8.46 GHz and in units of 10^{40} erg s^{-1}. T_{50} is in units of s. $L_{\rm pk}$ is in units of 10^{52} erg s^{-1} and in the 1–10^4 keV energy band. The adjusted R^2 is 0.6609. The number of GRBs in the sample is 38.

The $\log t_{\rm pkOpt}$–log HR–$\log \Gamma_0$ formula is

$$\log t_{\rm pkOpt} = (-0.28 \pm 0.045) \times \log {\rm HR} + (-1.2 \pm 0.047) \times \log \Gamma_0 + (5.3 \pm 0.11), \quad (266)$$

where $t_{\rm pkOpt}$ is in units of s. The adjusted R^2 is 0.4806. The number of GRBs in the sample is 39.

The $\log P_{\rm pk4}$–$\log t_{\rm burst}$–$\log t_{\rm pkOpt}$ formula is

$$\log P_{\rm pk4} = (-0.21 \pm 0.017) \times \log t_{\rm burst} + (-0.34 \pm 0.035) \times \log t_{\rm pkOpt} + (2.1 \pm 0.09), \quad (267)$$

where $P_{\rm pk4}$ is the peak photon flux in the 1 s time bin in 10–1000 keV and is in units of photons cm^{-2} s^{-1}. $t_{\rm burst}$ is in units of s. $t_{\rm pkOpt}$ is in units of s. The adjusted R^2 is 0.3097. The number of GRBs in the sample is 39.

The $\log F_{\rm X11hr}$–variability$_2$–$\log F_{\rm Opt11hr}$ formula is

$$\log F_{\rm X11hr} = (2.2 \pm 0.58) \times {\rm variability}_2 + (0.3 \pm 0.097) \times \log F_{\rm Opt11hr} + (-6.3 \pm 0.51), \quad (268)$$

where $F_{\rm X11hr}$ is in units of Jy. $F_{\rm Opt11hr}$ is in units of Jy. The adjusted R^2 is 0.3125. The number of GRBs in the sample is 39.

The $\log F_{\rm g}$–$\beta_{\rm X11hr}$–log Age formula is

$$\log F_{\rm g} = (-0.54 \pm 0.16) \times \beta_{\rm X11hr} + (-0.53 \pm 0.12) \times \log {\rm Age} + (2.7 \pm 0.34), \quad (269)$$

where $F_{\rm g}$ is in units of 10^{-6} erg cm^{-2} and in the 20–2000 keV energy band. Age is in units of Myr. The adjusted R^2 is 0.4175. The number of GRBs in the sample is 40.

The $\log F_{\rm Opt11hr}$–$\log F_{\rm pk2}$–$\log T_{\rm 90,i}$ formula is

$$\log F_{\rm Opt11hr} = (0.65 \pm 0.14) \times \log F_{\rm pk2} + (0.43 \pm 0.11) \times \log T_{\rm 90,i} + (-5.6 \pm 0.13), \quad (270)$$

where $F_{\rm Opt11hr}$ is in units of Jy. $F_{\rm pk2}$ is the peak energy flux in the 64 ms time bin in the rest-frame 1–10^4 keV energy band and is in units of 10^{-6} erg cm^{-2} s^{-1}. $T_{\rm 90,i}$ is in units of s. The adjusted R^2 is 0.5628. The number of GRBs in the sample is 40.

The log Age–log HR–$\beta_{\rm X11hr}$ formula is

$$\log {\rm Age} = (-0.63 \pm 0.14) \times \log {\rm HR} + (0.25 \pm 0.11) \times \beta_{\rm X11hr} + (2.4 \pm 0.2), \quad (271)$$

where Age is in units of Myr. The adjusted R^2 is 0.231. The number of GRBs in the sample is 40.

The $\log D_{\rm L}$–$\log \theta_{\rm j}$–log Age formula is

$$\log D_{\rm L} = (-0.46 \pm 0.074) \times \log \theta_{\rm j} + (-0.31 \pm 0.052) \times \log {\rm Age} + (0.44 \pm 0.21), \quad (272)$$

where $D_{\rm L}$ is in units of 10^{28} cm. $\theta_{\rm j}$ is in units of rad. Age is in units of Myr. The adjusted R^2 is 0.3565. The number of GRBs in the sample is 40.

The $\log F_{\rm Opt11hr}$–$\log \theta_{\rm j}$–$\log t_{\rm pkOpt}$ formula is

$$\log F_{\rm Opt11hr} = (0.45 \pm 0.19) \times \log \theta_{\rm j} + (0.32 \pm 0.1) \times \log t_{\rm pkOpt} + (-4.8 \pm 0.37), \quad (273)$$

where $F_{\rm Opt11hr}$ is in units of Jy. $\theta_{\rm j}$ is in units of rad. $t_{\rm pkOpt}$ is in units of s. The adjusted R^2 is 0.2278. The number of GRBs in the sample is 40.

The $\log E_{\rm p,cpl,i}$–$\log F_{\rm g}$–log SFR formula is

$$\log E_{\rm p,cpl,i} = (0.39 \pm 0.043) \times \log F_{\rm g} + (0.12 \pm 0.032) \times \log {\rm SFR} + (2.1 \pm 0.052), \quad (274)$$

where $E_{\rm p,cpl,i}$ is in units of keV. $F_{\rm g}$ is in units of 10^{-6} erg cm^{-2} and in the 20–2000 keV energy band. SFR is in units of $M_\odot$ yr^{-1}. The adjusted R^2 is 0.4204. The number of GRBs in the sample is 41.

The $\log F_{\rm g}$–$\log F_{\rm Opt11hr}$–metallicity formula is

$$\log F_{\rm g} = (0.27 \pm 0.066) \times \log F_{\rm Opt11hr} + (-0.64 \pm 0.25) \times {\rm metallicity} + (7.4 \pm 1.9), \quad (275)$$

where $F_{\rm g}$ is in units of 10^{-6} erg cm^{-2} and in the 20–2000 keV energy band. $F_{\rm Opt11hr}$ is in units of Jy. The metallicity is the value of 12 + log O/H. The adjusted R^2 is 0.242. The number of GRBs in the sample is 41.

The $\log \Gamma_0$–$\log P_{\rm pk4}$–$A_{\rm V}$ formula is

$$\log \Gamma_0 = (0.29 \pm 0.03) \times \log P_{\rm pk4} + (-0.26 \pm 0.13) \times A_{\rm V} + (2.1 \pm 0.042), \quad (276)$$

where $P_{\rm pk4}$ is the peak photon flux in the 1 s time bin in 10–1000 keV and is in units of photons cm^{-2} s^{-1}. The adjusted R^2 is 0.2218. The number of GRBs in the sample is 41.

The $\log t_{\rm pkOpt,i}$–$\log T_{\rm R45}$–$\log E_{\rm p,cpl}$ formula is

$$\log t_{\rm pkOpt,i} = (0.67 \pm 0.053) \times \log T_{\rm R45} + (-0.61 \pm 0.12) \times \log E_{\rm p,cpl} + (2.7 \pm 0.25), \quad (277)$$

where $t_{\rm pkOpt,i}$ is in units of s. $T_{\rm R45}$ is in units of s. $E_{\rm p,cpl}$ is in units of keV. The adjusted R^2 is 0.3051. The number of GRBs in the sample is 41.

The log SFR–$A_{\rm V}$–$\log t_{\rm burst,i}$ formula is

$$\log {\rm SFR} = (0.26 \pm 0.079) \times A_{\rm V} + (-0.46 \pm 0.077) \times \log t_{\rm burst,i} + (1.7 \pm 0.25), \quad (278)$$

where SFR is in units of $M_\odot$ yr^{-1}. $t_{\rm burst,i}$ is in units of s. The adjusted R^2 is 0.2794. The number of GRBs in the sample is 42.

The $\log L_{\rm pk}$–$\log F_{\rm g}$–$\log \Gamma_0$ formula is

$$\log L_{\rm pk} = (0.34 \pm 0.057) \times \log F_{\rm g} + (2 \pm 0.07) \times \log \Gamma_0 + (-4.8 \pm 0.14), \quad (279)$$

where $L_{\rm pk}$ is in units of $10^{52}\,{\rm erg\,s^{-1}}$ and in the 1–10^4 keV energy band. $F_{\rm g}$ is in units of $10^{-6}\,{\rm erg\,cm^{-2}}$ and in the 20–2000 keV energy band. The adjusted R^2 is 0.6858. The number of GRBs in the sample is 42.

The $\log E_{\rm p,cpl,i}$–$\log F_{\rm pk1}$–$\log$ SFR formula is

$$\log E_{\rm p,cpl,i} = (0.25 \pm 0.036) \times \log F_{\rm pk1} + (0.13 \pm 0.032) \times \log {\rm SFR} + (2.4 \pm 0.038), \quad (280)$$

where $E_{\rm p,cpl,i}$ is in units of keV. $F_{\rm pk1}$ is the peak energy flux in the 1 s time bin in the rest-frame 1–10^4 keV energy band and is in units of $10^{-6}\,{\rm erg\,cm^{-2}\,s^{-1}}$. The SFR is in units of $M_\odot\,{\rm yr^{-1}}$. The adjusted R^2 is 0.3181. The number of GRBs in the sample is 42.

The log SFR–$\log L_{\rm pk}$–$\log F_{\rm Opt11hr}$ formula is

$$\log {\rm SFR} = (0.3 \pm 0.053) \times \log L_{\rm pk} + (-0.33 \pm 0.08) \times \log F_{\rm Opt11hr} + (-0.88 \pm 0.4), \quad (281)$$

where the SFR is in units of $M_\odot\,{\rm yr^{-1}}$. $L_{\rm pk}$ is in units of $10^{52}\,{\rm erg\,s^{-1}}$ and in the 1–10^4 keV energy band. $F_{\rm Opt11hr}$ is in units of Jy. The adjusted R^2 is 0.3027. The number of GRBs in the sample is 42.

The $(-\beta_{\rm Band})$–$\log F_{\rm g}$–$\log N_{\rm H}$ formula is

$$(-\beta_{\rm Band}) = (0.21 \pm 0.087) \times \log F_{\rm g} + (-0.22 \pm 0.15) \times \log N_{\rm H} + (2.2 \pm 0.2), \quad (282)$$

where $F_{\rm g}$ is in units of $10^{-6}\,{\rm erg\,cm^{-2}}$ and in the 20–2000 keV energy band. $N_{\rm H}$ is in units of $10^{21}\,{\rm cm^{-2}}$. The adjusted R^2 is 0.2912. The number of GRBs in the sample is 43.

The $\log F_{\rm Opt11hr}$–$\log F_{\rm X11hr}$–$\log t_{\rm pkOpt,i}$ formula is

$$\log F_{\rm Opt11hr} = (0.25 \pm 0.1) \times \log F_{\rm X11hr} + (0.49 \pm 0.096) \times \log t_{\rm pkOpt,i} + (-3.9 \pm 0.77), \quad (283)$$

where $F_{\rm Opt11hr}$ is in units of Jy. $F_{\rm X11hr}$ is in units of Jy. $t_{\rm pkOpt,i}$ is in units of s. The adjusted R^2 is 0.3049. The number of GRBs in the sample is 43.

The Mag–$\log E_{\rm iso}$–$\log N_{\rm H}$ formula is

$$\mathrm{Mag} = (-1.1 \pm 0.34) \times \log E_{\rm iso} + (-1.5 \pm 0.61) \times \log N_{\rm H} + (-19 \pm 0.6), \quad (284)$$

where Mag is in units of magnitude. $E_{\rm iso}$ is in units of 10^{52} erg and in the rest-frame 1–10^4 keV energy band. $N_{\rm H}$ is in units of $10^{21}\,{\rm cm^{-2}}$. The adjusted R^2 is 0.4373. The number of GRBs in the sample is 44.

The Mag–$\log F_{\rm Opt11hr}$–$\log t_{\rm burst,i}$ formula is

$$\mathrm{Mag} = (0.39 \pm 0.39) \times \log F_{\rm Opt11hr} + (1.4 \pm 0.57) \times \log t_{\rm burst,i} + (-22 \pm 2.9), \quad (285)$$

where Mag is in units of magnitude. $F_{\rm Opt11hr}$ is in units of Jy. $t_{\rm burst,i}$ is in units of s. The adjusted R^2 is 0.4612. The number of GRBs in the sample is 44.

The Mag–log Mass–$\log E_{\rm p,cpl,i}$ formula is

$$\mathrm{Mag} = (-1.9 \pm 0.45) \times \log {\rm Mass} + (-0.37 \pm 0.76) \times \log E_{\rm p,cpl,i} + (-2.1 \pm 4.4), \quad (286)$$

where Mag is in units of magnitude. Mass is in units of $M_\odot$. $E_{\rm p,cpl,i}$is in units of keV. The adjusted R^2 is 0.8675. The number of GRBs in the sample is 44.

The $\log E_{\rm p,Band,i}$–$\log \theta_{\rm j}$–$\log$ Mass formula is

$$\log E_{\rm p,Band,i} = (-0.55 \pm 0.088) \times \log \theta_{\rm j} + (0.19 \pm 0.045) \times \log {\rm Mass} + (0.06 \pm 0.45), \quad (287)$$

where $E_{\rm p,Band,i}$ is in units of keV. $\theta_{\rm j}$ is in units of rad. Mass is in units of $M_\odot$. The adjusted R^2 is 0.2478. The number of GRBs in the sample is 44.

The $\log \Gamma_0$–$\log(1+z)$–$\log P_{\rm pk4}$ formula is

$$\log \Gamma_0 = (1.7 \pm 0.086) \times \log(1+z) + (0.4 \pm 0.022) \times \log P_{\rm pk4} + (1.2 \pm 0.04), \quad (288)$$

where $P_{\rm pk4}$ is the peak photon flux in the 1 s time bin in 10–1000 keV and is in units of photons $\rm cm^{-2}\,s^{-1}$. The adjusted R^2 is 0.6095. The number of GRBs in the sample is 44.

The Mag–$\log(1+z)$–$\log N_{\rm H}$ formula is

$$\mathrm{Mag} = (-5.3 \pm 1.9) \times \log(1+z) + (-1.2 \pm 0.6) \times \log N_{\rm H} + (-18 \pm 0.9), \quad (289)$$

where Mag is in units of magnitude. $N_{\rm H}$ is in units of $10^{21}\,{\rm cm^{-2}}$. The adjusted R^2 is 0.4667. The number of GRBs in the sample is 44.

The $\log E_{\rm iso}$–$\log E_{\rm p,cpl,i}$–$\log t_{\rm pkOpt,i}$ formula is

$$\log E_{\rm iso} = (0.9 \pm 0.11) \times \log E_{\rm p,cpl,i} + (-0.44 \pm 0.056) \times \log t_{\rm pkOpt,i} + (-0.66 \pm 0.37), \quad (290)$$

where $E_{\rm iso}$ is in units of 10^{52} erg and in the rest-frame 1–10^4 keV energy band. $E_{\rm p,cpl,i}$ is in units of keV. $t_{\rm pkOpt,i}$ is in units of s. The adjusted R^2 is 0.6507. The number of GRBs in the sample is 45.

The $\log t_{\rm pkOpt}$–$\log P_{\rm pk4}$–$\log E_{\rm p,cpl}$ formula is

$$\log t_{\rm pkOpt} = (-0.63 \pm 0.046) \times \log P_{\rm pk4} + (-0.43 \pm 0.11) \times \log E_{\rm p,cpl} + (3.8 \pm 0.24), \quad (291)$$

where $t_{\rm pkOpt}$ is in units of s. $P_{\rm pk4}$ is the peak photon flux in the 1 s time bin in 10–1000 keV and is in units of photons $\rm cm^{-2}\,s^{-1}$. $E_{\rm p,cpl}$ is in units of keV. The adjusted R^2 is 0.3112. The number of GRBs in the sample is 45.

The $\log D_{\rm L}$–$\log T_{50,\rm i}$–$\log t_{\rm radio,pk,i}$ formula is

$$\log D_{\rm L} = (-0.27 \pm 0.0097) \times \log T_{50,\rm i} + (-0.51 \pm 0.02) \times \log t_{\rm radio,pk,i} + (3.5 \pm 0.11), \quad (292)$$

where $D_{\rm L}$ is in units of 10^{28} cm. $T_{50,\rm i}$ is in units of s. $t_{\rm radio,pk,i}$ is in units of s. The adjusted R^2 is 0.205. The number of GRBs in the sample is 45.

The $\log t_{\rm pkOpt,i}$–$\log T_{90}$–$\log \Gamma_0$ formula is

$$\log t_{\rm pkOpt,i} = (0.29 \pm 0.026) \times \log T_{90} + (-1.4 \pm 0.028) \times \log \Gamma_0 + (4.6 \pm 0.067). \quad (293)$$

where $t_{\rm pkOpt,i}$ is in units of s. T_{90} is in units of s. The adjusted R^2 is 0.7005. The number of GRBs in the sample is 45.

The log SFR–$\log E_{\rm iso}$–$\log F_{\rm Opt11hr}$ formula is

$$\log {\rm SFR} = (0.38 \pm 0.049) \times \log E_{\rm iso} + (-0.34 \pm 0.073) \times \log F_{\rm Opt11hr} + (-1.1 \pm 0.35), \quad (294)$$

where SFR is in units of $M_\odot\,{\rm yr}^{-1}$. $E_{\rm iso}$ is in units of 10^{52} erg and in the rest-frame 1–10^4 keV energy band. $F_{\rm Opt11hr}$ is in units of Jy. The adjusted R^2 is 0.3405. The number of GRBs in the sample is 46.

The log Mass–metallicity–log SFR formula is

$$\log {\rm Mass} = (0.8 \pm 0.18) \times {\rm metallicity} + (0.55 \pm 0.054) \times \log {\rm SFR} + (2.2 \pm 1.6), \quad (295)$$

where Mass is in units of $M_\odot$. The metallicity is the value of $12 + \log {\rm O/H}$. SFR is in units of $M_\odot\,{\rm yr}^{-1}$. The adjusted R^2 is 0.6178. The number of GRBs in the sample is 46.

The $\log E_{\rm iso}$–$\log \theta_{\rm j}$–$\log t_{\rm radio,pk,i}$ formula is

$$\log E_{\rm iso} = (-0.98 \pm 0.18) \times \log \theta_{\rm j} + (-0.98 \pm 0.071) \times \log t_{\rm radio,pk,i} + (5.3 \pm 0.53), \quad (296)$$

where $E_{\rm iso}$ is in units of 10^{52} erg and in the rest-frame 1–10^4 keV energy band. $\theta_{\rm j}$ is in units of rad. $t_{\rm radio,pk,i}$ is in units of s. The adjusted R^2 is 0.2374. The number of GRBs in the sample is 46.

The $\log E_{\rm iso}$–$\log L_{\rm radio,pk}$–$\log \theta_{\rm j}$ formula is

$$\log E_{\rm iso} = (0.68 \pm 0.022) \times \log L_{\rm radio,pk} + (-0.78 \pm 0.12) \times \log \theta_{\rm j} + (-1.2 \pm 0.12), \quad (297)$$

where $E_{\rm iso}$ is in units of 10^{52} erg and in the rest-frame 1–10^4 keV energy band. $L_{\rm radio,pk}$ is in rest-frame 8.46 GHz and is in units of $10^{40}\,{\rm erg\,s^{-1}}$. $\theta_{\rm j}$ is in units of rad. The adjusted R^2 is 0.5004. The number of GRBs in the sample is 46.

The $\log F_{\rm Opt11hr}$–log Age–$\log T_{\rm R45,i}$ formula is

$$\log F_{\rm Opt11hr} = (0.3 \pm 0.13) \times \log {\rm Age} + (0.73 \pm 0.11) \times \log T_{\rm R45,i} + (-5.8 \pm 0.34), \quad (298)$$

where $F_{\rm Opt11hr}$ is in units of Jy. Age is in units of Myr. $T_{\rm R45,i}$ is in units of s. The adjusted R^2 is 0.3872. The number of GRBs in the sample is 47.

The $\log P_{\rm pk4}$–$\log E_{\rm p,Band}$–$\log F_{\rm X11hr}$ formula is

$$\log P_{\rm pk4} = (0.49 \pm 0.093) \times \log E_{\rm p,Band} + (0.42 \pm 0.043) \times \log F_{\rm X11hr} + (2.8 \pm 0.28), \quad (299)$$

where $P_{\rm pk4}$ is the peak photon flux in the 1 s time bin in 10–1000 keV and is in units of photons $\rm cm^{-2}\,s^{-1}$. $E_{\rm p,Band}$ is in units of keV. $F_{\rm X11hr}$ is in units of Jy. The adjusted R^2 is 0.6621. The number of GRBs in the sample is 47.

The $\log D_{\rm L}$–log HR–$\log \Gamma_0$ formula is

$$\log D_{\rm L} = (-0.24 \pm 0.031) \times \log {\rm HR} + (0.65 \pm 0.026) \times \log \Gamma_0 + (-0.8 \pm 0.053), \quad (300)$$

where $D_{\rm L}$ is in units of 10^{28} cm. The adjusted R^2 is 0.3027. The number of GRBs in the sample is 47.

The $\log F_{\rm g}$–$\log P_{\rm pk1}$–$\log F_{\rm Opt11hr}$ formula is

$$\log F_{\rm g} = (1.1 \pm 0.11) \times \log P_{\rm pk1} + (0.35 \pm 0.084) \times \log F_{\rm Opt11hr} + (1.5 \pm 0.52), \quad (301)$$

where $F_{\rm g}$ is in units of $10^{-6}\,{\rm erg\,cm^{-2}}$ and in the 20–2000 keV energy band. $P_{\rm pk1}$ is the peak photon flux in the 64 ms time bin in 10–1000 keV and is in units of photons $\rm cm^{-2}\,s^{-1}$. $F_{\rm Opt11hr}$ is in units of Jy. The adjusted R^2 is 0.6153. The number of GRBs in the sample is 48.

The log HR–variability$_3$–$(-\beta_{\rm Band})$ formula is

$$\log {\rm HR} = (7.9 \pm 3.2) \times {\rm variability}_3 + (-0.18 \pm 0.099) \times (-\beta_{\rm Band}) + (0.81 \pm 0.24), \quad (302)$$

The adjusted R^2 is 0.251. The number of GRBs in the sample is 48.

The $\log L_{\rm radio,pk}$–$\log L_{\rm pk}$–$A_{\rm V}$ formula is

$$\log L_{\rm radio,pk} = (0.5 \pm 0.026) \times \log L_{\rm pk} + (-0.35 \pm 0.076) \times A_{\rm V} + (1.9 \pm 0.053), \quad (303)$$

where $L_{\rm radio,pk}$ is in rest-frame 8.46 GHz and in units of $10^{40}\,{\rm erg\,s^{-1}}$. $L_{\rm pk}$ is in units of $10^{52}\,{\rm erg\,s^{-1}}$ and in the 1–10^4 keV energy band. The adjusted R^2 is 0.49. The number of GRBs in the sample is 48.

The $\log L_{\rm pk}$–$\log F_{\rm g}$–$\log F_{\rm radio,pk}$ formula is

$$\log L_{\rm pk} = (0.82 \pm 0.054) \times \log F_{\rm g} + (-0.85 \pm 0.06) \times \log F_{\rm radio,pk} + (-3.8 \pm 0.22), \quad (304)$$

where $L_{\rm pk}$ is in units of $10^{52}\,{\rm erg\,s^{-1}}$ and in the 1–10^4 keV energy band. $F_{\rm g}$ is in units of $10^{-6}\,{\rm erg\,cm^{-2}}$ and in the 20–2000 keV energy band. $F_{\rm radio,pk}$ is in units of Jy. The adjusted R^2 is 0.4055. The number of GRBs in the sample is 49.

The $\log L_{\rm pk}$–$\log F_{\rm g}$–$\log t_{\rm radio,pk,i}$ formula is

$$\log L_{\rm pk} = (0.74 \pm 0.055) \times \log F_{\rm g} + (-0.66 \pm 0.074) \times \log t_{\rm radio,pk,i} + (2.9 \pm 0.46), \quad (305)$$

where $L_{\rm pk}$ is in units of $10^{52}\,{\rm erg\,s^{-1}}$ and in the 1–10^4 keV energy band. $F_{\rm g}$ is in units of $10^{-6}\,{\rm erg\,cm^{-2}}$ and in the

20–2000 keV energy band. $t_{\rm radio,pk,i}$ is in units of s. The adjusted R^2 is 0.353. The number of GRBs in the sample is 49.

The $\log F_{\rm Opt11hr}$–$\log N_{\rm H}$–log Mass formula is

$$\log F_{\rm Opt11hr} = (-0.43 \pm 0.16) \times \log N_{\rm H} + (-0.52 \pm 0.11) \times \log {\rm Mass} + (0.074 \pm 1), \quad (306)$$

where $F_{\rm Opt11hr}$ is in units of Jy. $N_{\rm H}$ is in units of $10^{21}\,{\rm cm}^{-2}$. Mass is in units of $M_\odot$. The adjusted R^2 is 0.3336. The number of GRBs in the sample is 49.

The $\log F_{\rm g}$–variability$_3$–$\log T_{90,\rm i}$ formula is

$$\log F_{\rm g} = (43 \pm 6.6) \times {\rm variability}_3 + (0.78 \pm 0.039) \times \log T_{90,\rm i} + (-0.12 \pm 0.071), \quad (307)$$

where $F_{\rm g}$ is in units of $10^{-6}\,{\rm erg\,cm}^{-2}$ and in the 20–2000 keV energy band. $T_{90,\rm i}$ is in units of s. The adjusted R^2 is 0.4482. The number of GRBs in the sample is 49.

The $\log F_{\rm g}$–variability$_3$–$\log T_{\rm R45,i}$ formula is

$$\log F_{\rm g} = (47 \pm 6.9) \times {\rm variability}_3 + (0.78 \pm 0.054) \times \log T_{\rm R45,i} + (0.51 \pm 0.06), \quad (308)$$

where $F_{\rm g}$ is in units of $10^{-6}\,{\rm erg\,cm}^{-2}$ and in the 20–2000 keV energy band. $T_{\rm R45,i}$ is in units of s. The adjusted R^2 is 0.278. The number of GRBs in the sample is 49.

The $\log F_{\rm g}$–$\log(1+z)$–variability$_3$ formula is

$$\log F_{\rm g} = (-1.9 \pm 0.1) \times \log(1+z) + (35 \pm 6.9) \times {\rm variability}_3 + (1.7 \pm 0.086), \quad (309)$$

where $F_{\rm g}$ is in units of $10^{-6}\,{\rm erg\,cm}^{-2}$ and in the 20–2000 keV energy band. The adjusted R^2 is 0.3132. The number of GRBs in the sample is 49.

The $\log F_{\rm g}$–$\log D_{\rm L}$–variability$_3$ formula is

$$\log F_{\rm g} = (-0.86 \pm 0.042) \times \log D_{\rm L} + (37 \pm 6.9) \times {\rm variability}_3 + (1.3 \pm 0.069), \quad (310)$$

where $F_{\rm g}$ is in units of $10^{-6}\,{\rm erg\,cm}^{-2}$ and in the 20–2000 keV energy band. $D_{\rm L}$ is in units of $10^{28}\,{\rm cm}$. The adjusted R^2 is 0.2954. The number of GRBs in the sample is 50.

The log HR–$\log E_{\rm iso}$–$\log F_{\rm radio,pk}$ formula is

$$\log {\rm HR} = (0.24 \pm 0.018) \times \log E_{\rm iso} + (0.33 \pm 0.049) \times \log F_{\rm radio,pk} + (1.4 \pm 0.17), \quad (311)$$

where $E_{\rm iso}$ is in units of $10^{52}\,{\rm erg}$ and in the rest-frame 1–10^4 keV energy band. $F_{\rm radio,pk}$ is in units of Jy. The adjusted R^2 is 0.2991. The number of GRBs in the sample is 50.

The log Age–$\log F_{\rm Opt11hr}$–log SSFR formula is

$$\log {\rm Age} = (0.29 \pm 0.063) \times \log F_{\rm Opt11hr} + (-0.44 \pm 0.069) \times \log {\rm SSFR} + (4.1 \pm 0.31), \quad (312)$$

where Age is in units of Myr. $F_{\rm Opt11hr}$ is in units of Jy. log SSFR is in units of ${\rm Gyr}^{-1}$. The adjusted R^2 is 0.3771. The number of GRBs in the sample is 50.

The $\log E_{\rm p,Band,i}$–log HR–$\log\theta_{\rm j}$ formula is

$$\log E_{\rm p,Band,i} = (0.61 \pm 0.12) \times \log {\rm HR} + (-0.33 \pm 0.087) \times \log\theta_{\rm j} + (2 \pm 0.11), \quad (313)$$

where $E_{\rm p,Band,i}$ is in units of keV. $\theta_{\rm j}$ is in units of rad. The adjusted R^2 is 0.4157. The number of GRBs in the sample is 51.

The log SFR–$\log T_{90}$–$\log F_{\rm Opt11hr}$ formula is

$$\log {\rm SFR} = (0.5 \pm 0.068) \times \log T_{90} + (-0.4 \pm 0.072) \times \log F_{\rm Opt11hr} + (-2.1 \pm 0.36), \quad (314)$$

where SFR is in units of $M_\odot\,{\rm yr}^{-1}$. T_{90} is in units of s. $F_{\rm Opt11hr}$ is in units of Jy. The adjusted R^2 is 0.3356. The number of GRBs in the sample is 51.

The $\log L_{\rm radio,pk}$–$\log E_{\rm iso}$–$\log F_{\rm Opt11hr}$ formula is

$$\log L_{\rm radio,pk} = (0.67 \pm 0.023) \times \log E_{\rm iso} + (-0.23 \pm 0.074) \times \log F_{\rm Opt11hr} + (0.18 \pm 0.31), \quad (315)$$

where $L_{\rm radio,pk}$ is in rest-frame 8.46 GHz and in units of $10^{40}\,{\rm erg\,s}^{-1}$. $E_{\rm iso}$ is in units of $10^{52}\,{\rm erg}$ and in the rest-frame 1–10^4 keV energy band. $F_{\rm Opt11hr}$ is in units of Jy. The adjusted R^2 is 0.4846. The number of GRBs in the sample is 52.

The $\log F_{\rm Opt11hr}$–log Age–log Mass formula is

$$\log F_{\rm Opt11hr} = (0.42 \pm 0.11) \times \log {\rm Age} + (-0.45 \pm 0.098) \times \log {\rm Mass} + (-1.8 \pm 1), \quad (316)$$

where $F_{\rm Opt11hr}$ is in units of Jy. Age is in units of Myr. Mass is in units of $M_\odot$. The adjusted R^2 is 0.3177. The number of GRBs in the sample is 53.

The $\beta_{\rm X11hr}$–$\log E_{\rm p,Band}$–$\log F_{\rm X11hr}$ formula is

$$\beta_{\rm X11hr} = (-0.39 \pm 0.12) \times \log E_{\rm p,Band} + (-0.37 \pm 0.091) \times \log F_{\rm X11hr} + (-0.27 \pm 0.81), \quad (317)$$

where $E_{\rm p,Band}$ is in units of keV. $F_{\rm X11hr}$ is in units of Jy. The adjusted R^2 is 0.3324. The number of GRBs in the sample is 53.

The $\log E_{\rm p,Band,i}$–log HR–log Mass formula is

$$\log E_{\rm p,Band,i} = (0.83 \pm 0.1) \times \log {\rm HR} + (0.12 \pm 0.033) \times \log {\rm Mass} + (1.1 \pm 0.32), \quad (318)$$

where $E_{\rm p,Band,i}$ is in units of keV. Mass is in units of $M_\odot$. The adjusted R^2 is 0.6666. The number of GRBs in the sample is 53.

The log Age–log HR–log SSFR formula is

$$\log {\rm Age} = (-0.41 \pm 0.13) \times \log {\rm HR} + (-0.45 \pm 0.061) \times \log {\rm SSFR} + (2.8 \pm 0.083), \quad (319)$$

where Age is in units of Myr. log SSFR is in units of ${\rm Gyr}^{-1}$. The adjusted R^2 is 0.2396. The number of GRBs in the sample is 53.

The Mag–$\log L_{\rm pk}$–$\log P_{\rm pk4}$ formula is

$$\begin{aligned}\rm Mag = (-1.1 \pm 0.28) \times \log L_{pk} + (0.7 \pm 0.54) \\ \times \log P_{pk4} + (-21 \pm 0.48),\end{aligned} \quad (320)$$

where Mag is in units of magnitude. $L_{\rm pk}$ is in units of $10^{52}\,{\rm erg\,s^{-1}}$ and in the 1–10^4 keV energy band. $P_{\rm pk4}$ is the peak photon flux in the 1 s time bin in 10–1000 keV and is in units of photons $\rm cm^{-2}\,s^{-1}$. The adjusted R^2 is 0.3453. The number of GRBs in the sample is 53.

The log Mass–$\log L_{\rm pk}$–metallicity formula is

$$\begin{aligned}\log \rm Mass = (0.17 \pm 0.038) \times \log L_{pk} + (1.2 \pm 0.2) \\ \times \rm metallicity + (-0.7 \pm 1.7),\end{aligned} \quad (321)$$

where Mass is in units of $M_\odot$. $L_{\rm pk}$ is in units of $10^{52}\,{\rm erg\,s^{-1}}$ and in the 1–10^4 keV energy band. The metallicity is the value of $12 + \log {\rm O/H}$. The adjusted R^2 is 0.3348. The number of GRBs in the sample is 53.

The $\log F_{\rm Opt11hr}$–log Mass–$\log t_{\rm burst,i}$ formula is

$$\begin{aligned}\log F_{\rm Opt11hr} = (-0.29 \pm 0.11) \times \log \rm Mass + (0.63 \pm 0.12) \\ \times \log t_{\rm burst,i} + (-3.8 \pm 1.2),\end{aligned} \quad (322)$$

where $F_{\rm Opt11hr}$ is in units of Jy. Mass is in units of $M_\odot$. $t_{\rm burst,i}$ is in units of s. The adjusted R^2 is 0.2911. The number of GRBs in the sample is 53.

The log Age–$\log(1+z)$–$\log F_{\rm Opt11hr}$ formula is

$$\begin{aligned}\log \rm Age = (-1.7 \pm 0.34) \times \log(1+z) + (0.17 \pm 0.062) \\ \times \log F_{\rm Opt11hr} + (3.9 \pm 0.3),\end{aligned} \quad (323)$$

where Age is in units of Myr. $F_{\rm Opt11hr}$ is in units of Jy. The adjusted R^2 is 0.2579. The number of GRBs in the sample is 53.

The $\log L_{\rm radio,pk}$–$\log E_{\rm iso}$–$A_{\rm V}$ formula is

$$\begin{aligned}\log L_{\rm radio,pk} = (0.59 \pm 0.015) \times \log E_{\rm iso} + (-0.27 \pm 0.055 \\ \times A_{\rm V} + (1.3 \pm 0.041),\end{aligned} \quad (324)$$

where $L_{\rm radio,pk}$ is in rest-frame 8.46 GHz and is in untis of $10^{40}\,{\rm erg\,s^{-1}}$. $E_{\rm iso}$ is in units of $10^{52}\,{\rm erg}$ and in the rest-frame 1–10^4 keV energy band. The adjusted R^2 is 0.5084. The number of GRBs in the sample is 53.

The log Mass–$\beta_{\rm X11hr}$–Mag formula is

$$\begin{aligned}\log \rm Mass = (0.12 \pm 0.081) \times \beta_{X11hr} + (-0.11 \pm 0.029) \\ \times \rm Mag + (7 \pm 0.62),\end{aligned} \quad (325)$$

where Mass is in units of $M_\odot$. Mag is in units of magnitude. The adjusted R^2 is 0.8391. The number of GRBs in the sample is 54.

The $\log F_{\rm g}$–$\beta_{\rm X11hr}$–log SSFR formula is

$$\begin{aligned}\log F_{\rm g} = (-0.49 \pm 0.11) \times \beta_{\rm X11hr} + (0.4 \pm 0.051) \\ \times \log \rm SSFR + (1.5 \pm 0.17),\end{aligned} \quad (326)$$

where $F_{\rm g}$ is in units of $10^{-6}\,{\rm erg\,cm^{-2}}$ and in the 20–2000 keV energy band. log SSFR is in units of $\rm Gyr^{-1}$. The adjusted R^2 is 0.3069. The number of GRBs in the sample is 54.

The $\log T_{\rm 90,i}$–$\log E_{\rm p,Band}$–$\log F_{\rm X11hr}$ formula is

$$\begin{aligned}\log T_{\rm 90,i} = (0.34 \pm 0.054) \times \log E_{\rm p,Band} + (0.21 \pm 0.026) \\ \times \log F_{\rm X11hr} + (1.9 \pm 0.26),\end{aligned} \quad (327)$$

where $T_{\rm 90,i}$ is in units of s. $E_{\rm p,Band}$ is in units of keV. $F_{\rm X11hr}$ is in units of Jy. The adjusted R^2 is 0.2015. The number of GRBs in the sample is 54.

The $\log F_{\rm radio,pk}$–$\log F_{\rm Opt11hr}$–$\log t_{\rm radio,pk,i}$ formula is

$$\begin{aligned}\log F_{\rm radio,pk} = (0.27 \pm 0.04) \times \log F_{\rm Opt11hr} + (0.25 \pm 0.04) \\ \times \log t_{\rm radio,pk,i} + (-3.7 \pm 0.31),\end{aligned} \quad (328)$$

where $F_{\rm radio,pk}$ is in units of Jy. $F_{\rm Opt11hr}$ is in units of Jy. $t_{\rm radio,pk,i}$ is in units of s. The adjusted R^2 is 0.4246. The number of GRBs in the sample is 54.

The $\log F_{\rm Opt11hr}$–$\log F_{\rm radio,pk}$–$\log T_{\rm 90,i}$ formula is

$$\begin{aligned}\log F_{\rm Opt11hr} = (0.89 \pm 0.12) \times \log F_{\rm radio,pk} + (0.32 \pm 0.11) \\ \times \log T_{\rm 90,i} + (-1.6 \pm 0.46),\end{aligned} \quad (329)$$

where $F_{\rm Opt11hr}$ is in units of Jy. $F_{\rm radio,pk}$ is in units of Jy. $T_{\rm 90,i}$ is in units of s. The adjusted R^2 is 0.4369. The number of GRBs in the sample is 54.

The $\log D_{\rm L}$–$\log F_{\rm radio,pk}$–$A_{\rm V}$ formula is

$$\begin{aligned}\log D_{\rm L} = (-0.46 \pm 0.025) \times \log F_{\rm radio,pk} + (-0.12 \pm 0.028) \\ \times A_{\rm V} + (-1.2 \pm 0.084),\end{aligned} \quad (330)$$

where $D_{\rm L}$ is in units of $10^{28}\,{\rm cm}$. $F_{\rm radio,pk}$ is in units of Jy. The adjusted R^2 is 0.237. The number of GRBs in the sample is 54.

The log Mass–$\log T_{50}$–log SFR formula is

$$\begin{aligned}\log \rm Mass = (0.34 \pm 0.077) \times \log T_{50} + (0.62 \pm 0.047) \\ \times \log \rm SFR + (8.7 \pm 0.11),\end{aligned} \quad (331)$$

where Mass is in units of $M_\odot$. T_{50} is in units of s. SFR is in units of $M_\odot\,\rm yr^{-1}$. The adjusted R^2 is 0.6319. The number of GRBs in the sample is 54.

The $\log F_{\rm Opt11hr}$–$\log(1+z)$–$\log F_{\rm radio,pk}$ formula is

$$\begin{aligned}\log F_{\rm Opt11hr} = (-0.86 \pm 0.37) \times \log(1+z) + (0.79 \pm 0.15) \\ \times \log F_{\rm radio;pk} + (-1.3 \pm 0.45),\end{aligned} \quad (332)$$

where $F_{\rm Opt11hr}$ is in units of Jy. $F_{\rm radio,pk}$ is in units of Jy. R^2 is 0.4305. The number of GRBs in the sample is 54.

The $\log t_{\rm pkOpt}$–$\log F_{\rm g}$–$\log F_{\rm Opt11hr}$ formula is

$$\begin{aligned}\log t_{\rm pkOpt} = (-0.34 \pm 0.03) \times \log F_{\rm g} + (0.27 \pm 0.061) \\ \times \log F_{\rm Opt11hr} + (4 \pm 0.28),\end{aligned} \quad (333)$$

where $F_{\rm Opt11hr}$ is in units of Jy. $t_{\rm pkOpt}$ is in units of s. $F_{\rm g}$ is in units of $10^{-6}\,{\rm erg\,cm^{-2}}$ and in the 20–2000 keV energy band. The adjusted R^2 is 0.309. The number of GRBs in the sample is 55.

The log SFR–metallicity–A_V formula is

$$\log \mathrm{SFR} = (1.1 \pm 0.24) \times \mathrm{metallicity} + (0.24 \pm 0.07) \times A_V + (-8.9 \pm 2), \quad (334)$$

where SFR is in units of $M_\odot\,\mathrm{yr}^{-1}$. The metallicity is the value of $12 + \log \mathrm{O/H}$. The adjusted R^2 is 0.265. The number of GRBs in the sample is 55.

The Mag–log Mass–log $t_{\mathrm{burst,i}}$ formula is

$$\mathrm{Mag} = (-1.7 \pm 0.46) \times \log \mathrm{Mass} + (0.43 \pm 0.44) \times \log t_{\mathrm{burst,i}} + (-5.4 \pm 4.9), \quad (335)$$

where Mag is in units of magnitude. Mass is in units of $M_\odot$. $t_{\mathrm{burst,i}}$ is in units of s. The adjusted R^2 is 0.8658. The number of GRBs in the sample is 57.

The Mag–log T_{90}–log $t_{\mathrm{burst,i}}$ formula is

$$\mathrm{Mag} = (-1.1 \pm 0.81) \times \log T_{90} + (1.1 \pm 0.4) \times \log t_{\mathrm{burst,i}} + (-21 \pm 1.8), \quad (336)$$

where Mag is in units of magnitude. T_{90} is in units of s. $t_{\mathrm{burst,i}}$ is in units of s. The adjusted R^2 is 0.2815. The number of GRBs in the sample is 57.

The log HR–log θ_j–log $E_{\mathrm{p,cpl,i}}$ formula is

$$\log \mathrm{HR} = (0.18 \pm 0.064) \times \log \theta_j + (0.73 \pm 0.098) \times \log E_{\mathrm{p,cpl,i}} + (-1.6 \pm 0.26), \quad (337)$$

where θ_j is in units of rad. $E_{\mathrm{p,cpl,i}}$ is in units of keV. The adjusted R^2 is 0.605. The number of GRBs in the sample is 57.

The log L_{pk}–log θ_j–log $t_{\mathrm{burst,i}}$ formula is

$$\log L_{\mathrm{pk}} = (-0.75 \pm 0.12) \times \log \theta_j + (-0.43 \pm 0.047) \times \log t_{\mathrm{burst,i}} + (0.15 \pm 0.21), \quad (338)$$

where L_{pk} is in units of $10^{52}\,\mathrm{erg\,s}^{-1}$ and in the 1–10^4 keV energy band. θ_j is in units of rad. $t_{\mathrm{burst,i}}$ is in units of s. The adjusted R^2 is 0.2276. The number of GRBs in the sample is 57.

The log F_g–$(-\beta_{\mathrm{Band}})$–β_{X11hr} formula is

$$\log F_g = (0.22 \pm 0.13) \times (-\beta_{\mathrm{Band}}) + (-0.69 \pm 0.1) \times \beta_{\mathrm{X11hr}} + (1.5 \pm 0.4), \quad (339)$$

where F_g is in units of $10^{-6}\,\mathrm{erg\,cm}^{-2}$ and in the 20–2000 keV energy band. The adjusted R^2 is 0.4589. The number of GRBs in the sample is 58.

The log SFR–log E_{iso}–metallicity formula is

$$\log \mathrm{SFR} = (0.28 \pm 0.028) \times \log E_{\mathrm{iso}} + (0.97 \pm 0.2) \times \mathrm{metallicity} + (-7.8 \pm 1.7), \quad (340)$$

where SFR is in units of $M_\odot\,\mathrm{yr}^{-1}$. E_{iso} is in units of 10^{52} erg and in the rest-frame 1–10^4 keV energy band. The metallicity is the value of $12 + \log \mathrm{O/H}$. The adjusted R^2 is 0.3087. The number of GRBs in the sample is 58.

The log F_g–log $E_{\mathrm{p,Band}}$–β_{X11hr} formula is

$$\log F_g = (0.84 \pm 0.089) \times \log E_{\mathrm{p,Band}} + (-0.49 \pm 0.082) \times \beta_{\mathrm{X11hr}} + (-0.1 \pm 0.28), \quad (341)$$

where F_g is in units of $10^{-6}\,\mathrm{erg\,cm}^{-2}$ and in the 20–2000 keV energy band. $E_{\mathrm{p,Band}}$ is in units of keV. The adjusted R^2 is 0.6254. The number of GRBs in the sample is 58.

The log $E_{\mathrm{p,Band}}$–variability$_3$–log F_g formula is

$$\log E_{\mathrm{p,Band}} = (11 \pm 2.1) \times \mathrm{variability}_3 + (0.22 \pm 0.023) \times \log F_g + (1.8 \pm 0.051), \quad (342)$$

where $E_{\mathrm{p,Band}}$ is in units of keV. F_g is in units of $10^{-6}\,\mathrm{erg\,cm}^{-2}$ and in the 20–2000 keV energy band. The adjusted R^2 is 0.3281. The number of GRBs in the sample is 58.

The log SFR–log D_L–metallicity formula is

$$\log \mathrm{SFR} = (1.2 \pm 0.066) \times \log D_L + (0.89 \pm 0.17) \times \mathrm{metallicity} + (-7.1 \pm 1.5), \quad (343)$$

where SFR is in units of $M_\odot\,\mathrm{yr}^{-1}$. D_L is in units of 10^{28} cm. The metallicity is the value of $12 + \log \mathrm{O/H}$. The adjusted R^2 is 0.584. The number of GRBs in the sample is 59.

The log F_{pk1}–log $E_{\mathrm{p,Band}}$–β_{X11hr} formula is

$$\log F_{\mathrm{pk1}} = (0.98 \pm 0.091) \times \log E_{\mathrm{p,Band}} + (-0.33 \pm 0.07) \times \beta_{\mathrm{X11hr}} + (-1.5 \pm 0.25), \quad (344)$$

where F_{pk1} is the peak energy flux in the 1 s time bin in the rest-frame 1–10^4 keV energy band and is in units of $10^{-6}\,\mathrm{erg\,cm}^{-2}\,\mathrm{s}^{-1}$. $E_{\mathrm{p,Band}}$ is in units of keV. The adjusted R^2 is 0.5634. The number of GRBs in the sample is 59.

The log L_{pk}–Mag–log $T_{50,\mathrm{i}}$ formula is

$$\log L_{\mathrm{pk}} = (-0.13 \pm 0.037) \times \mathrm{Mag} + (-0.6 \pm 0.086) \times \log T_{50,\mathrm{i}} + (-2.1 \pm 0.79), \quad (345)$$

where L_{pk} is in units of $10^{52}\,\mathrm{erg\,s}^{-1}$ and in the 1–10^4 keV energy band. Mag is in units of magnitude. $T_{50,\mathrm{i}}$ is in units of s. The adjusted R^2 is 0.3217. The number of GRBs in the sample is 59.

The log SFR–log$(1 + z)$–metallicity formula is

$$\log \mathrm{SFR} = (4.6 \pm 0.26) \times \log(1 + z) + (0.79 \pm 0.17) \times \mathrm{metallicity} + (-7.3 \pm 1.4), \quad (346)$$

where SFR is in units of $M_\odot\,\mathrm{yr}^{-1}$. The metallicity is the value of $12 + \log \mathrm{O/H}$. The adjusted R^2 is 0.6034. The number of GRBs in the sample is 59.

The log F_g–log L_{pk}–metallicity formula is

$$\log F_g = (0.35 \pm 0.018) \times \log L_{\mathrm{pk}} + (-0.61 \pm 0.18) \times \mathrm{metallicity} + (6.3 \pm 1.5), \quad (347)$$

where F_g is in units of $10^{-6}\,\mathrm{erg\,cm}^{-2}$ and in the 20–2000 keV energy band. L_{pk} is in units of $10^{52}\,\mathrm{erg\,s}^{-1}$ and in the 1–10^4 keV energy band. The metallicity is the value of

$12 + \log \mathrm{O/H}$. The adjusted R^2 is 0.2819. The number of GRBs in the sample is 61.

The $\log E_{\rm iso}$–$\log L_{\rm radio,pk}$–$\log t_{\rm radio,pk}$ formula is

$$\log E_{\rm iso} = (0.71 \pm 0.015) \times \log L_{\rm radio,pk} + (-0.76 \pm 0.052) \times \log t_{\rm radio,pk} + (4.2 \pm 0.31), \quad (348)$$

where $E_{\rm iso}$ is in units of 10^{52} erg and in the rest-frame 1–10^4 keV energy band. $L_{\rm radio,pk}$ is in rest-frame 8.46 GHz and in units of $10^{40}\,{\rm erg\,s^{-1}}$. $t_{\rm radio,pk}$ is in units of s. The adjusted R^2 is 0.4832. The number of GRBs in the sample is 61.

The $\log L_{\rm radio,pk}$–$\log E_{\rm iso}$–$\log T_{90,\rm i}$ formula is

$$\log L_{\rm radio,pk} = (0.66 \pm 0.013) \times \log E_{\rm iso} + (-0.44 \pm 0.029) \times \log T_{90,\rm i} + (1.7 \pm 0.039), \quad (349)$$

where $L_{\rm radio,pk}$ is in rest-frame 8.46 GHz and in units of $10^{40}\,{\rm erg\,s^{-1}}$. $E_{\rm iso}$ is in units of 10^{52} erg and in the rest-frame 1–10^4 keV energy band. $T_{90,\rm i}$ is in units of s. The adjusted R^2 is 0.4534. The number of GRBs in the sample is 61.

The log Mass–$A_{\rm V}$–$\log E_{\rm p,cpl,i}$ formula is

$$\log \mathrm{Mass} = (0.32 \pm 0.093) \times A_{\rm V} + (0.48 \pm 0.13) \times \log E_{\rm p,cpl,i} + (8.2 \pm 0.36), \quad (350)$$

where Mass is in units of $M_\odot$. $E_{\rm p,cpl,i}$ is in units of keV. The adjusted R^2 is 0.2425. The number of GRBs in the sample is 62.

The Mag–$\log E_{\rm iso}$–$A_{\rm V}$ formula is

$$\mathrm{Mag} = (-0.84 \pm 0.31) \times \log E_{\rm iso} + (-0.49 \pm 0.36) \times A_{\rm V} + (-20 \pm 0.46), \quad (351)$$

where Mag is in units of magnitude. $E_{\rm iso}$ is in units of 10^{52} erg and in the rest-frame 1–10^4 keV energy band. The adjusted R^2 is 0.291. The number of GRBs in the sample is 62.

The $\log D_{\rm L}$–$\log F_{\rm radio,pk}$–$\log t_{\rm radio,pk,i}$ formula is

$$\log D_{\rm L} = (-0.41 \pm 0.026) \times \log F_{\rm radio,pk} + (-0.29 \pm 0.019) \times \log t_{\rm radio,pk,i} + (0.58 \pm 0.17), \quad (352)$$

where $D_{\rm L}$ is in units of 10^{28} cm. $F_{\rm radio,pk}$ is in units of Jy. $t_{\rm radio,pk,i}$ is in units of s. The adjusted R^2 is 0.242. The number of GRBs in the sample is 62.

The $\log L_{\rm pk}$–Mag–$\log T_{90,\rm i}$ formula is

$$\log L_{\rm pk} = (-0.13 \pm 0.036) \times \mathrm{Mag} + (-0.66 \pm 0.094) \times \log T_{90,\rm i} + (-1.8 \pm 0.74), \quad (353)$$

where $L_{\rm pk}$ is in units of $10^{52}\,{\rm erg\,s^{-1}}$ and in the 1–10^4 keV energy band. Mag is in units of magnitude. $T_{90,\rm i}$ is in units of s. The adjusted R^2 is 0.3448. The number of GRBs in the sample is 62.

The log SFR–$\log E_{\rm iso}$–log Mass formula is

$$\log \mathrm{SFR} = (0.19 \pm 0.035) \times \log E_{\rm iso} + (0.64 \pm 0.064) \times \log \mathrm{Mass} + (-5.5 \pm 0.6), \quad (354)$$

where SFR is in units of $M_\odot\,{\rm yr^{-1}}$. $E_{\rm iso}$ is in units of 10^{52} erg and in the rest-frame 1–10^4 keV energy band. Mass is in units of $M_\odot$. The adjusted R^2 is 0.5535. The number of GRBs in the sample is 63.

The log Mass–$\log E_{\rm iso}$–metallicity formula is

$$\log \mathrm{Mass} = (0.19 \pm 0.033) \times \log E_{\rm iso} + (1.2 \pm 0.17) \times \mathrm{metallicity} + (-0.96 \pm 1.5), \quad (355)$$

where Mass is in units of $M_\odot$. $E_{\rm iso}$ is in units of 10^{52} erg and in the rest-frame 1–10^4 keV energy band. The metallicity is the value of $12 + \log \mathrm{O/H}$. The adjusted R^2 is 0.3948. The number of GRBs in the sample is 63.

The log SSFR–$\log F_{\rm g}$–log Age formula is

$$\log \mathrm{SSFR} = (0.26 \pm 0.022) \times \log F_{\rm g} + (-0.41 \pm 0.054) \times \log \mathrm{Age} + (0.88 \pm 0.15), \quad (356)$$

where log SSFR is in units of ${\rm Gyr^{-1}}$. $F_{\rm g}$ is in units of $10^{-6}\,{\rm erg\,cm^{-2}}$ and in the 20–2000 keV energy band. Age is in units of Myr. The adjusted R^2 is 0.2893. The number of GRBs in the sample is 63.

The $\log \theta_{\rm j}$–$\log T_{90}$–$\log t_{\rm burst,i}$ formula is

$$\log \theta_{\rm j} = (-0.36 \pm 0.022) \times \log T_{90} + (0.14 \pm 0.019) \times \log t_{\rm burst,i} + (-0.82 \pm 0.06), \quad (357)$$

where $\theta_{\rm j}$ is in units of rad. T_{90} is in units of s. $t_{\rm burst,i}$ is in units of s. The adjusted R^2 is 0.2592. The number of GRBs in the sample is 63.

The $\log D_{\rm L}$–$\log \theta_{\rm j}$–$\log E_{\rm p,cpl,i}$ formula is

$$\log D_{\rm L} = (-0.47 \pm 0.048) \times \log \theta_{\rm j} + (0.33 \pm 0.057) \times \log E_{\rm p,cpl,i} + (-0.88 \pm 0.14), \quad (358)$$

where $D_{\rm L}$ is in units of 10^{28} cm. $\theta_{\rm j}$ is in units of rad. $E_{\rm p,cpl,i}$ is in units of keV. The adjusted R^2 is 0.299. The number of GRBs in the sample is 63.

The $\log D_{\rm L}$–$\log \theta_{\rm j}$–$\log t_{\rm burst,i}$ formula is

$$\log D_{\rm L} = (-0.38 \pm 0.044) \times \log \theta_{\rm j} + (-0.16 \pm 0.011) \times \log t_{\rm burst,i} + (0.54 \pm 0.073), \quad (359)$$

where $D_{\rm L}$ is in units of 10^{28} cm. $\theta_{\rm j}$ is in units of rad. $t_{\rm burst,i}$ is in units of s. The adjusted R^2 is 0.2289. The number of GRBs in the sample is 63.

The log Mass–$\log D_{\rm L}$–metallicity formula is

$$\log \mathrm{Mass} = (0.61 \pm 0.09) \times \log D_{\rm L} + (1.1 \pm 0.17) \times \mathrm{metallicity} + (-0.21 \pm 1.4), \quad (360)$$

where Mass is in units of $M_\odot$. $D_{\rm L}$ is in units of 10^{28} cm. The metallicity is the value of $12 + \log \mathrm{O/H}$. The adjusted R^2 is 0.4144. The number of GRBs in the sample is 64.

The Mag–$\log F_{\rm Opt11hr}$–log Mass formula is

$$\mathrm{Mag} = (0.29 \pm 0.32) \times \log F_{\rm Opt11hr} + (-1.7 \pm 0.43) \times \log \mathrm{Mass} + (-3.2 \pm 3.8), \quad (361)$$

where Mag is in units of magnitude. $F_{\rm Opt11hr}$ is in units of Jy. Mass is in units of $M_\odot$. The adjusted R^2 is 0.8621. The number of GRBs in the sample is 64.

The $\log(1+z)$–$\log\theta_{\rm j}$–$\log N_{\rm H}$ formula is

$$\log(1+z) = (-0.21 \pm 0.021) \times \log\theta_{\rm j} + (0.14 \pm 0.014) \times \log N_{\rm H} + (0.066 \pm 0.026), \quad (362)$$

where $\theta_{\rm j}$ is in units of rad. $N_{\rm H}$ is in units of $10^{21}\,{\rm cm}^{-2}$. The adjusted R^2 is 0.3328. The number of GRBs in the sample is 64.

The $\log D_{\rm L}$–$\log\theta_{\rm j}$–$\log N_{\rm H}$ formula is

$$\log D_{\rm L} = (-0.58 \pm 0.052) \times \log\theta_{\rm j} + (0.32 \pm 0.035) \times \log N_{\rm H} + (-0.45 \pm 0.064), \quad (363)$$

where $D_{\rm L}$ is in units of 10^{28} cm. $\theta_{\rm j}$ is in units of rad. $N_{\rm H}$ is in units of $10^{21}\,{\rm cm}^{-2}$. The adjusted R^2 is 0.3219. The number of GRBs in the sample is 64.

The log Mass–$\log(1+z)$–metallicity formula is

$$\log {\rm Mass} = (2.3 \pm 0.46) \times \log(1+z) + (1.1 \pm 0.16) \times {\rm metallicity} + (-0.52 \pm 1.4), \quad (364)$$

where Mass is in units of $M_\odot$. The metallicity is the value of $12 + \log {\rm O/H}$. The adjusted R^2 is 0.4282. The number of GRBs in the sample is 64.

The Mag–$\log(1+z)$–$\log F_{\rm Opt11hr}$ formula is

$${\rm Mag} = (-3.3 \pm 1.6) \times \log(1+z) + (0.54 \pm 0.31) \times \log F_{\rm Opt11hr} + (-17 \pm 1.5), \quad (365)$$

where Mag is in units of magnitude. $F_{\rm Opt11hr}$ is in units of Jy. The adjusted R^2 is 0.3878. The number of GRBs in the sample is 64.

The $\log F_{\rm g}$–$(-\beta_{\rm Band})$–$\log F_{\rm X11hr}$ formula is

$$\log F_{\rm g} = (0.11 \pm 0.15) \times (-\beta_{\rm Band}) + (0.64 \pm 0.046) \times \log F_{\rm X11hr} + (5.2 \pm 0.59), \quad (366)$$

where $F_{\rm g}$ is in units of $10^{-6}\,{\rm erg\,cm^{-2}}$ and in the 20–2000 keV energy band. $F_{\rm X11hr}$ is in units of Jy. The adjusted R^2 is 0.4304. The number of GRBs in the sample is 65.

The $\log F_{\rm g}$–$\log E_{\rm p,Band}$–$\log F_{\rm X11hr}$ formula is

$$\log F_{\rm g} = (1.1 \pm 0.079) \times \log E_{\rm p,Band} + (0.47 \pm 0.043) \times \log F_{\rm X11hr} + (2 \pm 0.39), \quad (367)$$

where $F_{\rm g}$ is in units of $10^{-6}\,{\rm erg\,cm^{-2}}$ and in the 20–2000 keV energy band. $E_{\rm p,Band}$ is in units of keV. $F_{\rm X11hr}$ is in units of Jy. The adjusted R^2 is 0.8306. The number of GRBs in the sample is 65.

The $\log F_{\rm pk1}$–$\log E_{\rm p,Band}$–$\log F_{\rm X11hr}$ formula is

$$\log F_{\rm pk1} = (1.1 \pm 0.088) \times \log E_{\rm p,Band} + (0.37 \pm 0.045) \times \log F_{\rm X11hr} + (0.37 \pm 0.38), \quad (368)$$

where $F_{\rm pk1}$ is the peak energy flux in the 1 s time bin in the rest-frame 1–10^4 keV energy band and is in units of $10^{-6}\,{\rm erg\,cm^{-2}\,s^{-1}}$. $E_{\rm p,Band}$ is in units of keV. $F_{\rm X11hr}$ is in units of Jy. The adjusted R^2 is 0.7179. The number of GRBs in the sample is 66.

The $\log E_{\rm p,Band,i}$–$\log F_{\rm g}$–$\log\theta_{\rm j}$ formula is

$$\log E_{\rm p,Band,i} = (0.22 \pm 0.019) \times \log F_{\rm g} + (-0.29 \pm 0.066) \times \log\theta_{\rm j} + (2 \pm 0.085), \quad (369)$$

where $E_{\rm p,Band,i}$ is in units of keV. $F_{\rm g}$ is in units of $10^{-6}\,{\rm erg\,cm^{-2}}$ and in the 20–2000 keV energy band. $\theta_{\rm j}$ is in units of rad. The adjusted R^2 is 0.223. The number of GRBs in the sample is 66.

The $\log P_{\rm pk4}$–$\log E_{\rm p,Band}$–$\log F_{\rm Opt11hr}$ formula is

$$\log P_{\rm pk4} = (0.58 \pm 0.1) \times \log E_{\rm p,Band} + (0.27 \pm 0.055) \times \log F_{\rm Opt11hr} + (0.83 \pm 0.37), \quad (370)$$

where $P_{\rm pk4}$ is the peak photon flux in the 1 s time bin in 10–1000 keV and is in units of photons $\,{\rm cm^{-2}\,s^{-1}}$. $E_{\rm p,Band}$ is in units of keV. $F_{\rm Opt11hr}$ is in units of Jy. The adjusted R^2 is 0.4235. The number of GRBs in the sample is 67.

The log Age–$\log(1+z)$–log HR formula is

$$\log {\rm Age} = (-2.1 \pm 0.45) \times \log(1+z) + (-0.36 \pm 0.12) \times \log {\rm HR} + (3.4 \pm 0.13), \quad (371)$$

where Age is in units of Myr. The adjusted R^2 is 0.3026. The number of GRBs in the sample is 67.

The log SSFR–log Age–log Mass formula is

$$\log {\rm SSFR} = (-0.39 \pm 0.059) \times \log {\rm Age} + (-0.29 \pm 0.061) \times \log {\rm Mass} + (3.8 \pm 0.61), \quad (372)$$

where log SSFR is in units of $\,{\rm Gyr^{-1}}$. Age is in units of Myr. Mass is in units of $M_\odot$. The adjusted R^2 is 0.2948. The number of GRBs in the sample is 68.

The log SSFR–$\log E_{\rm iso}$–log Age formula is

$$\log {\rm SSFR} = (0.15 \pm 0.013) \times \log E_{\rm iso} + (-0.33 \pm 0.051) \times \log {\rm Age} + (0.88 \pm 0.14), \quad (373)$$

where log SSFR is in units of $\,{\rm Gyr^{-1}}$. $E_{\rm iso}$ is in units of 10^{52} erg and in the rest-frame 1–10^4 keV energy band. Age is in units of Myr. The adjusted R^2 is 0.2254. The number of GRBs in the sample is 68.

The $\log E_{\rm p,Band,i}$–$\log F_{\rm g}$–log Mass formula is

$$\log E_{\rm p,Band,i} = (0.19 \pm 0.023) \times \log F_{\rm g} + (0.14 \pm 0.028) \times \log {\rm Mass} + (0.95 \pm 0.28), \quad (374)$$

where $E_{\rm p,Band,i}$ is in units of keV. $F_{\rm g}$ is in units of $10^{-6}\,{\rm erg\,cm^{-2}}$ and in the 20–2000 keV energy band. Mass is in units of $M_\odot$. The adjusted R^2 is 0.2071. The number of GRBs in the sample is 68.

The log SFR–$\log D_{\rm L}$–log Mass formula is

$$\log {\rm SFR} = (0.76 \pm 0.076) \times \log D_{\rm L} + (0.53 \pm 0.056) \times \log {\rm Mass} + (-4.5 \pm 0.52), \quad (375)$$

where the SFR is in units of $M_\odot\,\mathrm{yr}^{-1}$. D_L is in units of 10^{28} cm. Mass is in units of $M_\odot$. The adjusted R^2 is 0.6629. The number of GRBs in the sample is 69.

The $\log T_{90}$–$\log\theta_\mathrm{j}$–$\log E_\mathrm{p,Band,i}$ formula is

$$\log T_{90} = (-0.43 \pm 0.057) \times \log\theta_\mathrm{j} + (0.34 \pm 0.036) \times \log E_\mathrm{p,Band,i} + (0.21 \pm 0.082), \quad (376)$$

where T_{90} is in units of s. θ_j is in units of rad. $E_\mathrm{p,Band,i}$ is in units of keV. The adjusted R^2 is 0.2107. The number of GRBs in the sample is 69.

The log SFR–$\log(1+z)$–log Mass formula is

$$\log \mathrm{SFR} = (2.9 \pm 0.28) \times \log(1+z) + (0.46 \pm 0.058) \times \log \mathrm{Mass} + (-4.6 \pm 0.5), \quad (377)$$

where SFR is in units of $M_\odot\,\mathrm{yr}^{-1}$. Mass is in units of $M_\odot$. The adjusted R^2 is 0.687. The number of GRBs in the sample is 69.

The Mag–$\log(1+z)$–A_V formula is

$$\mathrm{Mag} = (-4.2 \pm 1.6) \times \log(1+z) + (-0.52 \pm 0.32) \times A_\mathrm{V} + (-19 \pm 0.79), \quad (378)$$

where Mag is in units of magnitude. The adjusted R^2 is 0.408. The number of GRBs in the sample is 69.

The $\log t_\mathrm{burst,i}$–$\log L_\mathrm{pk}$–$\log F_\mathrm{Opt11hr}$ formula is

$$\log t_\mathrm{burst,i} = (-0.18 \pm 0.021) \times \log L_\mathrm{pk} + (0.21 \pm 0.047) \times \log F_\mathrm{Opt11hr} + (3.4 \pm 0.24), \quad (379)$$

where $t_\mathrm{burst,i}$ is in units of s. L_pk is in units of $10^{52}\,\mathrm{erg\,s^{-1}}$ and in the 1–10^4 keV energy band. F_Opt11hr is in units of Jy. The adjusted R^2 is 0.2132. The number of GRBs in the sample is 70.

The $\log F_\mathrm{X11hr}$–$\log F_\mathrm{g}$–$\log\theta_\mathrm{j}$ formula is

$$\log F_\mathrm{X11hr} = (0.43 \pm 0.039) \times \log F_\mathrm{g} + (0.51 \pm 0.061) \times \log\theta_\mathrm{j} + (-6.9 \pm 0.089), \quad (380)$$

where F_X11hr is in units of Jy. F_g is in units of $10^{-6}\,\mathrm{erg\,cm^{-2}}$ and in the 20–2000 keV energy band. θ_j is in units of rad. The adjusted R^2 is 0.3077. The number of GRBs in the sample is 71.

The log Mass–$\log P_\mathrm{pk4}$–Mag formula is

$$\log \mathrm{Mass} = (-0.18 \pm 0.09) \times \log P_\mathrm{pk4} + (-0.14 \pm 0.023) \times \mathrm{Mag} + (6.8 \pm 0.5), \quad (381)$$

where Mass is in units of $M_\odot$. P_pk4 is the peak photon flux in the 1 s time bin in 10–1000 keV and is in units of photons $\mathrm{cm^{-2}\,s^{-1}}$. Mag is in units of magnitude. The adjusted R^2 is 0.8775. The number of GRBs in the sample is 72.

The $\log F_\mathrm{pk2}$–$(-\beta_\mathrm{Band})$–$\log E_\mathrm{p,Band,i}$ formula is

$$\log F_\mathrm{pk2} = (0.46 \pm 0.12) \times (-\beta_\mathrm{Band}) + (0.38 \pm 0.062) \times \log E_\mathrm{p,Band,i} + (-1.5 \pm 0.27), \quad (382)$$

where F_pk2 is the peak energy flux in the 64 ms time bin in the rest-frame 1–10^4 keV energy band and is in units of $10^{-6}\,\mathrm{erg\,cm^{-2}\,s^{-1}}$. $E_\mathrm{p,Band,i}$ is in units of keV. The adjusted R^2 is 0.2559. The number of GRBs in the sample is 73.

The log Mass–log HR–Mag formula is

$$\log \mathrm{Mass} = (-0.33 \pm 0.14) \times \log \mathrm{HR} + (-0.12 \pm 0.025) \times \mathrm{Mag} + (7.1 \pm 0.54), \quad (383)$$

where Mass is in units of $M_\odot$. Mag is in units of magnitude. The adjusted R^2 is 0.8604. The number of GRBs in the sample is 73.

The $\log E_\mathrm{iso}$–$\log P_\mathrm{pk1}$–$\log E_\mathrm{p,Band,i}$ formula is

$$\log E_\mathrm{iso} = (0.42 \pm 0.051) \times \log P_\mathrm{pk1} + (0.92 \pm 0.065) \times \log E_\mathrm{p,Band,i} + (-1.9 \pm 0.16), \quad (384)$$

where E_iso is in units of 10^{52} erg and in the rest-frame 1–10^4 keV energy band. P_pk1 is the peak photon flux in the 64 ms time bin in 10–1000 keV and is in units of photons $\mathrm{cm^{-2}\,s^{-1}}$. $E_\mathrm{p,Band,i}$ is in units of keV. The adjusted R^2 is 0.2987. The number of GRBs in the sample is 73.

The $\log F_\mathrm{pk2}$–$\log(1+z)$–$(-\beta_\mathrm{Band})$ formula is

$$\log F_\mathrm{pk2} = (-0.93 \pm 0.14) \times \log(1+z) + (0.5 \pm 0.13) \times (-\beta_\mathrm{Band}) + (-0.18 \pm 0.31), \quad (385)$$

where F_pk2 is the peak energy flux in the 64 ms time bin in the rest-frame 1–10^4 keV energy band and is in units of $10^{-6}\,\mathrm{erg\,cm^{-2}\,s^{-1}}$. The adjusted R^2 is 0.2389. The number of GRBs in the sample is 73.

The log Mass–$(-\beta_\mathrm{Band})$–$\log E_\mathrm{p,Band,i}$ formula is

$$\log \mathrm{Mass} = (-0.16 \pm 0.12) \times (-\beta_\mathrm{Band}) + (0.65 \pm 0.097) \times \log E_\mathrm{p,Band,i} + (8.2 \pm 0.36), \quad (386)$$

where Mass is in units of $M_\odot$. $E_\mathrm{p,Band,i}$ is in units of keV. The adjusted R^2 is 0.2063. The number of GRBs in the sample is 74.

The $\log E_\mathrm{p,Band,i}$–$\log D_\mathrm{L}$–log Mass formula is

$$\log E_\mathrm{p,Band,i} = (0.35 \pm 0.039) \times \log D_\mathrm{L} + (0.13 \pm 0.03) \times \log \mathrm{Mass} + (1.1 \pm 0.28), \quad (387)$$

where $E_\mathrm{p,Band,i}$ is in units of keV. D_L is in units of 10^{28} cm. Mass is in units of $M_\odot$. The adjusted R^2 is 0.2109. The number of GRBs in the sample is 74.

The $\log T_\mathrm{50,i}$–$(-\alpha_\mathrm{cpl})$–$\log t_\mathrm{burst,i}$ formula is

$$\log T_\mathrm{50,i} = (0.22 \pm 0.072) \times (-\alpha_\mathrm{cpl}) + (0.33 \pm 0.02) \times \log t_\mathrm{burst,i} + (-0.16 \pm 0.11), \quad (388)$$

where $T_\mathrm{50,i}$ is in units of s. $t_\mathrm{burst,i}$ is in units of s. The adjusted R^2 is 0.2056. The number of GRBs in the sample is 75.

The $\log F_\mathrm{pk1}$–log HR–log SFR formula is

$$\log F_\mathrm{pk1} = (0.93 \pm 0.11) \times \log \mathrm{HR} + (-0.17 \pm 0.035) \times \log \mathrm{SFR} + (-0.059 \pm 0.041), \quad (389)$$

where $F_{\rm pk1}$ is the peak energy flux in the 1 s time bin in the rest-frame 1–10^4 keV energy band and is in units of 10^{-6} erg cm^{-2} s^{-1}. SFR is in units of $M_\odot$ yr^{-1}. The adjusted R^2 is 0.2425. The number of GRBs in the sample is 76.

The $\log L_{\rm pk}$–$\log \theta_{\rm j}$–log Mass formula is

$$\log L_{\rm pk} = (-1.5 \pm 0.1) \times \log \theta_{\rm j} + (0.32 \pm 0.06) \times \log {\rm Mass} + (-4.9 \pm 0.56), \quad (390)$$

where $L_{\rm pk}$ is in units of 10^{52} erg s^{-1} and in the 1–10^4 keV energy band. $\theta_{\rm j}$ is in units of rad. Mass is in units of $M_\odot$. The adjusted R^2 is 0.2767. The number of GRBs in the sample is 76.

The $\log \theta_{\rm j}$–$\log(1+z)$–$\log F_{\rm X11hr}$ formula is

$$\log \theta_{\rm j} = (-0.84 \pm 0.073) \times \log(1+z) + (0.13 \pm 0.021) \times \log F_{\rm X11hr} + (0.073 \pm 0.14), \quad (391)$$

where $\theta_{\rm j}$ is in units of rad. $F_{\rm X11hr}$ is in units of Jy. The adjusted R^2 is 0.2238. The number of GRBs in the sample is 76.

The $\log D_{\rm L}$–$\log F_{\rm g}$–log Age formula is

$$\log D_{\rm L} = (0.12 \pm 0.01) \times \log F_{\rm g} + (-0.29 \pm 0.036) \times \log {\rm Age} + (0.77 \pm 0.1), \quad (392)$$

where $D_{\rm L}$ is in units of 10^{28} cm. $F_{\rm g}$ is in units of 10^{-6} erg cm^{-2} and in the 20–2000 keV energy band. Age is in units of Myr. The adjusted R^2 is 0.3209. The number of GRBs in the sample is 77.

The $\log F_{\rm g}$–$\log P_{\rm pk1}$–$A_{\rm V}$ formula is

$$\log F_{\rm g} = (1.1 \pm 0.04) \times \log P_{\rm pk1} + (-0.2 \pm 0.08) \times A_{\rm V} + (-0.08 \pm 0.083), \quad (393)$$

where $F_{\rm g}$ is in units of 10^{-6} erg cm^{-2} and in the 20–2000 keV energy band. $P_{\rm pk1}$ is the peak photon flux in the 64 ms time bin in 10–1000 keV and is in units of photons cm^{-2} s^{-1}. The adjusted R^2 is 0.4258. The number of GRBs in the sample is 77.

The $\log P_{\rm pk3}$–$\log(1+z)$–$(-\beta_{\rm Band})$ formula is

$$\log P_{\rm pk3} = (-0.82 \pm 0.067) \times \log(1+z) + (0.33 \pm 0.14) \times (-\beta_{\rm Band}) + (0.64 \pm 0.33), \quad (394)$$

where $P_{\rm pk3}$ is the peak photon flux in the 1024 ms time bin in 10–1000 keV and is in units of photons cm^{-2} s^{-1}. The adjusted R^2 is 0.2232. The number of GRBs in the sample is 77.

The $\log T_{\rm R45,i}$–$\log F_{\rm g}$–$\log t_{\rm pkOpt}$ formula is

$$\log T_{\rm R45,i} = (0.35 \pm 0.013) \times \log F_{\rm g} + (0.38 \pm 0.014) \times \log t_{\rm pkOpt} + (-0.76 \pm 0.043), \quad (395)$$

where $T_{\rm R45,i}$ is in units of s. $F_{\rm g}$ is in units of 10^{-6} erg cm^{-2} and in the 20–2000 keV energy band. $t_{\rm pkOpt}$ is in units of s. The adjusted R^2 is 0.3476. The number of GRBs in the sample is 78.

The $\log P_{\rm pk4}$–$\log F_{\rm g}$–log SFR formula is

$$\log P_{\rm pk4} = (0.45 \pm 0.022) \times \log F_{\rm g} + (-0.14 \pm 0.021) \times \log {\rm SFR} + (0.45 \pm 0.028), \quad (396)$$

where $P_{\rm pk4}$ is the peak photon flux in the 1 s time bin in 10–1000 keV and is in units of photons cm^{-2} s^{-1}. $F_{\rm g}$ is in units of 10^{-6} erg cm^{-2} and in the 20–2000 keV energy band. SFR is in units of $M_\odot$ yr^{-1}. The adjusted R^2 is 0.3386. The number of GRBs in the sample is 79.

The log SFR–$\log E_{\rm iso}$–$A_{\rm V}$ formula is

$$\log {\rm SFR} = (0.32 \pm 0.028) \times \log E_{\rm iso} + (0.29 \pm 0.073) \times A_{\rm V} + (0.25 \pm 0.069), \quad (397)$$

where SFR is in units of $M_\odot$ yr^{-1}. $E_{\rm iso}$ is in units of 10^{52} erg and in the rest-frame 1–10^4 keV energy band. The adjusted R^2 is 0.3195. The number of GRBs in the sample is 81.

The $\log P_{\rm pk4}$–$\log L_{\rm pk}$–$(-\beta_{\rm Band})$ formula is

$$\log P_{\rm pk4} = (0.28 \pm 0.04) \times \log L_{\rm pk} + (0.18 \pm 0.14) \times (-\beta_{\rm Band}) + (0.39 \pm 0.32), \quad (398)$$

where $P_{\rm pk4}$ is the peak photon flux in the 1 s time bin in 10–1000 keV and is in units of photons cm^{-2} s^{-1}. $L_{\rm pk}$ is in units of 10^{52} erg s^{-1} and in the 1–10^4 keV energy band. The adjusted R^2 is 0.2003. The number of GRBs in the sample is 81.

The $\log D_{\rm L}$–$\log \theta_{\rm j}$–log Mass formula is

$$\log D_{\rm L} = (-0.54 \pm 0.034) \times \log \theta_{\rm j} + (0.23 \pm 0.028) \times \log {\rm Mass} + (-2.4 \pm 0.26), \quad (399)$$

where $D_{\rm L}$ is in units of 10^{28} cm. $\theta_{\rm j}$ is in units of rad. Mass is in units of $M_\odot$. The adjusted R^2 is 0.3388. The number of GRBs in the sample is 81.

The $\log F_{\rm Opt11hr}$–$\beta_{\rm X11hr}$–log Mass formula is

$$\log F_{\rm Opt11hr} = (-0.3 \pm 0.098) \times \beta_{\rm X11hr} + (-0.34 \pm 0.074) \times \log {\rm Mass} + (-1.5 \pm 0.7), \quad (400)$$

where $F_{\rm Opt11hr}$ is in units of Jy. Mass is in units of $M_\odot$. The adjusted R^2 is 0.252. The number of GRBs in the sample is 82.

The log Mass–$\log T_{90}$–Mag formula is

$$\log {\rm Mass} = (0.49 \pm 0.094) \times \log T_{90} + (-0.12 \pm 0.022) \times {\rm Mag} + (6.2 \pm 0.45), \quad (401)$$

where Mass is in units of $M_\odot$. T_{90} is in units of s. Mag is in units of magnitude. The adjusted R^2 is 0.8661. The number of GRBs in the sample is 82.

The $\log t_{\rm burst,i}$–$\log P_{\rm pk4}$–$\log F_{\rm Opt11hr}$ formula is

$$\log t_{\rm burst,i} = (-0.29 \pm 0.055) \times \log P_{\rm pk4} + (0.27 \pm 0.043) \times \log F_{\rm Opt11hr} + (3.8 \pm 0.22), \quad (402)$$

where $t_{\rm burst,i}$ is in units of s. $P_{\rm pk4}$ is the peak photon flux in the 1 s time bin in 10–1000 keV and is in units of

photons $\mathrm{cm}^{-2}\,\mathrm{s}^{-1}$. F_{Opt11hr} is in units of Jy. The adjusted R^2 is 0.2451. The number of GRBs in the sample is 83.

The $\log P_{\mathrm{pk4}}$–$\log D_{\mathrm{L}}$–$\log t_{\mathrm{pkOpt}}$ formula is

$$\log P_{\mathrm{pk4}} = (-0.6 \pm 0.031) \times \log D_{\mathrm{L}} + (-0.48 \pm 0.021) \times \log t_{\mathrm{pkOpt}} + (2.2 \pm 0.052), \quad (403)$$

where P_{pk4} is the peak photon flux in the 1 s time bin in 10–1000 keV and is in units of photons $\mathrm{cm}^{-2}\,\mathrm{s}^{-1}$. D_{L} is in units of 10^{28} cm. t_{pkOpt} is in units of s. The adjusted R^2 is 0.38. The number of GRBs in the sample is 84.

The $\log F_{\mathrm{Opt11hr}}$–$\log F_{\mathrm{X11hr}}$–log Mass formula is

$$\log F_{\mathrm{Opt11hr}} = (0.22 \pm 0.079) \times \log F_{\mathrm{X11hr}} + (-0.38 \pm 0.069) \times \log \mathrm{Mass} + (0.0033 \pm 0.84), \quad (404)$$

where F_{Opt11hr} is in units of Jy. F_{X11hr} is in units of Jy. Mass is in units of $M_{\odot}$. The adjusted R^2 is 0.2405. The number of GRBs in the sample is 88.

The log SFR–$\log D_{\mathrm{L}}$–A_{V} formula is

$$\log \mathrm{SFR} = (1.1 \pm 0.055) \times \log D_{\mathrm{L}} + (0.24 \pm 0.061) \times A_{\mathrm{V}} + (0.24 \pm 0.057), \quad (405)$$

where the SFR is in units of $M_{\odot}\,\mathrm{yr}^{-1}$. D_{L} is in units of 10^{28} cm. The adjusted R^2 is 0.4998. The number of GRBs in the sample is 90.

The log SFR–$\log(1+z)$–A_{V} formula is

$$\log \mathrm{SFR} = (3.8 \pm 0.2) \times \log(1+z) + (0.2 \pm 0.056) \times A_{\mathrm{V}} + (-0.66 \pm 0.066), \quad (406)$$

where SFR is in units of $M_{\odot}\,\mathrm{yr}^{-1}$. The adjusted R^2 is 0.5415. The number of GRBs in the sample is 90.

The log HR–$\log T_{50}$–$\log E_{\mathrm{p,Band,i}}$ formula is

$$\log \mathrm{HR} = (-0.11 \pm 0.02) \times \log T_{50} + (0.33 \pm 0.032) \times \log E_{\mathrm{p,Band,i}} + (-0.2 \pm 0.097), \quad (407)$$

where T_{50} is in units of s. $E_{\mathrm{p,Band,i}}$ is in units of keV. The adjusted R^2 is 0.243. The number of GRBs in the sample is 96.

The $\log F_{\mathrm{g}}$–β_{X11hr}–log Mass formula is

$$\log F_{\mathrm{g}} = (-0.53 \pm 0.077) \times \beta_{\mathrm{X11hr}} + (-0.19 \pm 0.049) \times \log \mathrm{Mass} + (3.4 \pm 0.43), \quad (408)$$

where F_{g} is in units of $10^{-6}\,\mathrm{erg\,cm}^{-2}$ and in the 20–2000 keV energy band. Mass is in units of $M_{\odot}$. The adjusted R^2 is 0.2965. The number of GRBs in the sample is 97.

The $\log E_{\mathrm{iso}}$–$\log F_{\mathrm{X11hr}}$–$\log E_{\mathrm{p,cpl,i}}$ formula is

$$\log E_{\mathrm{iso}} = (0.55 \pm 0.05) \times \log F_{\mathrm{X11hr}} + (0.9 \pm 0.12) \times \log E_{\mathrm{p,cpl,i}} + (2.1 \pm 0.52), \quad (409)$$

where E_{iso} is in units of 10^{52} erg and in the rest-frame 1–10^4 keV energy band. F_{X11hr} is in units of Jy. $E_{\mathrm{p,cpl,i}}$ is in units of keV. The adjusted R^2 is 0.386. The number of GRBs in the sample is 97.

The $\log P_{\mathrm{pk4}}$–$\log F_{\mathrm{g}}$–$\log N_{\mathrm{H}}$ formula is

$$\log P_{\mathrm{pk4}} = (0.47 \pm 0.019) \times \log F_{\mathrm{g}} + (-0.18 \pm 0.037) \times \log N_{\mathrm{H}} + (0.39 \pm 0.033), \quad (410)$$

where P_{pk4} is the peak photon flux in the 1 s time bin in 10–1000 keV and is in units of photons $\mathrm{cm}^{-2}\,\mathrm{s}^{-1}$. F_{g} is in units of $10^{-6}\,\mathrm{erg\,cm}^{-2}$ and in the 20–2000 keV energy band. N_{H} is in units of $10^{21}\,\mathrm{cm}^{-2}$. The adjusted R^2 is 0.4773. The number of GRBs in the sample is 104.

The log Mass–$\log F_{\mathrm{Opt11hr}}$–$A_{\mathrm{V}}$ formula is

$$\log \mathrm{Mass} = (-0.31 \pm 0.049) \times \log F_{\mathrm{Opt11hr}} + (0.14 \pm 0.047) \times A_{\mathrm{V}} + (7.9 \pm 0.25), \quad (411)$$

where Mass is in units of $M_{\odot}$. F_{Opt11hr} is in units of Jy. The adjusted R^2 is 0.2312. The number of GRBs in the sample is 104.

The $\log F_{\mathrm{g}}$–$\log L_{\mathrm{pk}}$–$\log N_{\mathrm{H}}$ formula is

$$\log F_{\mathrm{g}} = (0.38 \pm 0.017) \times \log L_{\mathrm{pk}} + (-0.26 \pm 0.05) \times \log N_{\mathrm{H}} + (1.1 \pm 0.04), \quad (412)$$

where F_{g} is in units of $10^{-6}\,\mathrm{erg\,cm}^{-2}$ and in the 20–2000 keV energy band. L_{pk} is in units of $10^{52}\,\mathrm{erg\,s}^{-1}$ and in the 1–10^4 keV energy band. N_{H} is in units of $10^{21}\,\mathrm{cm}^{-2}$. The adjusted R^2 is 0.2658. The number of GRBs in the sample is 104.

The $\log F_{\mathrm{Opt11hr}}$–log Mass–$\log T_{50,\mathrm{i}}$ formula is

$$\log F_{\mathrm{Opt11hr}} = (-0.37 \pm 0.063) \times \log \mathrm{Mass} + (0.42 \pm 0.077) \times \log T_{50,\mathrm{i}} + (-1.9 \pm 0.61), \quad (413)$$

where F_{Opt11hr} is in units of Jy. Mass is in units of $M_{\odot}$. $T_{50,\mathrm{i}}$ is in units of s. The adjusted R^2 is 0.2729. The number of GRBs in the sample is 105.

The $\log F_{\mathrm{pk1}}$–$(-\alpha_{\mathrm{cpl}})$–β_{X11hr} formula is

$$\log F_{\mathrm{pk1}} = (-0.37 \pm 0.11) \times (-\alpha_{\mathrm{cpl}}) + (-0.35 \pm 0.069) \times \beta_{\mathrm{X11hr}} + (0.89 \pm 0.16), \quad (414)$$

where F_{pk1} is the peak energy flux in the 1 s time bin in the rest-frame 1–10^4 keV energy band and is in units of $10^{-6}\,\mathrm{erg\,cm}^{-2}\,\mathrm{s}^{-1}$. The adjusted R^2 is 0.2512. The number of GRBs in the sample is 108.

The $\log F_{\mathrm{g}}$–$\log E_{\mathrm{p,Band}}$–$\log F_{\mathrm{Opt11hr}}$ formula is

$$\log F_{\mathrm{g}} = (1.3 \pm 0.085) \times \log E_{\mathrm{p,Band}} + (0.21 \pm 0.041) \times \log F_{\mathrm{Opt11hr}} + (-0.71 \pm 0.29), \quad (415)$$

where F_{g} is in units of $10^{-6}\,\mathrm{erg\,cm}^{-2}$ and in the 20–2000 keV energy band. $E_{\mathrm{p,Band}}$ is in units of keV. F_{Opt11hr} is in units of Jy. The adjusted R^2 is 0.6036. The number of GRBs in the sample is 108.

The $\log F_{\mathrm{pk1}}$–$\log E_{\mathrm{p,cpl}}$–β_{X11hr} formula is

$$\log F_{\mathrm{pk1}} = (0.83 \pm 0.1) \times \log E_{\mathrm{p,cpl}} + (-0.36 \pm 0.065) \times \beta_{\mathrm{X11hr}} + (-1.3 \pm 0.26), \quad (416)$$

where $F_{\rm pk1}$ is the peak energy flux in the 1 s time bin in the rest-frame 1–10^4 keV energy band and is in units of 10^{-6} erg cm^{-2} s^{-1}. $E_{\rm p,cpl}$ is in units of keV. The adjusted R^2 is 0.4823. The number of GRBs in the sample is 108.

The log Mass–log $L_{\rm pk}$–$A_{\rm V}$ formula is

$$\log \mathrm{Mass} = (0.24 \pm 0.031) \times \log L_{\rm pk} + (0.3 \pm 0.068) \times A_{\rm V} + (9.3 \pm 0.065), \quad (417)$$

where Mass is in units of $M_\odot$. $L_{\rm pk}$ is in units of 10^{52} erg s^{-1} and in the 1–10^4 keV energy band. The adjusted R^2 is 0.208. The number of GRBs in the sample is 110.

The log $P_{\rm pk3}$–log$(1+z)$–log $F_{\rm g}$ formula is

$$\log P_{\rm pk3} = (-0.73 \pm 0.057) \times \log(1+z) + (0.47 \pm 0.011) \times \log F_{\rm g} + (0.74 \pm 0.033), \quad (418)$$

where $P_{\rm pk3}$ is the peak photon flux in the 1024 ms time bin in 10–1000 keV and is in units of photons cm^{-2} s^{-1}. $F_{\rm g}$ is in units of 10^{-6} erg cm^{-2} and in the 20–2000 keV energy band. The adjusted R^2 is 0.6368. The number of GRBs in the sample is 112.

The log $F_{\rm Opt11hr}$–log Mass–log $T_{\rm R45,i}$ formula is

$$\log F_{\rm Opt11hr} = (-0.38 \pm 0.062) \times \log \mathrm{Mass} + (0.42 \pm 0.083) \times \log T_{\rm R45,i} + (-1.6 \pm 0.59), \quad (419)$$

where $F_{\rm Opt11hr}$ is in units of Jy. Mass is in units of $M_\odot$. $T_{\rm R45,i}$ is in units of s. The adjusted R^2 is 0.2692. The number of GRBs in the sample is 115.

The log $F_{\rm g}$–$(-\beta_{\rm Band})$–log $T_{\rm R45,i}$ formula is

$$\log F_{\rm g} = (0.19 \pm 0.11) \times (-\beta_{\rm Band}) + (0.89 \pm 0.027) \times \log T_{\rm R45,i} + (0.33 \pm 0.25), \quad (420)$$

where $F_{\rm g}$ is in units of 10^{-6} erg cm^{-2} and in the 20–2000 keV energy band. $T_{\rm R45,i}$ is in units of s. The adjusted R^2 is 0.3425. The number of GRBs in the sample is 117.

The log $F_{\rm g}$–log $E_{\rm p,Band}$–log $T_{\rm R45,i}$ formula is

$$\log F_{\rm g} = (1.1 \pm 0.056) \times \log E_{\rm p,Band} + (0.69 \pm 0.035) \times \log T_{\rm R45,i} + (-1.4 \pm 0.11), \quad (421)$$

where $F_{\rm g}$ is in units of 10^{-6} erg cm^{-2} and in the 20–2000 keV energy band. $E_{\rm p,Band}$ is in units of keV. $T_{\rm R45,i}$ is in units of s. The adjusted R^2 is 0.6001. The number of GRBs in the sample is 117.

The log $E_{\rm p,Band}$–log $T_{\rm R45}$–log $P_{\rm pk4}$ formula is

$$\log E_{\rm p,Band} = (0.19 \pm 0.028) \times \log T_{\rm R45} + (0.31 \pm 0.043) \times \log P_{\rm pk4} + (1.6 \pm 0.047), \quad (422)$$

where $E_{\rm p,Band}$ is in units of keV. $T_{\rm R45}$ is in units of s. $P_{\rm pk4}$ is the peak photon flux in the 1 s time bin in 10–1000 keV and is in units of photons cm^{-2} s^{-1}. The adjusted R^2 is 0.2789. The number of GRBs in the sample is 118.

The log $F_{\rm Opt11hr}$–log $F_{\rm g}$–log Mass formula is

$$\log F_{\rm Opt11hr} = (0.33 \pm 0.055) \times \log F_{\rm g} + (-0.34 \pm 0.063) \times \log \mathrm{Mass} + (-2 \pm 0.6), \quad (423)$$

where $F_{\rm Opt11hr}$ is in units of Jy. $F_{\rm g}$ is in units of 10^{-6} erg cm^{-2} and in the 20–2000 keV energy band. Mass is in units of $M_\odot$. The adjusted R^2 is 0.2536. The number of GRBs in the sample is 120.

The log $E_{\rm iso}$–log $F_{\rm X11hr}$–$\beta_{\rm X11hr}$ formula is

$$\log E_{\rm iso} = (0.55 \pm 0.045) \times \log F_{\rm X11hr} + (-0.3 \pm 0.083) \times \beta_{\rm X11hr} + (5 \pm 0.29), \quad (424)$$

where $E_{\rm iso}$ is in units of 10^{52} erg and in the rest-frame 1–10^4 keV energy band. $F_{\rm X11hr}$ is in units of Jy. The adjusted R^2 is 0.2423. The number of GRBs in the sample is 121.

The $\beta_{\rm X11hr}$–log $P_{\rm pk4}$–log $T_{\rm R45,i}$ formula is

$$\beta_{\rm X11hr} = (-0.61 \pm 0.095) \times \log P_{\rm pk4} + (-0.16 \pm 0.067) \times \log T_{\rm R45,i} + (2.1 \pm 0.076), \quad (425)$$

where $P_{\rm pk4}$ is the peak photon flux in the 1 s time bin in 10–1000 keV and is in units of photons cm^{-2} s^{-1}. $T_{\rm R45,i}$ is in units of s. The adjusted R^2 is 0.3002. The number of GRBs in the sample is 123.

The log T_{90}–log $E_{\rm iso}$–log $N_{\rm H}$ formula is

$$\log T_{90} = (0.31 \pm 0.012) \times \log E_{\rm iso} + (0.17 \pm 0.032) \times \log N_{\rm H} + (1.3 \pm 0.024), \quad (426)$$

where T_{90} is in units of s. $E_{\rm iso}$ is in units of 10^{52} erg and in the rest-frame 1–10^4 keV energy band. $N_{\rm H}$ is in units of 10^{21} cm^{-2}. The adjusted R^2 is 0.2526. The number of GRBs in the sample is 125.

The log Mass–log $D_{\rm L}$–log $F_{\rm Opt11hr}$ formula is

$$\log \mathrm{Mass} = (0.48 \pm 0.066) \times \log D_{\rm L} + (-0.22 \pm 0.049) \times \log F_{\rm Opt11hr} + (8.3 \pm 0.24), \quad (427)$$

where Mass is in units of $M_\odot$. $D_{\rm L}$ is in units of 10^{28} cm. $F_{\rm Opt11hr}$ is in units of Jy. The adjusted R^2 is 0.2064. The number of GRBs in the sample is 126.

The log $D_{\rm L}$–log $\theta_{\rm j}$–$A_{\rm V}$ formula is

$$\log D_{\rm L} = (-0.44 \pm 0.036) \times \log \theta_{\rm j} + (-0.13 \pm 0.029) \times A_{\rm V} + (0.034 \pm 0.049), \quad (428)$$

where $D_{\rm L}$ is in units of 10^{28} cm. $\theta_{\rm j}$ is in units of rad. The adjusted R^2 is 0.2105. The number of GRBs in the sample is 126.

The log Mass–log$(1+z)$–log $F_{\rm Opt11hr}$ formula is

$$\log \mathrm{Mass} = (1.2 \pm 0.21) \times \log(1+z) + (-0.22 \pm 0.048) \times \log F_{\rm Opt11hr} + (8 \pm 0.23), \quad (429)$$

where Mass is in units of $M_{\odot}$. $F_{\rm Opt11hr}$ is in units of Jy. The adjusted R^2 is 0.2156. The number of GRBs in the sample is 126.

The $\log F_{\rm g}$–$\log L_{\rm pk}$–$(-\beta_{\rm Band})$ formula is

$$\log F_{\rm g} = (0.39 \pm 0.02) \times \log L_{\rm pk} + (0.19 \pm 0.1) \times (-\beta_{\rm Band}) + (0.67 \pm 0.24), \quad (430)$$

where $F_{\rm g}$ is in units of $10^{-6}\,{\rm erg\,cm^{-2}}$ and in the 20–2000 keV energy band. $L_{\rm pk}$ is in units of $10^{52}\,{\rm erg\,s^{-1}}$ and in the $1–10^4$ keV energy band. The adjusted R^2 is 0.2296. The number of GRBs in the sample is 127.

The $\log E_{\rm p,Band,i}$–$\log T_{90}$–$\log L_{\rm pk}$ formula is

$$\log E_{\rm p,Band,i} = (0.24 \pm 0.023) \times \log T_{90} + (0.29 \pm 0.012) \times \log L_{\rm pk} + (2.1 \pm 0.04), \quad (431)$$

where $E_{\rm p,Band,i}$ is in units of keV. T_{90} is in units of s. $L_{\rm pk}$ is in units of $10^{52}\,{\rm erg\,s^{-1}}$ and in the $1–10^4$ keV energy band. The adjusted R^2 is 0.4998. The number of GRBs in the sample is 127.

The $\log F_{\rm X11hr}$–$\beta_{\rm X11hr}$–$\log T_{50,\rm i}$ formula is

$$\log F_{\rm X11hr} = (-0.38 \pm 0.067) \times \beta_{\rm X11hr} + (0.36 \pm 0.038) \times \log T_{50,\rm i} + (-7 \pm 0.11), \quad (432)$$

where $F_{\rm X11hr}$ is in units of Jy. $T_{50,\rm i}$ is in units of s. The adjusted R^2 is 0.2084. The number of GRBs in the sample is 129.

The $\log P_{\rm pk4}$–$\log D_{\rm L}$–$\beta_{\rm X11hr}$ formula is

$$\log P_{\rm pk4} = (-0.26 \pm 0.035) \times \log D_{\rm L} + (-0.32 \pm 0.049) \times \beta_{\rm X11hr} + (1.2 \pm 0.082), \quad (433)$$

where $P_{\rm pk4}$ is the peak photon flux in the 1 s time bin in 10–1000 keV and is in units of photons $\rm cm^{-2}\,s^{-1}$. $D_{\rm L}$ is in units of 10^{28} cm. The adjusted R^2 is 0.3358. The number of GRBs in the sample is 130.

The $\log T_{50,\rm i}$–$\log E_{\rm iso}$–log Mass formula is

$$\log T_{50,\rm i} = (0.29 \pm 0.0082) \times \log E_{\rm iso} + (-0.15 \pm 0.022) \times \log {\rm Mass} + (2.1 \pm 0.21), \quad (434)$$

where $T_{50,\rm i}$ is in units of s. $E_{\rm iso}$ is in units of 10^{52} erg and in the rest-frame $1–10^4$ keV energy band. Mass is in units of $M_{\odot}$. The adjusted R^2 is 0.2199. The number of GRBs in the sample is 130.

The $\log F_{\rm g}$–$\log L_{\rm pk}$–log Mass formula is

$$\log F_{\rm g} = (0.44 \pm 0.017) \times \log L_{\rm pk} + (-0.26 \pm 0.035) \times \log {\rm Mass} + (3.5 \pm 0.33), \quad (435)$$

where $F_{\rm g}$ is in units of $10^{-6}\,{\rm erg\,cm^{-2}}$ and in the 20–2000 keV energy band. $L_{\rm pk}$ is in units of $10^{52}\,{\rm erg\,s^{-1}}$ and in the $1–10^4$ keV energy band. Mass is in units of $M_{\odot}$. The adjusted R^2 is 0.3385. The number of GRBs in the sample is 130.

The $\log P_{\rm pk4}$–$\log(1+z)$–$\beta_{\rm X11hr}$ formula is

$$\log P_{\rm pk4} = (-0.63 \pm 0.11) \times \log(1+z) + (-0.31 \pm 0.048) \times \beta_{\rm X11hr} + (1.4 \pm 0.084), \quad (436)$$

where $P_{\rm pk4}$ is the peak photon flux in the 1 s time bin in 10–1000 keV and is in units of photons $\rm cm^{-2}\,s^{-1}$. The adjusted R^2 is 0.3504. The number of GRBs in the sample is 130.

The $\log T_{90}$–$\rm variability_1$–$\log E_{\rm iso}$ formula is

$$\log T_{90} = (0.42 \pm 0.22) \times {\rm variability_1} + (0.22 \pm 0.0096) \times \log E_{\rm iso} + (1.4 \pm 0.017), \quad (437)$$

where T_{90} is in units of s. $E_{\rm iso}$ is in units of 10^{52} erg and in the rest-frame $1–10^4$ keV energy band. The adjusted R^2 is 0.2188. The number of GRBs in the sample is 132.

The $\log F_{\rm X11hr}$–$\beta_{\rm X11hr}$–$\log T_{90,\rm i}$ formula is

$$\log F_{\rm X11hr} = (-0.33 \pm 0.064) \times \beta_{\rm X11hr} + (0.41 \pm 0.035) \times \log T_{90,\rm i} + (-7.3 \pm 0.11), \quad (438)$$

where $F_{\rm X11hr}$ is in units of Jy. $T_{90,\rm i}$ is in units of s. The adjusted R^2 is 0.2234. The number of GRBs in the sample is 133.

The $(-\alpha_{\rm Band})$–log HR–$\log T_{90,\rm i}$ formula is

$$(-\alpha_{\rm Band}) = (-0.41 \pm 0.064) \times \log {\rm HR} + (0.11 \pm 0.02) \times \log T_{90,\rm i} + (1.1 \pm 0.044), \quad (439)$$

where $T_{90,\rm i}$ is in units of s. The adjusted R^2 is 0.2783. The number of GRBs in the sample is 135.

The log HR–$(-\alpha_{\rm Band})$–$\log E_{\rm p,Band,i}$ formula is

$$\log {\rm HR} = (-0.33 \pm 0.072) \times (-\alpha_{\rm Band}) + (0.34 \pm 0.04) \times \log E_{\rm p,Band,i} + (-0.033 \pm 0.14), \quad (440)$$

where $E_{\rm p,Band,i}$ is in units of keV. The adjusted R^2 is 0.442. The number of GRBs in the sample is 136.

The $\log L_{\rm pk}$–$\log P_{\rm pk4}$–$\log E_{\rm p,cpl,i}$ formula is

$$\log L_{\rm pk} = (0.87 \pm 0.054) \times \log P_{\rm pk4} + (0.63 \pm 0.097) \times \log E_{\rm p,cpl,i} + (-2.3 \pm 0.25), \quad (441)$$

where $L_{\rm pk}$ is in units of $10^{52}\,{\rm erg\,s^{-1}}$ and in the $1–10^4$ keV energy band. $P_{\rm pk4}$ is the peak photon flux in the 1 s time bin in 10–1000 keV and is in units of photons $\rm cm^{-2}\,s^{-1}$. $E_{\rm p,cpl,i}$ is in units of keV. The adjusted R^2 is 0.2905. The number of GRBs in the sample is 136.

The $\log F_{\rm g}$–$\log L_{\rm pk}$–$\log E_{\rm p,cpl,i}$ formula is

$$\log F_{\rm g} = (0.16 \pm 0.022) \times \log L_{\rm pk} + (0.45 \pm 0.076) \times \log E_{\rm p,cpl,i} + (-0.63 \pm 0.2), \quad (442)$$

where $F_{\rm g}$ is in units of $10^{-6}\,{\rm erg\,cm^{-2}}$ and in the 20–2000 keV energy band. $L_{\rm pk}$ is in units of $10^{52}\,{\rm erg\,s^{-1}}$ and in the $1–10^4$ keV energy band. $E_{\rm p,cpl,i}$ is in units of keV. The adjusted R^2 is 0.2238. The number of GRBs in the sample is 139.

The $\log L_{\rm pk}$–$\log F_{\rm g}$–$\log t_{\rm burst,i}$ formula is

$$\log L_{\rm pk} = (0.57 \pm 0.025) \times \log F_{\rm g} + (-0.46 \pm 0.027) \times \log t_{\rm burst,i} + (0.58 \pm 0.062), \quad (443)$$

where $L_{\rm pk}$ is in units of $10^{52}\,{\rm erg\,s^{-1}}$ and in the 1–10^4 keV energy band. $F_{\rm g}$ is in units of $10^{-6}\,{\rm erg\,cm^{-2}}$ and in the 20–2000 keV energy band. $t_{\rm burst,i}$ is in units of s. The adjusted R^2 is 0.2877. The number of GRBs in the sample is 140.

The $\log E_{\rm iso}$–$\log T_{\rm R45}$–$\log t_{\rm burst,i}$ formula is

$$\log E_{\rm iso} = (0.86 \pm 0.024) \times \log T_{\rm R45} + (-0.37 \pm 0.022) \times \log t_{\rm burst,i} + (0.66 \pm 0.05), \quad (444)$$

where $E_{\rm iso}$ is in units of 10^{52} erg and in the rest-frame 1–10^4 keV energy band. $T_{\rm R45}$ is in units of s. $t_{\rm burst,i}$ is in units of s. The adjusted R^2 is 0.2667. The number of GRBs in the sample is 140.

The log Mass–$\log(1+z)$–$A_{\rm V}$ formula is

$$\log {\rm Mass} = (1.8 \pm 0.23) \times \log(1+z) + (0.19 \pm 0.045) \times A_{\rm V} + (8.8 \pm 0.099), \quad (445)$$

where Mass is in units of $M_\odot$. The adjusted R^2 is 0.2586. The number of GRBs in the sample is 146.

The $\log E_{\rm iso}$–$\log T_{90}$–$\beta_{\rm X11hr}$ formula is

$$\log E_{\rm iso} = (0.82 \pm 0.025) \times \log T_{90} + (-0.39 \pm 0.052) \times \beta_{\rm X11hr} + (-0.028 \pm 0.098), \quad (446)$$

where $E_{\rm iso}$ is in units of 10^{52} erg and in the rest-frame 1–10^4 keV energy band. T_{90} is in units of s. The adjusted R^2 is 0.516. The number of GRBs in the sample is 149.

The $\log P_{\rm pk4}$–$\log E_{\rm p,cpl}$–$\log F_{\rm X11hr}$ formula is

$$\log P_{\rm pk4} = (0.18 \pm 0.05) \times \log E_{\rm p,cpl} + (0.22 \pm 0.013) \times \log F_{\rm X11hr} + (1.7 \pm 0.14), \quad (447)$$

where $P_{\rm pk4}$ is the peak photon flux in the 1 s time bin in 10–1000 keV and is in units of photons $\rm cm^{-2}\,s^{-1}$. $E_{\rm p,cpl}$ is in units of keV. $F_{\rm X11hr}$ is in units of Jy. The adjusted R^2 is 0.2295. The number of GRBs in the sample is 152.

The $\log F_{\rm X11hr}$–$\log E_{\rm iso}$–$\log F_{\rm Opt11hr}$ formula is

$$\log F_{\rm X11hr} = (0.28 \pm 0.016) \times \log E_{\rm iso} + (0.19 \pm 0.045) \times \log F_{\rm Opt11hr} + (-6.7 \pm 0.23), \quad (448)$$

where $F_{\rm X11hr}$ is in units of Jy. $E_{\rm iso}$ is in units of 10^{52} erg and in the rest-frame 1–10^4 keV energy band. $F_{\rm Opt11hr}$ is in units of Jy. The adjusted R^2 is 0.2229. The number of GRBs in the sample is 153.

The $\log E_{\rm iso}$–$\log T_{50}$–$\log F_{\rm X11hr}$ formula is

$$\log E_{\rm iso} = (0.63 \pm 0.021) \times \log T_{50} + (0.45 \pm 0.028) \times \log F_{\rm X11hr} + (3.1 \pm 0.22), \quad (449)$$

where $E_{\rm iso}$ is in units of 10^{52} erg and in the rest-frame 1–10^4 keV energy band. T_{50} is in units of s. $F_{\rm X11hr}$ is in units of Jy. The adjusted R^2 is 0.3408. The number of GRBs in the sample is 153.

The $\log F_{\rm g}$–$\log(1+z)$–$\beta_{\rm X11hr}$ formula is

$$\log F_{\rm g} = (0.71 \pm 0.15) \times \log(1+z) + (-0.56 \pm 0.064) \times \beta_{\rm X11hr} + (1.3 \pm 0.11), \quad (450)$$

where $F_{\rm g}$ is in units of $10^{-6}\,{\rm erg\,cm^{-2}}$ and in the 20–2000 keV energy band. The adjusted R^2 is 0.2953. The number of GRBs in the sample is 153.

The $\log F_{\rm pk1}$–log HR–log Mass formula is

$$\log F_{\rm pk1} = (1 \pm 0.07) \times \log {\rm HR} + (-0.15 \pm 0.03) \times \log {\rm Mass} + (1.1 \pm 0.29), \quad (451)$$

where $F_{\rm pk1}$ is the peak energy flux in the 1 s time bin in the rest-frame 1–10^4 keV energy band and is in units of $10^{-6}\,{\rm erg\,cm^{-2}\,s^{-1}}$. Mass is in units of $M_\odot$. The adjusted R^2 is 0.3515. The number of GRBs in the sample is 157.

The $\log E_{\rm iso}$–$\log F_{\rm pk1}$–$\log E_{\rm p,Band,i}$ formula is

$$\log E_{\rm iso} = (0.26 \pm 0.025) \times \log F_{\rm pk1} + (1.2 \pm 0.048) \times \log E_{\rm p,Band,i} + (-2.2 \pm 0.12), \quad (452)$$

where $E_{\rm iso}$ is in units of 10^{52} erg and in the rest-frame 1–10^4 keV energy band. $F_{\rm pk1}$ is the peak energy flux in the 1 s time bin in the rest-frame 1–10^4 keV energy band and is in units of $10^{-6}\,{\rm erg\,cm^{-2}\,s^{-1}}$. $E_{\rm p,Band,i}$ is in units of keV. The adjusted R^2 is 0.564. The number of GRBs in the sample is 158.

The $\log E_{\rm iso}$–$\log T_{90}$–$\log F_{\rm X11hr}$ formula is

$$\log E_{\rm iso} = (0.77 \pm 0.022) \times \log T_{90} + (0.36 \pm 0.028) \times \log F_{\rm X11hr} + (2 \pm 0.23), \quad (453)$$

where $E_{\rm iso}$ is in units of 10^{52} erg and in the rest-frame 1–10^4 keV energy band. T_{90} is in units of s. $F_{\rm X11hr}$ is in units of Jy. The adjusted R^2 is 0.3803. The number of GRBs in the sample is 159.

The $\log F_{\rm g}$–$\log L_{\rm pk}$–$\log F_{\rm Opt11hr}$ formula is

$$\log F_{\rm g} = (0.42 \pm 0.018) \times \log L_{\rm pk} + (0.28 \pm 0.034) \times \log F_{\rm Opt11hr} + (2.2 \pm 0.16), \quad (454)$$

where $F_{\rm g}$ is in units of $10^{-6}\,{\rm erg\,cm^{-2}}$ and in the 20–2000 keV energy band. $L_{\rm pk}$ is in units of $10^{52}\,{\rm erg\,s^{-1}}$ and in the 1–10^4 keV energy band. $F_{\rm Opt11hr}$ is in units of Jy. The adjusted R^2 is 0.3953. The number of GRBs in the sample is 171.

The $\log T_{90}$–$\log E_{\rm iso}$–log Mass formula is

$$\log T_{90} = (0.41 \pm 0.0082) \times \log E_{\rm iso} + (-0.17 \pm 0.021) \times \log {\rm Mass} + (2.9 \pm 0.2), \quad (455)$$

where T_{90} is in units of s. $E_{\rm iso}$ is in units of 10^{52} erg and in the rest-frame 1–10^4 keV energy band. Mass is in units of $M_\odot$. The adjusted R^2 is 0.3543. The number of GRBs in the sample is 172.

The $\log P_{\rm pk4}$–$\log F_{\rm g}$–$\log t_{\rm burst,i}$ formula is

$$\log P_{\rm pk4} = (0.43 \pm 0.021) \times \log F_{\rm g} + (-0.12 \pm 0.02) \times \log t_{\rm burst,i} + (0.45 \pm 0.043), \quad (456)$$

where $P_{\rm pk4}$ is the peak photon flux in the 1 s time bin in 10–1000 keV and is in units of photons $\rm cm^{-2}\,s^{-1}$. $F_{\rm g}$ is in units of 10^{-6} erg $\rm cm^{-2}$ and in the 20–2000 keV energy band. $t_{\rm burst,i}$ is in units of s. The adjusted R^2 is 0.3963. The number of GRBs in the sample is 172.

The $\log P_{\rm pk4}$–$\log {\rm HR}$–$\log F_{\rm X11hr}$ formula is

$$\log P_{\rm pk4} = (0.28 \pm 0.047) \times \log {\rm HR} + (0.23 \pm 0.016) \times \log F_{\rm X11hr} + (2.2 \pm 0.12), \quad (457)$$

where $P_{\rm pk4}$ is the peak photon flux in the 1 s time bin in 10–1000 keV and is in units of photons $\rm cm^{-2}\,s^{-1}$. $F_{\rm X11hr}$ is in units of Jy. The adjusted R^2 is 0.2558. The number of GRBs in the sample is 182.

The $\log F_{\rm g}$–$\log T_{\rm 50,i}$–$\log E_{\rm p,cpl,i}$ formula is

$$\log F_{\rm g} = (0.48 \pm 0.026) \times \log T_{\rm 50,i} + (0.57 \pm 0.056) \times \log E_{\rm p,cpl,i} + (-1.3 \pm 0.14), \quad (458)$$

where $F_{\rm g}$ is in units of 10^{-6} erg $\rm cm^{-2}$ and in the 20–2000 keV energy band. $T_{\rm 50,i}$ is in units of s. $E_{\rm p,cpl,i}$ is in units of keV. The adjusted R^2 is 0.4764. The number of GRBs in the sample is 185.

The $\log P_{\rm pk4}$–$\log T_{90}$–$\log F_{\rm X11hr}$ formula is

$$\log P_{\rm pk4} = (-0.13 \pm 0.013) \times \log T_{90} + (0.29 \pm 0.015) \times \log F_{\rm X11hr} + (2.8 \pm 0.12), \quad (459)$$

where $P_{\rm pk4}$ is the peak photon flux in the 1 s time bin in 10–1000 keV and is in units of photons $\rm cm^{-2}\,s^{-1}$. T_{90} is in units of s. $F_{\rm X11hr}$ is in units of Jy. The adjusted R^2 is 0.2226. The number of GRBs in the sample is 216.

The $\log F_{\rm g}$–$\log L_{\rm pk}$–$\log T_{\rm 50,i}$ formula is

$$\log F_{\rm g} = (0.39 \pm 0.013) \times \log L_{\rm pk} + (0.55 \pm 0.022) \times \log T_{\rm 50,i} + (0.38 \pm 0.019), \quad (460)$$

where $F_{\rm g}$ is in units of 10^{-6} erg $\rm cm^{-2}$ and in the 20–2000 keV energy band. $L_{\rm pk}$ is in units of $10^{52}\,\rm erg\,s^{-1}$ and in the 1–10^4 keV energy band. $T_{\rm 50,i}$ is in units of s. The adjusted R^2 is 0.4039. The number of GRBs in the sample is 218.

The $\log {\rm HR}$–$\rm variability_1$–$(-\beta_{\rm Band})$ formula is

$$\log {\rm HR} = (-0.54 \pm 0.49) \times {\rm variability_1} + (-0.15 \pm 0.054) \times (-\beta_{\rm Band}) + (1 \pm 0.14), \quad (461)$$

and the adjusted R^2 is 0.2164. The number of GRBs in the sample is 219.

The $\log L_{\rm pk}$–$\log F_{\rm g}$–$A_{\rm V}$ formula is

$$\log L_{\rm pk} = (0.51 \pm 0.021) \times \log F_{\rm g} + (-0.21 \pm 0.043) \times A_{\rm V} + (-0.35 \pm 0.037), \quad (462)$$

where $L_{\rm pk}$ is in units of $10^{52}\,\rm erg\,s^{-1}$ and in the 1–10^4 keV energy band. $F_{\rm g}$ is in units of 10^{-6} erg $\rm cm^{-2}$ and in the 20–2000 keV energy band. The adjusted R^2 is 0.2064. The number of GRBs in the sample is 220.

The $\log F_{\rm g}$–$\rm variability_1$–$\log P_{\rm pk1}$ formula is

$$\log F_{\rm g} = (-1.9 \pm 0.58) \times {\rm variability_1} + (0.83 \pm 0.038) \times \log P_{\rm pk1} + (0.41 \pm 0.055), \quad (463)$$

where $F_{\rm g}$ is in units of 10^{-6} erg $\rm cm^{-2}$ and in the 20–2000 keV energy band. $P_{\rm pk1}$ is the peak photon flux in the 64 ms time bin in 10–1000 keV and is in units of photons $\rm cm^{-2}\,s^{-1}$. The adjusted R^2 is 0.4694. The number of GRBs in the sample is 227.

The $\log E_{\rm iso}$–$(-\alpha_{\rm cpl})$–$\log E_{\rm p,cpl,i}$ formula is

$$\log E_{\rm iso} = (0.3 \pm 0.071) \times (-\alpha_{\rm cpl}) + (0.85 \pm 0.08) \times \log E_{\rm p,cpl,i} + (-2.2 \pm 0.23), \quad (464)$$

where $E_{\rm iso}$ is in units of 10^{52} erg and in the rest-frame 1–10^4 keV energy band. $E_{\rm p,cpl,i}$ is in units of keV. The adjusted R^2 is 0.2692. The number of GRBs in the sample is 228.

The $\log F_{\rm X11hr}$–$\log F_{\rm g}$–$\log F_{\rm Opt11hr}$ formula is

$$\log F_{\rm X11hr} = (0.52 \pm 0.023) \times \log F_{\rm g} + (0.16 \pm 0.026) \times \log F_{\rm Opt11hr} + (-7.1 \pm 0.13), \quad (465)$$

where $F_{\rm X11hr}$ is in units of Jy. $F_{\rm g}$ is in units of 10^{-6} erg $\rm cm^{-2}$ and in the 20–2000 keV energy band. $F_{\rm Opt11hr}$ is in units of Jy. The adjusted R^2 is 0.3134. The number of GRBs in the sample is 232.

The $\log F_{\rm g}$–$\log D_{\rm L}$–$\log E_{\rm p,cpl}$ formula is

$$\log F_{\rm g} = (0.27 \pm 0.029) \times \log D_{\rm L} + (0.63 \pm 0.059) \times \log E_{\rm p,cpl} + (-1.1 \pm 0.13), \quad (466)$$

where $F_{\rm g}$ is in units of 10^{-6} erg $\rm cm^{-2}$ and in the 20–2000 keV energy band. $D_{\rm L}$ is in units of 10^{28} cm. $E_{\rm p,cpl}$ is in units of keV. The adjusted R^2 is 0.2516. The number of GRBs in the sample is 248.

The $\log D_{\rm L}$–$\log T_{90}$–$\log E_{\rm p,cpl,i}$ formula is

$$\log D_{\rm L} = (0.2 \pm 0.0065) \times \log T_{90} + (0.29 \pm 0.028) \times \log E_{\rm p,cpl,i} + (-0.52 \pm 0.071), \quad (467)$$

where $D_{\rm L}$ is in units of 10^{28} cm. T_{90} is in units of s. $E_{\rm p,cpl,i}$ is in units of keV. The adjusted R^2 is 0.2192. The number of GRBs in the sample is 257.

The $\log F_{\rm g}$–$\log L_{\rm pk}$–$\log T_{\rm 90,i}$ formula is

$$\log F_{\rm g} = (0.37 \pm 0.011) \times \log L_{\rm pk} + (0.63 \pm 0.017) \times \log T_{\rm 90,i} + (0.1 \pm 0.022), \quad (468)$$

where $F_{\rm g}$ is in units of 10^{-6} erg $\rm cm^{-2}$ and in the 20–2000 keV energy band. $L_{\rm pk}$ is in units of $10^{52}\,\rm erg\,s^{-1}$ and in the 1–10^4 keV energy band. $T_{\rm 90,i}$ is in units of s. The adjusted R^2 is 0.4429. The number of GRBs in the sample is 312.

The $\log F_{\rm g}$–$\log T_{\rm R45}$–$\log E_{\rm p,cpl}$ formula is

$$\log F_{\rm g} = (0.59 \pm 0.019) \times \log T_{\rm R45} + (0.55 \pm 0.045) \times \log E_{\rm p,cpl} + (-1.2 \pm 0.098), \quad (469)$$

where $F_{\rm g}$ is in units of $10^{-6}\,{\rm erg\,cm^{-2}}$ and in the 20–2000 keV energy band. $T_{\rm R45}$ is in units of s. $E_{\rm p,cpl}$ is in units of keV. The adjusted R^2 is 0.5627. The number of GRBs in the sample is 362.

The $\log P_{\rm pk4}$–$\log D_{\rm L}$–$\log F_{\rm g}$ formula is

$$\log P_{\rm pk4} = (-0.25 \pm 0.013) \times \log D_{\rm L} + (0.39 \pm 0.013) \times \log F_{\rm g} + (0.45 \pm 0.011), \quad (470)$$

where $P_{\rm pk4}$ is the peak photon flux in the 1 s time bin in 10–1000 keV and is in units of photons $\rm cm^{-2}\,s^{-1}$. $D_{\rm L}$ is in units of 10^{28} cm. $F_{\rm g}$ is in units of $10^{-6}\,{\rm erg\,cm^{-2}}$ and in the 20–2000 keV energy band. The adjusted R^2 is 0.3421. The number of GRBs in the sample is 419.

The $\log {\rm HR}$–$\log F_{\rm pk2}$–$(-\alpha_{\rm spl})$ formula is

$$\log {\rm HR} = (0.17 \pm 0.036) \times \log F_{\rm pk2} + (-0.9 \pm 0.039) \times (-\alpha_{\rm spl}) + (2.2 \pm 0.075), \quad (471)$$

where $F_{\rm pk2}$ is the peak energy flux in the 64 ms time bin in the rest-frame 1–10^4 keV energy band and is in units of $10^{-6}\,{\rm erg\,cm^{-2}\,s^{-1}}$. The adjusted R^2 is 0.5718. The number of GRBs in the sample is 490.

The $\log {\rm HR}$–$\log T_{50}$–$(-\alpha_{\rm spl})$ formula is

$$\log {\rm HR} = (-0.11 \pm 0.014) \times \log T_{50} + (-0.87 \pm 0.035) \times (-\alpha_{\rm spl}) + (2.2 \pm 0.056), \quad (472)$$

where T_{50} is in units of s. The adjusted R^2 is 0.6123. The number of GRBs in the sample is 497.

The $\log {\rm HR}$–$\log F_{\rm pk1}$–$\log E_{\rm p,cpl}$ formula is

$$\log {\rm HR} = (0.15 \pm 0.02) \times \log F_{\rm pk1} + (0.92 \pm 0.045) \times \log E_{\rm p,cpl} + (-1.8 \pm 0.11), \quad (473)$$

where $F_{\rm pk1}$ is the peak energy flux in the 1 s time bin in the rest-frame 1–10^4 keV energy band and is in units of $10^{-6}\,{\rm erg\,cm^{-2}\,s^{-1}}$. $E_{\rm p,cpl}$ is in units of keV. The adjusted R^2 is 0.8214. The number of GRBs in the sample is 713.

The $\log P_{\rm pk3}$–$\log F_{\rm g}$–$(-\alpha_{\rm cpl})$ formula is

$$\log P_{\rm pk3} = (0.38 \pm 0.015) \times \log F_{\rm g} + (0.15 \pm 0.016) \times (-\alpha_{\rm cpl}) + (0.21 \pm 0.015), \quad (474)$$

where $P_{\rm pk3}$ is the peak photon flux in the 1024 ms time bin in 10–1000 keV and is in units of photons $\rm cm^{-2}\,s^{-1}$. $F_{\rm g}$ is in units of $10^{-6}\,{\rm erg\,cm^{-2}}$ and in the 20–2000 keV energy band. The adjusted R^2 is 0.4674. The number of GRBs in the sample is 913.

The $\log {\rm HR}$–$\log F_{\rm pk4}$–$(-\alpha_{\rm cpl})$ formula is

$$\log {\rm HR} = (0.42 \pm 0.024) \times \log F_{\rm pk4} + (-0.31 \pm 0.025) \times (-\alpha_{\rm cpl}) + (0.96 \pm 0.026), \quad (475)$$

where $F_{\rm pk4}$ is the peak energy flux in the 1024 ms time bin in the rest-frame 1–10^4 keV energy band and is in units of $10^{-6}\,{\rm erg\,cm^{-2}\,s^{-1}}$. The adjusted R^2 is 0.3125. The number of GRBs in the sample is 937.

The $\log {\rm HR}$–$\log P_{\rm pk1}$–$(-\beta_{\rm Band})$ formula is

$$\log {\rm HR} = (0.15 \pm 0.018) \times \log P_{\rm pk1} + (-0.18 \pm 0.034) \times (-\beta_{\rm Band}) + (0.83 \pm 0.085), \quad (476)$$

where $P_{\rm pk1}$ is the peak photon flux in the 64 ms time bin in 10–1000 keV and is in units of photons $\rm cm^{-2}\,s^{-1}$. The adjusted R^2 is 0.2471. The number of GRBs in the sample is 1092.

The $\log F_{\rm g}$–$\log P_{\rm pk1}$–$\log E_{\rm p,Band}$ formula is

$$\log F_{\rm g} = (0.58 \pm 0.027) \times \log P_{\rm pk1} + (0.63 \pm 0.025) \times \log E_{\rm p,Band} + (-1.1 \pm 0.053), \quad (477)$$

where $F_{\rm g}$ is in units of $10^{-6}\,{\rm erg\,cm^{-2}}$ and in the 20–2000 keV energy band. $P_{\rm pk1}$ is the peak photon flux in the 64 ms time bin in 10–1000 keV and is in units of photons $\rm cm^{-2}\,s^{-1}$. $E_{\rm p,Band}$ is in units of keV. The adjusted R^2 is 0.4116. The number of GRBs in the sample is 1121.

The $\log E_{\rm p,Band}$–$\log {\rm HR}$–$\log F_{\rm pk2}$ formula is

$$\log E_{\rm p,Band} = (0.42 \pm 0.019) \times \log {\rm HR} + (0.14 \pm 0.011) \times \log F_{\rm pk2} + (2 \pm 0.0099), \quad (478)$$

where $E_{\rm p,Band}$ is in units of keV. $F_{\rm pk2}$ is the peak energy flux in the 64 ms time bin in the rest-frame 1–10^4 keV energy band and is in units of $10^{-6}\,{\rm erg\,cm^{-2}\,s^{-1}}$. The adjusted R^2 is 0.6307. The number of GRBs in the sample is 1130.

The $\log T_{50}$–$\log {\rm HR}$–$(-\alpha_{\rm cpl})$ formula is

$$\log T_{50} = (-0.44 \pm 0.022) \times \log {\rm HR} + (0.35 \pm 0.032) \times (-\alpha_{\rm cpl}) + (0.53 \pm 0.04), \quad (479)$$

where T_{50} is in units of s. The adjusted R^2 is 0.2224. The number of GRBs in the sample is 1140.

The $\log {\rm HR}$–$\log T_{50}$–$(-\beta_{\rm Band})$ formula is

$$\log {\rm HR} = (-0.14 \pm 0.0073) \times \log T_{50} + (-0.11 \pm 0.024) \times (-\beta_{\rm Band}) + (0.97 \pm 0.06), \quad (480)$$

where T_{50} is in units of s. The adjusted R^2 is 0.201. The number of GRBs in the sample is 1183.

The $\log F_{\rm pk4}$–$(-\alpha_{\rm Band})$–$\log E_{\rm p,Band}$ formula is

$$\log F_{\rm pk4} = (0.11 \pm 0.025) \times (-\alpha_{\rm Band}) + (0.81 \pm 0.025) \times \log E_{\rm p,Band} + (-1.8 \pm 0.058), \quad (481)$$

where $F_{\rm pk4}$ is the peak energy flux in the 1024 ms time bin in the rest-frame 1–10^4 keV energy band and is in units of

10^{-6} erg cm^{-2} s^{-1}. $E_{\rm p,Band}$ is in units of keV. The adjusted R^2 is 0.3073. The number of GRBs in the sample is 1192.

The $\log T_{90}$–$\log F_{\rm g}$–$(-\alpha_{\rm cpl})$ formula is

$$\log T_{90} = (0.56 \pm 0.013) \times \log F_{\rm g} + (0.32 \pm 0.03) \times (-\alpha_{\rm cpl}) + (0.6 \pm 0.032), \quad (482)$$

where T_{90} is in units of s. $F_{\rm g}$ is in units of 10^{-6} erg cm^{-2} and in the 20–2000 keV energy band. The adjusted R^2 is 0.3263. The number of GRBs in the sample is 1347.

7. Discussions

There are many other interesting quantities that are not listed in this data sample, mainly because the quantities are limited to a few GRBs, or they are not quite well defined or not widely accepted. Readers may want to use the data shown here as a reservoir and add any other data they are interested in to perform statistical studies. With the Fourier transformation of the prompt LCs, the slope in the frequency domain can be obtained. The properties of the precursors are not included either, though they are thought to be not much different from those of the prompt emission (Burlon et al. 2008, 2009). Because of the universal behavior of the afterglow LCs (Zhang et al. 2006a), there are quite a few parameters, including the temporal decay index, the ending time, and spectral index, in each phase (they are in X-rays and mainly contain only one segment, i.e., there are no breaks in the spectra), while the phases include the steep decay phase, the plateau phase, the normal decay phase, and the jet break phase. There are also X-ray flare parameters in the afterglow, such as the number of flares, typical duration, rising temporal index, decay temporal index, spectrum index, and luminosities. Aside from the spectral indices, there are also plenty of detailed spectral lines from the afterglows and from the host galaxies, which can be used as characteristic quantities. One can use those data and the data listed in this paper for a combined analysis. On the other hand, the combination of parameters can also be taken as independent parameters, such as the average luminosity $L_{\rm iso} \equiv \frac{(1+z)E_{\rm iso}}{T_{90}}$ and the spectral index difference of the Band spectrum $\alpha - \beta$. For a detailed study on special quantities, one can obtain more data from the original data sets. For example, $P_{\rm pk}$ and $F_{\rm pk}$ have four time bins, mainly because different authors are interested in different time bins. It is not proper to simply take them as equal, and four different values are gathered in this work. In most cases, for each GRB, only a few time bins are available. One could obtain the $P_{\rm pk}$ in the 1024 ms bin (for example) if the original LCs are available. Therefore, digging into the original data from the satellites will provide much more extra data than those shown in this work. On the other hand, the LCs in different bands, the corresponding quantities for which are not shown here, are also interesting. One could expand the parameters by digging into the raw data.

One should be careful when using these data because of the variety of data sources. The energy band and sensitivity are different for different instruments. For example, T_{90} is energy dependent, therefore, the T_{90} from different instruments should not be taken as the same parameter if the energy bands for different instruments differ a lot. A proper way to handle this selection effect is to convert the LCs to the same energy band, in which case spectrum models are needed. However, in many cases, the spectrum model for each GRB is not the same, and for some GRBs, it is possible that two or more models have the same goodness for the spectrum fitting. Therefore, it is model dependent. Because of the complexity and the problem of model dependence, we only include directly available data, leaving these conversions for future work. The same problem also applies to T_{50}, the spectral lag, HR, fluence F, photon flux P, luminosity L, and isotropic equivalent energy $E_{\rm iso}$. To avoid these problems, we have converted them to the same band, either to a commonly used energy band or to a full band (like 1–10,000 keV), by employing spectral fitting parameters. However, these conversions are model dependent, as for different bursts, the spectral fitting model might be different, and the real model might not be the best fitting model. Even if the data can be converted into values in the same band, there are still cosmological effects. The same band is not the same band in the rest frame. Because of cosmological redshift, in order to compare within the same band, one should convert the quantities to the same band in the rest frame. However, even in the same band in the rest frame, the cosmological evolution effect is not removable. It is still unclear how GRBs evolve with the universe. On the other hand, with plenty of data at different redshifts, it is possible to study the evolution.

To avoid the problems that arise because of selection effects, we mainly concentrate on physical quantities (like luminosities and energies) rather than observational values (like fluence and photon flux), and we use the quantities in the rest frame rather than in the observer frame. However, they both rely on redshift detection, which is hard, and consequently, the sample size is much smaller. To balance this, one can use as much data as possible, while keeping in mind the reliability of GRBs without an obtained redshift. On the other hand, the relations between observational quantities may reveal the selection effect. If one finds properties that only appear in brighter GRBs (more photons observed), those are probably not intrinsic correlations.

Even with the selection effect considered, one can see from the figures shown in the figure sets that the correlations are not tight. Even though they are all consistent with previously found correlations, such as the Amati relation (Amati et al. 2002), the Ghirlanda relation (Ghirlanda et al. 2004b), the Yonetoku relation (Yonetoku et al. 2004) relation, the Liang–Zhang relation (Liang & Zhang 2005), etc., either they are able to be classified into several subgroups (e.g., the Amati relation is different for LGRBs and SGRBs), or the selected sample is still not tight enough (e.g., the standard candle relation is not good enough for precise cosmography; Xu et al. 2005; Wang et al. 2011). The probable reason might be the intrinsic variety of the GRBs. From the morphological view, they can be divided into different groups based on different properties. Based on the duration, there are LGRBs, SGRBs, and some of them may be classified as intermediate GRBs or ultra-LGRBs (Levan et al. 2014; Boër et al. 2015; Greiner et al. 2015). The physical mechanism responsible for ultra-LGRBs is thus far unclear. Greiner et al. (2015) provided an important clue for the ultra-LGRB 111209A, which is driven by the spindown radiation from a highly magnetized millisecond pulsar, known as a magnetar. Gompertz & Fruchter (2017) tried to place constraints on the magnetar model. Based on the spectrum (or hardness ratio), there are soft GRBs and hard GRBs, and some are very soft and thus classified as X-ray-rich GRBs or even X-ray flashes. Based on the luminosity, there are high-luminosity GRBs and low-luminosity GRBs. Based on connection with other phenomena, there are SN Ic-connected

GRBs, GRBs with no SN connection with a very dim flux, kilonova-connected GRBs, and strong GeV-connected GRBs. From the physical origin viewpoint, there are also different subgroups. Based on their progenitors, they can arise from massive stars, BH–NS binaries, NS–NS binaries, and even BH–WD binaries and NS–WD binaries. Based on the central engine, they can be BZ mechanism dominated, NDAF dominated, or magentar dominated. Based on the radiation mechanism, they can be synchrotron radiation dominated, inverse Compton scattering dominated, or photosphere emission dominated.

Therefore, direct analysis might not reveal the underlying pattern, mainly because of the selection effect and the clustering effect. For the selection effect, one should try to figure out each factor, if possible. For the clustering effect, one should try to find the subgroups from the full sample. A widely known clustering effect is that of long-soft GRBs and short-hard GRBs. However, it is very likely that GRBs should be classified into more subgroups. From the point of view of the central engine, they might be powered by an BH accretion disk system or neutron star. From the point of view of progenitors, they might arise from massive star collapsars, BH–WD mergers, BH–star mergers for LGRBs, and BH–NS mergers and NS–NS mergers for SGRBs. Other possibilities, such as NS–star mergers and NS–WD mergers, might also be hidden in the sample. For the radiation mechanism, it might be photosphere emission, synchrotron radiation, inverse Compton scattering (depending on the origins of the seed photons and the electrons/protons, many more subgroups could be needed), etc. For the ejecta, it could be highly relativistic or mildly relativistic. From the point of view of the environment, the number density could be uniformly distributed or have a wind-like distribution, and it could be either a dense environment or a thin one. For the optical counterpart, it could be supernova connected, kilonova connected, have no supernova connection, or even have a dim optical counterpart. From the point of view of the host galaxy, it might be a spiral galaxy, a field galaxy, or another type. More detailed or other classification criteria can be proposed. The different origins or mechanisms are represented by the properties of the data, and should be revealed by a detailed and comprehensive study of the data.

Clustering and correlation analyses actually affect each other. With the proper classification, such as whether NS–WD merger GRBs are grouped together based on some properties, the correlation between two or three parameters could be much tighter, and the correlation might be more useful for a standard candle relation or for a redshift indicator, etc. On the other hand, the correlation can be used as an indicator for clustering. For example, the $E_{\rm p}$–$E_{\rm iso}$ relation is often used as one of the indicators for certain GRBs being long or short. A GRB that lies on the Amati relation is more likely a collapsar-originated GRB, while an outlier is more likely a merger-originated GRB. Therefore, with more detailed clustering, the correlation within a certain group of GRBs is more reliable and reveals its deeper nature, which needs more data accumulation. Once a pure subset has been found, it could be used as a standard candle and could be an ideal tool for the cosmology in the high-redshift region.

For the clustering, an example is the classification of hard SGRBs and soft LGRBs. There are also other independent classifications, like ultralong GRBs and low-luminosity GRBs. These are classified using one or two parameters of the GRBs. Machine learning is a set of promising methods, such as the k-means, Support Vector Machine, and Principal Component Analysis (Zhou 2016). They are able to operate in a much higher dimension and in a highly nonlinear manner, similar to what has been done in other areas of astrophysics (e.g., Elorrieta et al. 2016). However, machine-learning methods are often like black boxes. It is easy to get the result of the clustering, but it is difficult to find the criteria for the clustering. One of the main aims is to figure out this black box, which reveals the intrinsic properties, similar to the clustering process shown in Zhang et al. (2009). Aside from clustering, machine learning can also be used for parameter predicting, for example, to predict the redshift, similar to what is being done with the SDSS galaxies (Hoyle et al. 2015). Given the lack of massive data used in general applications of machine learning, deep learning may also be a promising approach.

High-energy radiation in the GeV band has been detected in quite a few *Fermi* GRBs. From the binned LCs, they are likely from the afterglow (Ghisellini et al. 2010). However, there are many sources that can produce GeV photons. For example, the synchrotron and synchrotron self-inverse Compton scattering (SSC) emission from the long-lasting forward external shock can contribute these photons. The continuously active GRB central engines and the SSC emission of the continued internal shocks give rise to GeV photons. In a relativistic reverse shock formed, the prompt optical/X-ray/γ-ray photons are inversely Compton scattered by the accelerated electrons in the forward shock region. Finally, the external inverse Compton scattering (EIC) in the late-afterglow phase caused by X-ray flares may also give rise to GeV emission (Zou et al. 2009). It is still not clear which part dominates in the high-energy radiation. With the database of information on the other aspects of GRBs, the high-energy radiation may be used to compare with the database, and it may reveal some connections. One can use these connections to figure out the origin of the high-energy GeV emission, even though the high-energy data may come from several related instruments, including *Fermi*/LAT (Ackermann et al. 2013), HAWC (Abeysekara et al. 2012), H.E.S.S. (Aharonian et al. 2009), MAGIC (Albert et al. 2007), and Wukong (DAMPE; Chang et al. 2017).

A GW burst is accompanied by SGRBs, as they are believed to originate from a double compact object (NS–NS or NS–BH). An NS–NS origin has been identified from the detection of GW170817/GRB 170817A (Abbott et al. 2017c, 2017d). However, the observed GRB 170817A was a weak SGRB, which is much different from normal SGRBs. As the distance to GRB 170817A is much closer than to the other SGRBs, the birth rate is consequently much higher than the others, if we consider that they belong to two different subgroups. It is possible that NS–NS mergers may produce weak SGRBs, whereas BH–NS mergers may produce strong SGRBs, which are the SGRBs mostly observed. There are other GW bursts that have been observed, such as GW150914 (Abbott et al. 2016c). The presence of a BH that is tens of solar masses has been confirmed (for GW150914, it was the merger of a $36^{+5}_{-4}M_{\odot}$ BH and a $29^{+4}_{-4}M_{\odot}$ BH; Abbott et al. 2016c). Therefore, compared with an NS–NS merger, which is the merger of a several $M_{\odot}$ object and a several $M_{\odot}$ object, the BH–NS merger is the merger of tens of $M_{\odot}$ object and a several $M_{\odot}$ object. The BH–NS merger might be naturally stronger and consequently produce strong SGRBs. If the hypothesis is correct, these two different objects should have different properties in other

aspects. In the hundreds of observed SGRBs, these two origins should both have been included. Considering that LIGO had only been operating for just a few months when an NS–NS GRB (GRB 170817A) was observed indicates that there are many more of this kind of GRB that has been observed and archived when LIGO was not in operation. With the comprehensive table of the different aspects of all GRBs, one can try to figure out subgroups in the SGRBs. The NS–NS and NS–BH origin can be distinguished, and more subgroups of other origins might be uncovered. Until now, the BH–NS merger has not been confirmed by the GW detector. After it has been in operation for a longer time and with the enhanced instruments, the BH–NS merger should be identified in the future.

8. Conclusion

In this work, we collected a large number of data for 6289 GRBs from different works in the literature, GCNs, website databases, and calculations. The data include four parts: basic information, prompt emission, afterglow, and host galaxy (a total of 46 items for each GRB). With this complete table, we performed a comprehensive statistical study. When we performed the statistical analysis, we also changed some parameters from the observer frame to rest frame; we use the label "i" to denote this. For example, the duration of the 5%–95% γ-ray fluence (T_{90}) is in the observer frame, and $T_{90,i}$ is T_{90} in the rest frame. This work includes the following six items: (1) we imputed the missing errors through multiple imputation (Rubin 1987, 1996) by chained equations (MICE). (2) We calculated a small part of the peak energy flux (F_{pk}) in the rest-frame 1–10^4 keV energy band, the peak photon flux (P_{pk}) in the observer-frame 10–1000 keV energy band, the fluence (F_g) in the observer-frame 20–2000 keV energy band, the hardness ratio (HR) between the observer-frame 100–2000 and 20–100 keV energy bands, the isotropic γ-ray energy (E_{iso}) in the rest-frame 1–10^4 keV energy band, and the peak luminosity (L_{pk}) in the rest-frame 1–10^4 keV energy band. (3) We obtained all histograms for every parameter in the observer frame and for some parameters in the rest frame. (4) We obtained all scatter plots between two arbitrary parameters that are available for at least five GRBs. (5) We calculated the linear correlation coefficients and nonlinear correlation ratio between two arbitrary parameters that are available for at least five GRBs, and we excluded some correlations that are trivial, such as that between T_{90} and $T_{90,i}$. We do not need to put such correlations in the results. We also considered all errors using the Monte Carlo (MC) method. (6) We performed linear regression between two arbitrary parameters and three arbitrary parameters that are available for at least five GRBs; we also excluded some trivial results. We used the MC method to include all of the errors. Then, we analyzed some interesting results. Because there are many data and results, we created figure sets and several machine-readable tables. Only a small portion of the results are shown in this paper as examples. With this complete catalog, we can find more important relations, and we can reveal the intrinsic properties of GRBs.

We discussed the deficiencies of this comprehensive sample, which are mainly from the uncertainties and inconsistencies of the different instruments and the selection effect. To reveal more physical principles, one should try to classify the GRBs into more precise subgroups based on their physical origin, and the classification itself is a process to reveal the intrinsic properties of GRBs. With the detailed classifications, the correlations inside each group may be tighter and more physical. The correlations can then be used to study the radiation mechanism as well as the high-energy radiation, as indicators like the standard candle or pseudo-redshift, and to study the GWs of compact binary mergers.

We thank the anonymous referee for critically reading the manuscript and suggesting substantial improvements. We also thank the editors for the careful and enormous corrections on the manuscript. Y.C.Z. thanks Tsvi Piran, Bing Zhang, Zigao Dai, Kwong Sang Cheng, Daming Wei, Yongfeng Huang, Xiangyu Wang, Xuefeng Wu, Yizhong Fan, Enwei Liang, Fayin Wang, Yunwei Yu, Shuangxi Yi, Shiyong Liu, Haijun Tian, Gaochao Liu, Jun Liu, Deyi Ma, Sheng Cui, Reetanjali Moharana, Dingxiong Wang, Weihua Lei, Qingwen Wu, Jumpei Takata, Yan Wang, Biping Gong, Wei Xie, Wei Chen, Chao Yang, Lixiong Gan, Jiuzhou Wang, Wenbo Ma, Jun Tian, and Shuaibing Ma for helpful discussions. Y.C.Z. also thanks Jing Lv, Jingwen Xing, Yanhui Han, Max Oberndorfer, Chujun Yi, Zhengfu Xiong, Hualei Wang, Shaoping Huang, Xiaohao Cui, and Yuan Xue for their statistical studies on GRBs. Their works were mainly for their bachelor's degree theses or part of their research. Those were the prototypes or trials of the different aspects of this comprehensive statistical work, which was conceived in 2010 and started in 2012. The data were collected manually, stored in a Google spreadsheet, and checked by eye and by code. The originally collected data are available at: https://drive.google.com/drive/folders/0B9pJKjl_EXbvcFNMYnQ0WVFLTjQ. The codes in this work were compiled in R and Python. This work is supported by the National Basic Research Program of China (973 Program, grant No. 2014CB845800), by the National Natural Science Foundation of China (grants Nos. U1738132, 11773010, 11601267, and U1231101), and by the Humanity and Social Science Foundation of MOE of China (20171304). This research was supported in part by Perimeter Institute for Theoretical Physics. Research at Perimeter Institute is supported by the Government of Canada through the Department of Innovation, Science and Economic Development Canada and by the Province of Ontario through the Ministry of Economic Development, Job Creation and Trade.

ORCID iDs

Yuan-Chuan Zou https://orcid.org/0000-0002-5400-3261

References

Aasi, J., Abbott, B. P., Abbott, R., et al. 2014, PhRvD, 89, 122004
Abadie, J., Abbott, B. P., Abbott, R., et al. 2012, ApJ, 760, 12
Abbott, B. P., Abbott, R., Abbott, T. D., et al. 2016a, ApJS, 225, 8
Abbott, B. P., Abbott, R., Abbott, T. D., et al. 2016b, PhRvL, 116, 241103
Abbott, B. P., Abbott, R., Abbott, T. D., et al. 2016c, PhRvL, 116, 061102
Abbott, B. P., Abbott, R., Abbott, T. D., et al. 2017a, PhRvL, 118, 221101
Abbott, B. P., Abbott, R., Abbott, T. D., et al. 2017b, ApJL, 848, L13
Abbott, B. P., Abbott, R., Abbott, T. D., et al. 2017c, PhRvL, 119, 161101
Abbott, B. P., Abbott, R., Abbott, T. D., et al. 2017d, ApJL, 848, L12
Abbott, B. P., Abbott, R., Acernese, F., et al. 2010, ApJ, 715, 1438
Abeysekara, A. U., Aguilar, J. A., Aguilar, S., et al. 2012, APh, 35, 641
Ackermann, M., Ajello, M., Albert, A., et al. 2012, ApJS, 203, 4
Ackermann, M., Ajello, M., Asano, K., et al. 2013, ApJS, 209, 11
Acuner, Z., & Ryde, F. 2018, MNRAS, 475, 1708
Adrián-Martínez, S., Albert, A., Samarai, I. A., et al. 2013, A&A, 559, A9
Afonso, P., Schady, P., Kruehler, T., & Greiner, J. 2010, GCN, 10782, 1

Aharonian, F., Akhperjanian, A. G., Barres de Almeida, U., et al. 2009, A&A, 495, 505
Ahlgren, B., Larsson, J., Nymark, T., Ryde, F., & Pe'er, A. 2015, MNRAS, 454, L31
Aihara, H., Allende Prieto, C., An, D., et al. 2011, ApJS, 193, 29
Albert, J., Aliu, E., Anderhub, H., et al. 2007, ApJ, 667, 358
Allison, P., Auffenberg, J., Bard, R., et al. 2017, APh, 88, 7
Amati, L. 2006, MNRAS, 372, 233
Amati, L., Frontera, F., & Guidorzi, C. 2009, A&A, 508, 173
Amati, L., Frontera, F., Tavani, M., et al. 2002, A&A, 390, 81
Amati, L., Guidorzi, C., Frontera, F., et al. 2008, MNRAS, 391, 577
Antonelli, L. A., D'Avanzo, P., Perna, R., et al. 2009, A&A, 507, L45
Aptekar, R. L., Frederiks, D. D., Golenetskii, S. V., et al. 1995, SSRv, 71, 265
Arabsalmani, M., Møller, P., Fynbo, J. P. U., et al. 2015, MNRAS, 446, 990
Arabsalmani, M., Møller, P., Perley, D. A., et al. 2018, MNRAS, 473, 3312
Arcodia, R., Campana, S., & Salvaterra, R. 2016, A&A, 590, A82
Ashcraft, T., & Schaefer, B. E. 2007, ApJ, 671, 1896
Atteia, J.-L. 2003, A&A, 407, L1
Augusto, C. R. A., Navia, C. E., de Oliveira, M. N., et al. 2016, arXiv:1605.04274
Baird, D. C. 1994, Experimentation: An Introduction to Measurement Theory and Experiment Design (33rd ed.; Reading, MA: Benjamin Cummings: Addison-Wesley Professional)
Balázs, L. G., Bagoly, Z., Hakkila, J. E., et al. 2015, MNRAS, 452, 2236
Band, D., Matteson, J., Ford, L., et al. 1993, ApJ, 413, 281
Band, D. L., & Preece, R. D. 2005, ApJ, 627, 319
Barniol Duran, R. 2014, MNRAS, 442, 3147
Barraud, C., Olive, J.-F., Lestrade, J. P., et al. 2003, A&A, 400, 1021
Barthelmy, S. D., Amaral-Rogers, A., Cummings, J. R., et al. 2016a, GCN, 18944, 1
Barthelmy, S. D., Barbier, L. M., Cummings, J. R., et al. 2005, SSRv, 120, 143
Barthelmy, S. D., Barlow, B. N., Baumgartner, W. H., et al. 2012a, GCN, 13784, 1
Barthelmy, S. D., Baumgartner, W. H., Beardmore, A. P., et al. 2015a, GCN, 17761, 1
Barthelmy, S. D., Baumgartner, W. H., Cummings, J. R., et al. 2010a, GCN, 11388, 1
Barthelmy, S. D., Baumgartner, W. H., Cummings, J. R., et al. 2010b, GCN, 11218, 1
Barthelmy, S. D., Baumgartner, W. H., Cummings, J. R., et al. 2010c, GCN, 11058, 1
Barthelmy, S. D., Baumgartner, W. H., Cummings, J. R., et al. 2010d, GCN, 10417, 1
Barthelmy, S. D., Baumgartner, W. H., Cummings, J. R., et al. 2011a, GCN, 11757, 1
Barthelmy, S. D., Baumgartner, W. H., Cummings, J. R., et al. 2011b, GCN, 11811, 1
Barthelmy, S. D., Baumgartner, W. H., Cummings, J. R., et al. 2011c, GCN, 11921, 1
Barthelmy, S. D., Baumgartner, W. H., Cummings, J. R., et al. 2011d, GCN, 12445, 1
Barthelmy, S. D., Baumgartner, W. H., Cummings, J. R., et al. 2011e, GCN, 12689, 1
Barthelmy, S. D., Baumgartner, W. H., Cummings, J. R., et al. 2011f, GCN, 12602, 1
Barthelmy, S. D., Baumgartner, W. H., Cummings, J. R., et al. 2011g, GCN, 12507, 1
Barthelmy, S. D., Baumgartner, W. H., Cummings, J. R., et al. 2011h, GCN, 12399, 1
Barthelmy, S. D., Baumgartner, W. H., Cummings, J. R., et al. 2011i, GCN, 12035, 1
Barthelmy, S. D., Baumgartner, W. H., Cummings, J. R., et al. 2011j, GCN, 11783, 1
Barthelmy, S. D., Baumgartner, W. H., Cummings, J. R., et al. 2012b, GCN, 13052, 1
Barthelmy, S. D., Baumgartner, W. H., Cummings, J. R., et al. 2012c, GCN, 13572, 1
Barthelmy, S. D., Baumgartner, W. H., Cummings, J. R., et al. 2012d, GCN, 14068, 1
Barthelmy, S. D., Baumgartner, W. H., Cummings, J. R., et al. 2012e, GCN, 13659, 1
Barthelmy, S. D., Baumgartner, W. H., Cummings, J. R., et al. 2012f, GCN, 13633, 1
Barthelmy, S. D., Baumgartner, W. H., Cummings, J. R., et al. 2012g, GCN, 13594, 1
Barthelmy, S. D., Baumgartner, W. H., Cummings, J. R., et al. 2012h, GCN, 13404, 1
Barthelmy, S. D., Baumgartner, W. H., Cummings, J. R., et al. 2012i, GCN, 12983, 1
Barthelmy, S. D., Baumgartner, W. H., Cummings, J. R., et al. 2012j, GCN, 12955, 1
Barthelmy, S. D., Baumgartner, W. H., Cummings, J. R., et al. 2012k, GCN, 12889, 1
Barthelmy, S. D., Baumgartner, W. H., Cummings, J. R., et al. 2012l, GCN, 13869, 1
Barthelmy, S. D., Baumgartner, W. H., Cummings, J. R., et al. 2013a, GCN, 15620, 1
Barthelmy, S. D., Baumgartner, W. H., Cummings, J. R., et al. 2013b, GCN, 15457, 1
Barthelmy, S. D., Baumgartner, W. H., Cummings, J. R., et al. 2013c, GCN, 15456, 1
Barthelmy, S. D., Baumgartner, W. H., Cummings, J. R., et al. 2013d, GCN, 15370, 1
Barthelmy, S. D., Baumgartner, W. H., Cummings, J. R., et al. 2013e, GCN, 15041, 1
Barthelmy, S. D., Baumgartner, W. H., Cummings, J. R., et al. 2013f, GCN, 14899, 1
Barthelmy, S. D., Baumgartner, W. H., Cummings, J. R., et al. 2013g, GCN, 14736, 1
Barthelmy, S. D., Baumgartner, W. H., Cummings, J. R., et al. 2013h, GCN, 14693, 1
Barthelmy, S. D., Baumgartner, W. H., Cummings, J. R., et al. 2013i, GCN, 14343, 1
Barthelmy, S. D., Baumgartner, W. H., Cummings, J. R., et al. 2013j, GCN, 14315, 1
Barthelmy, S. D., Baumgartner, W. H., Cummings, J. R., et al. 2013k, GCN, 14296, 1
Barthelmy, S. D., Baumgartner, W. H., Cummings, J. R., et al. 2013l, GCN, 14146, 1
Barthelmy, S. D., Baumgartner, W. H., Cummings, J. R., et al. 2014a, GCN, 17239, 1
Barthelmy, S. D., Baumgartner, W. H., Cummings, J. R., et al. 2014b, GCN, 17011, 1
Barthelmy, S. D., Baumgartner, W. H., Cummings, J. R., et al. 2014c, GCN, 16845, 1
Barthelmy, S. D., Baumgartner, W. H., Cummings, J. R., et al. 2014d, GCN, 16615, 1
Barthelmy, S. D., Baumgartner, W. H., Cummings, J. R., et al. 2014e, GCN, 16404, 1
Barthelmy, S. D., Baumgartner, W. H., Cummings, J. R., et al. 2014f, GCN, 16105, 1
Barthelmy, S. D., Baumgartner, W. H., Cummings, J. R., et al. 2014g, GCN, 15908, 1
Barthelmy, S. D., Baumgartner, W. H., Cummings, J. R., et al. 2014h, GCN, 15847, 1
Barthelmy, S. D., Baumgartner, W. H., Cummings, J. R., et al. 2015b, GCN, 17539, 1
Barthelmy, S. D., Baumgartner, W. H., Cummings, J. R., et al. 2015c, GCN, 17426, 1
Barthelmy, S. D., Bernardini, M. G., Cummings, J. R., et al. 2015d, GCN, 18002, 1
Barthelmy, S. D., Cenko, S. B., Cummings, J. R., et al. 2015e, GCN, 18396, 1
Barthelmy, S. D., Cummings, J. R., D'Ai, A., et al. 2016b, GCN, 19181, 1
Barthelmy, S. D., Cummings, J. R., D'Avanzo, P., et al. 2016c, GCN, 19323, 1
Barthelmy, S. D., Cummings, J. R., D'Avanzo, P., et al. 2016d, GCN, 18998, 1
Barthelmy, S. D., Cummings, J. R., Evans, P. A., et al. 2015f, GCN, 18683, 1
Barthelmy, S. D., Cummings, J. R., Gehrels, N., et al. 2015g, GCN, 18754, 1
Barthelmy, S. D., Cummings, J. R., Gehrels, N., et al. 2015h, GCN, 18223, 1
Barthelmy, S. D., Cummings, J. R., Gehrels, N., et al. 2015i, GCN, 18110, 1
Barthelmy, S. D., Cummings, J. R., Gehrels, N., et al. 2016e, GCN, 19020, 1
Barthelmy, S. D., Cummings, J. R., Gehrels, N., et al. 2016f, GCN, 18929, 1
Barthelmy, S. D., & Norris, J. 2011, GCN, 12653, 1
Barthelmy, S. D., Sakamoto, T., Baumgartner, W. H., et al. 2010e, GCN, 10896, 1
Barthelmy, S. D., Sakamoto, T., Baumgartner, W. H., et al. 2012m, GCN, 12815, 1
Barthelmy, S. D., Sakamoto, T., Baumgartner, W. H., et al. 2012n, GCN, 12963, 1
Barthelmy, S. D., Sakamoto, T., & Stamatikos, M. 2011k, GCN, 11557, 1
Bartoli, B., Bernardini, P., Bi, X. J., et al. 2014, ApJ, 794, 82
Basilakos, S., & Perivolaropoulos, L. 2008, MNRAS, 391, 411
Baumgartner, W. H., Barthelmy, S. D., Cummings, J. R., et al. 2010a, GCN, 11414, 1

Baumgartner, W. H., Barthelmy, S. D., Cummings, J. R., et al. 2010b, GCN, 11281, 1
Baumgartner, W. H., Barthelmy, S. D., Cummings, J. R., et al. 2010c, GCN, 10801, 1
Baumgartner, W. H., Barthelmy, S. D., Cummings, J. R., et al. 2010d, GCN, 10501, 1
Baumgartner, W. H., Barthelmy, S. D., Cummings, J. R., et al. 2011a, GCN, 11764, 1
Baumgartner, W. H., Barthelmy, S. D., Cummings, J. R., et al. 2011b, GCN, 12049, 1
Baumgartner, W. H., Barthelmy, S. D., Cummings, J. R., et al. 2011c, GCN, 12551, 1
Baumgartner, W. H., Barthelmy, S. D., Cummings, J. R., et al. 2011d, GCN, 12175, 1
Baumgartner, W. H., Barthelmy, S. D., Cummings, J. R., et al. 2012a, GCN, 12946, 1
Baumgartner, W. H., Barthelmy, S. D., Cummings, J. R., et al. 2012b, GCN, 13291, 1
Baumgartner, W. H., Barthelmy, S. D., Cummings, J. R., et al. 2012c, GCN, 13472, 1
Baumgartner, W. H., Barthelmy, S. D., Cummings, J. R., et al. 2012d, GCN, 13581, 1
Baumgartner, W. H., Barthelmy, S. D., Cummings, J. R., et al. 2012e, GCN, 14111, 1
Baumgartner, W. H., Barthelmy, S. D., Cummings, J. R., et al. 2012f, GCN, 13961, 1
Baumgartner, W. H., Barthelmy, S. D., Cummings, J. R., et al. 2012g, GCN, 13942, 1
Baumgartner, W. H., Barthelmy, S. D., Cummings, J. R., et al. 2013, GCN, 15163, 1
Baumgartner, W. H., Barthelmy, S. D., Cummings, J. R., et al. 2014a, GCN, 17044, 1
Baumgartner, W. H., Barthelmy, S. D., Cummings, J. R., et al. 2014b, GCN, 16870, 1
Baumgartner, W. H., Barthelmy, S. D., Cummings, J. R., et al. 2014c, GCN, 16652, 1
Baumgartner, W. H., Barthelmy, S. D., Cummings, J. R., et al. 2014d, GCN, 16127, 1
Baumgartner, W. H., Barthelmy, S. D., Cummings, J. R., et al. 2014e, GCN, 15664, 1
Baumgartner, W. H., Barthelmy, S. D., Cummings, J. R., et al. 2015a, GCN, 17774, 1
Baumgartner, W. H., Barthelmy, S. D., Cummings, J. R., et al. 2015b, GCN, 17562, 1
Baumgartner, W. H., Barthelmy, S. D., Cummings, J. R., et al. 2015c, GCN, 17445, 1
Baumgartner, W. H., Barthelmy, S. D., Cummings, J. R., et al. 2015d, GCN, 17266, 1
Bégué, D., & Burgess, J. M. 2016, ApJ, 820, 68
Bellm, E. C., Bandstra, M. E., Boggs, S. E., et al. 2008, in AIP Conf. Ser. 1000, Gamma-Ray Bursts 2007, ed. M. Galassi, D. Palmer, & E. Fenimore (Melville, NY: AIP), 154
Berger, E. 2009, ApJ, 690, 231
Berger, E. 2014, ARA&A, 52, 43
Berger, E., Chornock, R., Holmes, T. R., et al. 2011, ApJ, 743, 204
Berger, E., Fong, W., & Chornock, R. 2013, ApJL, 774, L23
Berger, E., Kulkarni, S. R., & Frail, D. A. 2003, ApJ, 590, 379
Beskin, G. M., Oganesyan, G., Greco, G., & Karpov, S. 2015, AstBu, 70, 400
Bhat, P. N., Briggs, M. S., Connaughton, V., et al. 2012, ApJ, 744, 141
Bhatt, N., & Bhattacharyya, S. 2012, MNRAS, 420, 1706
Bhave, A., Kulkarni, S., Desai, S., & Srijith, P. K. 2017, arXiv:1708.05668
Bianco, F. B., Modjaz, M., Hicken, M., et al. 2014, ApJS, 213, 19
Bissaldi, E. 2015, GCN, 18299, 1
Bissaldi, E., & Burns, E. 2015, GCN, 18201, 1
Bissaldi, E., Connaughton, V., & von Kienlin, A. 2015a, GCN, 18041, 1
Bissaldi, E., Zhang, B., & Veres, P. 2015b, GCN, 18736, 1
Blanchard, P. K., Berger, E., & Fong, W.-f. 2016, ApJ, 817, 144
Blandford, R. D., & McKee, C. F. 1976, PhFl, 19, 1130
Bloom, J. S., Djorgovski, S. G., Kulkarni, S. R., & Frail, D. A. 1998, ApJL, 507, L25
Bloom, J. S., Frail, D. A., & Kulkarni, S. R. 2003, ApJ, 594, 674
Bloom, J. S., Frail, D. A., & Sari, R. 2001, AJ, 121, 2879
Bloom, J. S., Kulkarni, S. R., & Djorgovski, S. G. 2002, AJ, 123, 1111
Bloom, J. S., Perley, D. A., Li, W., et al. 2009, ApJ, 691, 723
Boella, G., Butler, R. C., Perola, G. C., et al. 1997, A&AS, 122, 299
Boër, M., Gendre, B., & Stratta, G. 2015, ApJ, 800, 16
Borgonovo, L., & Ryde, F. 2001, ApJ, 548, 770
Bosnjak, Z., Celotti, A., Ghirlanda, G., Della Valle, M., & Pian, E. 2006, A&A, 447, 121
Bošnjak, Ž., Götz, D., Bouchet, L., Schanne, S., & Cordier, B. 2014, A&A, 561, A25
Bromberg, O., Nakar, E., Piran, T., & Sari, R. 2013, ApJ, 764, 179
Buffington, A., Band, D. L., Jackson, B. V., Hick, P. P., & Smith, A. C. 2006, ApJ, 637, 880
Burgess, J. M., Connaughton, V., & Xiong, S. 2013, GCN, 14583, 1
Burlon, D., Ghirlanda, G., Ghisellini, G., et al. 2008, ApJL, 685, L19
Burlon, D., Ghirlanda, G., Ghisellini, G., Greiner, J., & Celotti, A. 2009, A&A, 505, 569
Burns, E. 2014a, GCN, 17150, 1
Burns, E. 2014b, GCN, 16626, 1
Burns, E. 2014c, GCN, 16579, 1
Burns, E. 2015a, GCN, 17432, 1
Burns, E. 2015b, GCN, 17328, 1
Burns, E., & Meegan, C. 2015a, GCN, 17807, 1
Burns, E., & Meegan, C. 2015b, GCN, 17525, 1
Burns, E., & Meegan, C. 2016, GCN, 19331, 1
Burns, E., & Yu, H.-F. 2015, GCN, 17408, 1
Burrows, D. N., Hill, J. E., Nousek, J. A., et al. 2005, SSRv, 120, 165
Butler, N. R., Bloom, J. S., & Poznanski, D. 2010, ApJ, 711, 495
Butler, N. R., Kocevski, D., Bloom, J. S., & Curtis, J. L. 2007, ApJ, 671, 656
Byrne, D. 2013, GCN, 14941, 1
Byrne, D., von Kienlin, A., & Paciesas, W. 2013, GCN, 14940, 1
Campana, S., Mangano, V., Blustin, A. J., et al. 2006, Natur, 442, 1008
Campana, S., Thöne, C. C., de Ugarte Postigo, A., et al. 2010, MNRAS, 402, 2429
Campisi, M. A., & Li, L.-X. 2008, MNRAS, 391, 935
Cano, Z., de Ugarte Postigo, A., Perley, D., et al. 2015, MNRAS, 452, 1535
Cano, Z., de Ugarte Postigo, A., Pozanenko, A., et al. 2014, A&A, 568, A19
Cano, Z., Wang, S.-Q., Dai, Z.-G., & Wu, X.-F. 2017, AdAst, 2017, 8929054
Capozziello, S., & Izzo, L. 2008, A&A, 490, 31
Cenko, S. B., Kelemen, J., Harrison, F. A., et al. 2009, ApJ, 693, 1484
Chandra, P., & Frail, D. A. 2012, ApJ, 746, 156
Chang, J., Ambrosi, G., An, Q., et al. 2017, APh, 95, 6
Chang, Z., Li, X., Lin, H.-N., et al. 2016, ChPhC, 40, 045102
Chaplin, V. 2013a, GCN, 14235, 1
Chaplin, V. 2013b, GCN, 14236, 1
Chaplin, V., & Fitzpatrick, G. 2013, GCN, 14346, 1
Chary, R., Becklin, E. E., & Armus, L. 2002, ApJ, 566, 229
Chattopadhyay, S., & Maitra, R. 2017, MNRAS, 469, 3374
Chen, S. L., Li, A., & Wei, D. M. 2006, ApJL, 647, L13
Chhotray, A., & Lazzati, D. 2015, ApJ, 802, 132
Christensen, L., Fynbo, J. P. U., Prochaska, J. X., et al. 2011, ApJ, 727, 73
Christensen, L., Hjorth, J., & Gorosabel, J. 2004, A&A, 425, 913
Church, R. P., Levan, A. J., Davies, M. B., & Tanvir, N. 2011, MNRAS, 413, 2004
Clocchiatti, A., Suntzeff, N. B., Covarrubias, R., & Candia, P. 2011, AJ, 141, 163
Cobb, B. E., Bailyn, C. D., van Dokkum, P. G., Buxton, M. M., & Bloom, J. S. 2004, ApJL, 608, L93
Collazzi, A. C. 2012, GCN, 13194, 1
Collazzi, A. C. 2013a, GCN, 15565, 1
Collazzi, A. C. 2013b, GCN, 15503, 1
Collazzi, A. C. 2013c, GCN, 15129, 1
Collazzi, A. C. 2013d, GCN, 15005, 1
Collazzi, A. C. 2013e, GCN, 14765, 1
Collazzi, A. C., Kouveliotou, C., van der Horst, A. J., et al. 2015, ApJS, 218, 11
Collazzi, A. C., & Schaefer, B. E. 2008, ApJ, 688, 456
Connaughton, V., Jenke, P., & Goldstein, A. 2015, GCN, 17511, 1
Connaughton, V., Zhang, B.-B., Fitzpatrick, G., & Roberts, O. 2014, GCN, 16419, 1
Contini, M. 2016, MNRAS, 460, 3232
Contopoulos, I., Nathanail, A., & Pugliese, D. 2014, ApJL, 780, L5
Covino, S., & Gotz, D. 2016, A&AT, 29, 205
Cucchiara, A., Cenko, S. B., Bloom, J. S., et al. 2011, ApJ, 743, 154
Cucchiara, A., Veres, P., Corsi, A., et al. 2015, ApJ, 812, 122
Cummings, J. R. 2014a, GCN, 17020, 1
Cummings, J. R. 2014b, GCN, 16111, 1
Cummings, J. R. 2014c, GCN, 16073, 1
Cummings, J. R., Amaral-Rogers, A., Barthelmy, S. D., et al. 2015a, GCN, 17457, 1
Cummings, J. R., & Barthelmy, S. D. 2011, GCN, 11546, 1

Cummings, J. R., Barthelmy, S. D., Baumgartner, W. H., et al. 2010a, GCN, 11069, 1
Cummings, J. R., Barthelmy, S. D., Baumgartner, W. H., et al. 2010b, GCN, 11289, 1
Cummings, J. R., Barthelmy, S. D., Baumgartner, W. H., et al. 2010c, GCN, 10803, 1
Cummings, J. R., Barthelmy, S. D., Baumgartner, W. H., et al. 2010d, GCN, 10660, 1
Cummings, J. R., Barthelmy, S. D., Baumgartner, W. H., et al. 2011a, GCN, 11937, 1
Cummings, J. R., Barthelmy, S. D., Baumgartner, W. H., et al. 2011b, GCN, 12581, 1
Cummings, J. R., Barthelmy, S. D., Baumgartner, W. H., et al. 2011c, GCN, 12457, 1
Cummings, J. R., Barthelmy, S. D., Baumgartner, W. H., et al. 2011d, GCN, 12201, 1
Cummings, J. R., Barthelmy, S. D., Baumgartner, W. H., et al. 2011e, GCN, 11776, 1
Cummings, J. R., Barthelmy, S. D., Baumgartner, W. H., et al. 2012a, GCN, 13604, 1
Cummings, J. R., Barthelmy, S. D., Baumgartner, W. H., et al. 2012b, GCN, 13481, 1
Cummings, J. R., Barthelmy, S. D., Baumgartner, W. H., et al. 2012c, GCN, 13310, 1
Cummings, J. R., Barthelmy, S. D., Baumgartner, W. H., et al. 2012d, GCN, 12968, 1
Cummings, J. R., Barthelmy, S. D., Baumgartner, W. H., et al. 2013, GCN, 15293, 1
Cummings, J. R., Barthelmy, S. D., Baumgartner, W. H., et al. 2014a, GCN, 17256, 1
Cummings, J. R., Barthelmy, S. D., Baumgartner, W. H., et al. 2014b, GCN, 17046, 1
Cummings, J. R., Barthelmy, S. D., Baumgartner, W. H., et al. 2014c, GCN, 16892, 1
Cummings, J. R., Barthelmy, S. D., Baumgartner, W. H., et al. 2014d, GCN, 16699, 1
Cummings, J. R., Barthelmy, S. D., Baumgartner, W. H., et al. 2014e, GCN, 16598, 1
Cummings, J. R., Barthelmy, S. D., Baumgartner, W. H., et al. 2014f, GCN, 16481, 1
Cummings, J. R., Barthelmy, S. D., Baumgartner, W. H., et al. 2014g, GCN, 16354, 1
Cummings, J. R., Barthelmy, S. D., Baumgartner, W. H., et al. 2014h, GCN, 16346, 1
Cummings, J. R., Barthelmy, S. D., Baumgartner, W. H., et al. 2014i, GCN, 15934, 1
Cummings, J. R., Barthelmy, S. D., Baumgartner, W. H., et al. 2014j, GCN, 15820, 1
Cummings, J. R., Barthelmy, S. D., Baumgartner, W. H., et al. 2015b, GCN, 17776, 1
Cummings, J. R., Barthelmy, S. D., Baumgartner, W. H., et al. 2015c, GCN, 17581, 1
Cummings, J. R., Barthelmy, S. D., Baumgartner, W. H., et al. 2015d, GCN, 17274, 1
Cummings, J. R., Barthelmy, S. D., D'Elia, V., et al. 2016a, GCN, 19188, 1
Cummings, J. R., Barthelmy, S. D., Gehrels, N., et al. 2015e, GCN, 18699, 1
Cummings, J. R., Barthelmy, S. D., Gehrels, N., et al. 2015f, GCN, 18410, 1
Cummings, J. R., Barthelmy, S. D., Gehrels, N., et al. 2015g, GCN, 18232, 1
Cummings, J. R., Barthelmy, S. D., Gehrels, N., et al. 2015h, GCN, 18013, 1
Cummings, J. R., Barthelmy, S. D., Gehrels, N., et al. 2015i, GCN, 18580, 1
Cummings, J. R., Barthelmy, S. D., Gehrels, N., et al. 2016b, GCN, 19328, 1
Cummings, J. R., Barthelmy, S. D., Gehrels, N., et al. 2016c, GCN, 18959, 1
Cummings, J. R., & Krimm, H. A. 2013, GCN, 14659, 1
Cummings, J. R., & Palmer, D. M. 2015, GCN, 17895, 1
Dado, S., & Dar, A. 2016, PhRvD, 94, 063007
Daigne, F., & Mochkovitch, R. 2003, MNRAS, 342, 587
Dainotti, M., Petrosian, V., Willingale, R., et al. 2015a, MNRAS, 451, 3898
Dainotti, M. G., & Amati, L. 2018, PASP, 130, 051001
Dainotti, M. G., Cardone, V. F., & Capozziello, S. 2008, MNRAS, 391, L79
Dainotti, M. G., Cardone, V. F., Piedipalumbo, E., & Capozziello, S. 2013a, MNRAS, 436, 82
Dainotti, M. G., & Del Vecchio, R. 2017, NewAR, 77, 23
Dainotti, M. G., Del Vecchio, R., Shigehiro, N., & Capozziello, S. 2015b, ApJ, 800, 31
Dainotti, M. G., Del Vecchio, R., & Tarnopolski, M. 2018, AdAst, 2018, 4969503
Dainotti, M. G., Fabrizio Cardone, V., Capozziello, S., Ostrowski, M., & Willingale, R. 2011a, ApJ, 730, 135
Dainotti, M. G., Ostrowski, M., & Willingale, R. 2011b, MNRAS, 418, 2202
Dainotti, M. G., Petrosian, V., Singal, J., & Ostrowski, M. 2013b, ApJ, 774, 157
Dainotti, M. G., Postnikov, S., Hernandez, X., & Ostrowski, M. 2016, ApJL, 825, L20
Dainotti, M. G., Willingale, R., Capozziello, S., Fabrizio Cardone, V., & Ostrowski, M. 2010, ApJL, 722, L215
Dar, A., & De Rujula, A. 2001, arXiv:astro-ph/0110162
D'Avanzo, P., Salvaterra, R., Bernardini, M. G., et al. 2014, MNRAS, 442, 2342
D'Avanzo, P., Salvaterra, R., Sbarufatti, B., et al. 2012, MNRAS, 425, 506
De Laurentis, M., Garufi, F., Giovanna Dainotti, M., & Milano, L. 2015, arXiv:1506.00106
D'Elia, V., Fynbo, J. P. U., Goldoni, P., et al. 2014, A&A, 564, A38
D'Elia, V., Kruehler, T., Wiersema, K., et al. 2015, GCN, 18187, 1
Demianski, M., Piedipalumbo, E., Sawant, D., & Amati, L. 2017, A&A, 598, A112
Deng, C.-M., Wang, X.-G., Guo, B.-B., et al. 2016, ApJ, 820, 66
de Pasquale, M., Piro, L., Gendre, B., et al. 2006, A&A, 455, 813
Dereli, H., Boer, M., Gendre, B., Amati, L., & Dichiara, S. 2015, arXiv:1506.05521
de Ugarte Postigo, A., Horváth, I., Veres, P., et al. 2011, A&A, 525, A109
de Ugarte Postigo, A., Xu, D., Malesani, D., & Tanvir, N. R. 2015, GCN, 17822, 1
Dichiara, S., Guidorzi, C., Amati, L., & Frontera, F. 2013a, MNRAS, 431, 3608
Dichiara, S., Guidorzi, C., Amati, L., Frontera, F., & Margutti, R. 2016, A&A, 589, A97
Dichiara, S., Guidorzi, C., Frontera, F., & Amati, L. 2013b, ApJ, 777, 132
Donato, D., Angelini, L., Padgett, C. A., et al. 2012, ApJS, 203, 2
Dong, Y.-Z., Gu, W.-M., Liu, T., & Wang, J. 2018, MNRAS, 475, L101
Eichler, D., Livio, M., Piran, T., & Schramm, D. N. 1989, Natur, 340, 126
Ellis, J., Mavromatos, N. E., Nanopoulos, D. V., Sakharov, A. S., & Sarkisyan, E. K. G. 2006, APh, 25, 402
Elorrieta, F., Eyheramendy, S., Jordán, A., et al. 2016, A&A, 595, A82
Evans, P. A., Beardmore, A. P., Page, K. L., et al. 2007, A&A, 469, 379
Evans, P. A., Beardmore, A. P., Page, K. L., et al. 2009, MNRAS, 397, 1177
Evans, P. A., Willingale, R., Osborne, J. P., et al. 2014, MNRAS, 444, 250
Feigelson, E. D., & Babu, G. J. 2012, Modern Statistical Methods for Astronomy (Cambridge: Cambridge Univ. Press)
Fenimore, E. E., & Ramirez-Ruiz, E. 2000, arXiv:astro-ph/0004176
Fermi Large Area Telescope Team, Ackermann, M., Ajello, M., et al. 2012, ApJ, 754, 121
Filgas, R., Greiner, J., Schady, P., et al. 2011, A&A, 535, A57
Firmani, C., Ghisellini, G., Avila-Reese, V., & Ghirlanda, G. 2006, MNRAS, 370, 185
Fisher, R. A. 1970, Statistical Methods for Research Workers (Edinburgh: Oliver and Boyd)
Fishman, G. J., Meegan, C. A., Wilson, R. B., et al. 1994, ApJS, 92, 229
Fitzpatrick, G. 2011, GCN, 12386, 1
Fitzpatrick, G. 2013, GCN, 14999, 1
Fitzpatrick, G., & Bhat, P. N. 2013, GCN, 15434, 1
Fitzpatrick, G., & Burgess, J. M. 2013, GCN, 14839, 1
Fitzpatrick, G., & Stanbro, M. 2014, GCN, 15935, 1
Fitzpatrick, G., & Xiong, S. 2013, GCN, 15332, 1
Fitzpatrick, G., & Younes, G. 2013, GCN, 15104, 1
Foley, S. 2010, GCN, 11434, 1
Foley, S., McGlynn, S., Hanlon, L., McBreen, S., & McBreen, B. 2008, A&A, 484, 143
Foley, S., & Meegan, C. 2013, GCN, 15011, 1
Fong, W., Berger, E., Chornock, R., et al. 2013, ApJ, 769, 56
Fong, W., Berger, E., & Fox, D. B. 2010a, ApJ, 708, 9
Fong, W., Berger, E., Margutti, R., & Zauderer, B. A. 2015, ApJ, 815, 102
Fong, W.-F., Berger, E., & Fox, D. 2010b, BAAS, 42, 228
Fragile, P. C., Mathews, G. J., Poirier, J., & Totani, T. 2004, APh, 20, 591
Frail, D. A., Kulkarni, S. R., Sari, R., et al. 2001, ApJL, 562, L55
Frederiks, D. 2010, GCN, 11439, 1
Frederiks, D., Golenetskii, S., Aptekar, R., et al. 2016, GCN, 19312, 1
Frederiks, D. D., Hurley, K., Svinkin, D. S., et al. 2013, ApJ, 779, 151
Friedman, A. S., & Bloom, J. S. 2005, ApJ, 627, 1
Friis, M., & Watson, D. 2013, ApJ, 771, 15
Frontera, F. 2004, in ASP Conf. Ser. 312, Gamma-Ray Bursts in the Afterglow Era, ed. M. Feroci et al. (San Francisco, CA: ASP), 3
Frontera, F., Amati, L., Costa, E., et al. 2000, ApJS, 127, 59

Frontera, F., Amati, L., Guidorzi, C., Landi, R., & in't Zand, J. 2012, ApJ, 754, 138
Frontera, F., Guidorzi, C., Montanari, E., et al. 2009, ApJS, 180, 192
Fruchter, A. S., Levan, A. J., Strolger, L., et al. 2006, Natur, 441, 463
Fujinuma, T., Tashiro, M., Terada, Y., et al. 2015, GCN, 17875, 1
Fynbo, J. P. U., Jakobsson, P., Prochaska, J. X., et al. 2009a, ApJS, 185, 526
Fynbo, J. P. U., Krühler, T., Leighly, K., et al. 2014, A&A, 572, A12
Fynbo, J. P. U., Prochaska, J. X., Sommer-Larsen, J., Dessauges-Zavadsky, M., & Møller, P. 2009b, in IAU Symp. 254, The Galaxy Disk in Cosmological Context, ed. J. Andersen, B. m. Nordströara, & J. Bland-Hawthorn, 41
Galama, T. J., Vreeswijk, P. M., van Paradijs, J., et al. 1998, Natur, 395, 670
Galli, M., Marisaldi, M., Fuschino, F., et al. 2013, A&A, 553, A33
Gao, H., Ding, X., Wu, X.-F., Dai, Z.-G., & Zhang, B. 2015a, ApJ, 807, 163
Gao, H., Lei, W.-H., You, Z.-Q., & Xie, W. 2016, ApJ, 826, 141
Gao, H., Wang, X.-G., Mészáros, P., & Zhang, B. 2015b, ApJ, 810, 160
Gao, H., Zhang, B.-B., & Zhang, B. 2012, ApJ, 748, 134
Gao, Y., & Dai, Z.-G. 2010, RAA, 10, 142
Gehrels, N., Barthelmy, S. D., Burrows, D. N., et al. 2008, ApJ, 689, 1161
Gehrels, N., Chincarini, G., Giommi, P., et al. 2004, ApJ, 611, 1005
Gehrels, N., Norris, J. P., Barthelmy, S. D., et al. 2006, Natur, 444, 1044
Gehrels, N., Ramirez-Ruiz, E., & Fox, D. B. 2009, ARA&A, 47, 567
Gehrels, N., & Razzaque, S. 2013, FrPhy, 8, 661
Geng, J. J., & Huang, Y. F. 2013, ApJ, 764, 75
Geng, J. J., & Huang, Y. F. 2016, AdAst, 2016, 159214
Geng, J. J., Wu, X. F., Huang, Y. F., Li, L., & Dai, Z. G. 2016, ApJ, 825, 107
Ghirlanda, G., Celotti, A., & Ghisellini, G. 2002, A&A, 393, 409
Ghirlanda, G., Ghisellini, G., & Celotti, A. 2004a, A&A, 422, L55
Ghirlanda, G., Ghisellini, G., Firmani, C., Celotti, A., & Bosnjak, Z. 2005, MNRAS, 360, L45
Ghirlanda, G., Ghisellini, G., & Lazzati, D. 2004b, ApJ, 616, 331
Ghirlanda, G., Ghisellini, G., Nava, L., & Burlon, D. 2011, MNRAS, 410, L47
Ghirlanda, G., Nappo, F., Ghisellini, G., et al. 2018, A&A, 609, A112
Ghirlanda, G., Nava, L., & Ghisellini, G. 2010, A&A, 511, A43
Ghirlanda, G., Nava, L., Ghisellini, G., et al. 2012, MNRAS, 420, 483
Ghirlanda, G., Nava, L., Ghisellini, G., Celotti, A., & Firmani, C. 2009, A&A, 496, 585
Ghirlanda, G., Nava, L., Ghisellini, G., & Firmani, C. 2007, A&A, 466, 127
Ghirlanda, G., Nava, L., Ghisellini, G., Firmani, C., & Cabrera, J. I. 2008, MNRAS, 387, 319
Ghirlanda, G., Salvaterra, R., Burlon, D., et al. 2013, MNRAS, 435, 2543
Ghisellini, G., Ghirlanda, G., Nava, L., & Celotti, A. 2010, MNRAS, 403, 926
Ghisellini, G., Ghirlanda, G., & Tavecchio, F. 2007, MNRAS, 375, L36
Ghisellini, G., Nardini, M., Ghirlanda, G., & Celotti, A. 2009, MNRAS, 393, 253
Giannios, D. 2006, A&A, 457, 763
Gibson, S. L., Wynn, G. A., Gompertz, B. P., & O'Brien, P. T. 2017, MNRAS, 470, 4925
Giommi, P., Perri, M., & Fiore, F. 2000, A&A, 362, 799
GLAST Facility Science Team, Gehrels, N., & Michelson, P. 1999, APh, 11, 277
Goldstein, A. 2013a, GCN, 15053, 1
Goldstein, A. 2013b, GCN, 14189, 1
Goldstein, A., Burgess, J. M., Preece, R. D., et al. 2012, ApJS, 199, 19
Goldstein, A., Connaughton, V., Briggs, M. S., & Burns, E. 2016, AAS/High Energy Astrophysics Division, 15, 306.07
Goldstein, A., & Meegan, C. A. 2012, GCN, 13951, 1
Goldstein, A., Preece, R. D., & Briggs, M. S. 2010, ApJ, 721, 1329
Goldstein, A., Preece, R. D., Mallozzi, R. S., et al. 2013, ApJS, 208, 21
Goldstein, A., Veres, P., Burns, E., et al. 2017, ApJL, 848, L14
Golenetskii, S., Aptekar, R., Frederiks, D., et al. 2010a, GCN, 11350, 1
Golenetskii, S., Aptekar, R., Frederiks, D., et al. 2010b, GCN, 11384, 1
Golenetskii, S., Aptekar, R., Frederiks, D., et al. 2011a, GCN, 11893, 1
Golenetskii, S., Aptekar, R., Frederiks, D., et al. 2011b, GCN, 12019, 1
Golenetskii, S., Aptekar, R., Frederiks, D., et al. 2011c, GCN, 12249, 1
Golenetskii, S., Aptekar, R., Frederiks, D., et al. 2011d, GCN, 12278, 1
Golenetskii, S., Aptekar, R., Frederiks, D., et al. 2011e, GCN, 12301, 1
Golenetskii, S., Aptekar, R., Frederiks, D., et al. 2011f, GCN, 12456, 1
Golenetskii, S., Aptekar, R., Frederiks, D., et al. 2011g, GCN, 12532, 1
Golenetskii, S., Aptekar, R., Frederiks, D., et al. 2011h, GCN, 12627, 1
Golenetskii, S., Aptekar, R., Frederiks, D., et al. 2011i, GCN, 12701, 1
Golenetskii, S., Aptekar, R., Frederiks, D., et al. 2012a, GCN, 12824, 1
Golenetskii, S., Aptekar, R., Frederiks, D., et al. 2012b, GCN, 13781, 1
Golenetskii, S., Aptekar, R., Frederiks, D., et al. 2012c, GCN, 12996, 1
Golenetskii, S., Aptekar, R., Frederiks, D., et al. 2012d, GCN, 13758, 1
Golenetskii, S., Aptekar, R., Frederiks, D., et al. 2012e, GCN, 13074, 1
Golenetskii, S., Aptekar, R., Frederiks, D., et al. 2012f, GCN, 13787, 1
Golenetskii, S., Aptekar, R., Frederiks, D., et al. 2012g, GCN, 13103, 1
Golenetskii, S., Aptekar, R., Frederiks, D., et al. 2012h, GCN, 13100, 1
Golenetskii, S., Aptekar, R., Frederiks, D., et al. 2012i, GCN, 13158, 1
Golenetskii, S., Aptekar, R., Frederiks, D., et al. 2012j, GCN, 13268, 1
Golenetskii, S., Aptekar, R., Frederiks, D., et al. 2012k, GCN, 13272, 1
Golenetskii, S., Aptekar, R., Frederiks, D., et al. 2012l, GCN, 13315, 1
Golenetskii, S., Aptekar, R., Frederiks, D., et al. 2012m, GCN, 13341, 1
Golenetskii, S., Aptekar, R., Frederiks, D., et al. 2012n, GCN, 13354, 1
Golenetskii, S., Aptekar, R., Frederiks, D., et al. 2012o, GCN, 13378, 1
Golenetskii, S., Aptekar, R., Frederiks, D., et al. 2012p, GCN, 13445, 1
Golenetskii, S., Aptekar, R., Frederiks, D., et al. 2012q, GCN, 13440, 1
Golenetskii, S., Aptekar, R., Frederiks, D., et al. 2012r, GCN, 13552, 1
Golenetskii, S., Aptekar, R., Frederiks, D., et al. 2012s, GCN, 13707, 1
Golenetskii, S., Aptekar, R., Frederiks, D., et al. 2012t, GCN, 13674, 1
Golenetskii, S., Aptekar, R., Frederiks, D., et al. 2012u, GCN, 13621, 1
Golenetskii, S., Aptekar, R., Frederiks, D., et al. 2012v, GCN, 13676, 1
Golenetskii, S., Aptekar, R., Frederiks, D., et al. 2012w, GCN, 14104, 1
Golenetskii, S., Aptekar, R., Frederiks, D., et al. 2012x, GCN, 14022, 1
Golenetskii, S., Aptekar, R., Frederiks, D., et al. 2012y, GCN, 14005, 1
Golenetskii, S., Aptekar, R., Frederiks, D., et al. 2012z, GCN, 13979, 1
Golenetskii, S., Aptekar, R., Frederiks, D., et al. 2012aa, GCN, 13789, 1
Golenetskii, S., Aptekar, R., Frederiks, D., et al. 2013a, GCN, 15549, 1
Golenetskii, S., Aptekar, R., Frederiks, D., et al. 2013b, GCN, 15125, 1
Golenetskii, S., Aptekar, R., Frederiks, D., et al. 2013c, GCN, 15095, 1
Golenetskii, S., Aptekar, R., Frederiks, D., et al. 2013d, GCN, 15023, 1
Golenetskii, S., Aptekar, R., Frederiks, D., et al. 2013e, GCN, 14872, 1
Golenetskii, S., Aptekar, R., Frederiks, D., et al. 2013f, GCN, 14809, 1
Golenetskii, S., Aptekar, R., Frederiks, D., et al. 2013g, GCN, 14698, 1
Golenetskii, S., Aptekar, R., Frederiks, D., et al. 2013h, GCN, 14356, 1
Golenetskii, S., Aptekar, R., Frederiks, D., et al. 2013i, GCN, 14275, 1
Golenetskii, S., Aptekar, R., Frederiks, D., et al. 2014a, GCN, 16807, 1
Golenetskii, S., Aptekar, R., Frederiks, D., et al. 2014b, GCN, 16755, 1
Golenetskii, S., Aptekar, R., Frederiks, D., et al. 2014c, GCN, 16389, 1
Golenetskii, S., Aptekar, R., Frederiks, D., et al. 2014d, GCN, 16351, 1
Golenetskii, S., Aptekar, R., Frederiks, D., et al. 2014e, GCN, 16328, 1
Golenetskii, S., Aptekar, R., Frederiks, D., et al. 2014f, GCN, 16025, 1
Golenetskii, S., Aptekar, R., Frederiks, D., et al. 2014g, GCN, 15943, 1
Golenetskii, S., Aptekar, R., Frederiks, D., et al. 2015a, GCN, 18356, 1
Golenetskii, S., Aptekar, R., Frederiks, D., et al. 2015b, GCN, 18259, 1
Golenetskii, S., Aptekar, R., Frederiks, D., et al. 2015c, GCN, 18073, 1
Golenetskii, S., Aptekar, R., Frederiks, D., et al. 2015d, GCN, 17918, 1
Golenetskii, S., Aptekar, R., Frederiks, D., et al. 2015e, GCN, 17727, 1
Golenetskii, S., Aptekar, R., Frederiks, D., et al. 2016a, GCN, 18867, 1
Golenetskii, S., Aptekar, R., Frederiks, D., et al. 2016b, GCN, 18837, 1
Golenetskii, S., Aptekar, R., Frederiks, D., et al. 2017, ApJ, 834, 170
Golenetskii, S., Aptekar, R., Mazets, E., et al. 2010c, GCN, 11408, 1
Golenetskii, S., Aptekar, R., Mazets, E., et al. 2011j, GCN, 11951, 1
Golenetskii, S., Aptekar, R., Mazets, E., et al. 2012ab, GCN, 13295, 1
Golenetskii, S., Aptekar, R., Mazets, E., et al. 2012ac, GCN, 13351, 1
Golenetskii, S., Aptekar, R., Mazets, E., et al. 2013j, GCN, 14135, 1
Golenetskii, S., Aptekar, R., Pal'Shin, V., et al. 2014h, GCN, 15754, 1
Golenetskii, S., Aptekar, R., Pal'Shin, V., et al. 2015f, GCN, 17351, 1
Golkhou, V. Z., & Butler, N. R. 2014, AAS/High Energy Astrophysics Division, 14, 112.04
Golkhou, V. Z., Butler, N. R., & Littlejohns, O. M. 2015, ApJ, 811, 93
Gompertz, B., & Fruchter, A. 2017, ApJ, 839, 49
Gorbovskoy, E. S., Lipunov, V. M., Buckley, D. A. H., et al. 2016, MNRAS, 455, 3312
Gorbovskoy, E. S., Lipunova, G. V., Lipunov, V. M., et al. 2012, MNRAS, 421, 1874
Gorosabel, J., Castro-Tirado, A. J., Ramirez-Ruiz, E., et al. 2006, ApJL, 641, L13
Gorosabel, J., Lund, N., Brandt, S., Westergaard, N. J., & Castro Cerón, J. M. 2004, A&A, 427, 87
Graham, J. F., & Fruchter, A. S. 2013, ApJ, 774, 119
Granot, J., Guetta, D., & Gill, R. 2017, ApJL, 850, L24
Greiner, J., Fox, D. B., Schady, P., et al. 2015, ApJ, 809, 76
Greiner, J., Krühler, T., Klose, S., et al. 2011, A&A, 526, A30
Greiner, J., Krühler, T., Nardini, M., et al. 2013, A&A, 560, A70
Greiner, J., Michałowski, M. J., Klose, S., et al. 2016, A&A, 593, A17
Greiner, J., Yu, H.-F., Krühler, T., et al. 2014, A&A, 568, A75
Gruber, D. 2012a, GCN, 13339, 1
Gruber, D. 2012b, GCN, 137541, 1
Gruber, D., Goldstein, A., Weller von Ahlefeld, V., et al. 2014, ApJS, 211, 12
Grupe, D., Nousek, J. A., Veres, P., Zhang, B.-B., & Gehrels, N. 2013, ApJS, 209, 20

Guetta, D., & Pian, E. 2009, arXiv:0910.2134
Guetta, D., Pian, E., & Waxman, E. 2011, A&A, 525, A53
Guidorzi, C., Dichiara, S., & Amati, L. 2016, A&A, 589, A98
Guidorzi, C., Frontera, F., Montanari, E., et al. 2005, MNRAS, 363, 315
Guidorzi, C., Lacapra, M., Frontera, F., et al. 2011, A&A, 526, A49
Guiriec, S., Briggs, M. S., Connaugthon, V., et al. 2010, ApJ, 725, 225
Guiriec, S., Kouveliotou, C., Hartmann, D. H., et al. 2016, ApJL, 831, L8
Hakkila, J., Giblin, T. W., Young, K. C., et al. 2007, ApJS, 169, 62
Hakkila, J., Lien, A., Sakamoto, T., et al. 2015, ApJ, 815, 134
Han, X. H., Hammer, F., Liang, Y. C., et al. 2010, A&A, 514, A24
Hartoog, O. E., Malesani, D., Fynbo, J. P. U., et al. 2015, A&A, 580, A139
Heussaff, V., Atteia, J.-L., & Zolnierowski, Y. 2013, A&A, 557, A100
Hjorth, J., & Bloom, J. S. 2012, in The Gamma-Ray Burst–Supernova Connection, ed. C. Kouveliotou, R. A. M. J. Wijers, & S. Woosley (Cambridge: Cambridge Univ. Press), 169
Hjorth, J., Malesani, D., Jakobsson, P., et al. 2012, ApJ, 756, 187
Hjorth, J., Sollerman, J., Møller, P., et al. 2003, Natur, 423, 847
Horesh, A., Cenko, S. B., Perley, D. A., et al. 2015, ApJ, 812, 86
Horváth, I. 1998, ApJ, 508, 757
Horváth, I. 2002, A&A, 392, 791
Horváth, I. 2009, Ap&SS, 323, 83
Horváth, I., Balázs, L. G., Bagoly, Z., & Veres, P. 2008, A&A, 489, L1
Horváth, I., & Tóth, B. G. 2016, Ap&SS, 361, 155
Hoyle, B., Rau, M. M., Paech, K., et al. 2015, MNRAS, 452, 4183
Hron, K., Filzmoser, P., & Thompson, K. 2012, Journal of Applied Statistics, 14, 1115
Hu, Y.-D., Liang, E.-W., Xi, S.-Q., et al. 2014, ApJ, 789, 145
Huang, K. Y., Urata, Y., Kuo, P. H., et al. 2007, ApJL, 654, L25
Hui, C. M. 2016, GCN, 19198, 1
Hui, C. M., & Bissaldi, E. 2016, GCN, 19056, 1
Huja, D., Mészáros, A., & Řípa, J. 2009, A&A, 504, 67
Hurley, K., Atteia, J.-L., Barraud, C., et al. 2011a, ApJS, 197, 34
Hurley, K., Briggs, M. S., Kippen, R. M., et al. 2011b, ApJS, 196, 1
Hurley, K., Guidorzi, C., Frontera, F., et al. 2010, ApJS, 191, 179
Hurley, K., Pal'shin, V. D., Aptekar, R. L., et al. 2013, ApJS, 207, 39
Ioka, K., Hotokezaka, K., & Piran, T. 2016, ApJ, 833, 110
Irwin, C. M., & Chevalier, R. A. 2016, MNRAS, 460, 1680
Izzo, L., Capozziello, S., Covone, G., & Capaccioli, M. 2009, arXiv:0906.4888
Izzo, L., Muccino, M., Zaninoni, E., Amati, L., & Della Valle, M. 2015, A&A, 582, A115
Japelj, J., Kopač, D., Kobayashi, S., et al. 2014, ApJ, 785, 84
Japelj, J., Vergani, S. D., Salvaterra, R., et al. 2016, A&A, 590, A129
Jenke, P. 2013a, GCN, 15331, 1
Jenke, P. 2013b, GCN, 14663, 1
Jenke, P. 2014a, GCN, 17241, 1
Jenke, P. 2014b, GCN, 17220, 1
Jenke, P. 2014c, GCN, 17094, 1
Jenke, P. 2014d, GCN, 16762, 1
Jenke, P. 2014e, GCN, 16115, 1
Jenke, P. 2015a, GCN, 18130, 1
Jenke, P. 2015b, GCN, 18015, 1
Jenke, P. 2015c, GCN, 17994, 1
Jenke, P., & Fitzpatrick, G. 2014, GCN, 16084, 1
Jenke, P., & von Kienlin, A. 2015, GCN, 17364, 1
Jenke, P., von Kienlin, A., & Burns, E. 2014, GCN, 17189, 1
Jenke, P., & Yu, H.-F. 2014, GCN, 16599, 1
Jeong, S., Castro-Tirado, A. J., Bremer, M., et al. 2014, A&A, 569, A93
Jia, L.-W., Uhm, Z. L., & Zhang, B. 2016, ApJS, 225, 17
Jimenez, R., Band, D., & Piran, T. 2001, ApJ, 561, 171
Jin, Z.-P., Hotokezaka, K., Li, X., et al. 2016, NatCo, 7, 12898
Kagawa, Y., Yonetoku, D., Sawano, T., et al. 2015, ApJ, 811, 4
Kaneko, Y., Bostancı, Z. F., Göğüş, E., & Lin, L. 2015, MNRAS, 452, 824
Kaneko, Y., Preece, R. D., Briggs, M. S., et al. 2006, ApJS, 166, 298
Kann, D. A., Klose, S., Zhang, B., et al. 2010, ApJ, 720, 1513
Kann, D. A., Schady, P., Olivares, E. F., et al. 2019, A&A, 624, A143
Kasliwal, M. M., Cenko, S. B., Kulkarni, S. R., et al. 2008, ApJ, 678, 1127
Katz, J. I. 1994, ApJL, 432, L107
Kawakubo, Y., Yoshida, A., Sakamoto, T., et al. 2015, GCN, 18724, 1
Kelly, P. L., Filippenko, A. V., Fox, O. D., Zheng, W., & Clubb, K. I. 2013, ApJL, 775, L5
Kelly, P. L., & Kirshner, R. P. 2012, ApJ, 759, 107
Kendall, M. G. 1938, Biometrika, 30, 81
Kewley, L. J., & Ellison, S. L. 2008, ApJ, 681, 1183
King, A., Olsson, E., & Davies, M. B. 2007, MNRAS, 374, L34
Klebesadel, R. W., Strong, I. B., & Olson, R. A. 1973, ApJL, 182, L85
Kobulnicky, H. A., & Kewley, L. J. 2004, ApJ, 617, 240
Kocevski, D., Ryde, F., & Liang, E. 2003, ApJ, 596, 389
Kocevski, D., & West, A. A. 2011, ApJL, 735, L8
Kopač, D., D'Avanzo, P., Melandri, A., et al. 2012, MNRAS, 424, 2392
Kopač, D., Kobayashi, S., Gomboc, A., et al. 2013, ApJ, 772, 73
Kopač, D., Mundell, C. G., Japelj, J., et al. 2015, ApJ, 813, 1
Kounine, A. 2012, IJMPE, 21, 1230005
Kouveliotou, C., Meegan, C. A., Fishman, G. J., et al. 1993, ApJL, 413, L101
Kouveliotou, C., Wijers, R. A., & Woosley, S. 2012, Gamma-ray Bursts, Vol. 51 (Cambridge: Cambridge Univ. Press)
Krimm, H. A., Barthelmy, S. D., Baumgartner, W. H., et al. 2010a, GCN, 11312, 1
Krimm, H. A., Barthelmy, S. D., Baumgartner, W. H., et al. 2010b, GCN, 10964, 1
Krimm, H. A., Barthelmy, S. D., Baumgartner, W. H., et al. 2011a, GCN, 11793, 1
Krimm, H. A., Barthelmy, S. D., Baumgartner, W. H., et al. 2011b, GCN, 12476, 1
Krimm, H. A., Barthelmy, S. D., Baumgartner, W. H., et al. 2013a, GCN, 15499, 1
Krimm, H. A., Barthelmy, S. D., Baumgartner, W. H., et al. 2013b, GCN, 14833, 1
Krimm, H. A., Barthelmy, S. D., Baumgartner, W. H., et al. 2013c, GCN, 14726, 1
Krimm, H. A., Barthelmy, S. D., Baumgartner, W. H., et al. 2013d, GCN, 14399, 1
Krimm, H. A., Barthelmy, S. D., Baumgartner, W. H., et al. 2014a, GCN, 17083, 1
Krimm, H. A., Barthelmy, S. D., Baumgartner, W. H., et al. 2014b, GCN, 16893, 1
Krimm, H. A., Barthelmy, S. D., Baumgartner, W. H., et al. 2014c, GCN, 16721, 1
Krimm, H. A., Barthelmy, S. D., Baumgartner, W. H., et al. 2014d, GCN, 16370, 1
Krimm, H. A., Barthelmy, S. D., Baumgartner, W. H., et al. 2014e, GCN, 16186, 1
Krimm, H. A., Barthelmy, S. D., Baumgartner, W. H., et al. 2014f, GCN, 15962, 1
Krimm, H. A., Barthelmy, S. D., Baumgartner, W. H., et al. 2014g, GCN, 15738, 1
Krimm, H. A., Barthelmy, S. D., Baumgartner, W. H., et al. 2015a, GCN, 17795, 1
Krimm, H. A., Barthelmy, S. D., Baumgartner, W. H., et al. 2015b, GCN, 17596, 1
Krimm, H. A., Barthelmy, S. D., Baumgartner, W. H., et al. 2015c, GCN, 17471, 1
Krimm, H. A., Barthelmy, S. D., Cummings, J. R., et al. 2015d, GCN, 18752, 1
Krimm, H. A., Barthelmy, S. D., Cummings, J. R., et al. 2015e, GCN, 18593, 1
Krimm, H. A., Barthelmy, S. D., Cummings, J. R., et al. 2015f, GCN, 18429, 1
Krimm, H. A., Barthelmy, S. D., Cummings, J. R., et al. 2015g, GCN, 18256, 1
Krimm, H. A., Barthelmy, S. D., Cummings, J. R., et al. 2015h, GCN, 18129, 1
Krimm, H. A., Barthelmy, S. D., Cummings, J. R., et al. 2015i, GCN, 18020, 1
Krimm, H. A., Barthelmy, S. D., Cummings, J. R., et al. 2016a, GCN, 19216, 1
Krimm, H. A., Barthelmy, S. D., Cummings, J. R., et al. 2016b, GCN, 19038, 1
Krimm, H. A., & Cummings, J. R. 2013, GCN, 14694, 1
Krimm, H. A., Yamaoka, K., Sugita, S., et al. 2009, ApJ, 704, 1405
Krühler, T., Greiner, J., Afonso, P., et al. 2009, A&A, 508, 593
Krühler, T., Greiner, J., Schady, P., et al. 2011, A&A, 534, A108
Krühler, T., Ledoux, C., Fynbo, J. P. U., et al. 2013, A&A, 557, A18
Krühler, T., Malesani, D., Fynbo, J. P. U., et al. 2015, A&A, 581, A125
Kulkarni, S., & Desai, S. 2017, Ap&SS, 362, 70
Kumar, P., & Zhang, B. 2015, PhR, 561, 1
Lamb, D. Q., Ricker, G. R., Atteia, J.-L., et al. 2004, NewAR, 48, 423
Laskar, T., Alexander, K. D., Berger, E., et al. 2016, ApJ, 833, 88
Laskar, T., Berger, E., Margutti, R., et al. 2015, ApJ, 814, 1
Lee, H. K., Wijers, R. A. M. J., & Brown, G. E. 2000, PhR, 325, 83
Le Floc'h, E., Duc, P.-A., Mirabel, I. F., et al. 2002, ApJL, 581, L81
Leibler, C. N., & Berger, E. 2010, ApJ, 725, 1202
Lennarz, D., & Taboada, I. 2015, Proc. ICRC (The Hague, The Netherlands), 34, 715
Levan, A. J., Tanvir, N. R., Starling, R. L. C., et al. 2014, ApJ, 781, 13
Levesque, E. M., Bloom, J. S., Butler, N. R., et al. 2010a, MNRAS, 401, 963
Levesque, E. M., Kewley, L. J., Berger, E., & Zahid, H. J. 2010b, AJ, 140, 1557
Levesque, E. M., Soderberg, A. M., Kewley, L. J., & Berger, E. 2010c, ApJ, 725, 1337
Li, L., Liang, E.-W., Tang, Q.-W., et al. 2012a, ApJ, 758, 27

Li, L.-B., Zhang, Z.-B., Huang, Y.-F., et al. 2015, MNRAS, 451, 1815
Li, L.-X., & Paczyński, B. 1998, ApJL, 507, L59
Li, M.-H., & Lin, H.-N. 2015, A&A, 582, A111
Li, Y., Li, A., & Wei, D. M. 2008, in AIP Conf. Ser. 1065, 2008 Nanjing Gamma-Ray Burst Conf., ed. Y.-F. Huang, Z.-G. Dai, & B. Zhang (Melville, NY: AIP), 123
Li, Y., Zhang, B., & Lü, H.-J. 2016, ApJS, 227, 7
Li, Z., Chen, L., & Wang, D. 2012b, PASP, 124, 297
Liang, E., & Zhang, B. 2005, ApJ, 633, 611
Liang, E.-W., Lin, T.-T., Lü, J., et al. 2015, ApJ, 813, 116
Liang, E.-W., Lü, H.-J., Hou, S.-J., Zhang, B.-B., & Zhang, B. 2009, ApJ, 707, 328
Liang, E.-W., Racusin, J. L., Zhang, B., Zhang, B.-B., & Burrows, D. N. 2008a, ApJ, 675, 528
Liang, E.-W., Yi, S.-X., Zhang, J., et al. 2010, ApJ, 725, 2209
Liang, E.-W., Zhang, B.-B., & Zhang, B. 2008b, in AIP Conf. Ser. 1065, 2008 Nanjing Gamma-Ray Burst Conf., ed. Y.-F. Huang, Z.-G. Dai, & B. Zhang (Melville, NY: AIP), 25
Lien, A., Sakamoto, T., Barthelmy, S. D., et al. 2016a, ApJ, 829, 7
Lien, A. Y., Barthelmy, S. D., Baumgartner, W. H., et al. 2013a, GCN, 15508, 1
Lien, A. Y., Barthelmy, S. D., Baumgartner, W. H., et al. 2014a, GCN, 17127, 1
Lien, A. Y., Barthelmy, S. D., Baumgartner, W. H., et al. 2014b, GCN, 16916, 1
Lien, A. Y., Barthelmy, S. D., Baumgartner, W. H., et al. 2014c, GCN, 16736, 1
Lien, A. Y., Barthelmy, S. D., Baumgartner, W. H., et al. 2015a, GCN, 17880, 1
Lien, A. Y., Barthelmy, S. D., Baumgartner, W. H., et al. 2015b, GCN, 17814, 1
Lien, A. Y., Barthelmy, S. D., Baumgartner, W. H., et al. 2015c, GCN, 17604, 1
Lien, A. Y., Barthelmy, S. D., Baumgartner, W. H., et al. 2015d, GCN, 17329, 1
Lien, A. Y., Barthelmy, S. D., Cummings, J. R., et al. 2013b, GCN, 15234, 1
Lien, A. Y., Barthelmy, S. D., Cummings, J. R., et al. 2013c, GCN, 15076, 1
Lien, A. Y., Barthelmy, S. D., Cummings, J. R., et al. 2015e, GCN, 18751, 1
Lien, A. Y., Barthelmy, S. D., Cummings, J. R., et al. 2015f, GCN, 18604, 1
Lien, A. Y., Barthelmy, S. D., Cummings, J. R., et al. 2015g, GCN, 18452, 1
Lien, A. Y., Barthelmy, S. D., Cummings, J. R., et al. 2015h, GCN, 18268, 1
Lien, A. Y., Barthelmy, S. D., Cummings, J. R., et al. 2015i, GCN, 18038, 1
Lien, A. Y., Barthelmy, S. D., Cummings, J. R., et al. 2015j, GCN, 18034, 1
Lien, A. Y., Barthelmy, S. D., Cummings, J. R., et al. 2016b, GCN, 19234, 1
Lien, A. Y., Barthelmy, S. D., Cummings, J. R., et al. 2016c, GCN, 19043, 1
Lin, H.-N., Li, X., & Chang, Z. 2016, MNRAS, 459, 2501
Lin, L. 2011, GCN, 11952, 1
Lipunov, V. M., Gorosabel, J., Pruzhinskaya, M. V., et al. 2016, MNRAS, 455, 712
Little, R. J. A. 1988, Journal of Business Economic Statistics, 6, 287
Littlejohns, O. M., Butler, N. R., Cucchiara, A., et al. 2015, MNRAS, 449, 2919
Liu, T., Lin, Y.-Q., Hou, S.-J., & Gu, W.-M. 2015, ApJ, 806, 58
Liu, T., Xue, L., Zhao, X.-H., Zhang, F.-W., & Zhang, B. 2016, ApJ, 821, 132
Lloyd, N. M., & Petrosian, V. 1999, ApJ, 511, 550
Lloyd, N. M., Petrosian, V., & Mallozzi, R. S. 2000a, ApJ, 534, 227
Lloyd, N. M., Petrosian, V., & Preece, R. D. 2000b, in AIP Conf. Ser. 526. Gamma-ray Bursts, 5th Huntsville Symp., ed. R. M. Kippen, R. S. Mallozzi, & G. J. Fishman (Melville, NY: AIP), 155
Lloyd-Ronning, N. M., & Petrosian, V. 2002, ApJ, 565, 182
Lloyd-Ronning, N. M., & Ramirez-Ruiz, E. 2002, ApJ, 576, 101
Lü, H.-J., & Zhang, B. 2014, ApJ, 785, 74
Lü, H.-J., Zhang, B., Liang, E.-W., Zhang, B.-B., & Sakamoto, T. 2014, MNRAS, 442, 1922
Lü, J., Zou, Y.-C., Lei, W.-H., et al. 2012, ApJ, 751, 49
Lu, R.-J., Hou, S.-J., & Liang, E.-W. 2010, ApJ, 720, 1146
Lu, R.-J., Wei, J.-J., Liang, E.-W., et al. 2012a, ApJ, 756, 112
Lu, R.-J., Wei, J.-J., Qin, S.-F., & Liang, E.-W. 2012b, ApJ, 745, 168
Lu, Y., Huang, Y. F., & Zhang, S. N. 2008, ApJ, 684, 1330
Lundman, C., Pe'er, A., & Ryde, F. 2013, MNRAS, 428, 2430
Lyutikov, M., & Toonen, S. 2017, arXiv:1709.02221
MacLachlan, G. A., Shenoy, A., Sonbas, E., et al. 2013, MNRAS, 432, 857
Maeder, A., & Meynet, G. 2012, RvMP, 84, 25
Maiolino, R., Nagao, T., Grazian, A., et al. 2008, A&A, 488, 463
Malesani, D., Covino, S., D'Avanzo, P., et al. 2007, A&A, 473, 77
Malesani, D., Tanvir, N. R., Kruehler, T., et al. 2015, GCN, 18540, 1
Mallozzi, R. S., Paciesas, W. S., Pendleton, G. N., et al. 1995, ApJ, 454, 597
Mangano, V., Sbarufatti, B., & Stratta, G. 2012, MSAIS, 21, 143
Mannucci, F., Salvaterra, R., & Campisi, M. A. 2011, MNRAS, 414, 1263
Margutti, R., Berger, E., Fong, W., et al. 2012, ApJ, 756, 63
Margutti, R., Zaninoni, E., Bernardini, M. G., et al. 2013, MNRAS, 428, 729
Markwardt, C. B., Amaral-Rogers, A., Barthelmy, S. D., et al. 2015a, GCN, 18622, 1
Markwardt, C. B., Amaral-Rogers, A., Barthelmy, S. D., et al. 2015b, GCN, 17628, 1
Markwardt, C. B., Barthelmy, S. D., Baumgartner, W. H., et al. 2010, GCN, 10972, 1
Markwardt, C. B., Barthelmy, S. D., Baumgartner, W. H., et al. 2011a, GCN, 12620, 1
Markwardt, C. B., Barthelmy, S. D., Baumgartner, W. H., et al. 2011b, GCN, 12485, 1
Markwardt, C. B., Barthelmy, S. D., Baumgartner, W. H., et al. 2011c, GCN, 11804, 1
Markwardt, C. B., Barthelmy, S. D., Baumgartner, W. H., et al. 2012a, GCN, 13154, 1
Markwardt, C. B., Barthelmy, S. D., Baumgartner, W. H., et al. 2012b, GCN, 13333, 1
Markwardt, C. B., Barthelmy, S. D., Baumgartner, W. H., et al. 2012c, GCN, 13807, 1
Markwardt, C. B., Barthelmy, S. D., Baumgartner, W. H., et al. 2012d, GCN, 13535, 1
Markwardt, C. B., Barthelmy, S. D., Baumgartner, W. H., et al. 2012e, GCN, 12998, 1
Markwardt, C. B., Barthelmy, S. D., Baumgartner, W. H., et al. 2013a, GCN, 15521, 1
Markwardt, C. B., Barthelmy, S. D., Baumgartner, W. H., et al. 2013b, GCN, 14133, 1
Markwardt, C. B., Barthelmy, S. D., Baumgartner, W. H., et al. 2014a, GCN, 17140, 1
Markwardt, C. B., Barthelmy, S. D., Baumgartner, W. H., et al. 2014b, GCN, 16927, 1
Markwardt, C. B., Barthelmy, S. D., Baumgartner, W. H., et al. 2014c, GCN, 16756, 1
Markwardt, C. B., Barthelmy, S. D., Baumgartner, W. H., et al. 2014d, GCN, 16402, 1
Markwardt, C. B., Barthelmy, S. D., Baumgartner, W. H., et al. 2014e, GCN, 15996, 1
Markwardt, C. B., Barthelmy, S. D., Baumgartner, W. H., et al. 2014f, GCN, 15769, 1
Markwardt, C. B., Barthelmy, S. D., Baumgartner, W. H., et al. 2015c, GCN, 18292, 1
Markwardt, C. B., Barthelmy, S. D., Baumgartner, W. H., et al. 2015d, GCN, 18148, 1
Markwardt, C. B., Barthelmy, S. D., Baumgartner, W. H., et al. 2015e, GCN, 18048, 1
Markwardt, C. B., Barthelmy, S. D., Baumgartner, W. H., et al. 2015f, GCN, 17890, 1
Markwardt, C. B., Barthelmy, S. D., Baumgartner, W. H., et al. 2015g, GCN, 17491, 1
Markwardt, C. B., Barthelmy, S. D., Baumgartner, W. H., et al. 2015h, GCN, 17330, 1
Markwardt, C. B., Barthelmy, S. D., Cummings, J. R., et al. 2013c, GCN, 15083, 1
Markwardt, C. B., Barthelmy, S. D., Cummings, J. R., et al. 2015i, GCN, 18469, 1
Markwardt, C. B., Barthelmy, S. D., Cummings, J. R., et al. 2016a, GCN, 19240, 1
Markwardt, C. B., Barthelmy, S. D., Cummings, J. R., et al. 2016b, GCN, 19066, 1
Mazets, E. P., Aptekar, R. L., Frederiks, D. D., et al. 2002, arXiv:astro-ph/0209219
McGlynn, S. 2012, GCN, 13741, 1
Meegan, C., Lichti, G., Bhat, P. N., et al. 2009, ApJ, 702, 791
Meegan, C. A., Fishman, G. J., Wilson, R. B., et al. 1992, Natur, 355, 143
Meegan, C. A., Pendleton, G. N., Briggs, M. S., et al. 1996, ApJS, 106, 65
Melandri, A., Bernardini, M. G., D'Avanzo, P., et al. 2015, A&A, 581, A86
Melandri, A., Covino, S., Rogantini, D., et al. 2014, A&A, 565, A72
Melandri, A., Mundell, C. G., Kobayashi, S., et al. 2008, ApJ, 686, 1209
Melandri, A., Sbarufatti, B., D'Avanzo, P., et al. 2012, MNRAS, 421, 1265
Mereghetti, S., Götz, D., Borkowski, J., Walter, R., & Pedersen, H. 2003, A&A, 411, L291
Mereghetti, S., Gotz, D., Ferrigno, C., Bozzo, E., & Borkowski, J. 2015, GCN, 17476, 1
Mereghetti, S., Gotz, D., Ferrigno, C., Bozzo, E., & Borkowski, J. 2016, GCN, 19251, 1

Mészáros, A., Řípa, J., & Ryde, F. 2011, A&A, 529, A55
Mészáros, P. 1998, in AIP Conf. Proc. 428, 4th Huntsville Gamma-ray Burst Symp. (Melville, NY: AIP), 647
Mészáros, P. 2006, RPPh, 69, 2259
Mészáros, P., & Rees, M. J. 2000, ApJ, 530, 292
Mészáros, P., & Rees, M. J. 2001, ApJL, 556, L37
Metzger, B. D., Martínez-Pinedo, G., Darbha, S., et al. 2010, MNRAS, 406, 2650
Michałowski, M. J., Gentile, G., Hjorth, J., et al. 2015, A&A, 582, A78
Minaev, P. Y., Pozanenko, A. S., & Loznikov, V. M. 2010, AstL, 36, 707
Minaev, P. Y., Pozanenko, A. S., Molkov, S. V., & Grebenev, S. A. 2014, AstL, 40, 235
Molinari, E., Vergani, S. D., Malesani, D., et al. 2007, A&A, 469, L13
Morgan, A. N., Long, J., Richards, J. W., et al. 2012, ApJ, 746, 170
Moriyama, M., Yoshida, A., Sakamoto, T., et al. 2016, GCN, 18810, 1
Mosquera Cuesta, H. J., Dumet, M. H., & Furlanetto, C. 2008, JCAP, 7, 004
Nagao, T., Maiolino, R., & Marconi, A. 2006, A&A, 459, 85
Nakahira, S., Yoshida, A., Sakamoto, T., et al. 2016, GCN, 18845, 1
Nakar, E. 2007, PhR, 442, 166
Nakar, E., & Piran, T. 2005, MNRAS, 360, L73
Nappo, F., Ghisellini, G., Ghirlanda, G., et al. 2014, MNRAS, 445, 1625
Nappo, F., Pescalli, A., Oganesyan, G., et al. 2017, A&A, 598, A23
Narayan, R., Paczynski, B., & Piran, T. 1992, ApJL, 395, L83
Narayana Bhat, P., Meegan, C. A., von Kienlin, A., et al. 2016, ApJS, 223, 28
Nardini, M., Elliott, J., Filgas, R., et al. 2014, A&A, 562, A29
Nardini, M., Ghisellini, G., Ghirlanda, G., & Celotti, A. 2010, MNRAS, 403, 1131
Nardini, M., Greiner, J., Krühler, T., et al. 2011, A&A, 531, A39
Nava, L., Ghirlanda, G., Ghisellini, G., & Celotti, A. 2011, A&A, 530, A21
Nava, L., Ghirlanda, G., Ghisellini, G., & Firmani, C. 2008, MNRAS, 391, 639
Nava, L., Salvaterra, R., Ghirlanda, G., et al. 2012, MNRAS, 421, 1256
Nava, L., Sironi, L., Ghisellini, G., Celotti, A., & Ghirlanda, G. 2013, MNRAS, 433, 2107
Nemmen, R. S., Georganopoulos, M., Guiriec, S., et al. 2012, Sci, 338, 1445
Nicuesa Guelbenzu, A., Klose, S., Michałowski, M. J., et al. 2014, ApJ, 789, 45
Nicuesa Guelbenzu, A., Klose, S., Palazzi, E., et al. 2015, A&A, 583, A88
Niino, Y., Aoki, K., Hashimoto, T., et al. 2016, LPICo, 1962, 4039
Norris, J., & Barthelmy, S. D. 2012, GCN, 13015, 1
Norris, J., Sakamoto, T., Barthelmy, S. D., & Gehrels, N. 2013, GCN, 14306, 1
Norris, J. P., & Bonnell, J. T. 2006, ApJ, 643, 266
Norris, J. P., Gehrels, N., & Scargle, J. D. 2010, ApJ, 717, 411
Norris, J. P., Marani, G. F., & Bonnell, J. T. 2000, ApJ, 534, 248
Nysewander, M., Fruchter, A. S., & Pe'er, A. 2009, ApJ, 701, 824
Oates, S. R., Page, M. J., De Pasquale, M., et al. 2012, MNRAS, 426, L86
Oates, S. R., Page, M. J., Schady, P., et al. 2009, MNRAS, 395, 490
Oates, S. R., Racusin, J. L., De Pasquale, M., et al. 2015, MNRAS, 453, 4121
Oates, S. R., Racusin, J. L., & De Pasquale, M. 2016, LPICo, 1962, 4060
Ozawa, S., Yoshida, A., Sakamoto, T., et al. 2016, GCN, 19085, 1
Paciesas, W. S., Meegan, C. A., Pendleton, G. N., et al. 1999, ApJS, 122, 465
Paciesas, W. S., Meegan, C. A., von Kienlin, A., et al. 2012, ApJS, 199, 18
Paczynski, B. 1991, AcA, 41, 257
Page, K. L., Starling, R. L. C., Fitzpatrick, G., et al. 2011, MNRAS, 416, 2078
Pal'shin, V. D., Hurley, K., Svinkin, D. S., et al. 2013, ApJS, 207, 38
Palmer, D. M., Amaral-Rogers, A., Barthelmy, S. D., et al. 2015a, GCN, 17637, 1
Palmer, D. M., Barthelmy, S. D., Baumgartner, W. H., et al. 2010a, GCN, 10988, 1
Palmer, D. M., Barthelmy, S. D., Baumgartner, W. H., et al. 2010b, GCN, 10509, 1
Palmer, D. M., Barthelmy, S. D., Baumgartner, W. H., et al. 2010c, GCN, 10351, 1
Palmer, D. M., Barthelmy, S. D., Baumgartner, W. H., et al. 2011a, GCN, 11818, 1
Palmer, D. M., Barthelmy, S. D., Baumgartner, W. H., et al. 2011b, GCN, 12292, 1
Palmer, D. M., Barthelmy, S. D., Baumgartner, W. H., et al. 2011c, GCN, 12504, 1
Palmer, D. M., Barthelmy, S. D., Baumgartner, W. H., et al. 2012a, GCN, 13007, 1
Palmer, D. M., Barthelmy, S. D., Baumgartner, W. H., et al. 2012b, GCN, 13186, 1
Palmer, D. M., Barthelmy, S. D., Baumgartner, W. H., et al. 2012c, GCN, 13360, 1
Palmer, D. M., Barthelmy, S. D., Baumgartner, W. H., et al. 2012d, GCN, 13669, 1
Palmer, D. M., Barthelmy, S. D., Baumgartner, W. H., et al. 2012e, GCN, 13828, 1
Palmer, D. M., Barthelmy, S. D., Baumgartner, W. H., et al. 2013a, GCN, 15272, 1
Palmer, D. M., Barthelmy, S. D., Baumgartner, W. H., et al. 2013b, GCN, 15092, 1
Palmer, D. M., Barthelmy, S. D., Baumgartner, W. H., et al. 2013c, GCN, 14925, 1
Palmer, D. M., Barthelmy, S. D., Baumgartner, W. H., et al. 2013d, GCN, 14554, 1
Palmer, D. M., Barthelmy, S. D., Baumgartner, W. H., et al. 2013e, GCN, 14163, 1
Palmer, D. M., Barthelmy, S. D., Baumgartner, W. H., et al. 2014a, GCN, 17175, 1
Palmer, D. M., Barthelmy, S. D., Baumgartner, W. H., et al. 2014b, GCN, 16935, 1
Palmer, D. M., Barthelmy, S. D., Baumgartner, W. H., et al. 2014c, GCN, 16768, 1
Palmer, D. M., Barthelmy, S. D., Baumgartner, W. H., et al. 2014d, GCN, 16423, 1
Palmer, D. M., Barthelmy, S. D., Baumgartner, W. H., et al. 2014e, GCN, 16240, 1
Palmer, D. M., Barthelmy, S. D., Baumgartner, W. H., et al. 2014f, GCN, 15774, 1
Palmer, D. M., Barthelmy, S. D., Baumgartner, W. H., et al. 2015b, GCN, 17907, 1
Palmer, D. M., Barthelmy, S. D., Baumgartner, W. H., et al. 2015c, GCN, 17374, 1
Palmer, D. M., Barthelmy, S. D., Cummings, J. R., et al. 2015d, GCN, 18496, 1
Palmer, D. M., Barthelmy, S. D., Cummings, J. R., et al. 2015e, GCN, 18328, 1
Palmer, D. M., Barthelmy, S. D., Cummings, J. R., et al. 2015f, GCN, 18157, 1
Palmer, D. M., Barthelmy, S. D., Cummings, J. R., et al. 2015g, GCN, 18055, 1
Palmer, D. M., Barthelmy, S. D., Cummings, J. R., et al. 2016a, GCN, 19263, 1
Palmer, D. M., Barthelmy, S. D., Cummings, J. R., et al. 2016b, GCN, 19091, 1
Palmer, D. M., Barthelmy, S. D., Cummings, J. R., et al. 2016c, GCN, 18882, 1
Palmer, D. M., Barthelmy, S. D., Cummings, J. R., et al. 2016d, GCN, 18829, 1
Pe'er, A., Barlow, H., O'Mahony, S., et al. 2015, ApJ, 813, 127
Pe'er, A., Mészáros, P., & Rees, M. J. 2006a, ApJ, 642, 995
Pe'er, A., Mészáros, P., & Rees, M. J. 2006b, ApJ, 652, 482
Pe'er, A., Ryde, F., Wijers, R. A. M. J., Mészáros, P., & Rees, M. J. 2007, ApJL, 664, L1
Pearson, K. 1895, RSPS, 58, 240
Pélangeon, A., Atteia, J.-L., Nakagawa, Y. E., et al. 2008, A&A, 491, 157
Pelassa, V. 2012a, GCN, 13013, 1
Pelassa, V. 2012b, GCN, 13872, 1
Pelassa, V. 2012c, GCN, 13773, 1
Pelassa, V. 2013a, GCN, 15599, 1
Pelassa, V. 2013b, GCN, 14962, 1
Pelassa, V. 2013c, GCN, 14271, 1
Pelassa, V. 2013d, GCN, 14154, 1
Pelassa, V. 2014a, GCN, 16900, 1
Pelassa, V. 2014b, GCN, 16835, 1
Pelassa, V. 2014c, GCN, 16658, 1
Pelassa, V. 2015, GCN, 17388, 1
Pelassa, V., & Connaughton, V. 2012, GCN, 13771, 1
Pelassa, V., Fitzpatrick, G., Meegan, C., & Bhat, N. 2014, GCN, 16066, 1
Pelassa, V., & Meegan, C. 2013, GCN, 15573, 1
Pelassa, V., & Yu, H.-F. 2015, GCN, 17389, 1
Peng, Z. Y., Zhao, X. H., Yin, Y., Bao, Y. Y., & Ma, L. 2012, ApJ, 752, 132
Perets, H. B., Li, Z., Lombardi, J. C., Jr., & Milcarek, S. R., Jr. 2016, ApJ, 823, 113
Perley, D. A., Bloom, J. S., Butler, N. R., et al. 2008, ApJ, 672, 449
Perley, D. A., Bloom, J. S., Klein, C. R., et al. 2010, MNRAS, 406, 2473
Perley, D. A., Cenko, S. B., Bloom, J. S., et al. 2009, AAS Meeting, 214, 603.18
Perley, D. A., Cenko, S. B., Corsi, A., et al. 2014, ApJ, 781, 37
Perley, D. A., Krühler, T., Schulze, S., et al. 2016a, ApJ, 817, 7
Perley, D. A., Levan, A. J., Tanvir, N. R., et al. 2013, ApJ, 778, 128
Perley, D. A., Morgan, A. N., Updike, A., et al. 2011, AJ, 141, 36
Perley, D. A., Perley, R. A., Hjorth, J., et al. 2015, ApJ, 801, 102
Perley, D. A., Tanvir, N. R., Hjorth, J., et al. 2016b, ApJ, 817, 8
Pescalli, A., Ghirlanda, G., Salvaterra, R., et al. 2016, A&A, 587, A40

Piran, T. 1999, PhR, 314, 575
Piran, T. 2004, RvMP, 76, 1143
Piran, T., Shemi, A., & Narayan, R. 1993, MNRAS, 263, 861
Piranomonte, S., Japelj, J., Vergani, S. D., et al. 2015, MNRAS, 452, 3293
Piro, A. L., & Thrane, E. 2012, ApJ, 761, 63
Planck Collaboration, Ade, P. A. R., Aghanim, N., et al. 2016, A&A, 594, A13
Postnov, K. A. 2000, arXiv:astro-ph/0010031
Pozanenko, A. S., Barkov, M. V., Minaev, P. Y., et al. 2018, ApJL, 852, L30
Preece, R. D., Briggs, M. S., Mallozzi, R. S., et al. 2000, ApJS, 126, 19
Prochaska, J. X., Chen, H.-W., Bloom, J. S., et al. 2007, ApJS, 168, 231
Produit, N., Bao, T. W., Batsch, T., et al. 2018, NIMPA, 877, 259
Qin, Y., Liang, E.-W., Liang, Y.-F., et al. 2013, ApJ, 763, 15
Qin, Y.-P., & Chen, Z.-F. 2013, MNRAS, 430, 163
Quilligan, F., McBreen, B., Hanlon, L., et al. 2002, A&A, 385, 377
Racusin, J. L., Oates, S. R., de Pasquale, M., & Kocevski, D. 2016, ApJ, 826, 45
Rácz, I. I., Balázs, L. G., Horvath, I., Tóth, L. V., & Bagoly, Z. 2018, MNRAS, 475, 306
Ramirez-Ruiz, E., Lazzati, D., & Blain, A. W. 2002, ApJL, 565, L9
Rau, A. 2012, GCN, 12950, 1
Rau, A. 2013, GCN, 14435, 1
Rau, A., Kienlin, A. V., Hurley, K., & Lichti, G. G. 2005, A&A, 438, 1175
Rau, A., & Meegan, C. 2012, GCN, 12806, 1
Rau, A., Savaglio, S., Krühler, T., et al. 2010, ApJ, 720, 862
Rea, N., Gullón, M., Pons, J. A., et al. 2015, ApJ, 813, 92
Rees, M. J., & Meszaros, P. 1992, MNRAS, 258, 41P
Rees, M. J., & Meszaros, P. 1994, ApJL, 430, L93
Rees, M. J., & Mészáros, P. 2005, ApJ, 628, 847
Reichart, D. E., Lamb, D. Q., Fenimore, E. E., et al. 2001, ApJ, 552, 57
Resmi, L. 2017, JApA, 38, 56
Ricciarini, S., Yoshida, A., Sakamoto, T., et al. 2016, GCN, 19345, 1
Ricker, G. R., Atteia, J.-L., Crew, G. B., et al. 2003, in AIP Conf. Ser. 662, Gamma-Ray Burst and Afterglow Astronomy 2001: A Workshop Celebrating the First Year of the HETE Mission, ed. G. R. Ricker & R. K. Vanderspek (Melville, NY: AIP), 3
Ripa, J. 2011, PhD thesis
Řípa, J., Mészáros, A., Veres, P., & Park, I. H. 2012, ApJ, 756, 44
Řípa, J., Mészáros, A., Wigger, C., et al. 2009, A&A, 498, 399
Rizzuto, D., Guidorzi, C., Romano, P., et al. 2007, MNRAS, 379, 619
Roberts, O. 2014a, GCN, 16889, 1
Roberts, O. 2014b, GCN, 16708, 1
Roberts, O., & Meegan, C. 2014, GCN, 16700, 1
Roberts, O., & Stanbro, M. 2014, GCN, 16680, 1
Roberts, O. J. 2014c, GCN, 16971, 1
Roberts, O. J. 2014d, GCN, 17249, 1
Roberts, O. J. 2014e, GCN, 17143, 1
Roberts, O. J. 2014f, GCN, 17133, 1
Roberts, O. J. 2014g, GCN, 17001, 1
Roberts, O. J. 2014h, GCN, 16987, 1
Roberts, O. J. 2015a, GCN, 18190, 1
Roberts, O. J. 2015b, GCN, 17906, 1
Roberts, O. J. 2016, GCN, 19265, 1
Roberts, O. J., & Burns, E. 2016, GCN, 18861, 1
Roberts, O. J., Fitzpatrick, G., & Veres, P. 2016, GCN, 19411, 1
Roberts, O. J., & Stanbro, M. 2015, GCN, 17561, 1
Roberts, O. J., von Kienlin, A., & Meegan, C. 2015a, GCN, 18358, 1
Roberts, O. J., & Younes, G. 2015a, GCN, 18229, 1
Roberts, O. J., & Younes, G. 2015b, GCN, 17793, 1
Roberts, O. J., Zhang, B.-B., & Meegan, C. 2015b, GCN, 17819, 1
Robertson, B. E., & Ellis, R. S. 2012, ApJ, 744, 95
Roming, P. W. A., Koch, T. S., Oates, S. R., et al. 2009, ApJ, 690, 163
Rossi, F., Guidorzi, C., Amati, L., et al. 2008, MNRAS, 388, 1284
Rowlinson, A., Gompertz, B. P., Dainotti, M., et al. 2014, MNRAS, 443, 1779
Rowlinson, A., & O'Brien, P. 2012, in Proc. of the Gamma-Ray Bursts 2012 Conf. (GRB 2012) (Munich), 100
Rubin, D. B. 1976, Biometrika, 63, 581
Rubin, D. B. 1987, Multiple Imputation For Nonresponse In Surveys (New York: Wiley)
Rubin, D. B. 1996, J. Am. Stat. Assoc., 91, 473
Ruffini, R., Rueda, J. A., Muccino, M., et al. 2016, ApJ, 832, 136
Ruggeri, A. C., & Capozziello, S. 2016, Ap&SS, 361, 279
Ryde, F. 2005, ApJL, 625, L95
Ryde, F., & Pe'er, A. 2009, ApJ, 702, 1211
Rykoff, E. S., Aharonian, F., Akerlof, C. W., et al. 2009, ApJ, 702, 489
Saez, D., & Götz, D. 2015, arXiv:1507.06491
Sahu, K. C., Livio, M., Petro, L., et al. 1997, Natur, 387, 476
Sakamoto, T., Barthelmy, S. D., Barbier, L., et al. 2008, ApJS, 175, 179
Sakamoto, T., Barthelmy, S. D., Baumgartner, W. H., et al. 2009, GCN, 10180, 1
Sakamoto, T., Barthelmy, S. D., Baumgartner, W. H., et al. 2010a, GCN, 10993, 1
Sakamoto, T., Barthelmy, S. D., Baumgartner, W. H., et al. 2010b, GCN, 11358, 1
Sakamoto, T., Barthelmy, S. D., Baumgartner, W. H., et al. 2010c, GCN, 11169, 1
Sakamoto, T., Barthelmy, S. D., Baumgartner, W. H., et al. 2010d, GCN, 10371, 1
Sakamoto, T., Barthelmy, S. D., Baumgartner, W. H., et al. 2011a, ApJS, 195, 2
Sakamoto, T., Barthelmy, S. D., Baumgartner, W. H., et al. 2011b, GCN, 12464, 1
Sakamoto, T., Barthelmy, S. D., Baumgartner, W. H., et al. 2011c, GCN, 12312, 1
Sakamoto, T., Barthelmy, S. D., Baumgartner, W. H., et al. 2011d, GCN, 11677, 1
Sakamoto, T., Barthelmy, S. D., Baumgartner, W. H., et al. 2012a, GCN, 13917, 1
Sakamoto, T., Barthelmy, S. D., Baumgartner, W. H., et al. 2012b, GCN, 13689, 1
Sakamoto, T., Barthelmy, S. D., Baumgartner, W. H., et al. 2012c, GCN, 13195, 1
Sakamoto, T., Barthelmy, S. D., Baumgartner, W. H., et al. 2012d, GCN, 13836, 1
Sakamoto, T., Barthelmy, S. D., Baumgartner, W. H., et al. 2013a, GCN, 15584, 1
Sakamoto, T., Barthelmy, S. D., Baumgartner, W. H., et al. 2013b, GCN, 14942, 1
Sakamoto, T., Barthelmy, S. D., Baumgartner, W. H., et al. 2013c, GCN, 14613, 1
Sakamoto, T., Barthelmy, S. D., Baumgartner, W. H., et al. 2014a, GCN, 17176, 1
Sakamoto, T., Barthelmy, S. D., Baumgartner, W. H., et al. 2014b, GCN, 16942, 1
Sakamoto, T., Barthelmy, S. D., Baumgartner, W. H., et al. 2014c, GCN, 16799, 1
Sakamoto, T., Barthelmy, S. D., Baumgartner, W. H., et al. 2014d, GCN, 16573, 1
Sakamoto, T., Barthelmy, S. D., Baumgartner, W. H., et al. 2015a, GCN, 17930, 1
Sakamoto, T., Barthelmy, S. D., Cummings, J. R., et al. 2015b, GCN, 18648, 1
Sakamoto, T., Barthelmy, S. D., Cummings, J. R., et al. 2015c, GCN, 18514, 1
Sakamoto, T., Barthelmy, S. D., Cummings, J. R., et al. 2015d, GCN, 18368, 1
Sakamoto, T., Barthelmy, S. D., Cummings, J. R., et al. 2015e, GCN, 18170, 1
Sakamoto, T., Barthelmy, S. D., Cummings, J. R., et al. 2015f, GCN, 17675, 1
Sakamoto, T., Barthelmy, S. D., Cummings, J. R., et al. 2015g, GCN, 17519, 1
Sakamoto, T., Barthelmy, S. D., Cummings, J. R., et al. 2015h, GCN, 17401, 1
Sakamoto, T., Barthelmy, S. D., Cummings, J. R., et al. 2016a, GCN, 19276, 1
Sakamoto, T., Barthelmy, S. D., Cummings, J. R., et al. 2016b, GCN, 19106, 1
Sakamoto, T., Barthelmy, S. D., Gehrels, N., et al. 2012e, GCN, 13405, 1
Sakamoto, T., Barthelmy, S. D., & Norris, J. 2011e, GCN, 12477, 1
Sakamoto, T., Lamb, D. Q., Graziani, C., et al. 2004, ApJ, 602, 875
Sakamoto, T., Lamb, D. Q., Kawai, N., et al. 2005, NCimC, 28, 339
Sako, M., Harrison, F. A., & Rutledge, R. E. 2005, ApJ, 623, 973
Salmonson, J. D. 2000, ApJL, 544, L115
Sang, Y., Lin, H.-N., & Chang, Z. 2016, MNRAS, 460, 2282
Sari, R., & Piran, T. 1999, ApJ, 520, 641
Sari, R., Piran, T., & Narayan, R. 1998, ApJL, 497, L17
Sato, G., Barthelmy, S. D., Baumgartner, W. H., et al. 2013, GCN, 15298
Savaglio, S., Glazebrook, K., & Le Borgne, D. 2009, ApJ, 691, 182
Sazonov, S. Y., Sunyaev, R. A., Terekhov, O. V., et al. 1998, A&AS, 129, 1
Schady, P., Page, M. J., Oates, S. R., et al. 2010, MNRAS, 401, 2773
Schady, P., Savaglio, S., Krühler, T., Greiner, J., & Rau, A. 2011, A&A, 525, A113
Schaefer, B. E. 2003a, ApJL, 583, L71
Schaefer, B. E. 2003b, ApJL, 583, L67
Schaefer, B. E. 2007, ApJ, 660, 16
Schaefer, B. E., Cline, T. L., Hurley, K. C., & Laros, J. G. 1998, ApJS, 118, 353
Schaefer, B. E., Deng, M., & Band, D. L. 2001, ApJL, 563, L123
Schulze, S., Chapman, R., Hjorth, J., et al. 2015, ApJ, 808, 73
Schulze, S., Klose, S., Björnsson, G., et al. 2011, A&A, 526, A23
Senuma, K., Yoshida, A., Sakamoto, T., et al. 2015, GCN, 18792, 1
Serino, M., Sakamoto, T., Kawai, N., et al. 2014, PASJ, 66, 87

Shahmoradi, A., & Nemiroff, R. J. 2010, MNRAS, 407, 2075
Shao, L., Fan, Y.-Z., & Wei, D.-M. 2010, ApJL, 719, L172
Si, S.-K., Qi, Y.-Q., Xue, F.-X., et al. 2018, ApJ, 863, 50
Siellez, K., Boer, M., Gendre, B., & Regimbau, T. 2016, arXiv:1606.03043
Simić, S., & C. Popović, L. 2012, IJMPD, 21, 1250028
Smith, D. A., Levine, A., Bradt, H., et al. 2002, ApJS, 141, 415
Sokolov, V. V., Fatkhullin, T. A., Castro-Tirado, A. J., et al. 2001, A&A, 372, 438
Song, C.-Y., Liu, T., Gu, W.-M., & Tian, J.-X. 2016, MNRAS, 458, 1921
Sparre, M., Hartoog, O. E., Krühler, T., et al. 2014, ApJ, 785, 150
Sparre, M., & Starling, R. L. C. 2012, MNRAS, 427, 2965
Spearman, C. 1987, American Journal of Psychology, 100, 441
Stamatikos, M., Barthelmy, S. D., Baumgartner, W. H., et al. 2010a, GCN, 11202, 1
Stamatikos, M., Barthelmy, S. D., Baumgartner, W. H., et al. 2010b, GCN, 10732, 1
Stamatikos, M., Barthelmy, S. D., Baumgartner, W. H., et al. 2011a, GCN, 12016, 1
Stamatikos, M., Barthelmy, S. D., Baumgartner, W. H., et al. 2011b, GCN, 12651, 1
Stamatikos, M., Barthelmy, S. D., Baumgartner, W. H., et al. 2011c, GCN, 11691, 1
Stamatikos, M., Barthelmy, S. D., Baumgartner, W. H., et al. 2011d, GCN, 11527, 1
Stamatikos, M., Barthelmy, S. D., Baumgartner, W. H., et al. 2012, GCN, 13039, 1
Stamatikos, M., Barthelmy, S. D., Baumgartner, W. H., et al. 2013a, GCN, 15613, 1
Stamatikos, M., Barthelmy, S. D., Baumgartner, W. H., et al. 2013b, GCN, 15108, 1
Stamatikos, M., Barthelmy, S. D., Baumgartner, W. H., et al. 2013c, GCN, 15016, 1
Stamatikos, M., Barthelmy, S. D., Baumgartner, W. H., et al. 2013d, GCN, 14952, 1
Stamatikos, M., Barthelmy, S. D., Baumgartner, W. H., et al. 2014a, GCN, 17202, 1
Stamatikos, M., Barthelmy, S. D., Baumgartner, W. H., et al. 2014b, GCN, 16960, 1
Stamatikos, M., Barthelmy, S. D., Baumgartner, W. H., et al. 2014c, GCN, 16827, 1
Stamatikos, M., Barthelmy, S. D., Baumgartner, W. H., et al. 2014d, GCN, 16584, 1
Stamatikos, M., Barthelmy, S. D., Baumgartner, W. H., et al. 2014e, GCN, 16462, 1
Stamatikos, M., Barthelmy, S. D., Baumgartner, W. H., et al. 2014f, GCN, 16292, 1
Stamatikos, M., Barthelmy, S. D., Baumgartner, W. H., et al. 2014g, GCN, 16284, 1
Stamatikos, M., Barthelmy, S. D., Baumgartner, W. H., et al. 2014h, GCN, 16063, 1
Stamatikos, M., Barthelmy, S. D., Baumgartner, W. H., et al. 2014i, GCN, 15836, 1
Stamatikos, M., Barthelmy, S. D., Baumgartner, W. H., et al. 2015a, GCN, 17941, 1
Stamatikos, M., Barthelmy, S. D., Baumgartner, W. H., et al. 2015b, GCN, 17701, 1
Stamatikos, M., Barthelmy, S. D., Baumgartner, W. H., et al. 2015c, GCN, 17516, 1
Stamatikos, M., Barthelmy, S. D., Cenko, S. B., et al. 2015d, GCN, 18086, 1
Stamatikos, M., Barthelmy, S. D., Cummings, J. R., et al. 2015e, GCN, 18668, 1
Stamatikos, M., Barthelmy, S. D., Cummings, J. R., et al. 2015f, GCN, 18527, 1
Stamatikos, M., Barthelmy, S. D., Cummings, J. R., et al. 2015g, GCN, 18387, 1
Stamatikos, M., Barthelmy, S. D., Cummings, J. R., et al. 2015h, GCN, 18196, 1
Stamatikos, M., Barthelmy, S. D., Cummings, J. R., et al. 2016a, GCN, 19302, 1
Stamatikos, M., Barthelmy, S. D., Cummings, J. R., et al. 2016b, GCN, 19113, 1
Stamatikos, M., Barthelmy, S. D., Cummings, J. R., et al. 2016c, GCN, 18899, 1
Stamatikos, M., Markwardt, C. B., Barthelmy, S. D., et al. 2015i, GCN, 17406, 1
Stanbro, M. 2014a, GCN, 16636, 1
Stanbro, M. 2014b, GCN, 16385, 1
Stanbro, M. 2014c, GCN, 16347, 1
Stanbro, M. 2014d, GCN, 15977, 1
Stanbro, M. 2014e, GCN, 15975, 1
Stanbro, M. 2015a, GCN, 18639, 1
Stanbro, M. 2015b, GCN, 17658, 1
Stanbro, M. 2015c, GCN, 17353, 1
Stanbro, M. 2015d, GCN, 17308, 1
Stanbro, M. 2015e, GCN, 17295, 1
Stanbro, M. 2015f, GCN, 17276, 1
Stanbro, M., & Meegan, C. 2015, GCN, 18570, 1
Stanbro, M., & Troja, E. 2014, GCN, 16319, 1
Stanbro, M., & Yu, H.-F. 2015, GCN, 17292, 1
Stanek, K. Z., Dai, X., Prieto, J. L., et al. 2007, ApJL, 654, L21
Stanek, K. Z., Garnavich, P. M., Nutzman, P. A., et al. 2005, ApJL, 626, L5
Stanek, K. Z., Matheson, T., Garnavich, P. M., et al. 2003, ApJL, 591, L17
Stanway, E. R., Levan, A. J., & Davies, L. J. M. 2014, MNRAS, 444, 2133
Starling, R. L. C., Page, K. L., Pe'Er, A., Beardmore, A. P., & Osborne, J. P. 2012, MNRAS, 427, 2950
Starling, R. L. C., Wiersema, K., Levan, A. J., et al. 2011, MNRAS, 411, 2792
Stern, B. E., Tikhomirova, Y., Kompaneets, D., Svensson, R., & Poutanen, J. 2001, ApJ, 563, 80
Stratta, G., Dainotti, M. G., Dall'Osso, S., Hernandez, X., & De Cesare, G. 2018, ApJ, 869, 155
Stratta, G., Gendre, B., Atteia, J. L., et al. 2013, ApJ, 779, 66
Svensson, K. M., Levan, A. J., Tanvir, N. R., Fruchter, A. S., & Strolger, L.-G. 2010, MNRAS, 405, 57
Swenson, C. A., & Roming, P. W. A. 2014, ApJ, 788, 30
Swenson, C. A., Roming, P. W. A., De Pasquale, M., & Oates, S. R. 2013, ApJ, 774, 2
Tanvir, N., Pak, S., Priddey, R., et al. 2005, GCN, 3031, 1
Tanvir, N. R., Kruehler, T., Malesani, D., et al. 2015a, GCN, 18524, 1
Tanvir, N. R., Levan, A. J., Fruchter, A. S., et al. 2013, Natur, 500, 547
Tanvir, N. R., Xu, D., Zafar, T., Covino, S., & Schulze, S. 2015b, GCN, 18080, 1
Tarnopolski, M. 2015, A&A, 581, A29
Tarnopolski, M. 2016, Ap&SS, 361, 125
Tavani, M. 1996, ApJ, 466, 768
Terekhov, O. V., Denisenko, D. V., Lobachev, V. A., et al. 1994, AstL, 20, 265
Thoene, C. C., de Ugarte Postigo, A., & Ricci, D. 2008, GCN, 8135, 1
Thompson, C., Mészáros, P., & Rees, M. J. 2007, ApJ, 666, 1012
Thöne, C. C., de Ugarte Postigo, A., Fryer, C. L., et al. 2011, Natur, 480, 72
Tierney, D. 2011, GCN, 12529, 1
Tierney, D. 2012, GCN, 14039, 1
Tierney, D. 2013, GCN, 14329, 1
Toelge, K., & Bissaldi, E. 2015, GCN, 18727, 1
Toelge, K., & Hui, M. 2016, GCN, 19161, 1
Trentham, N., Ramirez-Ruiz, E., & Blain, A. W. 2002, MNRAS, 334, 983
Troja, E., King, A. R., O'Brien, P. T., Lyons, N., & Cusumano, G. 2008, MNRAS, 385, L10
Troja, E., Sakamoto, T., Cenko, S. B., et al. 2016, ApJ, 827, 102
Tsutsui, R., Nakamura, T., Yonetoku, D., et al. 2008, in AIP Conf. Ser. 1000, Gamma-Ray Bursts 2007, ed. M. Galassi, D. Palmer, & E. Fenimore (Melville, NY: AIP), 28
Tsutsui, R., Nakamura, T., Yonetoku, D., et al. 2009, JCAP, 8, 015
Tsutsui, R., Nakamura, T., Yonetoku, D., et al. 2011, PASJ, 63, 741
Tsutsui, R., Nakamura, T., Yonetoku, D., Murakami, T., & Takahashi, K. 2010, arXiv:1012.3009
Tsutsui, R., Nakamura, T., Yonetoku, D., Takahashi, K., & Morihara, Y. 2013a, PASJ, 65, 3
Tsutsui, R., & Shigeyama, T. 2013, PASJ, 65, L3
Tsutsui, R., & Shigeyama, T. 2014, PASJ, 66, 42
Tsutsui, R., Yonetoku, D., Nakamura, T., Takahashi, K., & Morihara, Y. 2013b, MNRAS, 431, 1398
Tu, Z. L., & Wang, F. Y. 2018, ApJL, 869, L23
Tunnicliffe, R. L., Levan, A. J., Tanvir, N. R., et al. 2014, MNRAS, 437, 1495
Turpin, D., Heussaff, V., Dezalay, J.-P., et al. 2016, ApJ, 831, 28
Ukwatta, T. N., Barthelmy, D., Cummings, J. R., et al. 2015a, GCN, 18542, 1
Ukwatta, T. N., Barthelmy, S. D., Baumgartner, W. H., et al. 2010a, GCN, 11207, 1
Ukwatta, T. N., Barthelmy, S. D., Baumgartner, W. H., et al. 2011a, GCN, 11703, 1
Ukwatta, T. N., Barthelmy, S. D., Baumgartner, W. H., et al. 2011b, GCN, 11902, 1
Ukwatta, T. N., Barthelmy, S. D., Baumgartner, W. H., et al. 2011c, GCN, 12030, 1

Ukwatta, T. N., Barthelmy, S. D., Baumgartner, W. H., et al. 2012a, GCN, 13041, 1
Ukwatta, T. N., Barthelmy, S. D., Baumgartner, W. H., et al. 2012b, GCN, 13880, 1
Ukwatta, T. N., Barthelmy, S. D., Baumgartner, W. H., et al. 2012c, GCN, 13568, 1
Ukwatta, T. N., Barthelmy, S. D., Baumgartner, W. H., et al. 2012d, GCN, 13450, 1
Ukwatta, T. N., Barthelmy, S. D., Baumgartner, W. H., et al. 2012e, GCN, 12924, 1
Ukwatta, T. N., Barthelmy, S. D., Baumgartner, W. H., et al. 2013a, GCN, 15354, 1
Ukwatta, T. N., Barthelmy, S. D., Baumgartner, W. H., et al. 2013b, GCN, 15116, 1
Ukwatta, T. N., Barthelmy, S. D., Baumgartner, W. H., et al. 2013c, GCN, 15031, 1
Ukwatta, T. N., Barthelmy, S. D., Baumgartner, W. H., et al. 2013d, GCN, 14636, 1
Ukwatta, T. N., Barthelmy, S. D., Baumgartner, W. H., et al. 2013e, GCN, 14197, 1
Ukwatta, T. N., Barthelmy, S. D., Baumgartner, W. H., et al. 2014a, GCN, 17213, 1
Ukwatta, T. N., Barthelmy, S. D., Baumgartner, W. H., et al. 2014b, GCN, 17010, 1
Ukwatta, T. N., Barthelmy, S. D., Baumgartner, W. H., et al. 2014c, GCN, 16839, 1
Ukwatta, T. N., Barthelmy, S. D., Baumgartner, W. H., et al. 2014d, GCN, 16613, 1
Ukwatta, T. N., Barthelmy, S. D., Baumgartner, W. H., et al. 2014e, GCN, 16306, 1
Ukwatta, T. N., Barthelmy, S. D., Baumgartner, W. H., et al. 2014f, GCN, 16103, 1
Ukwatta, T. N., Barthelmy, S. D., Baumgartner, W. H., et al. 2014g, GCN, 15906, 1
Ukwatta, T. N., Barthelmy, S. D., Baumgartner, W. H., et al. 2015b, GCN, 17740, 1
Ukwatta, T. N., Barthelmy, S. D., Baumgartner, W. H., et al. 2015c, GCN, 17410, 1
Ukwatta, T. N., Barthelmy, S. D., Beardmore, A. P., et al. 2016a, GCN, 19148, 1
Ukwatta, T. N., Barthelmy, S. D., Cummings, J. R., et al. 2015d, GCN, 18670, 1
Ukwatta, T. N., Barthelmy, S. D., Cummings, J. R., et al. 2015e, GCN, 18382, 1
Ukwatta, T. N., Barthelmy, S. D., Cummings, J. R., et al. 2015f, GCN, 18214, 1
Ukwatta, T. N., Barthelmy, S. D., Cummings, J. R., et al. 2015g, GCN, 18091, 1
Ukwatta, T. N., Barthelmy, S. D., Cummings, J. R., et al. 2015h, GCN, 17973, 1
Ukwatta, T. N., Barthelmy, S. D., Cummings, J. R., et al. 2016b, GCN, 19301, 1
Ukwatta, T. N., Barthelmy, S. D., Cummings, J. R., et al. 2016c, GCN, 18919, 1
Ukwatta, T. N., Dhuga, K. S., Stamatikos, M., et al. 2012f, MNRAS, 419, 614
Ukwatta, T. N., Msu, S., Barthelmy, S. D., et al. 2011d, GCN, 12671, 1
Ukwatta, T. N., Stamatikos, M., Dhuga, K. S., et al. 2010b, ApJ, 711, 1073
Urata, Y., Huang, K., Yamazaki, R., & Sakamoto, T. 2015, ApJ, 806, 222
Valan, V., Larsson, J., & Ahlgren, B. 2018, MNRAS, 474, 2401
van Dongen, S., & Enright, A. J. 2012, arXiv:1208.3145
van Putten, M. H. P. M. 2015, ApJ, 810, 7
Veres, P. 2016, GCN, 18796, 1
Veres, P., Connaughton, V., & Meegan, C. 2015a, GCN, 18066, 1
Veres, P., & Meegan, C. 2016, GCN, 18844, 1
Veres, P., Meegan, C., & von Kienlin, A. 2015b, GCN, 18787, 1
Vetere, L., Soffitta, P., Massaro, E., Giommi, P., & Costa, E. 2007, A&A, 473, 347
Vianello, G., Götz, D., & Mereghetti, S. 2009, A&A, 495, 1005
Virgili, F. J., Qin, Y., Zhang, B., & Liang, E. 2012, MNRAS, 424, 2821
Volnova, A. A., Pozanenko, A. S., Gorosabel, J., et al. 2014, MNRAS, 442, 2586
von Kienlin, A. 2010, GCN, 11002, 1
von Kienlin, A. 2011, GCN, 11671, 1
von Kienlin, A. 2013a, GCN, 15528, 1
von Kienlin, A. 2013b, GCN, 15396, 1
von Kienlin, A. 2013c, GCN, 14560, 1
von Kienlin, A. 2013d, GCN, 14442, 1
von Kienlin, A. 2014a, GCN, 16905, 1
von Kienlin, A. 2014b, GCN, 16754, 1
von Kienlin, A. 2014c, GCN, 16450, 1
von Kienlin, A. 2014d, GCN, 15811, 1
von Kienlin, A. 2014e, GCN, 15790, 1
von Kienlin, A. 2015a, GCN, 18628, 1
von Kienlin, A. 2015b, GCN, 17623, 1
von Kienlin, A., & Bhat, P. N. 2014, GCN, 15651, 1
von Kienlin, A., & Burns, E. 2015, GCN, 17319, 1
von Kienlin, A., & Connaughton, V. 2014, GCN, 15716, 1
von Kienlin, A., & Jenke, P. 2013, GCN, 15401, 1
von Kienlin, A., & Meegan, C. 2013a, GCN, 15591, 1
von Kienlin, A., & Meegan, C. 2013b, GCN, 15300, 1
von Kienlin, A., & Meegan, C. 2014, GCN, 16850, 1
von Kienlin, A., & Meegan, C. 2015, GCN, 17481, 1
von Kienlin, A., Meegan, C. A., Paciesas, W. S., et al. 2014, ApJS, 211, 13
von Kienlin, A., & Younes, G. 2013, GCN, 14530, 1
von Kienlin, A., & Younes, G. 2014, GCN, 16042, 1
von Kienlin, A., Yu, H.-F., & Toelge, K. 2016, GCN, 19061, 1
Vurm, I., & Beloborodov, A. M. 2016, ApJ, 831, 175
Wainwright, C., Berger, E., & Penprase, B. E. 2007, ApJ, 657, 367
Wang, F.-F., Zou, Y.-C., Liu, Y., Liao, B., & Moharana, R. 2018, JHEAp, 18, 21
Wang, F. Y., & Dai, Z. G. 2014, ApJS, 213, 15
Wang, F. Y., Dai, Z. G., & Liang, E. W. 2015, NewAR, 67, 1
Wang, F.-Y., Qi, S., & Dai, Z.-G. 2011, MNRAS, 415, 3423
Wang, J. S., Wang, F. Y., Cheng, K. S., & Dai, Z. G. 2016, A&A, 585, A68
Wang, X.-G., Liang, E.-W., Li, L., et al. 2013, ApJ, 774, 132
Wang, Y.-Z., Huang, Y.-J., Liang, Y.-F., et al. 2017, ApJL, 851, L20
Wei, H. 2010, JCAP, 8, 020
Wei, J.-J., Wu, X.-F., Gao, H., & Mészáros, P. 2016, JCAP, 8, 031
Wei, J.-J., Wu, X.-F., Melia, F., Wei, D.-M., & Feng, L.-L. 2014, MNRAS, 439, 3329
Wiersema, K., Curran, P. A., Krühler, T., et al. 2012, MNRAS, 426, 2
Wijers, R. A. M. J., Rees, M. J., & Meszaros, P. 1997, MNRAS, 288, L51
Willingale, R., Genet, F., Granot, J., & O'Brien, P. T. 2010, MNRAS, 403, 1296
Willingale, R., O'Brien, P. T., Goad, M. R., et al. 2007a, arXiv:0710.3727
Willingale, R., O'Brien, P. T., Osborne, J. P., et al. 2007b, ApJ, 662, 1093
Wiseman, P., Graham, J., Schady, P., & Greiner, J. 2015, GCN, 17336, 1
Woosley, S. E. 1993, ApJ, 405, 273
Woosley, S. E., & Bloom, J. S. 2006, ARA&A, 44, 507
Woźniak, P. R., Vestrand, W. T., Wren, J. A., et al. 2006, ApJL, 642, L99
Wu, Q., Zou, Y.-C., Cao, X., Wang, D.-X., & Chen, L. 2011, ApJL, 740, L21
Xiao, D., Liu, L.-D., Dai, Z.-G., & Wu, X.-F. 2017, arXiv:1710.05910
Xiao, L., & Schaefer, B. E. 2009a, ApJ, 707, 387
Xiao, L., & Schaefer, B. E. 2009b, ApJ, 698, 803
Xiao, L., & Schaefer, B. E. 2011, ApJ, 731, 103
Xie, C., Fang, T., Wang, J., Liu, T., & Jiang, X. 2016, ApJL, 824, L17
Xiong, S. 2011, GCN, 12073, 1
Xiong, S. 2013a, GCN, 15315, 1
Xiong, S. 2013b, GCN, 14903, 1
Xiong, S. 2014a, GCN, 15751, 1
Xiong, S. 2014b, GCN, 15687, 1
Xiong, S., Byrne, D., & Meegan, C. 2012, GCN, 13860, 1
Xiong, S., & Chaplin, V. 2013, GCN, 14283, 1
Xiong, S., Connaughton, V., & Singer, L. P. 2014, GCN, 15688, 1
Xiong, S., & Meegan, C. 2013, GCN, 15175, 1
Xu, D., Dai, Z. G., & Liang, E. W. 2005, ApJ, 633, 603
Xu, D., de Ugarte Postigo, A., Leloudas, G., et al. 2013, ApJ, 776, 98
Xu, D., Levan, A. J., Fynbo, J. P. U., et al. 2014, GCN, 16983, 1
Xu, D., Tanvir, N. R., Malesani, D., & Fynbo, J. 2015, GCN, 18505, 1
Xu, M., & Huang, Y. F. 2012, A&A, 538, A134
Yamada, Y., Yoshida, A., Sakamoto, T., et al. 2016, GCN, 18814, 1
Yamazaki, R. 2009, ApJL, 690, L118
Yang, B., Jin, Z.-P., Li, X., et al. 2015, NatCo, 6, 7323
Yang, E.-B., Zhang, Z.-B., Choi, C.-S., & Chang, H.-Y. 2016a, arXiv:1603.03680
Yang, E. B., Zhang, Z. B., & Jiang, X. X. 2016b, Ap&SS, 361, 257
Yi, S.-X., Xi, S.-Q., Yu, H., et al. 2016, ApJS, 224, 20
Yi, S.-X., Yu, H., Wang, F. Y., & Dai, Z.-G. 2017, ApJ, 844, 79
Yonetoku, D., Murakami, T., Nakamura, T., et al. 2004, ApJ, 609, 935
Yonetoku, D., Murakami, T., Tsutsui, R., et al. 2010, PASJ, 62, 1495
Yoshida, A., Sakamoto, T., Takahashi, I., et al. 2015, GCN, 18605, 1
Yost, S. A., & Moore, T. M. 2015, MNRAS, 454, 3567

Younes, G. 2012, GCN, 13214, 1
Younes, G. 2014a, GCN, 16189, 1
Younes, G. 2014b, GCN, 15709, 1
Younes, G. 2015a, GCN, 17813, 1
Younes, G. 2015b, GCN, 18081, 1
Younes, G., Connaughton, V., Meegan, C., & von Kienlin, A. 2014a, GCN, 16014, 1
Younes, G., & Meegan, C. 2014, GCN, 16447, 1
Younes, G., von Kienlin, A., & Meegan, C. 2014b, GCN, 16452, 1
Yu, H., Wang, F. Y., Dai, Z. G., & Cheng, K. S. 2015a, ApJS, 218, 13
Yu, H.-F. 2013a, GCN, 15554, 1
Yu, H.-F. 2013b, GCN, 14801, 1
Yu, H.-F. 2014a, GCN, 17216, 1
Yu, H.-F. 2014b, GCN, 16203, 1
Yu, H.-F. 2014c, GCN, 16199, 1
Yu, H.-F. 2014d, GCN, 16081, 1
Yu, H.-F. 2015a, GCN, 18715, 1
Yu, H.-F. 2015b, GCN, 17863, 1
Yu, H.-F. 2015c, GCN, 17579, 1
Yu, H.-F., & Burns, E. 2015, GCN, 18178, 1
Yu, H.-F., Burns, E., Connaughton, V., Goldstein, A., & Gibby, M. 2015b, GCN, 17975, 1
Yu, H.-F., Goldstein, A., & Pelassa, V. 2013, GCN, 15070, 1
Yu, H.-F., Greiner, J., van Eerten, H., et al. 2015c, A&A, 573, A81
Yu, H.-F., & Jenke, P. 2015, GCN, 18149, 1
Yu, H.-F., Preece, R. D., Greiner, J., et al. 2016, A&A, 588, A135
Yu, H.-F., & von Kienlin, A. 2014, GCN, 16032, 1
Yu, H.-F., & Xiong, S. 2013, GCN, 14261, 1
Yu, H.-F., Younes, G., & Meegan, C. 2015d, GCN, 17891, 1
Zaninoni, E., Bernardini, M. G., Margutti, R., & Amati, L. 2016, MNRAS, 455, 1375
Zaninoni, E., Bernardini, M. G., Margutti, R., Oates, S., & Chincarini, G. 2013, A&A, 557, A12
Zhang, B. 2007, ChJAA, 7, 1
Zhang, B. 2018, The Physics of Gamma-Ray Bursts (Cambridge: Cambridge Univ. Press)
Zhang, B., Fan, Y. Z., Dyks, J., et al. 2006a, ApJ, 642, 354
Zhang, B., & Mészáros, P. 2004, IJMPA, 19, 2385
Zhang, B., Zhang, B.-B., Liang, E.-W., et al. 2007, ApJL, 655, L25
Zhang, B., Zhang, B.-B., Virgili, F. J., et al. 2009, ApJ, 703, 1696
Zhang, B.-B. 2011, ApJL, 726, L2
Zhang, B.-B. 2013a, GCN, 15382, 1
Zhang, B.-B. 2013b, GCN, 15360, 1
Zhang, B.-B. 2014a, GCN, 17021, 1
Zhang, B.-B. 2014b, GCN, 16798, 1
Zhang, B.-B. 2014c, GCN, 16775, 1
Zhang, B.-B. 2014d, GCN, 16669, 1
Zhang, B.-B. 2014e, GCN, 16590, 1
Zhang, B.-B. 2014f, GCN, 16561, 1
Zhang, B.-B. 2014g, GCN, 16537, 1
Zhang, B.-B. 2014h, GCN, 15866, 1
Zhang, B.-B. 2015, GCN, 17674, 1
Zhang, B.-B., Foley, S., & Bhat, N. 2013a, GCN, 15219, 1
Zhang, B.-B., van Eerten, H., Burrows, D. N., et al. 2015a, ApJ, 806, 15
Zhang, B.-B., Zhang, B., Liang, E.-W., et al. 2011, ApJ, 730, 141
Zhang, B.-B., Zhang, B., Murase, K., Connaughton, V., & Briggs, M. S. 2014a, ApJ, 787, 66
Zhang, F.-W., Fan, Y.-Z., Shao, L., & Wei, D.-M. 2013b, ApJL, 778, L11
Zhang, F.-W., Shao, L., Yan, J.-Z., & Wei, D.-M. 2012, ApJ, 750, 88
Zhang, G. Q., & Wang, F. Y. 2018, ApJ, 852, 1
Zhang, Q., Huang, Y.-F., & Zong, H.-S. 2015b, ApJ, 811, 83
Zhang, Q., Huang, Y. F., & Zong, H. S. 2016a, ApJ, 823, 156
Zhang, S., Jin, Z.-P., Zhang, F.-W., et al. 2017, ApJ, 844, 55
Zhang, S., Lu, F. J., Zhang, S. N., & Li, T. P. 2014b, Proc. SPIE, 9144, 914421
Zhang, Z., Xie, G. Z., Deng, J. G., & Jin, W. 2006b, MNRAS, 373, 729
Zhang, Z.-B., Yang, E.-B., Choi, C.-S., & Chang, H.-Y. 2016b, MNRAS, 462, 3243
Zheng, W., Filippenko, A. V., Yuk, H., Zhu, Y., & Perley, D. A. 2015, GCN, 18273, 1
Zheng, W.-K., Deng, J.-S., & Wang, J. 2009, RAA, 9, 1103
Zhou, Z. H. 2016, Machine Learning (In Chinese) (Beijing: Tsinghua Univ. Press)
Zitouni, H., Guessoum, N., Azzam, W. J., & Mochkovitch, R. 2015, Ap&SS, 357, 7
Zou, Y.-C., Cheng, K. S., & Wang, F. Y. 2015, ApJL, 800, L23
Zou, Y.-C., Fan, Y.-Z., & Piran, T. 2009, MNRAS, 396, 1163
Zou, Y.-C., & Piran, T. 2010, MNRAS, 402, 1854
Zou, Y.-C., Wang, F.-F., Moharana, R., et al. 2018, ApJL, 852, L1